A new Synthetic Approach Toward Rylene Dyes

Dissertation

zur Erlangung des Grades

“Doktor der Naturwissenschaften”

im Promotionsfach Chemie

am Fachbereich Chemie, Pharmazie, Geographie und Geowissenschaften der

Johannes Gutenberg-Universität Mainz

vorgelegt von

Daniel Uersfeld

geboren in Koblenz

Mainz, März 2019

Dekan:

1. Berichterstatter:

2. Berichterstatter:

Tag der mündlichen Prüfung: 29.05.2019

Die folgende Arbeit wurde im Zeitraum von März 2015 bis September 2018 am Max-Planck-Institut für Polymerforschung in Mainz sowie der Johannes Gutenberg-Universität Mainz angefertigt. Diese Dissertation wurde eigenständig und ohne unerlaubte Hilfe erarbeitet.

As if all this was something more

Than another footnote on a postcard from nowhere

Another chapter in the handbook for exercises in futility

TABLE OF CONTENTS

LIST OF FIGURES

LIST OF SCHEMES

List of Abbrevations and Acronyms

AcOH	Acetic acid
Bpin	Boronic acid pinacol ester
B_2pin_2	Bis(pinacolato)diboron
Bu	Butyl
CB[8]	Cucurbit[8]uril
dba	dibenzylideneacetone
DBN	1,5-Diazabicyclo[4.3.0]non-5-ene
DBU	1,8-Diazabicyclo[5.4.0]undec-7-ene
DIPP	Di*iso*propylphenyl
DMF	Dimethylformamide
DMSO	Dimethyl sulfoxide
Dppf	1,1′-Bis(diphenylphosphino)ferrocene
EET	Excitation energy transfer
FD-MS	Field desorption mass spectrometry
HBC	Hexa-*peri*-hexabenzocoronene
HOMO	Highest Occupied Molecular Orbital
HS	High Spin
ISC	Intersystem crossing
KOAc	Potassium acetate
LED	Light-emitting diode
LIESST	Light-Induced Excited Spin-State Trapping
LS	Low Spin
LUMO	Lowest Unoccupied Molecular Orbital
MALDI-TOF	Matrix-assisted laser desorption/ionization time of flight
NDA	Naphthalene-3,4,7,8-tetracarboxylic dianhydride
NDE	Naphthalene-3,4-dicarboxylic ester
NMA	Naphthalene-3,4-dicarboxylic monoanhydride
NMP	*N*-methyl-2-pyrrolidon
NMI	Naphthalene-3,4-dicarboxylic monoimide
PAH	Polycyclic aromatic hydrocarbon
PCy_3	Tricyclohexylphosphine
PDA	Perylene-3,4,9,10-tetracarboxylic dianhydride

$Pd_2(dba)_3$	Tris(dibenzylideneacetone)dipalladium(0)
PDI	Perylene-3,4,9,10-tetracarboxylic diimide
$Pd(OAc)_2$	Palladium(II) acetate
$Pd(PPh_3)_4$	Tetrakis(triphenylphosphine)palladium(0)
PMI	Perylene-3,4-dicarboxylic monoimide
PPh_3	Triphenylphosphine
PTE	Perylene-3,4,9,10-tetracarboxylic tetraester
p-TsOH	*p*-Toluenesulfonic acid
RET	Resonance Energy Transfer
R_f	Refractive index
SCO	Spin crossover
SPhos	2-Dicyclohexylphosphino-2',6'-dimethoxybiphenyl
TBAHFP	Tetrabutylammonium hexafluorophosphate
t-BuONa	Sodium *tert*-butoxide
TDA	Terrylene-3,4,11,12-tetracarboxylic dianhydride
TDI	Terrylene-3,4,11,12-tetracarboxylic diimide
TFA	Trifluoroacetic acid
THF	Tetrahydrofuran
TLC	Thin layer chromatography
TMS	Trimethylsilyl
TTE	Terrylene-3,4,11,12-tetracarboxylic tetraester
QDI	Quaterrylene-3,4,14,15-tetracarboxylic diimide

Chapter 1
INTRODUCTION AND MOTIVATION

The discovery of the aniline-based mauveine by *William Henry Perkin* in 1856 marked the beginning of the industrial production of synthetic dyes. While dyes have been traditionally used in the textile industry, the rapid increase in production volume of synthetic dyes and pigments made them abundant colorants for everyday items.[1] Intensive research lead to new synthetic methods to produce previously known natural dyes like alizarin,[2] but also new classes like azo dyes.[3]

Today, scientific interest in dyes and pigments has shifted towards functional materials.[4] The modern toolkit of synthetic chemistry allows for the design of functional dyes with tunable material properties like absorbance and photoluminescence, photochromism, adjustable frontier orbital energy levels and solubility, amongst others.[5] New dyes can be engineered, and properties can be fine-tuned to fit the necessary requirements in a rapidly growing field with ongoing developments. Contemporary dyes find use as organic semiconductors,[6] as well as photoconductive and photovoltaic devices.[7] Their fluorescing and phosphorescing properties are utilized in commercial as well as academic applications, such as organic LEDs (light emitting diodes) and lasers,[8,9] or as fluorescent probes in modern biology.[10] These state-of-the-art dyes, custom-tailored for each specific application on a molecular level, are oftentimes central to the success of a project.

The family of rylenes, which describes a series of *peri*-linked naphthalene units (Figure 1-1) following the terminology by *Clar*,[11] was first mentioned in 1910, when *Scholl* synthesized non-functionalized perylene.[12] Extending perylene with additional naphthalene units results in terrylene, quaterrylene, pentarylene and hexarylene. More important than unfunctionalized rylenes, however, are the electron deficient rylene imides, first described by *Kardos* in the form of perylene diimide (PDI) in 1913 (Figure 1-1).[13] Owing to their chemical, thermal and photochemical

stability, rylene imides are now, more than 100 years after the first discovery of perylene, among the most powerful functional materials, both in an industrial and academic environment.[14,15] The series of rylene imides Applications range from colorants in the automotive industry,[16] to high-tech areas such as light absorbers in dye sensitized solar cells,[17] as electron transporting materials in organic field-effect transistors,[18] as fluorescent solar collectors,[19] and as probes in bio imaging.[20]

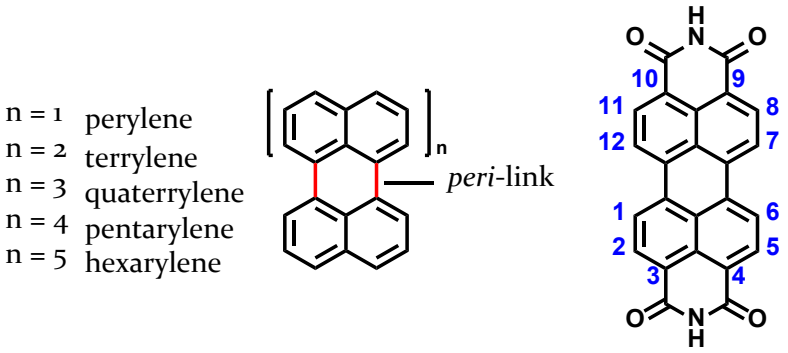

Figure 1-1. Perylene (left, n = 1) and perylene diimide (right, numbering of the perylene-scaffold in blue) as first described by *Scholl* (1910) and *Kardos* (1913).

1.1 Properties of Rylene Imides

The unique combination of properties of rylene imides are inherent to their electronic structure. Due to the increased electron delocalization caused by the electron withdrawing carboxylic imides substituents, rylene imides possess high chemical and thermal stability. The low reactivity of cyclic aromatic imides results in relative inertness of the carboxylic imide groups towards a wide range of reaction conditions. Typically, hydrolysis requires boiling the rylene imide in alcoholic solution with a large excess of potassium hydroxide, whereas PDI pigments dissolved in concentrated sulfuric acid show no signs of decomposition.[21] High thermal stability up to 490 °C makes high-temperature reactions as well as purification via sublimation without thermal decay possible.[21,22] Comparison of the first oxidation potentials of perylene, terrylene and quaterrylene diimide (1.67 V, 1.12 V, 0.82 V) show that rylene

imides are generally resistant to oxidation, but oxidation becomes easier when the distance between the electron withdrawing imide substituents increases.[23]

The electron deficiency of rylene imides is the reason for their high photochemical stability, as photooxidation (reaction of excited triplet-states with oxidizing agents like oxygen) as the major destructive mechanism of dyes and pigments is disfavored.[15] For example, investigation into the photophysical properties of TDI allowed the tracking of the chromophores for several minutes before irreversible photobleaching.[24]

The introduction of additional naphthalene units into the conjugated rylene scaffold rises the HOMO (highest occupied molecular orbital) levels considerably, while LUMO (lowest unoccupied molecular orbital) levels are mostly unaffected, as it is shown in the series of diimides in Figure 1-2.[25] Furthermore, due to the decoupling of the imide substituent from the rylene core, the choice of imide substituent shows no significant influence on the energy levels.[17]

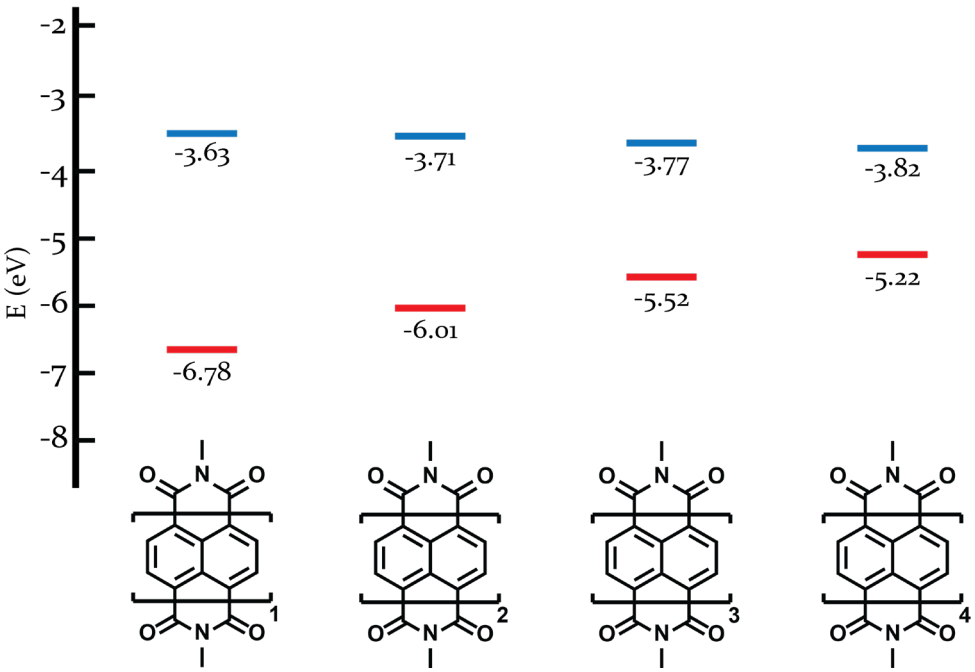

Figure 1-2. Energy levels of NDI, PDI, TDI and QDI. LUMO (blue) determined by cyclic voltammetric measurements, HOMO (red) estimated from HOMO = LUMO – E_{gap}. Further details (imide substituents, experimental setup) are described in the referred literature.[25]

Another effect that stems from extension of the conjugated π-system becomes apparent in Figure 1-2. With each additional naphthalene unit, the HOMO-LUMO energy gap decreases and a bathochromic shift of the absorption maximum of approximately 100 nm can be observed (Figure 1-3).[26] The absorption coefficients increase in a similar, linear manner, which is in accordance to the expected increasing absorption cross section. Higher rylenes also possess some of the highest absorption coefficients in the NIR region amongst all known organic dyes.[27] Whereas the absorptivity generally increases upon elongation of the rylene imide π-system, starting from quaterrylene diimide (QDI), fluorescence intensity drops dramatically.[28] It is suggested that with a decreasing energy gap, the probability for radiationless transitions increases exponentially, leading to an estimated quantum yield of φ_{fl} = 5 % in the case of QDI.[29] Nonetheless, some rylene imides exhibit outstanding fluorescence quantum yields.[30]

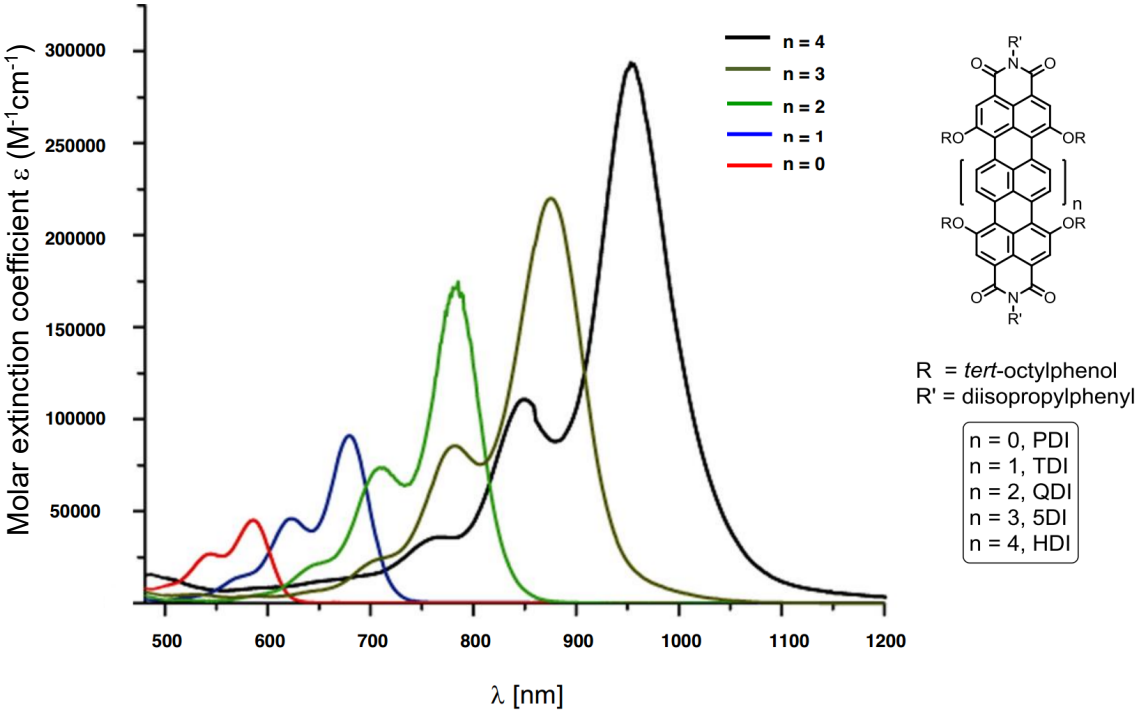

Figure 1-3. Absorption spectra of a rylene diimide series in $CHCl_3$.[26]

The extended aromatic scaffolds of rylene imides not only determine the photophysical properties, but also influence their behavior in solution. The aromatic hydrocarbon backbone of unsubstituted perylene diimides is almost perfectly flat,[31] leading to large stacks of aggregating PDI molecules driven by energetically favorable π-π interactions.[32] Figure 1-4 demonstrates how the flat PDI backbone of N,N'-dipropyl-PDI results in tight packing in the crystal structure.

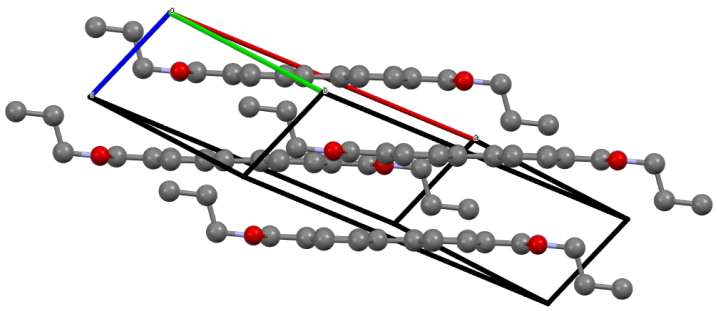

Figure 1-4. Crystal structure and packing of N,N'-Dipropyl-PDI.[33]

Consequently, the first synthesized perylene diimides were pigments and insoluble in almost every solvent except in sulfuric acid. For the same reason, the highly fluorescent nature of perylene diimides was only discovered in 1959, when longer, solubility-enhancing imide substituents were introduced, which were able to diminish aggregates in solution (see Figure 1-5).[34]

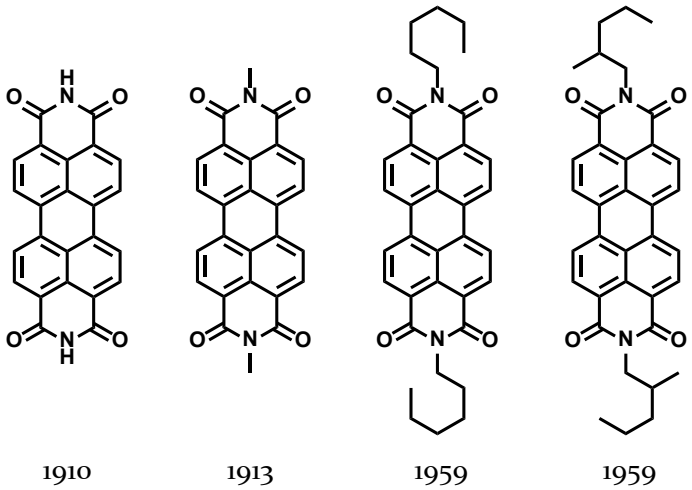

Figure 1-5. First ever synthesized PDI pigments (R = H, CH_3), first ever synthesized PDIs with significant fluorescence (R = hexyl, 2-methylpentyl).

Predicting the π-π stacking interactions via simple physical relationships for an individual rylene imide structure is difficult and depends on several factors. An extensive study on the π-π stacking behavior of a variety of dyes in different solvents has been conducted by the *Würthner* group.[32] They concluded that a combination of electrostatic interactions, dispersion interactions, orbital interactions and solvophobic effects determine the rate of aggregation and are influenced by the size and electronic structure of the aromatic backbone of the molecule, the nature of the peripheral substituents as well as the solvent.

When stacking of π-conjugated molecules occurs, the aggregation can lead to J- or H-type aggregates. These cases describe aggregating behavior where the absorption maximum is shifted to either longer (bathochromically shifted, J-type) or shorter (hypsochromically shifted, H-type) wavelengths with respect to the monomer absorption. In the case of H-aggregation, the fluorescence is typically quenched. Figure 1-6 shows how an increasing concentration of a tetra-phenoxylated PDI in methylcyclohexane leads to a J-type, bathochromically shifted absorption maximum.[35]

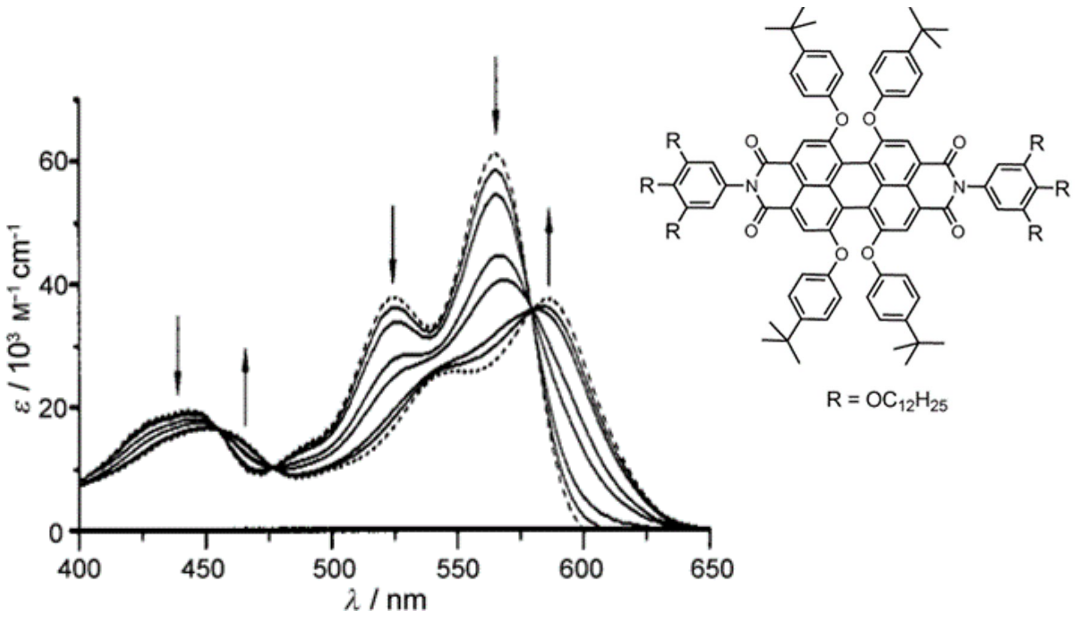

Figure 1-6. Concentration-dependant UV/Vis absorption spectra in methylcyclohexane demonstrating J-type aggregation behavior. The arrows indicate the changes in the spectra with increasing concentration.[35]

1.2 Synthetic Concepts of Rylene Imides

The history of modifying and substituting rylene imides started in 1913 (Figure 1-5), and new developments still emerge more than hundred years after the discovery of the first PDI. Figure 1-7 shows the accessible functionalization positions and Scheme 1-1 an exemplary overview of functionalization methods that will be discussed in this section.

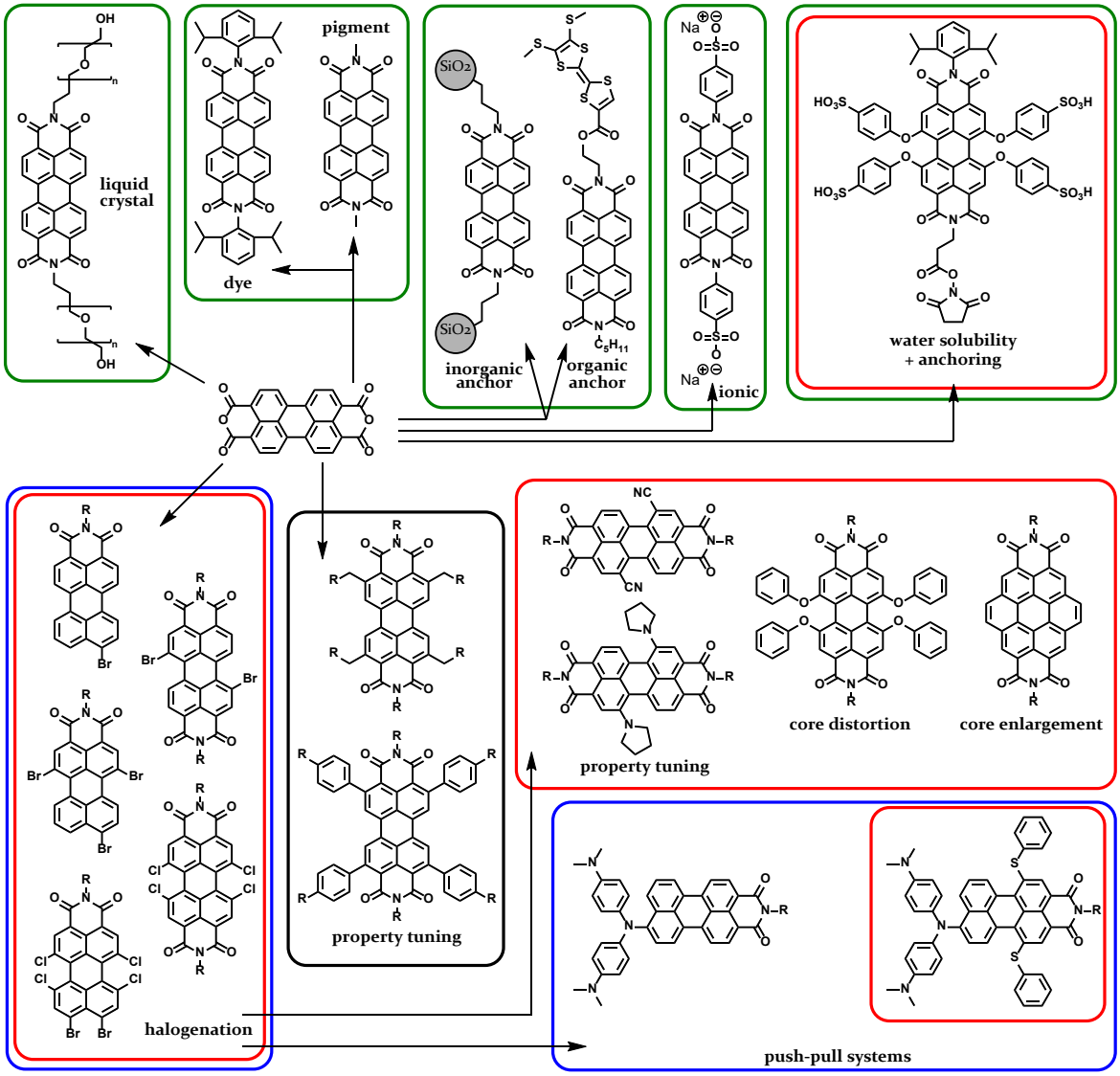

Scheme 1-1. Exemplary overview of functionalization methods of rylene imides, as discussed in this chapter.

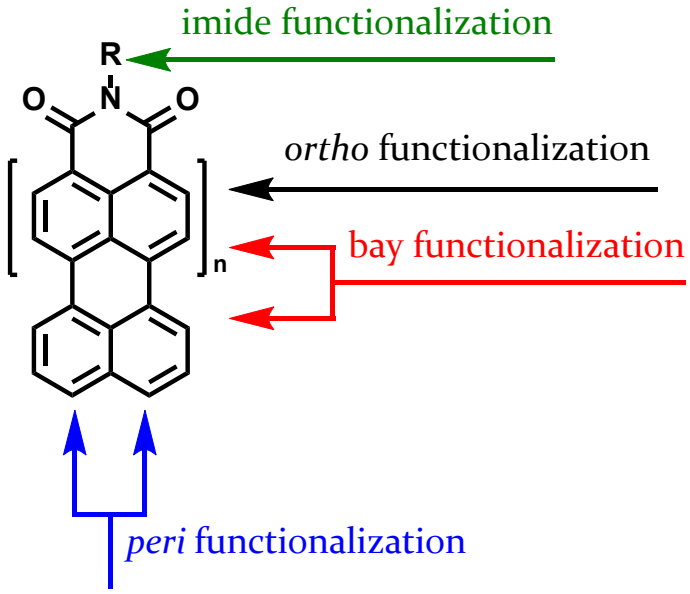

Figure 1-7. Accessible functionalization positions of rylene imides.

1.2.1 IMIDE FUNCTIONALIZATION

Chronologically, the variation of the imide position was the first method of synthetically functionalizing PDIs and efforts were led by the pigment industry. The influence of imide substituents on the solid state packing, and thus on the color of the pigment, is explored in the field of crystallochromy.[36] The expansion from pigment to dye chemistry of rylene imides started when bulkier substituents capable of preventing tight π-stacking were introduced.[37,38] In the exemplary case of N,N'-bis(2,6-di*iso*propylphenyl)-3,4,9,10-perylenetetracarboxylic diimide, the dihedral angle between substituent and perylene core is 88.3° in the solid state.[39] The resulting twist and steric demand effectively diminish π-interactions in solution and increase solubility in organic solvents significantly.

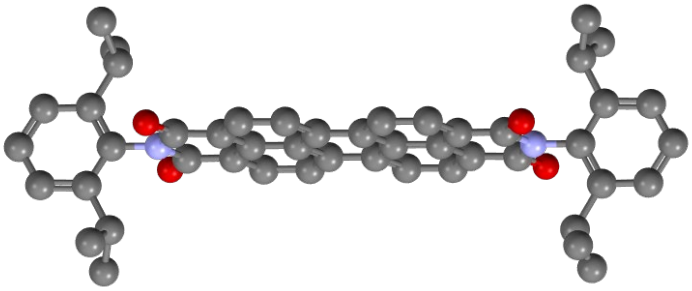

Figure 1-8. Crystal structure of N,N'-bis(2,6-di*iso*propylphenyl)-3,4,9,10-perylenetetracarboxylic diimide showing the dihedral angle between bulky imide substituents and the perylene backbone.[39]

Imide functionalization is not limited to adjusting the solubility or absorption/emission properties, however. The substituent most importantly impacts the self-organizing properties and,[40] if chosen well, can be used to anchor the rylene imide to organic as well as to inorganic compounds,[41,42] or to introduce ionic species.[43] Figure 1-9 shows two of those examples, where different imide substituents either lead to self-organization of the PDI to form liquid crystals (left),[40] or enabled the attachment of the PDI to a tetrathiafulvalene donor via an anchor group (right).[42]

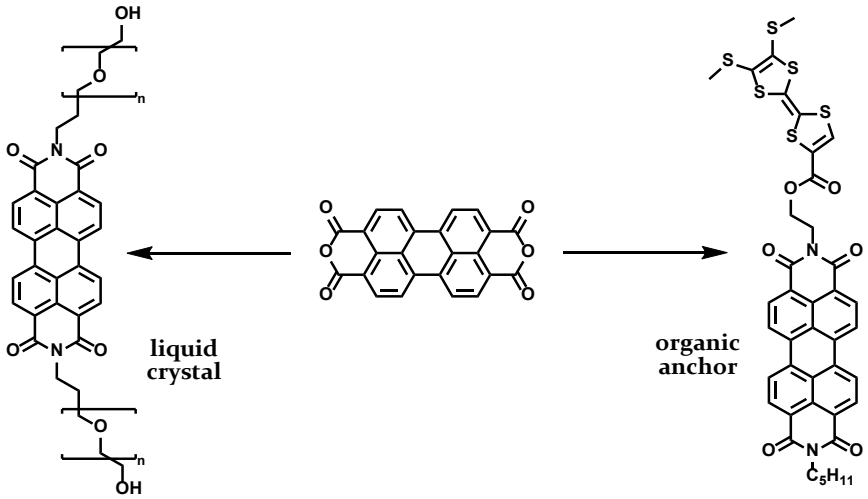

Figure 1-9. Imide-functionalized PDIs. Liquid crystal (left), organic anchor (right).

The preparation of asymmetric PDIs poses a major synthetic obstacle. It is generally not possible to obtain asymmetric PDI **1-3** in two successive imidization steps

from perylene-3,4,9,10-tetracarboxylic dianhydride (PDA) **1-1** only by controlling the ratio of PDA to primary amine (Figure 1-10). Even when using ratios lower than 1:1 of PDA to amine, symmetric PDI **1-3** ($R^1 = R^2$) and PDA **1-1** will be recovered as a mixture.[44] If two amines of similar reactivity are mixed, **1-3** ($R^1 \neq R^2$) can only be obtained after difficult purification.

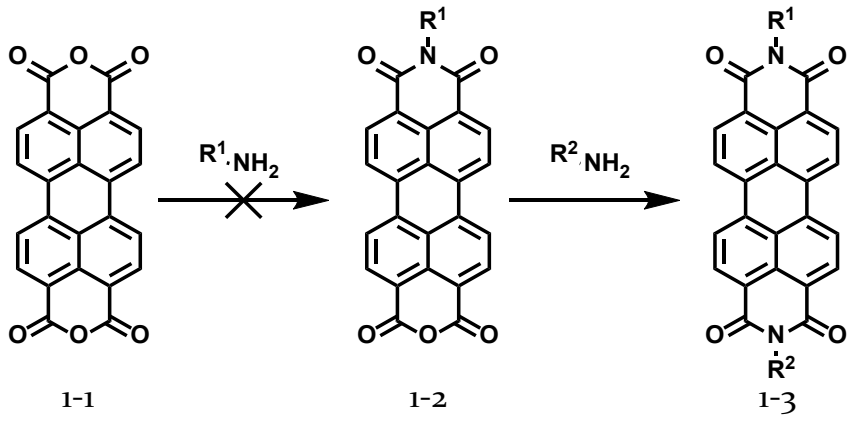

1-1 1-2 1-3

Figure 1-10. Unsuccessful method of synthesizing asymmetric PDI from PDA in two imidziation steps.

It is therefore necessary to synthesize asymmetric building blocks **1-4** or **1-7** in a first step (Scheme 1-2). The potassium salt of the monoanhydride **1-4** can be obtained by converting PDA **1-1** to the tetrapotassium salt and precipitating **1-4** by slow addition of acetic acid.[45] The monoanhydride potassium salt is only soluble in water, and consequently, the scope of this reaction limited.

Alternatively, perylene-3,4,9,10-tetracarboxylic esters **1-5** (PTE) can be converted to 3,4-dialkylcarboxylate-perylene-9,10-dicarboxylic anhydride **1-6** in high yield.[46,47] The reactivity difference between carboxylic anhydride and carboxylic ester groups leads to selective substitution of the carboxylic anhydride, resulting in asymmetric monoimide dicarboxylic esters **1-7.** The asymmetric building block can then be converted to the asymmetric PDI **1-3** in a second imidization step.

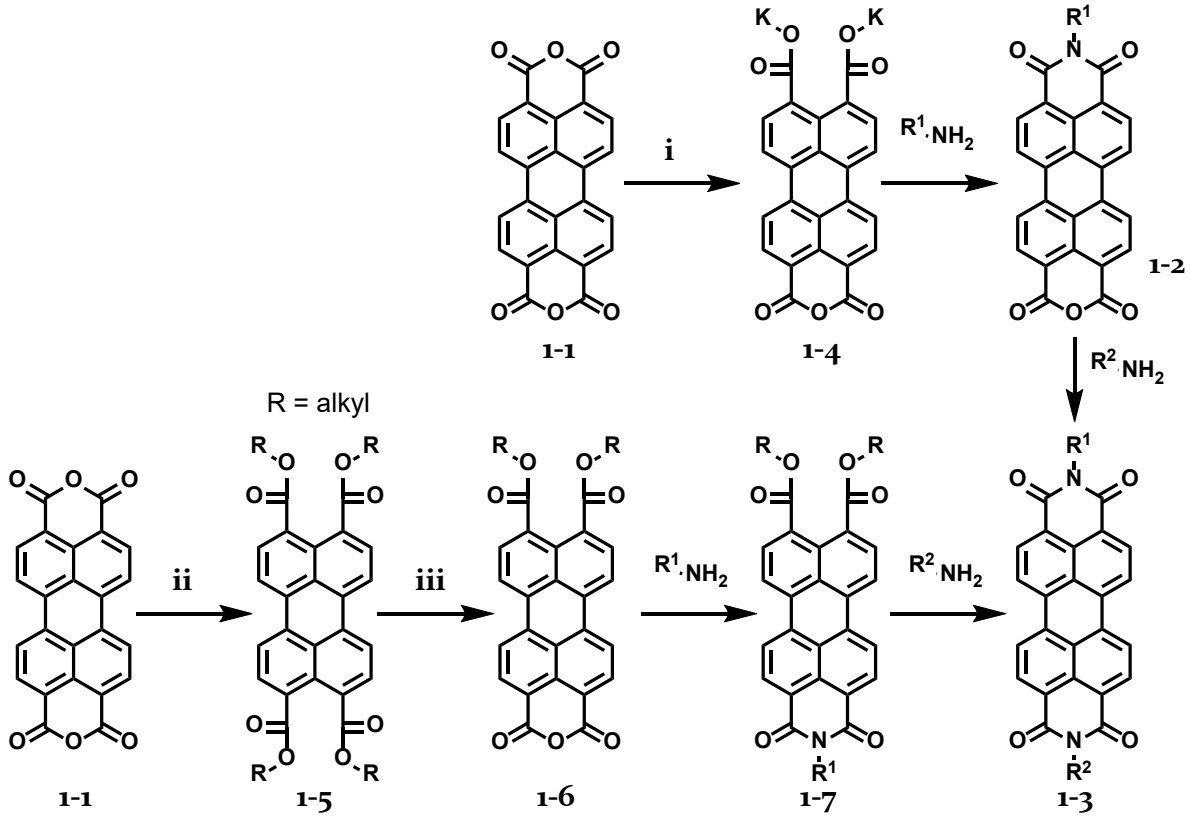

Scheme 1-2. Methods for obtaining asymmetric PDIs. Conditions: i) KOH, H_2O, 90 °C, AcOH, 99 °C; ii) KOH, alkylamine, Aliquat 336®, H_2O, reflux, 95 %; iii) *p*-TsOH, toluene, reflux, 78 %.

1.2.2 CORE FUNCTIONALIZATION

Contrary to imide functionalization, the introduction of substituents into the conjugated rylene system (i.e. ortho, peri or bay) typically affects the optical and electronic properties and is used to tune these properties accordingly. Figure 1-11 shows the frontier orbitals of perylene-3,4-dicarboxylic monoimide (PMI). The electron distribution demonstrates how substitution at the aromatic core can influence electronic properties, as electron withdrawing or donating substituents would directly alter the electron density. The electron distribution also explains why the choice of imide substituent generally has no influence on the electronic distribution of the rylene core, as the nodes at the nitrogen lead to electronic decoupling of imide substituent and rylene core.

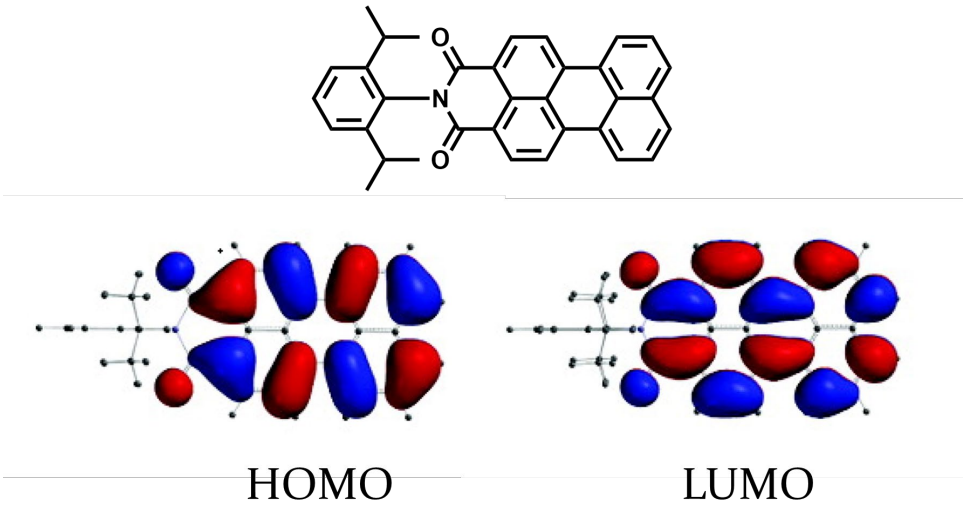

Figure 1-11. Frontier orbitals of PMI.[48]

Access to the *bay*- and *peri*-positions is usually achieved via halogenation. Similar to the effects of bulky imide substituents, halogenation (or introduction of other bulky substituents) at the *bay*-positions increases solubility caused by a twist induced along the long molecular axis. This is accompanied by changes in optical, electronic and physical properties, and was first described by BASF for 1,6,7,12 chlorinated perylene diimides.[49] Figure 1-12 demonstrates this twist in the crystal structure with a twisting angle of 37°.[50]

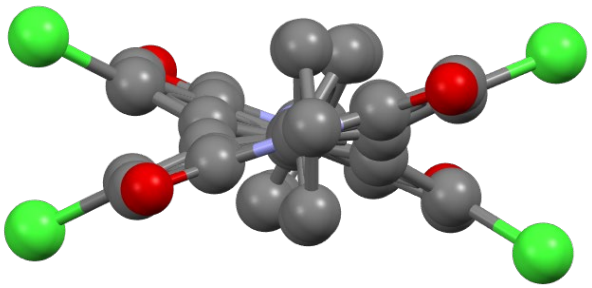

Figure 1-12. Twist along the long molecular axis of *bay*-tetrachlorinated PDI.[50]

When PMI is used in bromination reactions, the first bromination occurs at one *peri*-position, followed by two simultaneous halogenations at the 1 and 6 positions, which is explained by a change of HOMO and LUMO distribution along the π-

system.[17] Selective, double-*peri*-bromination can be achieved by a modified *Hunsdiecker* reaction developed by *Zagranyarski* in 2014 (Scheme 1-3).[51]

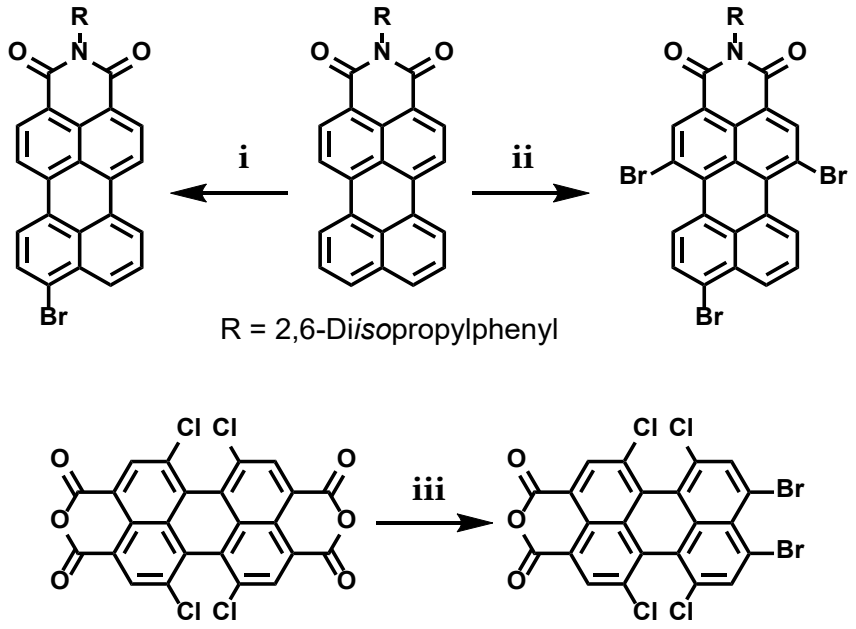

Scheme 1-3. Bromination of PMI (top) and PDA (bottom). Conditions: i) Br_2, AcOH, RT; ii) Br_2, $CHCl_3$, reflux; iii) NaOH, AcOH, Br_2, 80 °C.

Halogenated rylene imides serve as building blocks for a wide variety of functional materials. A prominent example are *bay*-phenoxylated rylene imides, first synthesized by BASF by nucleophilic substitution in 1986.[52] Phenoxylation at the *bay*-positions increases solubility dramatically, because of the conformational isomerism arising from different orientations of the *bay*-phenoxy substituents (Figure 1-13).[53]

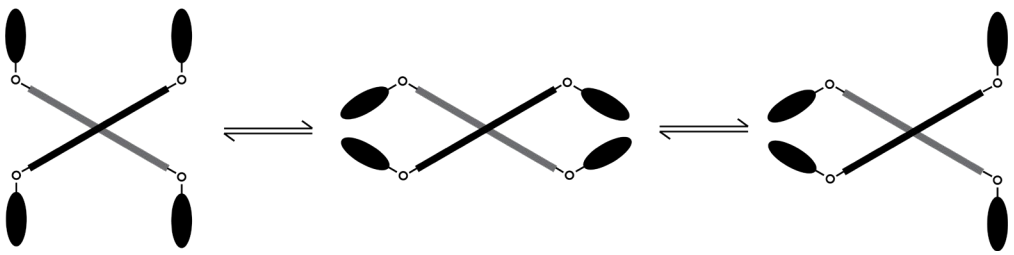

Figure 1-13. Schematic representation of the conformational isomerism in *bay*-phenoxylated PDIs.

Further functionalization is possible, as demonstrated in the synthesis of a variety of highly fluorescent, water soluble dyes by *Kohl* in 2004.[54] The combination of imide- and *bay*-substitution made water soluble rylene imides accessible that could successfully be attached to proteins, thus allowing enzyme-activity tracking by single molecule spectroscopy (Figure 1-14, left).[55]

Functionalization in the *bay*-positions was utilized to tune optical and electronic properties. π–Donating substituents like amines cause large bathochromic shifts due to a push-pull substructure,[15] while electron withdrawing groups such as in *ortho*- or *bay*-cyano PDI derivatives lower the LUMO levels even further as a matter of increased electron deficiency (Figure 1-14, right).[56]

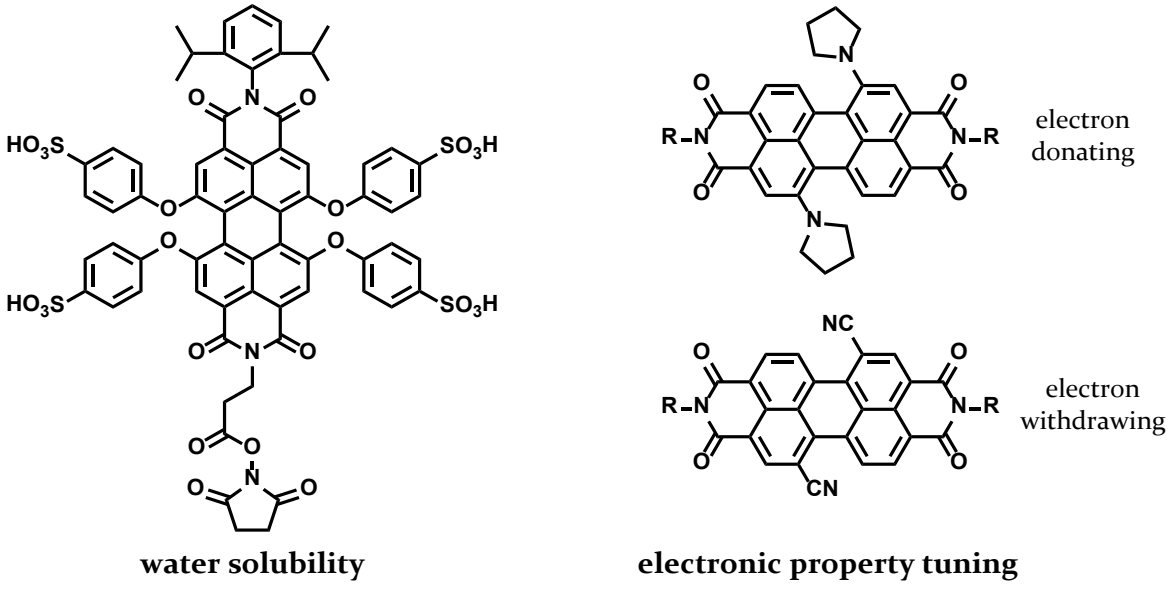

Figure 1-14. Demonstration of different effects of *bay*-substitution. Induced water solubility (left) and electronic property tuning (right).

The halogenated *peri*-position can be accessed in the same ways as described above. Most noteworthy are push-pull type PMIs with controllable optical and electrochemical properties.[57] These types of PMIs are amongst the most efficient materials found in dye-sensitized solar cells, due to their stability, ease of access and handling.[58]

1.2.3 Cross-coupling Based Functionalization of Perylenes

Halogenated rylene imides can also be modified by metal-catalyzed cross coupling reactions, such as *Suzuki-Miyaura*, *Stille* or *Sonogashira* reactions. Palladium-catalyzed reactions are central elements to the synthesis of core-expanded rylenes, such as coronene diimides or heterocyclic annelated perylene diimides, which find use in a wide range of applications.[28,59]

One of the more recent achievements to be mentioned is the *ortho*-functionalization of rylene imides by the *Shinokubo* group.[60] This synthetic protocol enables the selective introduction of alkyl and aryl substituents at the 2, 5, 8 and 11 positions of perylene diimides. The novelty of *ortho*-functionalized PDIs is the introduction of substituents without a distortion of the rylene core, as it is the case in *bay*-functionalized rylene imides. This allows tuning optical and electrochemical properties in applications where altering the solid-state packing is not desirable.

Some of the described functionalization methods are also applicable to the higher homologues of the rylene imide series and are discussed as necessary, but to date, functional perylene imides remain the most researched and developed materials of the rylene imide family.

1.3 Synthesis of Terrylene Diimides

The first TDI was synthesized in 1997, much later than QDI (1992) and PDI (1913).[61–63] Until now, TDIs have only attracted academic but no industrial attention. Even though their chemical, thermal and photochemical stabilities are similar to those of the widely researched class of PDIs, the to this date low yielding, multiple-step syntheses available have hindered widespread application. This fact is also reflected by comparison of the number of publications containing either of these representatives: whereas more than 4000 publications contain any form of perylene imide, it is less than 100 for terrylene imides. However, in these 100 cases the unique absorption and emission profile of TDI was essential to the respective field of

research, demonstrating the key importance of these terrylene compounds to science.[20,64–70]

Initial protocols, based on palladium-catalyzed cross coupling reactions, relied on highly toxic organotin compounds, required time-consuming purification (multiple steps including purification via column chromatography on at least three of these steps) and suffered from low yields (Scheme 1-4, top). Development of alternative methods was undertaken to overcome these drawbacks, as achieved by e.g. *Suzuki-Miyaura* based cross-coupling protocols. This approach avoided the toxic intermediates and long reaction times, although the other remaining downsides persisted.[71]

Base-induced oxidative coupling of PMI and naphthalene-1,8-dicarboxylic monoimide (NMI, Scheme 1-4, bottom) leads - due to the non-existing selectivity – to a mixture of PDI, TDI and QDI. With moderate to poor solubility of TDI and QDI, separation is tiresome and not profitably executable. Furthermore, harsh reaction conditions limit the scope of imide substituents that tolerate these coupling conditions.[72]

Due to its 'asymmetric' nature (coupling of one perylene to one naphthalene unit), the key step in every TDI synthesis developed so far relies on the preparation of PMI from PDA or PDI. While the small-scale preparation of PMI is manageable, the requirement of high-pressure reaction vessels as well as the tedious workup procedures severely limit the accessibility of PMI on a larger scale. Furthermore, alternative imide substituents than 2,6-di*iso*propylphenyl require additional saponification and imidization steps, adding more expensive and time-consuming reactions to the sequence.

However, for academic purposes, *Suzuki-Miyaura* and *Stille* cross coupling reactions are feasible. Comparatively mild reaction conditions allow for a wider range of imide substituents compared to the base-induced oxidative coupling. The imide substituents have to be introduced at the beginning of each reaction sequence, as saponification of a generic TDI would lead to insoluble terrylene dianhydride, and subsequent imidization would be impossible. Therefore, each application would call for

the whole reaction sequence for every different imide substituent to be repeated. These problems make the currently available approaches to TDI synthesis too difficult and time-consuming to gain the same impact in an academic and industrial environment as PDIs have.

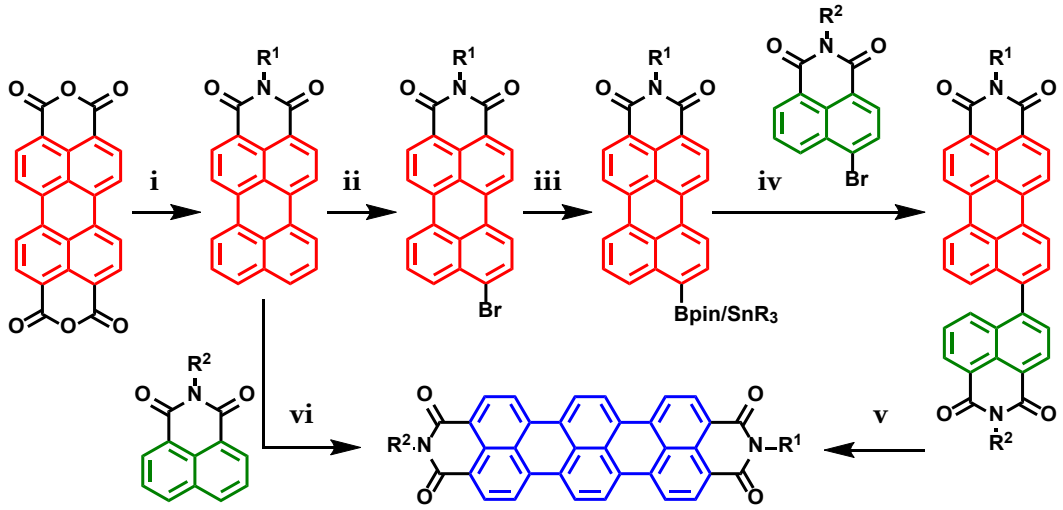

Scheme 1-4. Syntheses of TDI following common procedures. Conditions: i) 2,6-di*iso*propylaniline, Cu_2O, quinoline, > 220 °C, high pressure, 79 %; ii) Br_2, AcOH, RT, 5-7 h, 95 %; iii.a) B_2pin_2, 1,4-dioxane, 70 °C, 20 h, 95 %; iii.b) $Sn_2(Bu)_6$, $Pd(PPh_3)_4$, toluene, reflux, 4 d, 88 %; iv.a) $Pd(PPh_3)_4$, K_2CO_3, toluene/H_2O/EtOH, 85 °C, 18 h, 60 %; iv.b) $Pd(PPh_3)_4$, toluene, reflux, 4 d, 70 %; v) ethanolamine, K_2CO_3, 160 °C, 18 h, 70-90 %; vi) diglyme, DBN, *t*BuONa, 130 °C, 3 h, 15-42 %.

1.4 Photophysical Processes

Fluorescence spectroscopy is a powerful method for investigations into the photophysical processes of rylene imides. Detailed knowledge about these processes is essential for the molecular and experimental design and the underlying radiative and non-radiative transitions are typically illustrated by a *Jablonski* energy level diagram (Figure 1-15). When a molecule absorbs light (vertical, straight arrows in Figure 1-15), it is excited from the ground electronic state ($S_{0,0}$) to a vibrational (v = 0, 1, 2, etc.) level of an excited electronic state (S_1 or S_2) within 10^{-15} s, a timespan that is too short for significant nuclear displacement (*Franck-Condon* principle).[73] The typical absorption-band pattern of rylene diimides (top-right part of Figure 1-15) correlates with the 0-0, 0-1 and 0-2 vibronic transitions.

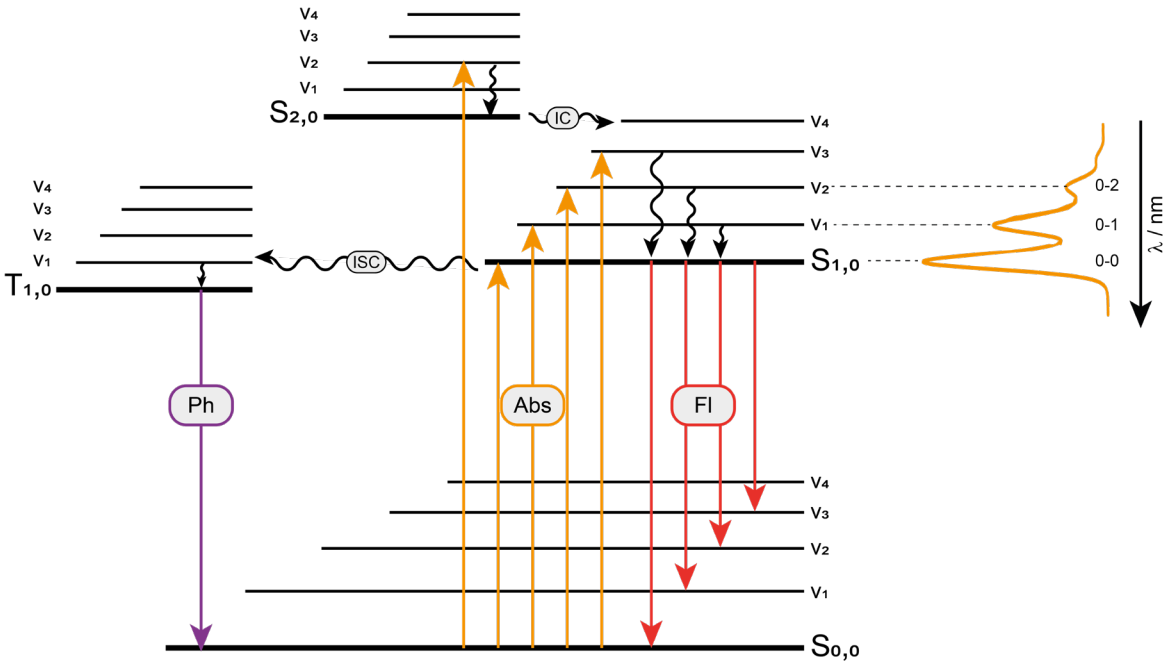

Figure 1-15. Jablonski diagram including radiative and radiationless transitions.

Excited molecules rapidly relax (10^{-14} – 10^{-12} s) to the lowest vibrational level of the excited electronic state in a non-radiative process (vertical, wavy arrows in Figure 1-15). If a molecule is excited to a higher excited electronic state than S_1, a rapid, non-radiative transition called 'internal conversion' (IC) occurs, followed by vibrational relaxation to the lowest vibrational level of the first excited electronic state $S_{1,0}$.

From $S_{1,0}$, several radiative and non-radiative transitions can happen. The most relevant transition for this work is fluorescence, defined as emission of photons from singlet-excited states. In the case of phosphorescence, a prior 'intersystem crossing' (ISC) from $S_{1,0}$ to the first excited electronic triplet state is necessary. Both ISC and phosphorescence are less likely to happen and take place more slowly than the already discussed processes due to the spin-forbidden transitions between electronic states of differing spin multiplicity. Radiating transitions are generally of lesser energy due to energy dissipation in the excited states.

Besides phosphorescence, other, non-radiative transitions are possible that compete with fluorescence. Amongst those are quenching processes including excited-

state reactions, molecular rearrangements, ground-state complex formations and energy transfer.

An important quenching process and the basis for many fluorescence spectroscopy experiments conducted on rylene imides is the resonance energy transfer (RET). RET describes the energy transfer of the excited-state energy from a donor molecule D (excited states of higher energy) to an acceptor molecule A (excited states of lesser energy, Figure 1-16). Energy transfer is a non-radiative process that occurs when donor and acceptor are electronically coupled by long-range dipole-dipole interactions. After the energy transfer from donor to acceptor, all aforementioned processes are possible, including detectable fluorescence from the acceptor.

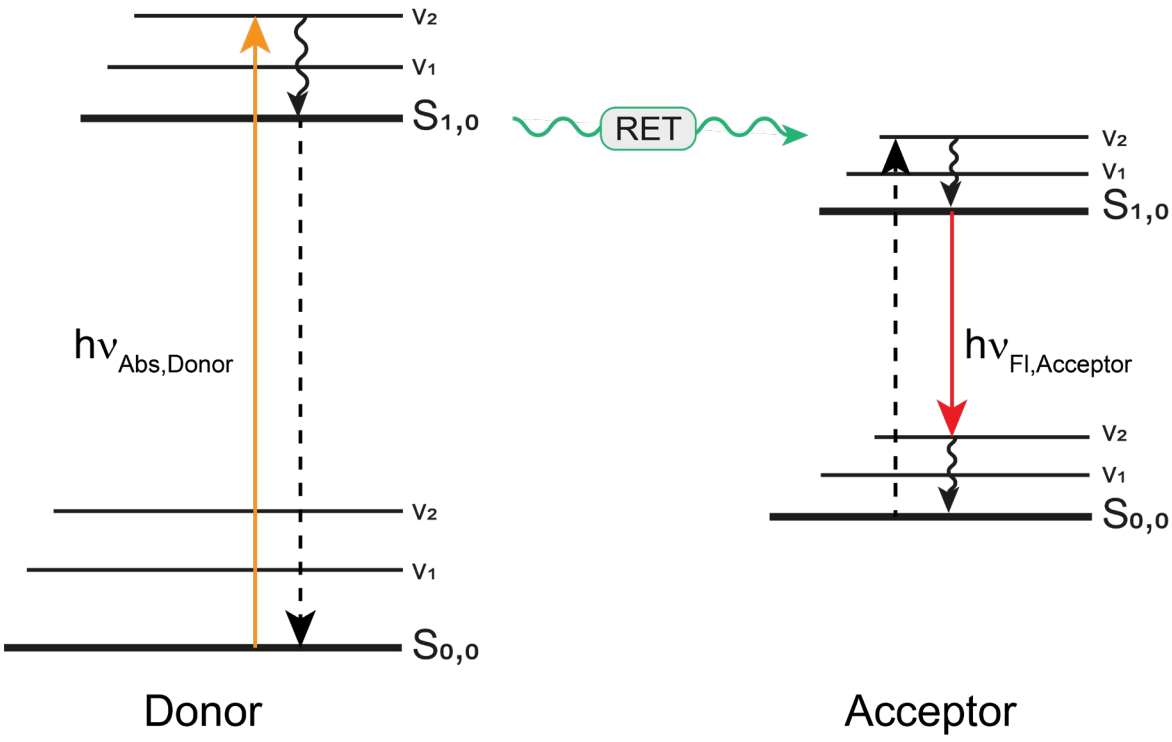

Figure 1-16. Jablonski diagram of excited energy transfer from a donor D to an acceptor A.

A prerequisite for RET is the spectral overlap between the donor emission spectrum and the acceptor absorption spectrum (Figure 1-17). The degree of the spectral overlap as well as the donor-acceptor distance determine the extent of resonance energy transfer. The efficiency of this mechanism, called *Förster resonance energy*

transfer (FRET), can be described by the *Förster* distance at which RET is 50 % efficient.[74]

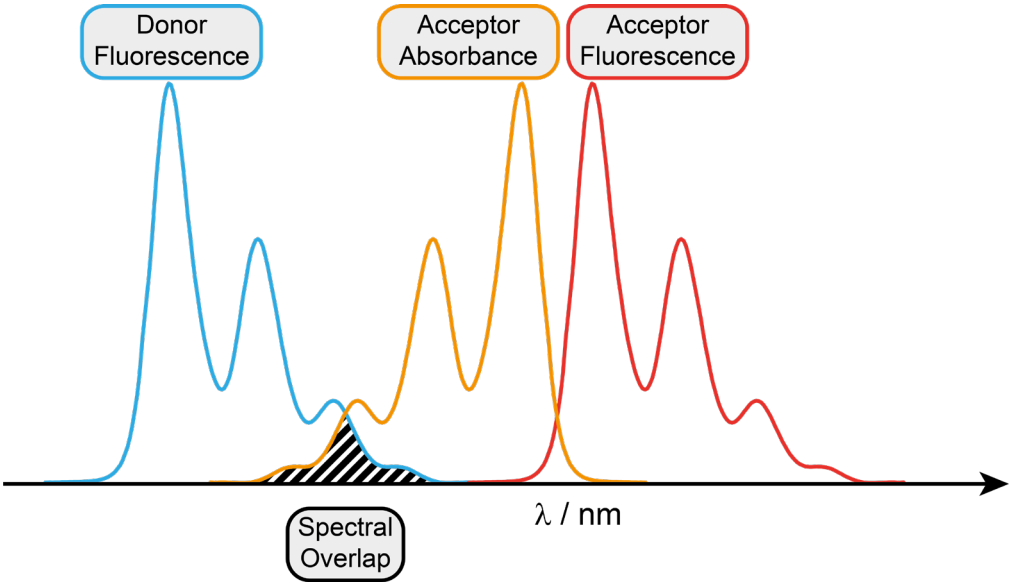

Figure 1-17. Spectral overlap in energy transfer processes.

Because the RET efficiency is highly dependent on the donor-acceptor distance, the rate of energy transfer has been successfully used as an instrument to measure distances and conformational changes in the past, for example in the elucidation of protein conformation and interaction.[75–78] Coupled with single-molecule spectroscopy, RET can be an efficient tool to probe internal dynamics and photophysical properties such as the influence of the local surroundings and triplet-state lifetimes of a molecule, as was investigated in a PDI-TDI dyad in 2013.[75]

1.5 Motivation

Rylene imides have proven to be essential building blocks in applications where their high thermal, chemical and photochemical stability, exceptionally good optical and electronic properties or excellent colorant characteristics are important. Some of these applications have already been described; however, literature survey demonstrates the gap between utilization of perylene imides and the other members of the rylene family for said applications. This is not because of inferior properties or lack

of interest from academic and industrial side in these other rylene based materials. In fact, expanding the absorption and emission profile beyond the available wavelengths of perylene imides would be highly beneficial. Essentially though, time-consuming synthetic approaches currently available are a significant obstacle. Oftentimes, molecules are designed with specific goals in mind, but actual synthesis might deviate from theory, sometimes demanding a complete overhaul of reaction sequences. In other cases, the target compound does not provide the necessary properties or functionality the application calls for, and derivatives of a compound need to be synthesized. In these situations, reliable, reproducible and economic synthetic concepts are crucial for projects to move forward in a reasonable time period, in academia as well as industry.

The primary, but not sole, focus of this thesis is the synthesis of terrylene based, functional materials. For this task, a revolutionary one-pot concept for the synthesis of rylene based compounds will be presented in chapter 2 that tries to address and eliminate the obstacles described in the previous section. Literature-reported terrylene diimides will be synthesized in order to compare the different approaches, followed by the exploration of the scopes and limits of this new concept.

Previously available synthetic methods were not suitable for several reasons:

A) The envisioned project did not justify the high amount of workload in cases where the target compounds are only the starting point of a more complex research project
B) The project required derivatization on-demand at molecular positions that up until now needed to be addressed at the beginning of the reaction sequence
C) The project demanded substitution patterns that were unknown to recent research

As our decades-long presence in rylene imide synthesis shows, the demand for a reliable, economic access to terrylene based compounds is very high, which justifies the effort for more fundamental research on the known structures of TDI in the same

way it was done for PDI due to its high potential for many scientific innovations in past and present.

Many projects discussed in this work will be interdisciplinary, with the main focus on the synthesis and the chromophore's properties as the basis for its role as probes in single molecule spectroscopy. Chapter 3 and 4 will show two different ways of utilizing TDI as a probe for the investigation of the spin states of a graphene-based system. While chapter 3 would ultimately see the TDI covalently attached to graphene-based materials to allow insights into the spin states at the edges of defined graphene nanoribbons, in chapter 4, the TDI acts as a ligand in a coordination complex. In this envisioned coordination complex based on the principles of the *LIESST*-effect, switching between high-spin and low-spin states after irradiation at certain wavelengths could be visualized with the help of the TDI probe. In both cases, single molecule spectroscopy is the tool to analyze these physical effects, but the unique photophysical properties of TDI are essential to make these experiments possible.

In chapter 5, imide functionalization of TDI will provide quaternized, water-soluble chromophores for host-guest based chemosensors. Ultimately, these host-guest systems could be used to monitor biocatalytic activity, as has been demonstrated in the past where PDI served as the chromophore.

Chapter 6 will explore how the newly developed synthetic concept can be used in the preparation of electron-deficient polycyclic aromatic hydrocarbon (PAH) structures that incorporate heteroatoms or graphene-type motifs into the rylene scaffold. Here, the goal is to build up compounds with novel architectures in a one- or two-step synthesis that could provide new, unique properties in the future.

Chapter 7 will focus on the synthesis of a rigid, triangular shaped system of three donor and acceptor molecules. The intention of a design like this is to gain insight into the energy- or electron-transfer processes on a single molecular basis. This chapter will also demonstrate the current limitations of the one-pot approach and how this constraint influenced the design choices necessary.

The topics discussed in this work will show how a new approach to old, established methods can lower the bar of entry into the synthesis of historically difficult to synthesize materials. It will also become obvious where this method still lacks reliability and how the room for improvement in these not fully explored areas can elevate the impact of this work from the academic to the industrial scale.

Chapter 2

A NEW SYNTHETIC CONCEPT FOR RYLENE IMIDES AND ESTERS

2.1 INTRODUCTION

One of the main obstacles in all syntheses of terrylene based compounds is the large number of steps, many of them relying on complicated purification procedures of intermediate products with poor solubility. A major culprit of the complexity of previously available methods is the necessary utilization of PMI as one of the building blocks for TDI. The asymmetric nature of TDI (which can formally be assembled by one naphthalene and one perylene monoimide) requires the synthesis of PMI prior to the formation of TDI, and the accompanying downsides have been described elaborately in the previous chapter.

As an alternative strategy to build up terrylene compounds, three naphthalene units could be used instead, and such a strategy has been applied in 1990 (Scheme 2-1).[79] *Bohnen et al.*, however, used alkali metal induced cyclization of *peri*-linked oligonaphthalene precursors followed by oxidization of the intermediate anions. This strategy could not be applied to the synthesis of the corresponding imide compounds due to their electron deficient nature. However, the underlying strategy of constructing the terrylene core from three naphthalene units will be used as the basis for the new concept discussed in this chapter.

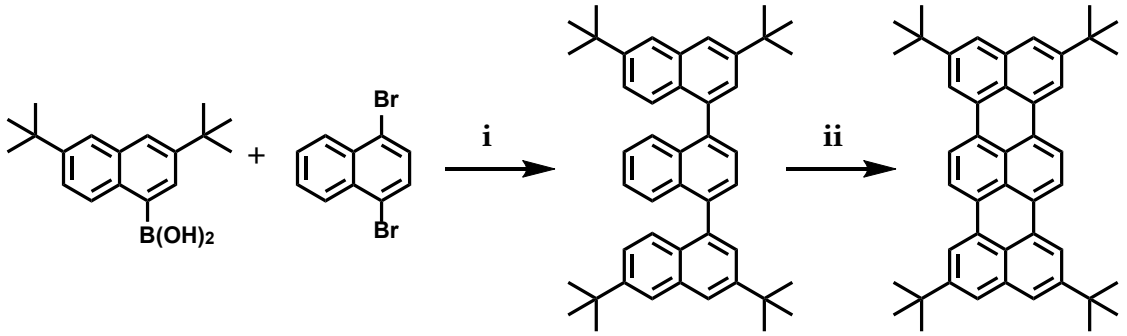

Scheme 2-1. Synthesis of terrylene via cyclization of a ternaphthalene precursor. Conditions: i) $Pd(PPh_3)_4$, K_2CO_3, toluene, reflux, 3 d, 83 %; ii) K, dimethoxyethane, $CdCl_2$, RT, 7 d, 42 %.[80]

2.2 Reaction Design

In order to justify a new synthetic concept for terrylene based compounds that avoids the downsides of previous methods, the new approach should

i) use readily available materials (commercial availability or high-yielding synthesis),
ii) minimize the number of synthetic steps,
iii) limit the need for complicated (chromatographic) purification, and
iv) allow variation of substituents for further functionalization.

Basing the new concept on a coupling reaction between three naphthalene units will comply with the first condition, as naphthalenes are generally commercially available in a variety of substitution patterns. To meet the second condition, reactants and reaction conditions need to be chosen in a way that allows a 'one-pot reaction'. In contrast to the coupling → oxidative cyclization sequence of earlier methods, a series of chemical reactions without purification of intermediate products in the same reaction is preferable. Minimizing the number of reaction steps will coincidentally reduce the workload for purification processes, which will in turn comply with the third condition. Condition four will be discussed separately as it has only a minor influence on the reaction design.

In 2012, *Zagranyarski* selectively brominated 1,6,7,12-tetrachloro-3,4,9,10-perylentetracarboxilyc acid dianhydride (**2-1**) in the 9 and 10 *peri*-positions using a modified

Hunsdiecker reaction protocol (**2-2**, Figure 2-1).[81] Expanding this reaction to 1,4,5,8-naphthalenetetracarboxylix dianhydride (**2-3**, NDA) would result in 4,5-dibromo-1,8-naphthalenedicarboxylic anhydride (**2-4,** dibromo-NMA), which will first be explored as the main building block for further development on this new approach.

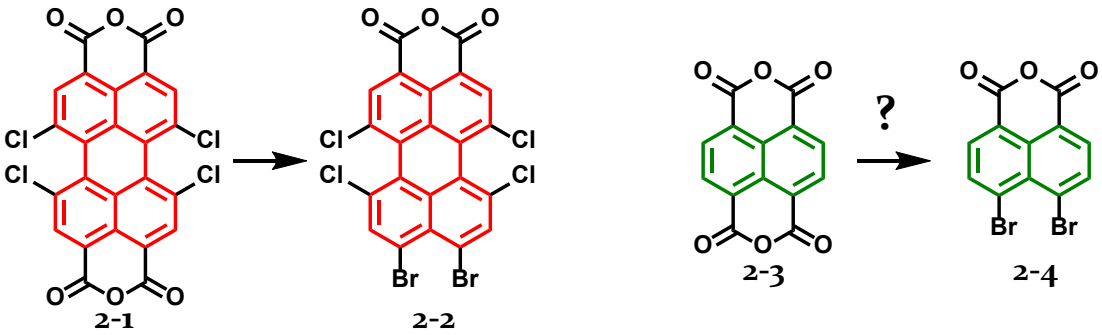

Figure 2-1. *Hunsdiecker* reaction conditions for the *peri*-bromination PDA and possible expansion towards *peri*-bromination of NDA. Conditions: NaOH, AcOH, Br_2, 80 °C.

Addressing the problem of low solubility in the synthesis of rylene imides is often case specific. One strategy to bypass solubility issues during a reaction sequence towards rylene imides is the use of carboxylic ester intermediates instead of their poorly soluble carboxylic anhydride counterparts.[82] In some instances like the synthesis of the bifunctional *N*,*N*-bis(4-bromo-2,6-di*iso*propylphenyl)perylene-3,4,9,10-tetracarboxylic diimide (**2-8,** Scheme 2-2), where the low reactivity of the amine inhibits the imidization reaction with PDA, only the utilization of carboxylic esters instead of the anhydrides guarantees the success.[83,84]

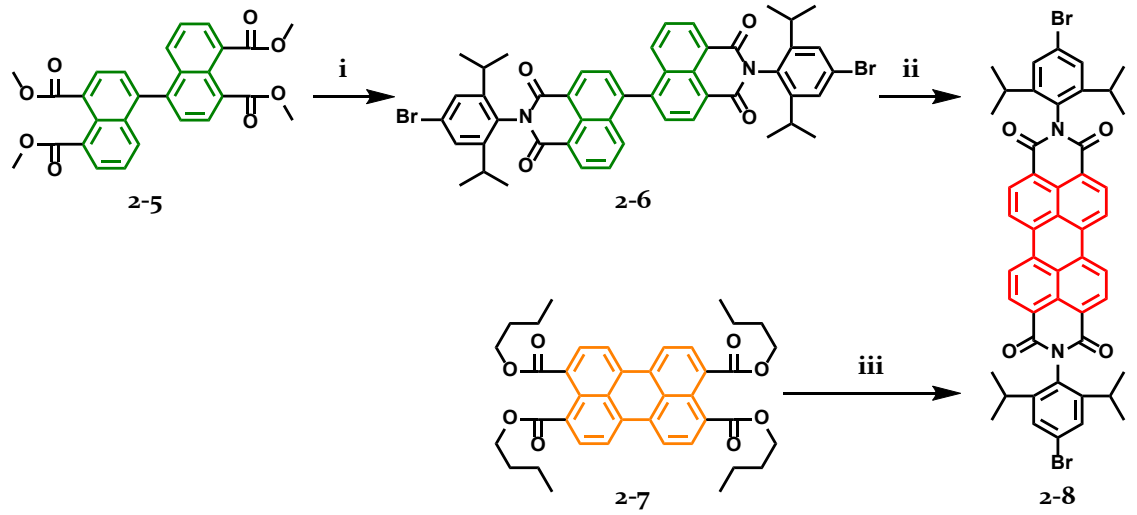

Scheme 2-2. Synthesis of para-dibromo-PDI **2-8** via two different carboxylic ester precursors. Conditions: i) 4-bromo-2,6-di*iso*propylaniline, $ZnCl_2$, imidazole, 140 °C, 99 %; ii) K_2CO_3, ethanolamine, 100 °C, 60 %; iii) 4-bromo-2,6-di*iso*propylaniline, $ZnCl_2$, imidazole, 180 °C, 82 %.

On this basis, a legitimate question is whether the same strategy could solve many of the problems which the previous TDI syntheses suffer from. Analogous to perylene-3,4,9,10-tetra(*n*-butylcarboxylate) (**2-7**, PTE), the envisioned universal building block for the synthesis of symmetrical TDIs is its higher homologue terrylene-3,4,11,12-tetra(*n*-butylcarboxylate) (**2-9**, TTE, Scheme 2-3). For this purpose, dibromo-NMA **2-4** will be transformed into 4,5-dibromonaphthalene-1,8-di(*n*-butylcarboxylate) (**2-10**, dibromo-NDE) as the 'terminal' naphthalene unit.

The structure of the 'core' naphthalene unit is dictated by its eligibility for cross-coupling reactions as well as its ease of access. Recently, fourfold *Yamamoto* cross-coupling conditions have been utilized in the single-step synthesis of graphene nanoribbons.[85] This would require a 1,4,5,8 tetrasubstituted naphthalene as the 'core' naphthalene unit (Scheme 2-3) with X=Y=Br. However, 1,4,5,8 tetrasubstituted naphthalenes are not commercially available and can only be synthesized in low yields, which rules out a *Yamamoto*-based approach in the synthesis of TTE **2-9** based on condition i).

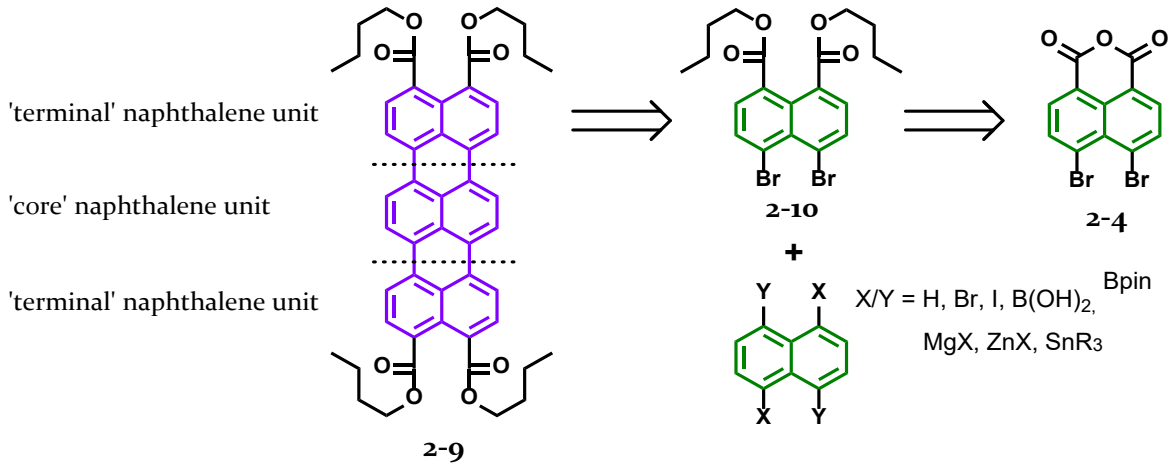

Scheme 2-3. Possible cross-coupling reaction based approaches for the synthesis of TTE.

Eligible aryl-aryl cross-coupling protocols that were proven to be compatible with 1,5 disubstituted naphthalenes are *Suzuki-Miyaura*, *Kumada*/*Negishi* and the *Stille* reactions. Organomagnesium or organozinc compounds necessary for *Kumada* and *Negishi* cross-couplings generally require air- and water-free reaction conditions and are therefore difficult to handle.[86] Conversion of arylhalides to their boronic acid pinacol esters on the other hand reliably produces air and water stable compounds in good yields.[87] Furthermore, boronic esters don't rely on toxic organotin compounds necessary for *Stille* coupling reactions. Additionally, the higher reactivity of boronic esters compared to organostannanes ensures a much higher reaction rate than in *Stille* cases.[61,71]

Together with 1,4-naphthalenediboronic acid pinacol ester as the central naphthalene unit, **2-4** will be converted to TTE in a palladium-catalyzed cascade reaction, consisting of a *Suzuki-Miyaura* cross-coupling and subsequent C-H arylation (Scheme 2-4).[88,89] This proposed one-pot reaction is expected to meet the four conditions due to the easy access to readily available starting material with good solubility and the flexibility of further functionalization based on the universal TTE building block.

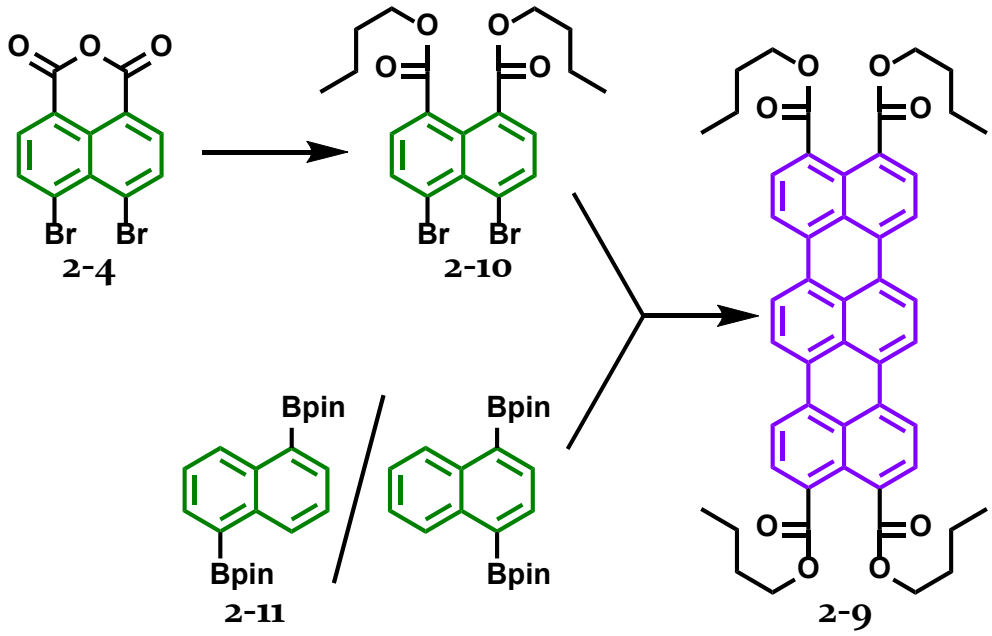

Scheme 2-4. Concept for the synthesis of TTE **2-9** via *Suzuki-Miyaura* cross-coupling reaction.

2.3 Synthesis of the Terrylene Tetraester

As the first step in the synthesis of the required TTE precursor, a protocol had to be established to apply the modified *Hunsdiecker* conditions to NDA **2-3**. Dissolving **2-3** in aqueous KOH at 85 °C and adding bromine led to immediate precipitation of dibromo-NMA **2-4**. After stirring the reaction until it reached room temperature, the precipitate was filtered, washed and dried to receive a pale-yellow solid in quantitative yield (Scheme 2-5).

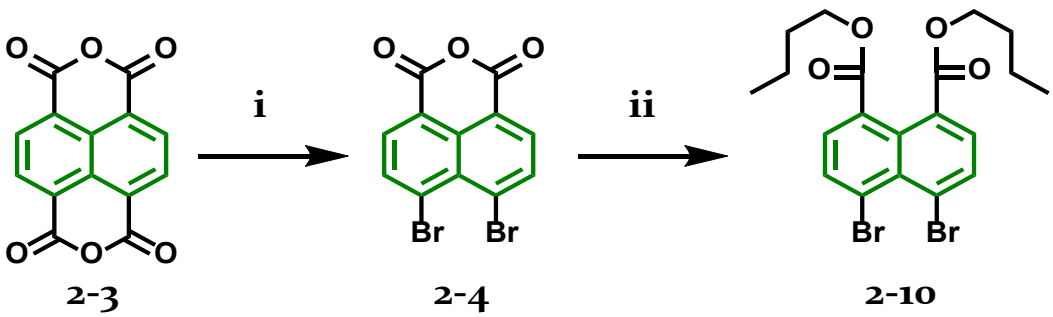

Scheme 2-5. Synthesis of dibromo-NDE. Conditions: i) KOH, H_2O, Br_2, 85 °C, 1 h, quant.; ii) KOH, KI, *n*-butylbromide, H_2O, Aliquat 336®, reflux, 6 h, 65 %.

The following esterification step was explored via two different routes.[90,91] The first approach utilized DBU as base in DMF as solvent, resulting in **2-10** in yields exceeding 80 %. However, column chromatography was mandatory, which is why the second route was found to be more convenient.

Dibromo-NMA **2-4** was dissolved in aqueous KOH with Aliquat 336® as a phase transfer catalyst. The reaction mixture was stirred under reflux until the aqueous phase turned colorless. The organic phase was filtered over a pad of silica and concentrated under reduced pressure. Diluting with hexane and cooling in liquid nitrogen led to immediate precipitation of **2-10**. The precipitate was filtered and washed with $N_{2,liq}$-cooled hexane and was received in 65 % yield in high purity (see ^{1}H NMR in Figure 2-2). Avoiding column chromatography meets condition iii) of the requirements for a new TDI synthesis.

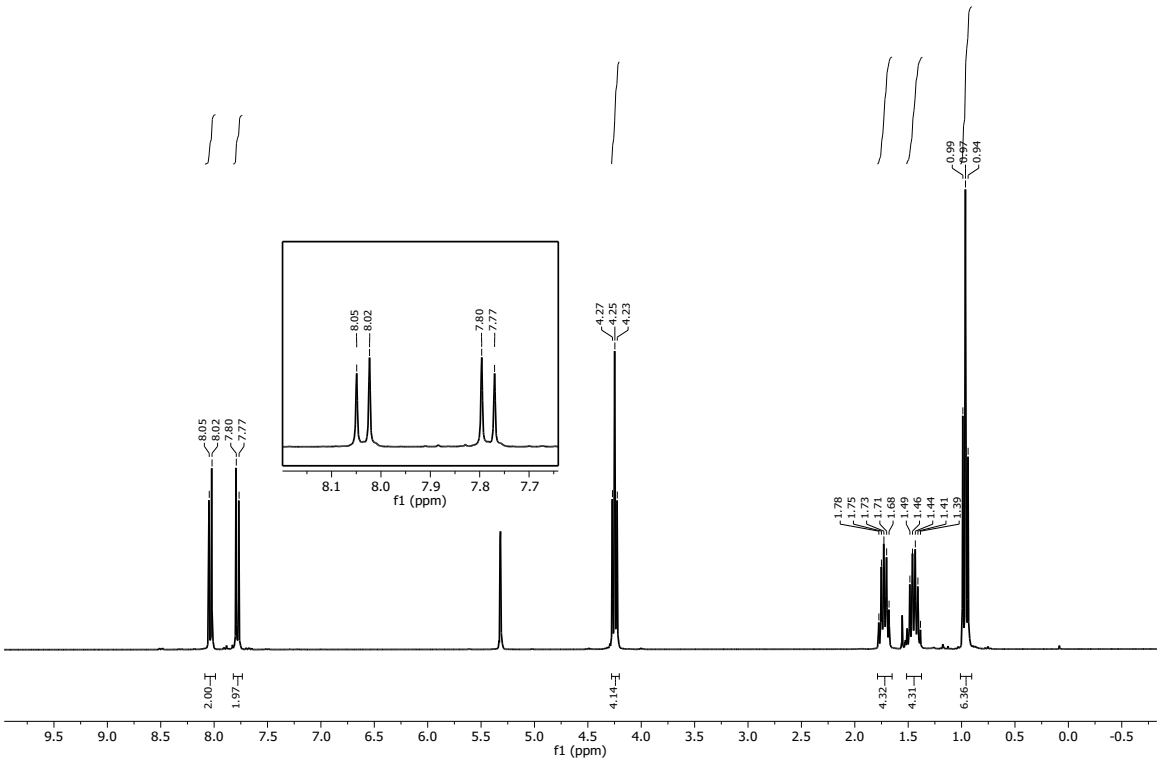

Figure 2-2. ^{1}H NMR (300 MHz, CD_2Cl_2, 300 K) of dibromo-NDE **2-10**.

At first, the reaction between the precursors **2-10** and **2-11** was carried out under standard Suzuki-Miyaura conditions; thereby, toluene was used as the solvent with ethanol/H_2O as co-solvent to dissolve the base K_2CO_3. After degassing and purging with argon, tetrakis(triphenylphosphine)palladium(0) ($Pd(PPh_3)_4$) was added and the reaction was refluxed until all starting material had been converted to ternaphthalene unit **2-12** (Scheme 2-6, checked via TLC and FD MS). Then, palladium(II)-acetate ($Pd(OAc)_2$) and tricyclohexylphosphine (PCy_3) were added and the reaction was refluxed for additional 16 h.

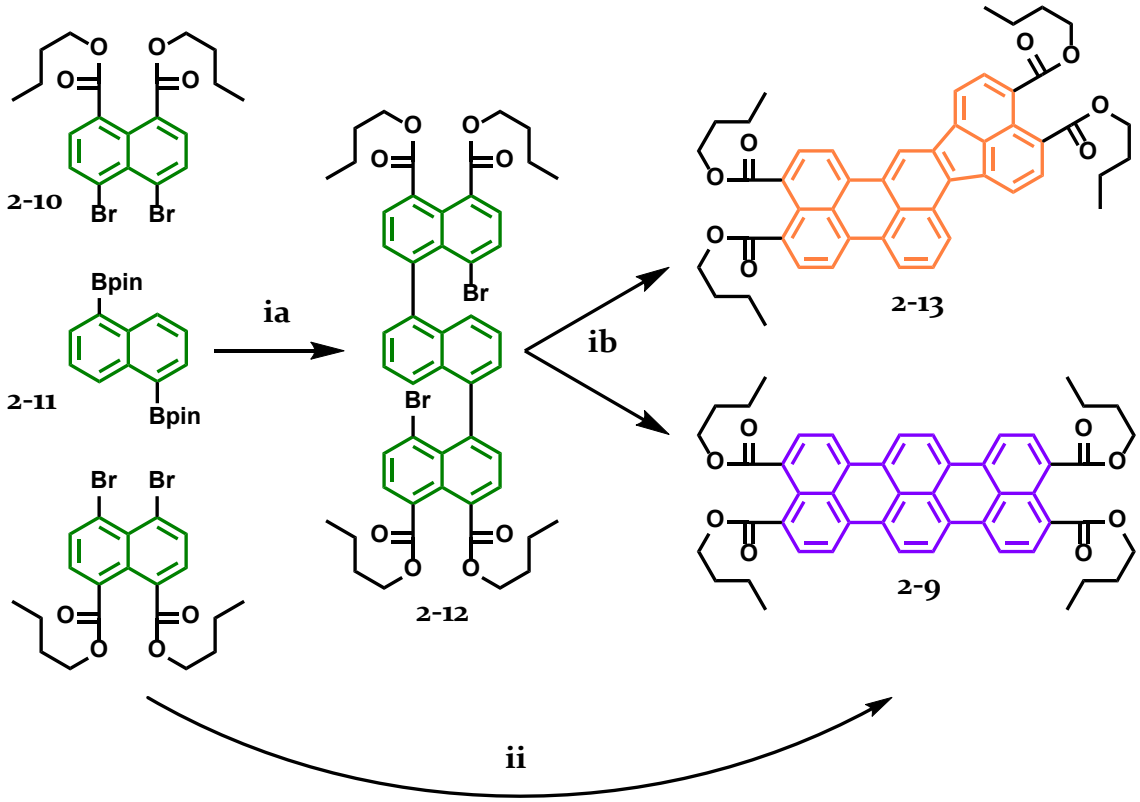

Scheme 2-6. Sequential (i) vs. single-step (ii) one-pot synthesis of TTE. Conditions: see Table 2-1.

TLC separation of the reaction mixture revealed bright yellow, red-orange and violet compounds. Further investigation via FD MS confirmed the presence of TTE **2-9** (violet), next to bright yellow (**B** in Figure 2-3), orange (**2-13**) and colorless (**2-12**) spots. This first test reaction proved that the new strategy was, in principle, successful. However, separation of the described mixture was impossible due to only small

R_f-value differences between the side-products. For this reaction to be viable, determining conditions that completely avoid these unwanted side reactions was crucial.

Table 2-1 lists the tested conditions that were used to determine the best combination of solvent, catalyst system and base for the synthesis of TTE **2-9**, as judged by TLC analysis. The ratio of products (see Figure 2-3) was estimated by TLC analysis.

Table 2-1. Conditions for the one-pot cross-coupling of **2-10** and **2-11**. The ratio of colored reaction products was estimated from TLC analysis.

	SOLVENT	**CATALYST**	**BASE**	**TEMP.**	**RATIO A:B:C**
1	Toluene/H_2O/EtOH	$Pd(PPh_3)_4$ $Pd(OAc)_2/PCy_3$	K_2CO_3	65 °C - reflux	15:70:15
2	Toluene/H_2O Aliquat 336	$Pd(PPh_3)_4$ $Pd(OAc)_2/PCy_3$	K_2CO_3	65 °C - reflux	15:70:15
3	1,4-Dioxane/H_2O	$Pd(PPh_3)_4$ $Pd(OAc)_2/PCy_3$	K_2CO_3	reflux	10:80:10
4	Toluene	$Pd(PPh_3)_4$ $Pd(OAc)_2/PCy_3$	DBU	reflux	10:70:20
5	1,4-Dioxane	$Pd(PPh_3)_4$ $Pd(OAc)_2/PCy_3$	DBU	reflux	10:60:30
6	DMF	$Pd(PPh_3)_4$ $Pd(OAc)_2/PCy_3$	DBU	reflux	5:70:25
7	DMSO	$Pd(PPh_3)_4$ $Pd(OAc)_2/PCy_3$	DBU	reflux	5:70:25
8	*o*-Xylene	$Pd(PPh_3)_4$ $Pd(OAc)_2/PCy_3$	DBU	reflux	10:40:50
9	*o*-Xylene	$Pd(PPh_3)_4$ $Pd(OAc)_2/PCy_3$	K_2CO_3	reflux	50:40:10
10	*o*-Xylene	$Pd(OAc)_2$/SPhos	K_2CO_3	reflux	40:40:20
11	*o*-Xylene	$Pd_2(dba)_3$/SPhos	K_2CO_3	reflux	40:40:20
12	*o*-Xylene	$Pd_2(dba)_3$/ P(*o*-tolyl)$_3$	K_2CO_3	reflux	40:40:20
13	*o*-Xylene	$Pd_2(dba)_3/PCy_3$	K_2CO_3	reflux	80:15:5

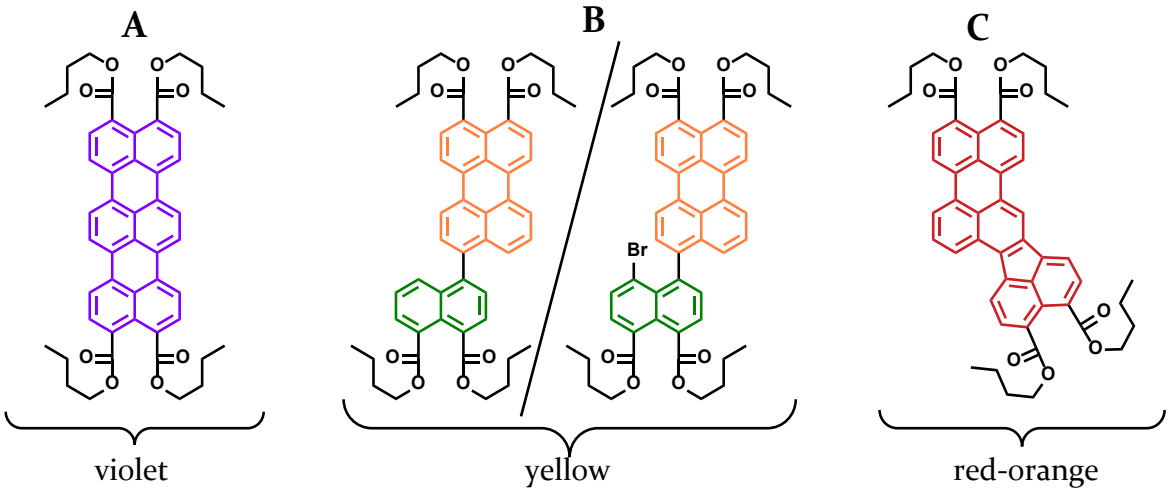

Figure 2-3. Colored reaction products of the reaction conditions in Table 2-1.

As conducting these test reactions was an iterative process, it became obvious that high temperatures and unpolar solvents influence the ratio in favor of TTE **2-9** over the unwanted side reactions. Polar solvents (including added water to dissolve inorganic bases) or organic bases such as DBU, favored the side products instead of TTE **2-9**. Additionally, the successive addition of the different catalysts led to worse results compared to simultaneous addition at the beginning of the reaction.

The best results on a milligram scale were obtained with anhydrous *o*-xylene as the solvent, K_2CO_3 as a base and $Pd_2(dba)_3/PCy_3$ as the catalyst system (entry #13, Table 2-1). Interestingly, the *Suzuki-Miyaura* coupling was successful even without the addition of water. Residual water from K_2CO_3 appears to produce enough active borate anions to allow *Suzuki-Miyaura* reaction to take place.

Although the five-membered analogue **2-13** could not be separated from the complicated reaction mixtures for further characterization, mechanistic studies by *Shoyama et al.* investigating the influence of the base on the coupling mechanism corroborate the probability for this competing cyclization.[92] In their findings, they proposed a cross-coupling mechanism in which DBU serves as an auxiliary base that promotes the cyclization of five-membered polycyclic dicarboximides instead of their six-membered analogues that are congruent with the results discussed in this section.

If this new synthetic approach towards higher rylene structures should be established as a reliable method, the drawbacks criticized earlier need to be addressed. On an academic scale, the main downside of earlier methods was the difficulty of purification at several reaction steps. Surprisingly, even if conversion of the starting material was not complete, as long as no five-membered **2-13** was present, it was possible to purify TTE **2-9** by liquid/liquid extraction and precipitation (Figure 2-4). Because both the starting material and the non-cyclized reaction intermediates are highly soluble, only TTE precipitated and could be obtained in high purity, as evidenced in the ^{1}H NMR spectrum in Figure 2-5.

Additionally, scaling up is always of interest for compounds serving as universal building-blocks. With this procedure, several grams of terrylene compound **2-9** were produced in 75 % yield in a short amount of time, which was previously hardly possible.

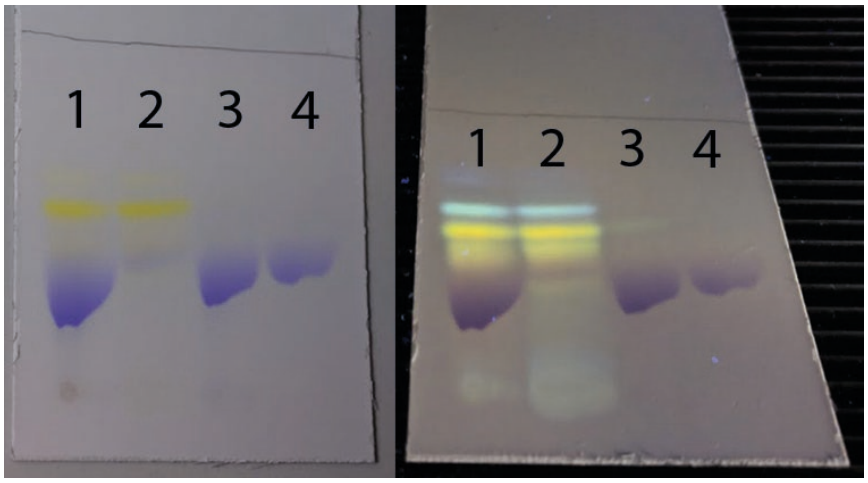

Figure 2-4. Purification steps of TTE **2-9**. Left: under ambient light; right: under UV-light. 1) crude reaction mixture. 2) filtrate after initial precipitation. 3) solid after initial precipitation. 4) solid after full workup.

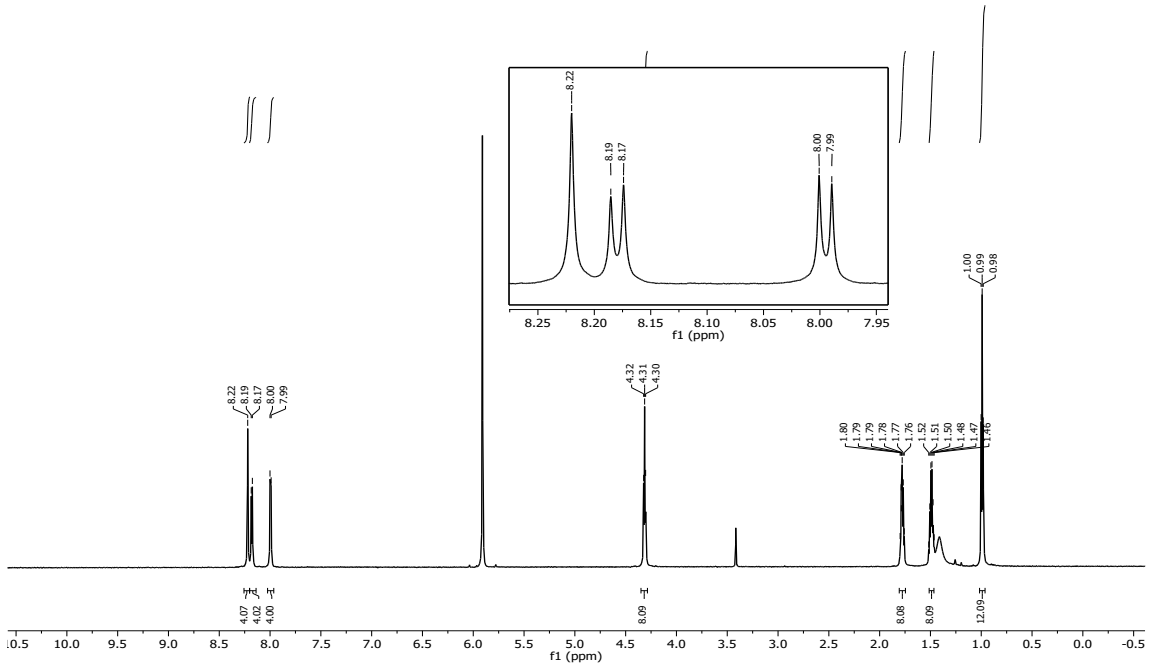

Figure 2-5. ^{1}H NMR (700 MHz, $C_2D_2Cl_2$, 373 K) of TTE **2-9** after precipitation.

The main advantages compared to old methods are evident; for the first time, a scalable, four-step synthesis of a terrylene based compound has been established that completely avoided any column chromatography, instead relying on precipitation due to the large differences in the solubilities of side products and the target compound.

2.4 Syntheses of Terrylene Diimides

Even though rylene esters have some academic significance, mainly due to their good phase forming properties,[93–96] the vast majority of rylene related research is based on rylene imides. While TTE **2-9** itself possesses some mentionable properties like a fluorescence quantum yield of 100 %,[97] the academic and industrial significance of this compound lies in its role as a potential universal building block for a wide range of different terrylene imides.

Two different approaches based on the cascade cross-coupling reaction were established and are shown in Scheme 2-7:

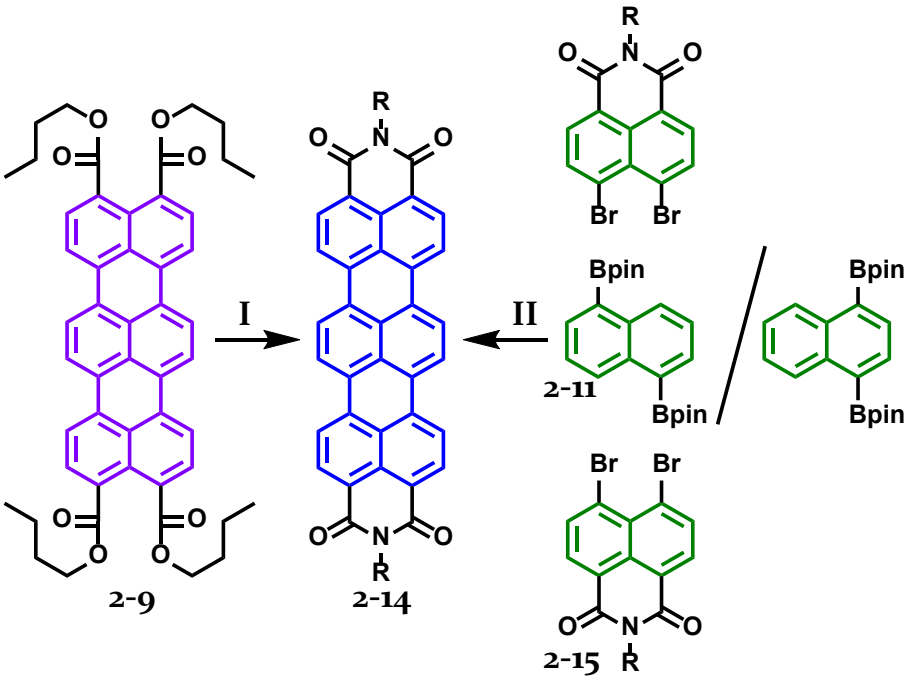

Scheme 2-7. Synthesis of TDI via imidization (**I**) and cascade reaction (**II**).

The most straight forward strategy of synthesizing symmetric TDIs via imidization of TTE **2-9** with the respective amine (Scheme 2-7, **I**). This is known to be an essential strategy for PDIs when imidization with poorly reactive amines/anilines has to be performed, as has been discussed in chapter 1.2.1 (page 8).[83] Even though carboxylic anhydrides are much more reactive than carboxylic esters,[98] the low solubility of PDA reduces its reactivity, thus no reaction can be observed in these rare cases. As the solubility of terrylene-3,4,11,12-tetracarboxy dianhydride (TDA) in any suitable solvent is even worse than that of PDA, no literature-known procedure for any TDI compound that arises from unsubstituted TDA exists to this date. TTE **2-9** therefore is a promising building block for the synthesis of TDIs.

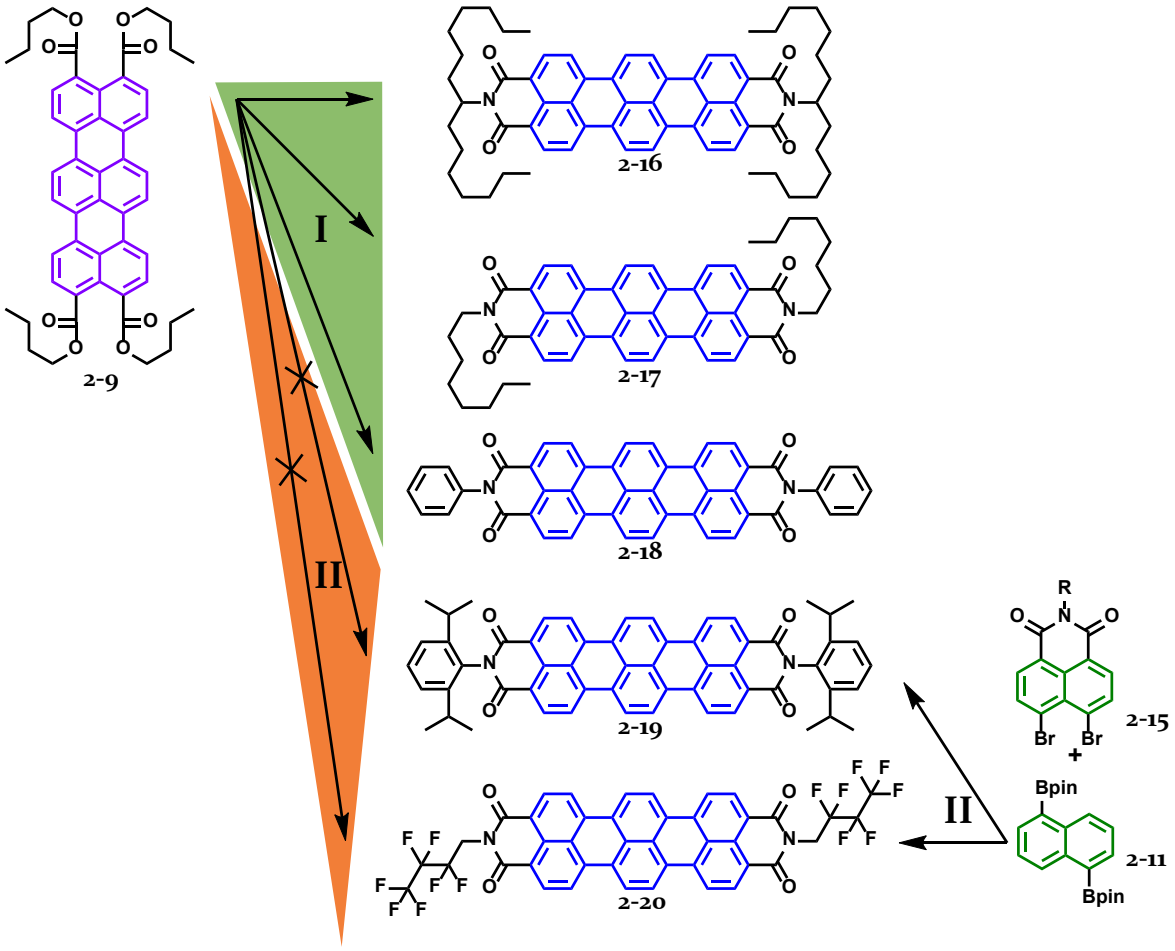

Scheme 2-8. Scope and limitations in the choice of amines/anilines for two new routes towards TDIs. Conditions: I) amine/aniline, imidazole, pressure vessel, 170 °C, 16 h, 60 % for **2-16**, 72 % for **2-17**, 75 % for **2-18**; II) $Pd_2(dba)_3$, PCy_3, K_2CO_3, *o*-xylene, 145 °C, 16 h, 60 % for **2-19**, 33 % for **2-20**.

The second approach towards synthesizing TDIs, namely the direct cross coupling of 4,5-dibromo NMI with naphthalene diboronic acid pinacol ester, can be seen in Scheme 2-7 **II**. This direct cross-coupling adds the additional step of synthesizing the required 4,5-dibromo naphthalene imides, but potentially expands the range of eligible amines/anilines in cases where approach **I** is not applicable or insufficient.

Each of these two routes faces drawbacks in terms of applicable amines, which will be discussed in this as well as in the following chapters. Scheme 2-8 depicts the successful TDI syntheses via the imidization (**I**) and cascade coupling routes (**II**).

When comparing the successful and unsuccessful TDI syntheses in Scheme 2-8, the probability that direct imidization of TTE **2-9** is successful seems to be higher for

unhindered amines/anilines with good solubility. Whilst TDI **2-16** is a well-known, highly soluble compound due to its α-branched imide-substituent, thus imidization in imidazole at 170 °C can be performed effortlessly, TDIs **2-17** and **2-18** were proven to be pigments. The combination of reactivity and solubility of butyl substituted TTE with *n*-octylamine and aniline however was compatible and imidization was successful.

Unpredictable was the fact that TDI **2-19** could not be obtained via route **I**. Independent of the chosen solvent, temperature or added catalyst, either no reaction at all, or hydrolysis/decarboxylation was observed. TDI pigment **2-20** could not be obtained via route **I** as well, as the low boiling point of the fluoroalkylamine is too low for any reaction to take place.

Fortunately, the cascade reaction pathway **II** is not limited to the dibromo-NDE **2-10**. Using 4,5-dibromo-NMIs as the coupling partners resulted in the TDIs **2-19** and **2-20** under the same reaction conditions as determined earlier (Scheme 2-9).

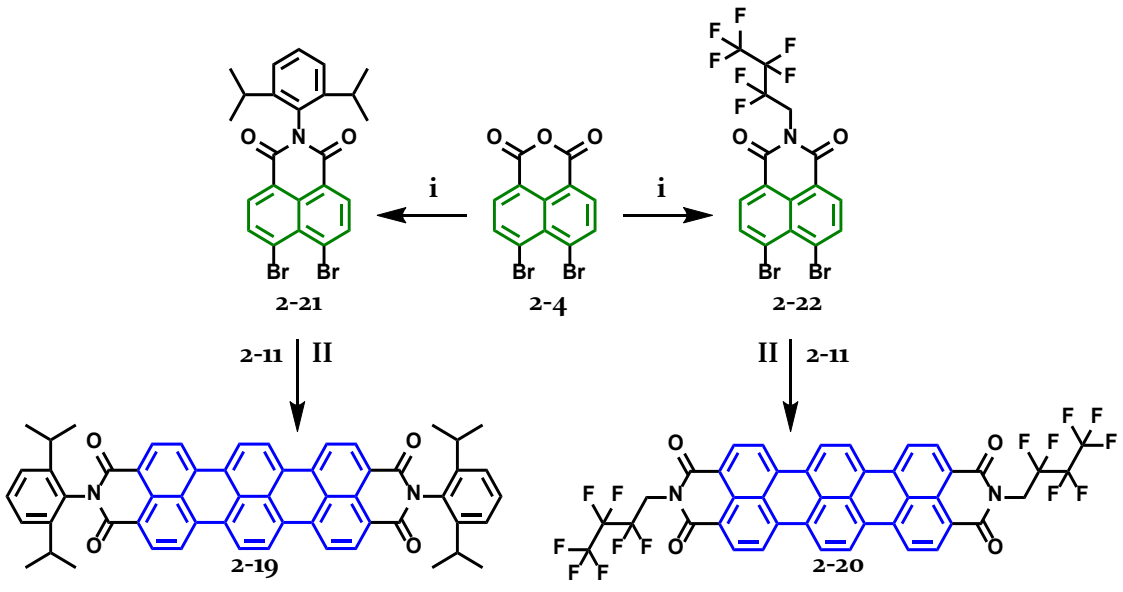

Scheme 2-9. Synthesis of 2,6-di*iso*propyl and 2,2,3,3,4,4,4-heptafluorobutyl substituted 4,5-dibromo NMIs **2-21** and **2-22** and TDIs **2-19** and **2-20**. Conditions: i) amine/aniline, NMP/propionic acid 1:1, 160 °C, 16 h, 55 % for **2-21** and **2-22**; II) see Scheme 2-8.

Synthesis of 4,5-dibromo naphthalene imides (e.g. **2-21** and **2-22**) however is subject to a different set of limitations in terms of reaction conditions. As *peri*-halogenated rylenes are susceptible towards substitution reaction in the *peri*-positions, the choice of solvent is critical. Typically, imidization reactions with halogenated rylenes are carried out in acidic solvents or solvent mixtures like acetic or propionic acid with *N*-methyl-2-pyrrolidon (NMP) as co-solvent. Synthesis of 2,6-di*iso*propylphenyl and 2,2,3,3,4,4,4-heptafluorobutyl substituted 4,5-dibromo NMI **2-21** and **2-22** was successful, while the 1-heptyloctylamine substituted derivative could not be obtained in the same way (Scheme 2-9). A possible explanation could be the hydrophobic nature of 1-heptyloctylamine that results in polymer-like contraction or micelle-formation of the alkyl chain in 'bad' solvents, thus rendering the amine inactive as a nucleophile. This behavior demonstrates the main drawback of route **II**, as nucleophiles must be stable as well as reactive under acidic conditions.

Nonetheless, pathway **II** serves as an additional tool to expand the range of accessible TDIs. Fluoroalkyl- and 2,5-di*iso*propylphenyl substituted 4,5-dibromo naphthalene imides allowed for successful synthesis of TDI **2-19** and **2-20** that were unattainable via direct imidization. In the case of the TDI pigment **2-20**, the target compound precipitated in 33 % yield. Remaining starting material and catalyst could be removed after the compound was filtered and rinsed with diluted acid and organic solvents, in which the fluorinated TDI was insoluble. The MALDI-TOF spectrum in Figure 2-6 shows **2-20** after the described purification procedure without any impurities present. Due to their pigment-like characters, no further purity-confirming characterization was successful on TDIs **2-17**, **2-18** and **2-20**.

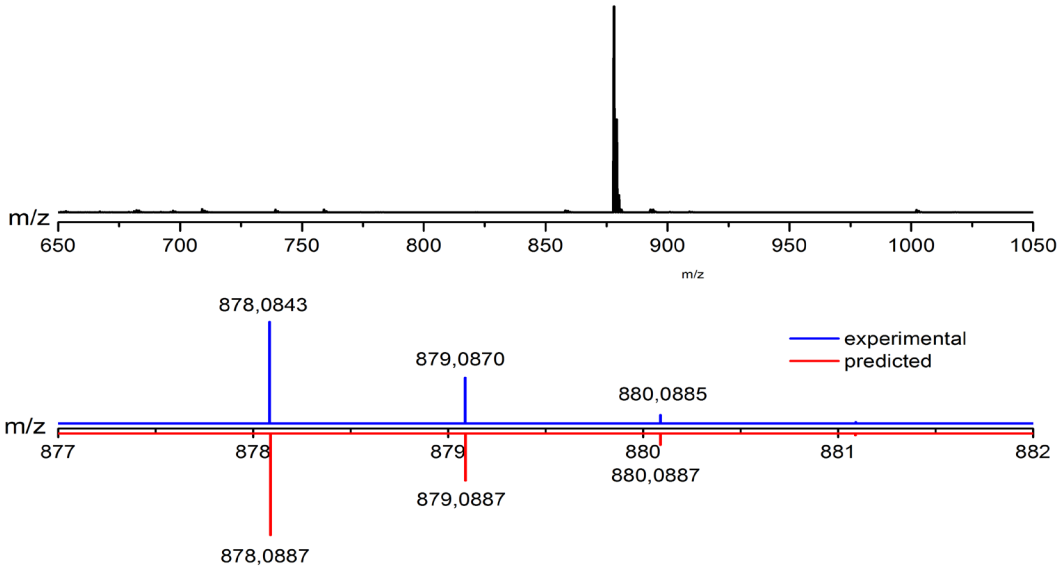

Figure 2-6. MALDI-TOF spectrum of TDI **2-20**.

2,6-Di*iso*propylphenyl substituted TDI **2-19** on the other hand required comparatively elaborated workup procedures, as well as chromatographic purification via a short silica column to remove residual starting material. Contrary to butyl substituted dibromo-NDE **2-10**, *N*-(2,6-di*iso*propylphenyl)-4,5-dibromo-1,8-naphthalimide **2-21** could not be removed during the filtration step due to its lower solubility. The yield, however, was 60 % on a 500 mg scale.

Although the overall cascade-coupling yield for DIPP-TDI **2-19** with 30 % seems low, it helps to put the synthetic steps necessary into perspective when comparing 2005's approach (55 %) and the one presented here. Previously, PMI syntheses required highly elaborated laboratory equipment (pressure vessels) and purification skills (chromatography). Furthermore, vacuum filtration is highly ineffective in removing the decomposition products and copper-oxides from the pasty, slurry-like reaction mixture, making the preparation of PMI in significant amounts very labor-intensive.[99] In the following reaction sequence (see Scheme 1-4), purification via column chromatography is required in three of these steps.

With this new naphthalene-based synthesis on the other hand, the 'terminal' and the 'core' naphthalene precursor units can be prepared from inexpensive materials in

a total of three steps. Precipitation and removal of residual reaction materials is sufficient to receive both naphthalene coupling partners in high yields. In the subsequent cross-coupling reaction, the effort necessary for purifying the final terrylene compounds is dependent on the solubility of the cross-coupling building blocks, as has been demonstrated in the two cases in Scheme 2-9. In the case of the fluoroalkyl-substituted TDI, the solubility of TDI **2-20** in organic solvents is low enough to remove the fluoroalkyl substituted dibromo-NMI **2-22** and other residual reaction material by rinsing TDI with organic solvents and diluted acid. In the case of 2,6-di*iso*-propylphenyl substituted TDI **2-19**, the difference in solubility between cross-coupling product and starting material is not large enough to separate the compounds by precipitation and column chromatography becomes necessary. However, as this is the only chromatographic purification step in the reaction sequence, this improved reaction protocol is a significant addition to the toolbox of rylene diimide syntheses when flexibility in the choice of imide-substituent and quick access to the desired TDI is more important than the overall yield.

2.5 Synthesis of Rylene Monoimides

PMIs have shown to be versatile chromophore building blocks with controllable optical and electrochemical properties.[57] As a consequence, they are of great interest to academic research and industrial applications, both as intermediate compounds as well as for their functional qualities as colorants of semiconducting material.[100–105] Push-pull type PMIs of the structure demonstrated in Figure 2-7 are amongst the most efficient materials found in dye-sensitized solar cells.[58] For dye-sensitized solar cells, charge separation is an important characteristic to avoid recombination between injected electrons and oxidized dye molecules.[17] The frontier orbitals in Figure 2-7 are clearly separated between the HOMO, located on the donor part of the structure, and the LUMO which is mainly located at the perylene core, an electronic configuration that cannot be realized in rylene diimides as effectively.

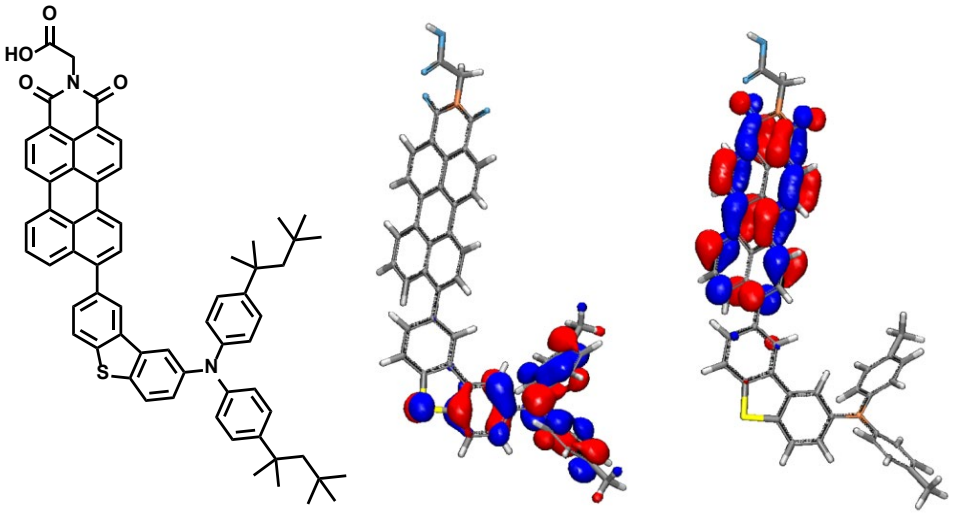

Figure 2-7. Push-pull type PMI (left), calculated HOMO (center) and LUMO (right).[106]

All currently available syntheses of rylene monoimides have a special difficulty in common which has already been discussed in the previous sections for the DIPP-PMI case. Expanding this structural motif via one naphthalene unit to terrylene monoimides (TMI), these circumstances gain even greater relevance. Thus, *bay*-unsubstituted TMIs have, up to this point, not been fully characterized and utilized. Yet,

their role as colorants and semiconductors make rylene monoimides interesting building blocks that would benefit from more accessible synthetic protocols than available before.

In Scheme 2-10, a retro-synthetic concept based on the previously discussed cascade cross-coupling reaction for the synthesis of the displayed perylene and terrylene monoimides composed of readily available coupling partners is presented. In contrast to the 'top-down' method of decarboxylation-imidization starting from the rylene dianhydride, a 'bottom-up' approach will be utilized to construct perylene and terrylene monoimides from naphthalene and perylene precursors.

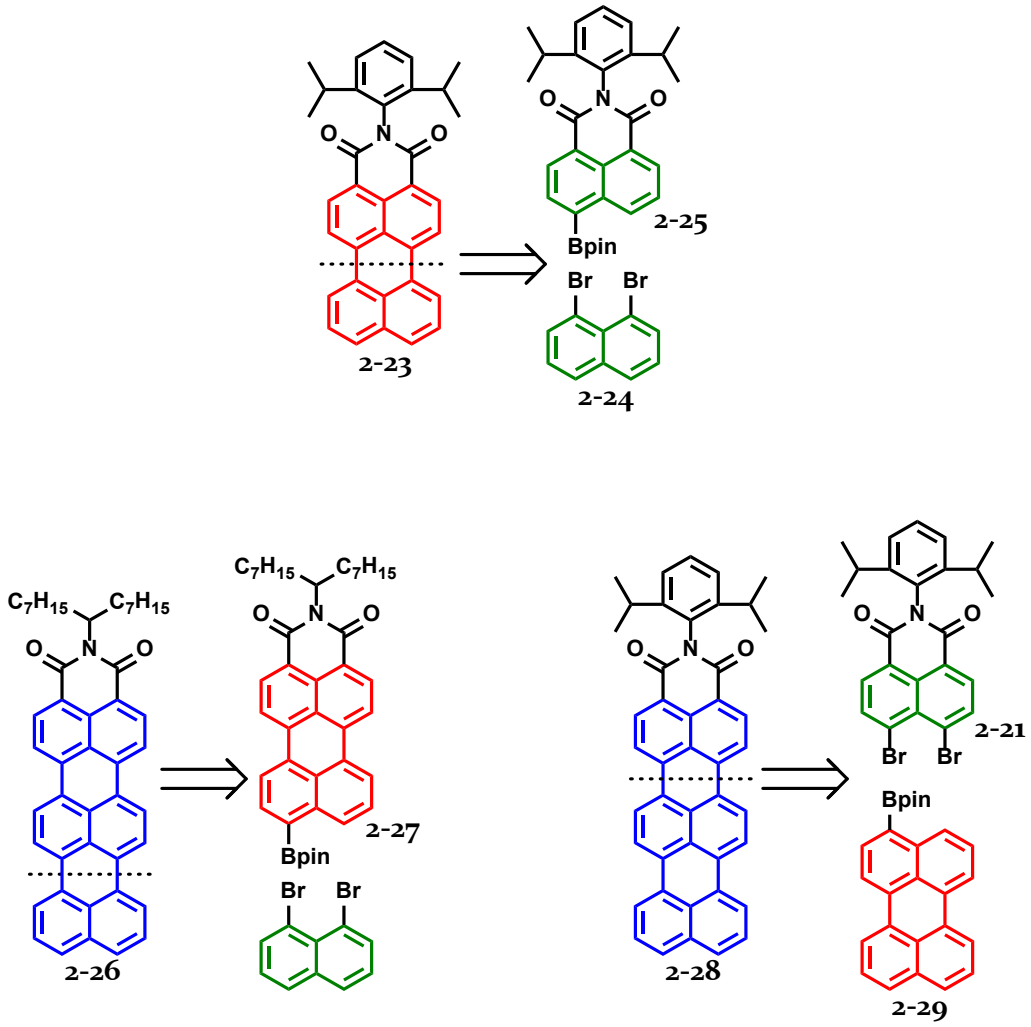

Scheme 2-10. Retro-synthetical concept for the syntheses of perylene (top) and terrylene monoimides (bottom).

2.5.1 Synthesis of Perylene Monoimide

Following a literature-known procedure, the boronic acid pinacol ester of 2,6-di*iso*propylphenyl substituted NMI **2-25** was prepared in two steps in an overall yield of 57 % (Scheme 2-11).[107] Under the cascade cross-coupling conditions established in the previous section, **2-25** was coupled with 1,8-dibromo naphthalene **2-24** in yields exceeding 65 %. Although column chromatography was mandatory to separate PMI **2-23** from the naphthalene building blocks, purification was more efficient compared to the previous protocols that relied on the separation of PMI from anhydrides with poor solubility.

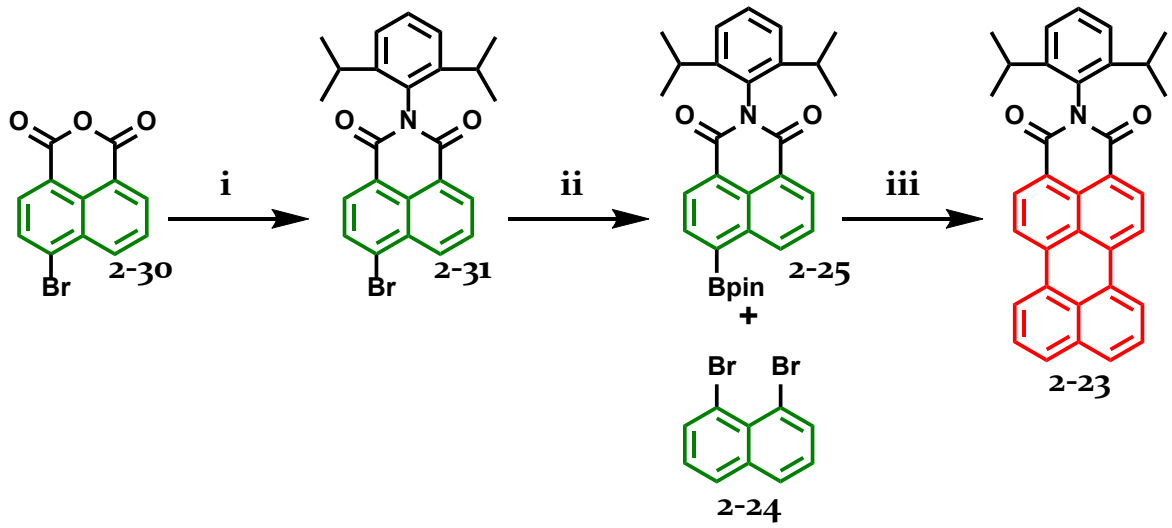

Scheme 2-11. Synthesis of PMI **2-23**. Conditions: i) 2,6-di*iso*propylaniline, AcOH, reflux, 3 d, 95 %; ii) B_2pin_2, KOAc, $Pd(dppf)Cl_2$, 1,4-dioxane, 90 °C, 60 %;[107] iii) $Pd_2(dba)_3$, PCy_3, K_2CO_3, *o*-dichlorobenzene, 160 °C, 16 h, 65 %.

2.5.2 Syntheses of Terrylene Monoimides

Starting from PMA **2-23**, imidization and further conversion to the boronic acid of the 1-heptyloctylamine substituted PMI **2-27** in three steps followed previously reported procedures (Scheme 2-12).[108] 1,8-Dibromonaphthalene **2-24** proved to be a viable coupling partner for PMI **2-27** as well, resulting in 1-heptyloctyl substituted TMI **2-26** in 30 % yield. The synthesis of 2,6-di*iso*propylphenyl substituted TMI **2-28** succeeded with the combination of 4,5-dibromo NMI **2-21** and the 3-boronic acid

pinacol ester of perylene **2-29** in 40 % yield. After repeated precipitation of both TMIs from dichloromethane in methanol, **2-26** and **2-28** were obtained in 30 % and 40 % yield, respectively. Their identity was confirmed via MALDI-TOF MS and NMR spectroscopy. In the case of 2,6-di*iso*propylphenyl substituted TMI **2-28** however, the solubility was low, and no signals could be resolved in the ^{13}C NMR spectrum, even at elevated temperatures.

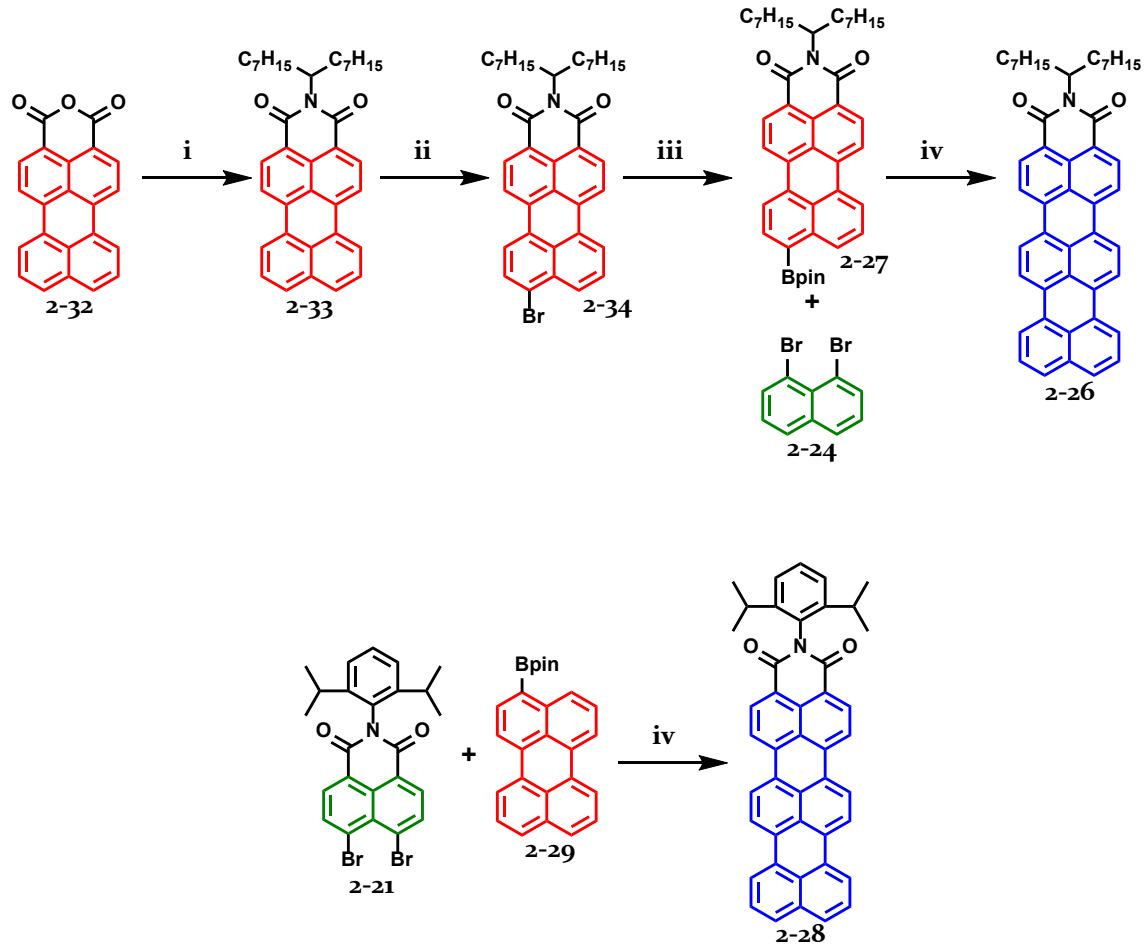

Scheme 2-12. Synthesis of 1-heptyloctyl substituted TMI **2-26** (top) and 2,6-di*iso*-propylphenyl substituted TMI **2-28** (bottom). Conditions: iv) $Pd_2(dba)_3$, PCy_3, K_2CO_3, *o*-dichlorobenzene, 160 °C, 16 h, 30 % for **2-26**, 40 % for **2-28**.

This series of different rylene monoimides synthesized by the same cascade cross-coupling condition demonstrates the flexibility of the cascade cross-coupling reaction. The electron deficient coupling partner (monoimide) can either bear the halide

substituents or the boronic ester, which has been shown by the syntheses of TMIs **2-26** and **2-28**. Consequently, coupling partners can be chosen based upon their accessibility and are not limited to naphthalene compounds. As an example, PMI has been synthesized in 65 % yield without the need for extensive filtration and removal of copper-oxides. The flexibility in the choice of imide substituent (a variety of 4-bromo-naphthalene-1,8-dicarboximides are reported in the literature) furthermore illustrates the utility of the cascade cross-coupling reaction in the synthesis of the PMI building block that doesn't rely on elaborate saponification and subsequent imidization of 2,6-di*iso*propylphenyl substituted PMIs.[62]

Additionally, the 'bottom-up' approach made the synthesis of core-unsubstituted TMIs possible. Due to the insolubility of TDA, the decarboxylation-imidization protocol that is employed in the conversion of PDA to PMI is not suitable for the preparation of TMIs, and multi-step syntheses were necessary.[71] Using the cascade cross-coupling reaction however, TMIs with variable imide-substituents became accessible in good yields, making them potential candidates in applications that were so far limited to PMIs.

2.6 Optical and Electronic Properties

In order to gain insight into the optical and electronic properties of the newly synthesized terrylene compounds shown in Figure 2-8, TTE **2-9** and 1-heptyloctyl substituted TMI **2-26** were characterized by UV-Vis and fluorescence spectroscopy (Figure 2-9) as well as cyclic voltammetry (Figure 2-10), of which the results are summarized in Table 2-2. Both compounds were compared to literature-known TDI **2-16**.

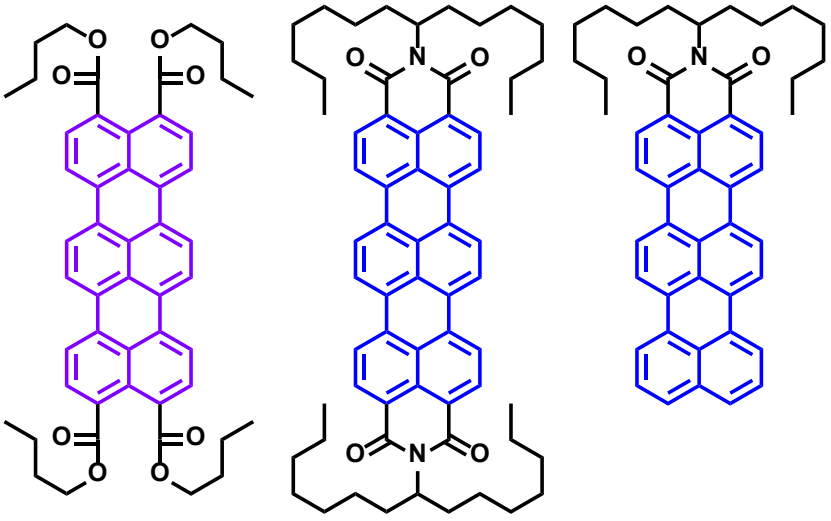

2-9 **2-16** **2-26**

Figure 2-8. Terrylene compounds characterized by UV/Vis spectroscopy and cyclic voltammetry.

Similar to TDI **2-16**, TTE **2-9** reveals three characteristic absorption bands ascribed to different electronic S_0–S_n transitions. The comparatively higher degree of electron deficiency of **2-16** compared to **2-9**, which is due to the stronger electron-withdrawing nature of the two imide groups compared to four ester groups, results in a bathochromic shift of the absorption and emission bands of TDI **2-16** in regard to TTE **2-9**. The molar absorptivity of TTE **2-9** is approx. 20% lower than that of TDI **2-16**, which is a similar difference in absorptivity as found in their perylene derivatives (41000 $M^{-1}cm^{-1}$ for PTE,[109] 52100 $M^{-1}cm^{-1}$ for PDI[110]), whereas the fluorescence quantum yield of **2-9** (ϕ_{fl} = 1.00 ± 0.03) is significantly higher than that of TDI

(ϕ_{fl} = 0.70 ± 0.01). In contrast, TMI **2-26** exhibits a relatively low absorptivity (ε_{max} = 46200 M^{-1} cm^{-1}) and emission (ϕ_{fl} = 0.20 ± 0.01), which can be attributed to the low solubility of TMI, probably due to strong π–π interactions in solution. This assumption is further established by the fact that the absorption band of TMI is very broad, displaying a poorly separated band structure with a Stokes shift (1878 cm^{-1}) larger than that of TDIs (generally less than 350 cm^{-1}).

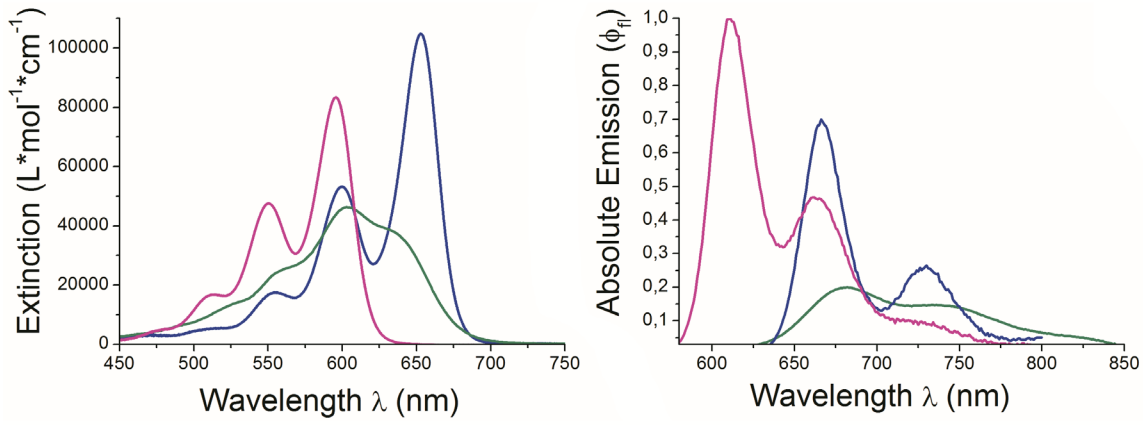

Figure 2-9. UV-Vis absorption (left) and emission (right) spectra of compound **2-9** (magenta), **2-16** (blue), and **2-26** (green) in CH_2Cl_2, c ≈ 10^{-6}M.

Table 2-2. Optical and electrochemical properties of **2-9**, **2-16** and **2-26**.

	$\lambda_{abs,max}$ (nm)	ε_0 ($M^{-1}cm^{-1}$)	$\lambda_{em,max}$ (nm)	φ_{fl}	*LUMO* (eV)	*HOMO* (eV)
2-9	595	83400	610	1.0 ± 0.03	-3.4	-5.3
2-16	652	105000	666	0.7 ± 0.01	-3.7	-5.5
2-26	603	46200	680	0.2 ± 0.01	-3.5	-5.3

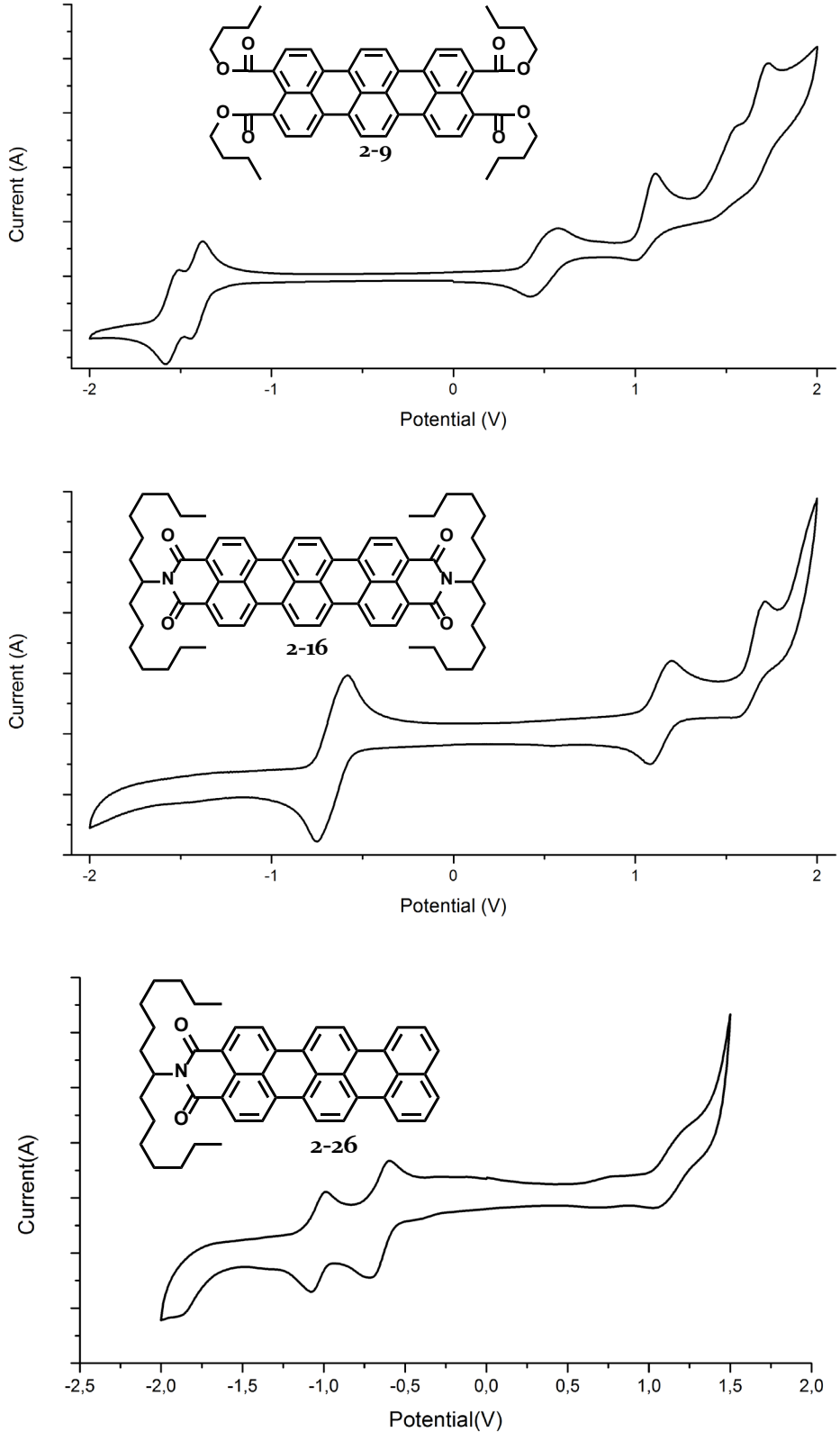

Figure 2-10. Cyclic voltammograms of **2-9** (top) and **2-16** (center) in 0.1 M solution of Bu_4NPF_6 in dichloromethane, **2-26** (bottom) in 0.1 M solution of Bu_4NPF_6 in THF, 100 mV/s.

All three terrylene compounds **2-9**, **2-16** and **2-26** revealed reversible oxidation and reduction processes in the accessible scanning range in cyclo-voltammetric measurements (Figure 2-10). Both fully peri-functionalized TTE **2-9** and TDI **2-16** exhibit two reversible oxidation waves. Their first oxidation potentials have the same onset demonstrating the same HOMO levels of -5.3 eV, which, is more positive than that of TDI (-5.5 eV). Thus, TTE and TMI are both easier to be oxidized than TDI, which can be attributed to the two imide substituents.[97] No reversible oxidation could be determined for TMI **2-26** in the accessible scanning range, hinting at the possibility of *peri*-coupling of the oxidized TMI. Additionally, irreversible oxidation occurs at higher voltages in the case of TTE **2-9**. Within the accessible scanning potential range in CH_2Cl_2 and THF, TDI displays one, TTE and TMI two reversible reduction waves. The first reduction potential shifts positively following the order from TDI **2-16** to TTE **2-9**, indicating that TTE **2-9** has a more positive LUMO level (-3.4 eV) than TDI **2-16** (-3.7 eV), which is easier to be reduced due to the electron deficiency caused by the imide substituents.

2.7 Summary

A powerful synthetic method has been developed to gain access to a wide variety of different terrylene compounds as well as perylene and terrylene monoimides. Some compounds like TDIs **2-16** and **2-19** have been synthesized previously, but were available in small quantities only, mainly because synthesis and purification required a great deal of effort and time. Other compounds, especially TTE **2-9** as a universal building block, remained unreported so far. Generally, the number of steps needed towards final compounds have been greatly reduced. In addition, this novel protocol was proven to reduce the efforts necessary for analytically pure material in gram-scale, only relying on precipitation and filtration methods, whereas previous methods inevitably relied on column chromatographic purification of intermediates and target compounds.

It was shown that TTE **2-9** serves as the go-to building block for symmetric TDIs where the amine/aniline is sufficiently reactive in nucleophilic substitution reactions. In situations where imidization with TTE did not yield the desired TDI, an alternate pathway via the respective 4,5-dibromo NMI was used for direct synthesis of the target compounds.

This new synthetic concept proved to be not limited to dyes; pigments were successfully synthesized, as showcased with TDIs **2-17**, **2-18** and **2-20** which has thus far been unprecedented. This is noteworthy, especially because the reactions in question proceeded cleanly, thus avoiding complicated or impossible purification of pigments. Even though the three pigments synthesized for this work did not show any exceptional performance as functional semiconductors in FET devices, this approach paves the way for a variety of TDI pigments that are otherwise not attainable.

For the first time, TMIs without bay substituents have been synthesized and characterized. This opens up the possibility of designing *peri*-functionalized TMIs, similar to PMI-motifs that have been used in the past, for applications ranging from push-pull type systems in dye-sensitized solar cells to their role in the self-assembly properties of peptide-chromophore conjugates.[111–113]

The following chapters will focus on utilizing this new cascade reaction for the synthesis of different terrylene based compounds and will also discuss the current difficulties and limitations that remain to be solved.

Chapter 3
SYNTHESIS OF AN ASYMMETRIC, MONOFUNCTIONAL TDI

3.1 INTRODUCTION

So far, the newly developed approach only focused on synthesizing symmetric TDIs. There is, however, a large interest in connecting mono-functional rylene imides to structural motifs, as evidenced in past and present research.[114–122] Of particular interest is the probing of excited electronic states in polycyclic aromatic hydrocarbons (PAH), especially hexa-*peri*-hexabenzocoronene (HBC) and its derivatives, via single-molecule studies. Due to the highly efficient intersystem crossing (ISC) into long-lived triplet states preventing luminescence detection, these electronic states can be observed and monitored only indirectly by photophysical characterization of multichromophoric structures.[123] In a multichromophore consisting of HBC and energy acceptors, the excitation of HBC leads to partial excitation energy transfer (EET) to the attached probe (e.g. PMIs), which in turn shows detectable fluorescence. The temporal ceasing of PMI fluorescence, in return, can give insights into the electronic structure of HBC, as demonstrated by *Fückel et al.* (Figure 3-1).[124] In this special multichromophore, however, the EET to ISC ratio exceeded expectations by far, hampering investigations on the desired photophysical properties of HBC. Linking TDI instead of PMI to the PAH could eliminate the push-pull character of the resulting donor-*peri*-acceptor dyad, turn down the EET efficiency and allow more detailed investigation into HBCs and other PAHs photophysical characteristics.

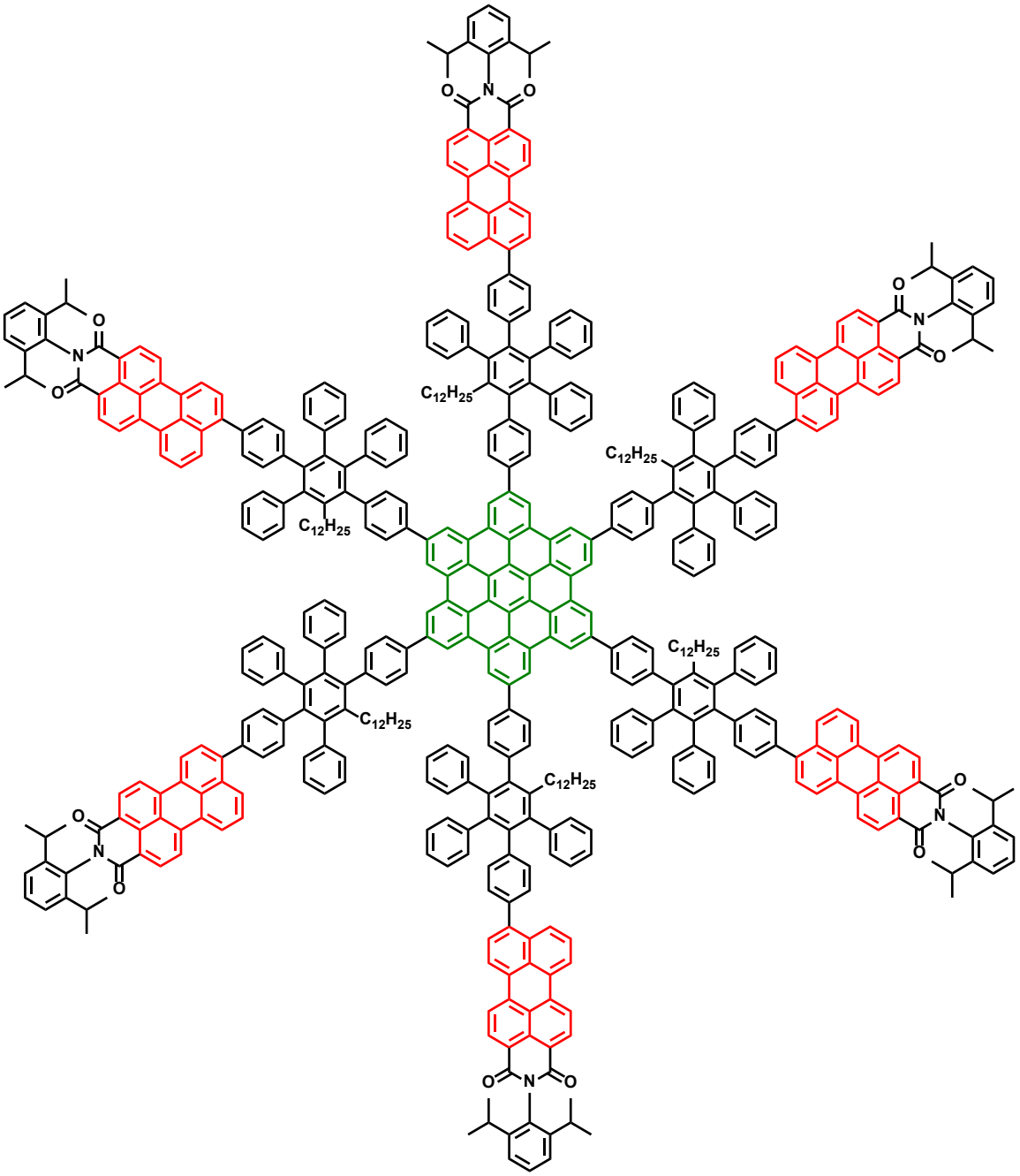

Figure 3-1. Molecular structure of HBC-6PMI.[124]

The challenge on the synthetic chemist's side arises from the necessity of a desymmetrized TDI which can be coupled to any PAH via an anchor. Retro-synthetically, two approaches are possible following the cascade cross-coupling protocol to synthesize a monofunctional, asymmetric TDI (Scheme 3-1).

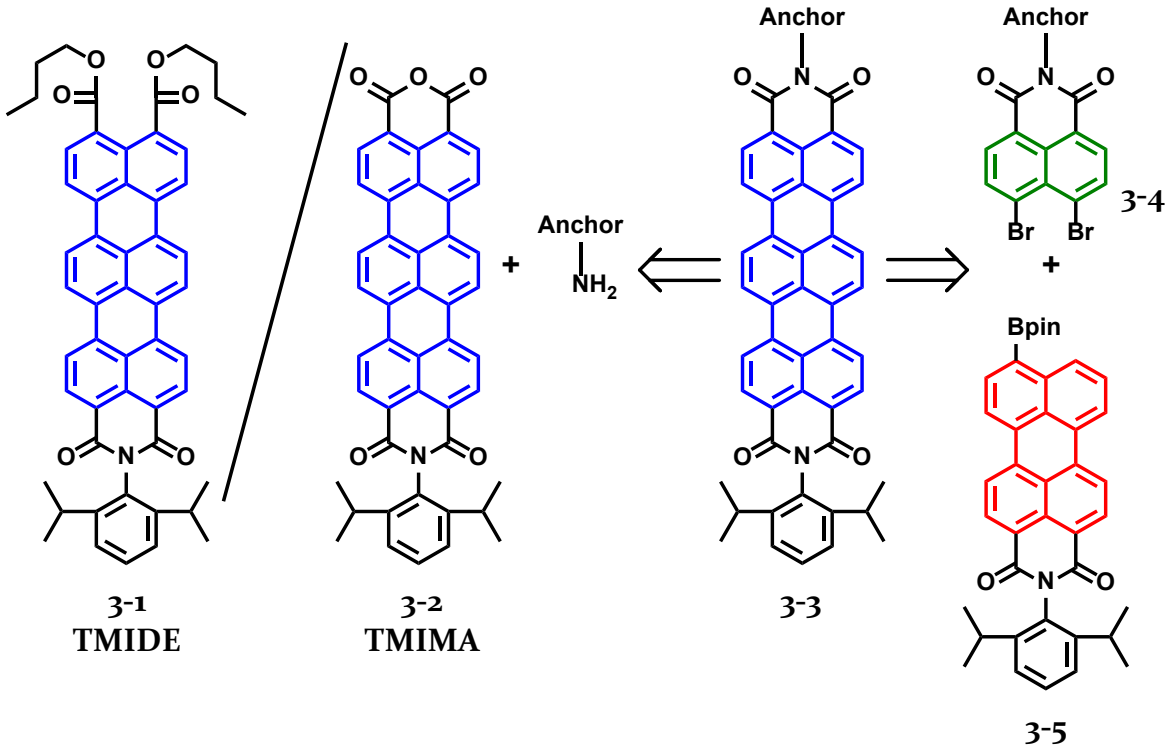

Scheme 3-1. Retro-synthetic concept for the synthesis of monofunctional, asymmetric TDI **3-3**.

These two approaches resemble approach **I** and **II** discussed in chapter 2. Here, imidization of precursors **3-1**/**3-2** (TMIDE and TMIMA, Scheme 3-1) with the anchor-bearing amine/aniline on the one hand, and cascade cross-coupling of anchor-bearing dibromo-NMI **3-4** with PMI **3-5** on the other hand are viable strategies in the synthesis of the monofunctional TDI **3-3**.

The choice of anchor is dependent on two factors. 1) In the subsequent step, cross-coupling with a halide-functionalized PAH must be possible and 2) the anchor must be stable under cross-coupling and imidization reaction conditions.

Both *Suzuki-Miyaura* and *Sonogashira* aryl-aryl cross-coupling reaction protocols rely on functional groups that are known to be stable under imidization conditions.[125,126] Consequently, this chapter will discuss the synthesis of the asymmetric TDI building blocks TMIDE/TMIMA and the possibilities of synthesizing a monofunctional TDI suitable for aryl-aryl cross-coupling reactions.

3.2 Synthesis of Asymmetric TDIs

Chapter 2 has already proven that 9-boronic esters of PMI can act as the coupling partner in the cascade reaction towards TDIs. Unsurprisingly, with dibromo-NDE **2-10**, the synthesis of TMIDE **3-1** succeeded in excellent yields of 65 % on a gram scale (Scheme 3-2). Purification was particularly easy by filtering over a pad of silica; rinsing with pure DCM removed all the starting material, while the target compound eluted in ethyl acetate as pure compound. Figure 3-2 shows the NMR spectrum of TMIDE **3-1** without any further purification.

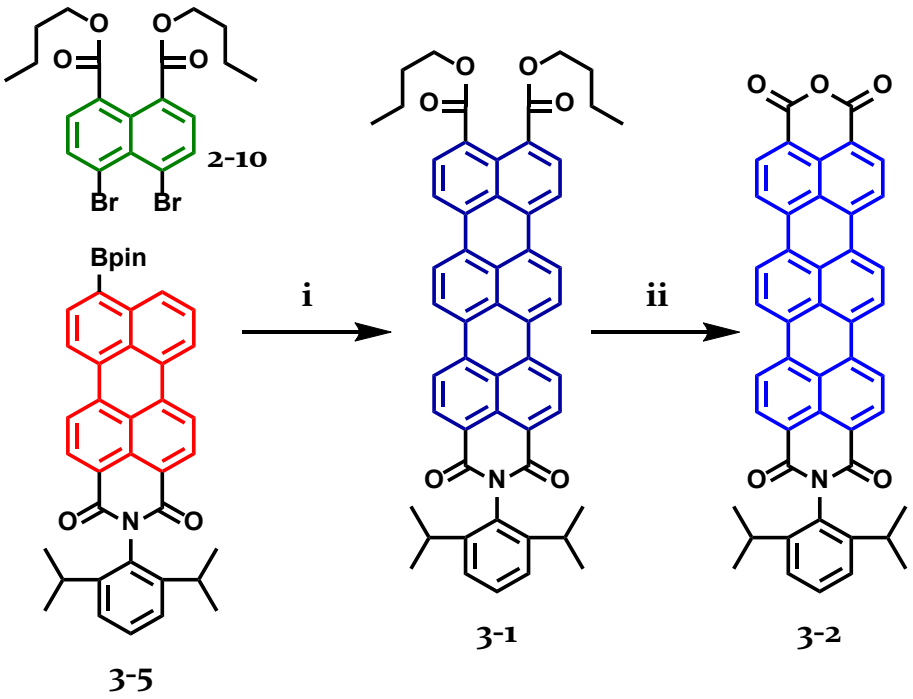

Scheme 3-2. Synthesis of TMIDE and TMIMA. Conditions: i) K_2CO_3, $Pd_2(dba)_3$, PCy_3, o-dichlorobenzene, 180 °C, 6 h, 65 %; ii) AcOH, H_2SO_4, 110 °C, 100 %.

Since the carboxylic ester **2-9** was insufficiently reactive in nucleophilic substitution reactions, TMIDE **3-1** was further converted to the respective monoanhydride TMIMA **3-2** by stirring in a mixture of acetic and sulfuric acid (1:3) at 110 °C. The single remaining DIPP imide substituent was chosen for two important reasons: 1) providing sufficient solubility for the remaining imidization reactions and 2) hydrolytic stability.

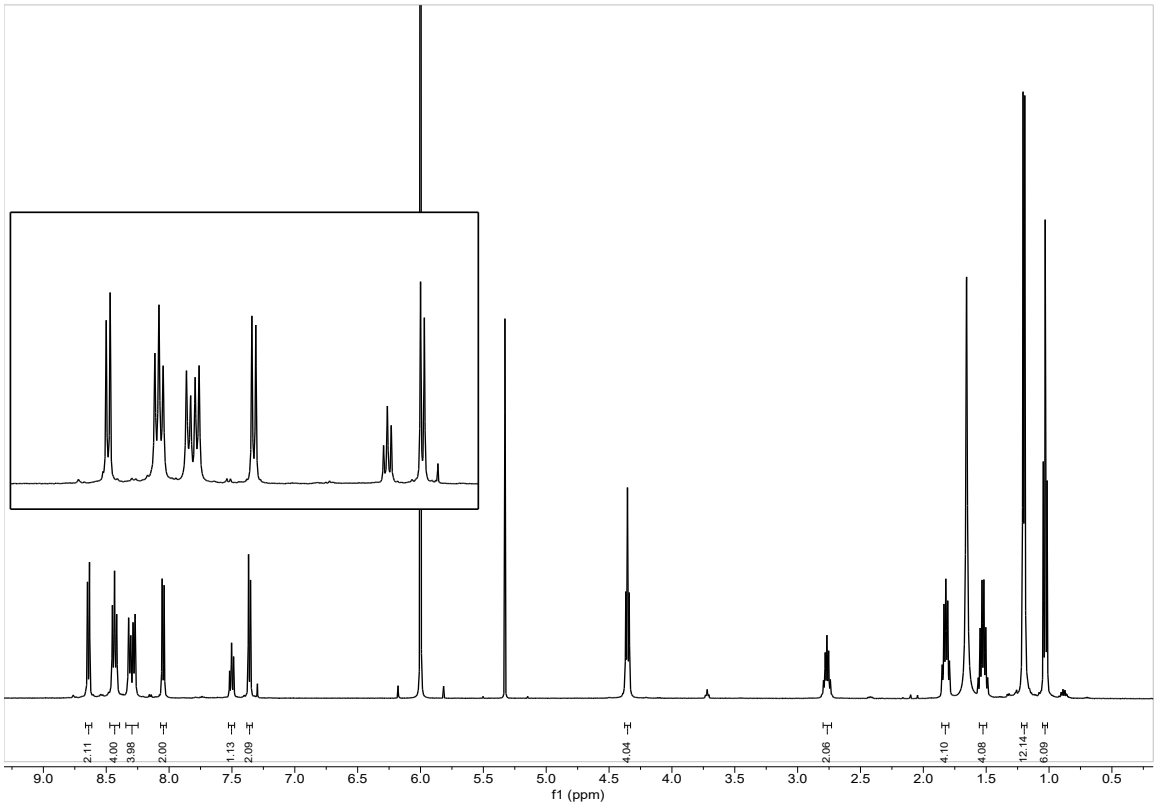

Figure 3-2. ^{1}H NMR of TMIDE, $C_2D_2Cl_4$, 298 K.

3.2.1 SUZUKI-MIYAURA ANCHOR

In order to introduce a substituent capable of *Suzuki-Miyaura* cross coupling reactions, a bromo- and Bpin-bearing imide substituent with 1) sufficient solubility and 2) shortest distance between TDI and future cross-coupled PAH was chosen. Scheme 3-3 displays the three possible approaches, based on imidization of the TMIDE and TMIMA **3-1** and **3-2**, and direct cascade cross-coupling with the respective dibromo-NMI **3-8**.

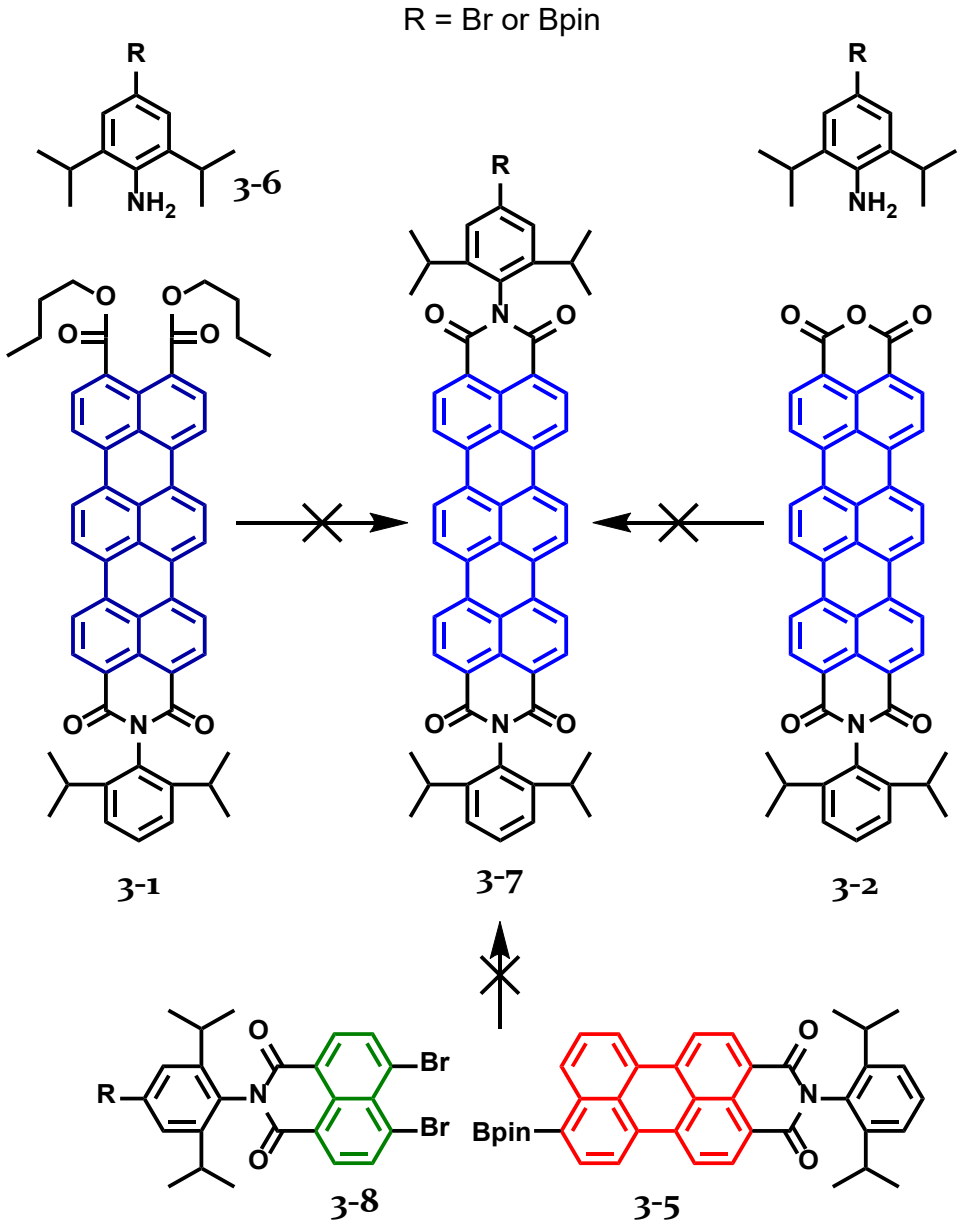

Scheme 3-3. Unsuccessful attempts of imidization of 4-bromo-2,6-di*iso*propylaniline with TMIDE and TMIMA (top) and cascade reaction towards Br-TDI (bottom).

Cascade reaction of 9-Bpin-PMI **3-5** and bromo functionalized NMI **3-8** (Scheme 3-3, bottom) failed, because the bromo-group on the DIPP substituent acted as an additional reaction center in cross-coupling reactions. This, in turn, resulted in several unwanted side-reactions whose structures were assumed based on TLC and MS analysis and are shown in Scheme 3-4. Additionally, the reactivity of **3-6** seemed to be much lower compared to its unsubstituted counterpart **2-21**, as at typical temperatures (140 °C – 180 °C), no reaction could be observed. After increasing the

temperature to 180 °C and beyond, *Suzuki-Miyaura* cross-coupling could be observed, as evidenced by TLC analysis. These harsh conditions, however, also lead to increasing amounts of dehalogenated starting material and resulting intermediates. This further complicated purification procedures, rendering this approach unviable.

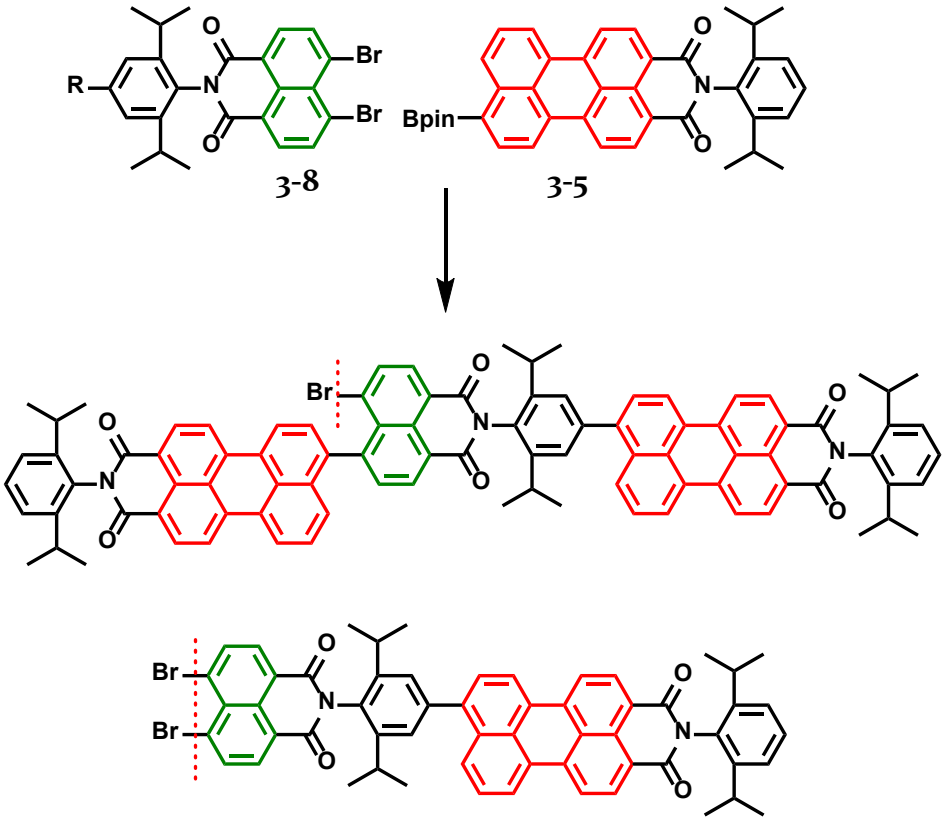

Scheme 3-4. Unintended side-reactions of the cascade cross-coupling approach, assumed from TLC and MS analysis.

As an alternative, 4-bromo-2,6-di*iso*propylaniline (**3-6**) was explored as the nucleophile in imidization reactions with TMIDE **3-1** and TMIMA **3-2** (Scheme 3-3, top), a strategy that was successful in the past.[84] In this instance however, this was not the case, and the attempted reaction conditions are summarized in Table 3-1.

Table 3-1. Conditions for the imidization of **3-6** with TDI precursors **3-1** and **3-2**. [a)] Temperature increase in increments of 20 °C.

	SOLVENT	CATALYST	TEMPERATURE[a)]
1	Imidazole		140 °C – 220 °C
2	Imidazole	$ZnCl_2$	140 °C – 220 °C
3	Imidazole	$Zn(OAc)_2$	160 °C – 220 °C
4	Imidazole	HATU/DIPEA	140 °C – 200 °C
5	Imidazole	4-DMAP	140 °C – 200 °C
6	Quinoline		140 °C – 220 °C
7	Quinoline	$ZnCl_2$	140 °C – 220 °C
8	Quinoline	$Zn(OAc)_2$	160 °C – 220 °C
9	Quinoline	HATU/DIPEA	140 °C – 220 °C
10	Quinoline	4-DMAP	140 °C – 220 °C
11	*o*-Xylene		reflux
12	*o*-Xylene	$Zn(OAc)_2$	reflux
13	NMP	$Zn(OAc)_2$	160 °C – reflux
14	DMF	$Zn(OAc)_2$	120 °C - reflux
15	DMF	HATU/DIPEA	120 °C – reflux

Generally, only reactions in mildly basic solvents, namely in imidazole and quinoline, were, even if unsatisfactory, reproducible. With unreactive nucleophiles in the rylene imide synthesis, imidazole and quinoline are the only solvents that in general enable these unfavorable imidization reactions.[30,127] Up to temperatures of 180 °C, no reaction could be observed in any solvent and catalyst combination. Adding catalysts like $ZnCl_2$ and $Zn(OAc)_2$ as well as increasing the temperatures above 180 °C lead to increasing amounts of TMIMA (if TMIDE was used as the starting material) and TMI (due to decarboxylation of the carboxylic anhydride) in imidazole and quinoline, while the starting material remained unreactive in other solvents. Evidence for hydrolysis as the main reaction in pure quinoline can be drawn from the MALDI-TOF spectrum in Figure 3-3, giving mainly anhydride TMIMA **3-2**. Adding $Zn(OAc)_2$ at the beginning of the reaction, however, lead to an increased amount of the decarboxylation product TMI.

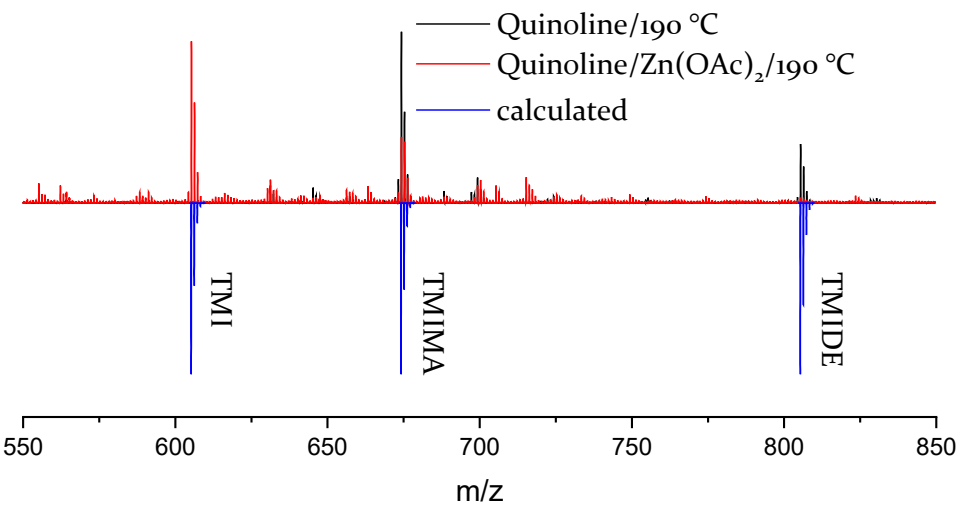

Figure 3-3. MALDI-TOF spectrum of reaction conditions #6 and #8 resulting in decarboxylation.

Interestingly, comparable reaction conditions are known to facilitate the synthesis of PMI from PDA.[128] Similar problems lead to the development of a direct coupling strategy of naphthalene imides in chapter 2, where the conversion of TTE **2-9** and 2,6-diisopropylaniline to DIPP-TDI **2-19** was not successful. Without surprise, however, was the further decrease in nucleophilicity of the bromo-substituted aniline due to its increased electron-deficiency. Similar results were obtained when TMIMA was used as the starting material instead of TMIDE, even though the anhydride should be more reactive, as has already been discussed. Adding catalysts like HATU (hexafluorophosphate azabenzotriazole tetramethyl uronium) and 4-DMAP (4-dimethylaminopyridine) known to catalyze the imidization reaction via intermediately formed activated esters,[129] thus allowing lower reaction temperatures (and in turn avoid decarboxylation), was also not successful.

Derivatives of aniline **3-6** and dibromo-NMI **3-8** with R = Bpin instead of R = Br were synthesized. The same reaction conditions discussed previously were carried out with both boronic ester analogues. The results were similar however: either too many side reactions made any purification efforts futile (cascade approach), or the target compound could not be observed (imidization with TMIDE **3-1** and TMIMA **3-2**).

In the case of a demand for a monofunctionalized TDI suitable for *Suzuki-Miyaura* cross coupling reactions in the future, the (current) synthetic limitations would require the design and synthesis of an anchor group that increases solubility and/or reactivity in imidization reactions. Due to the intended purpose of this monofunctionalized TDI however, it is preferable for the TDI and the PAH to be in as close vicinity as possible. Introduction of a spacer that limits the impact of said restrictions is therefore not desirable. Consequently, further work focused on the introduction of an anchor group that is suitable for *Sonogashira* cross coupling reactions.

3.2.2 SONOGASHIRA ANCHOR

In a first step, 4-trimethylsilyl(ethynyl)aniline and 2,6-di*iso*propyl-4-trimethylsilyl(ethynyl)aniline **3-10** were synthesized from 4-bromoaniline and 2,6-di*iso*propyl-4-bromaniline, respectively (Scheme 3-5). With both anilines, TMIMA **3-2** was used as the starting material for imidization reactions with conditions #1 - #10 in Table 3-1.

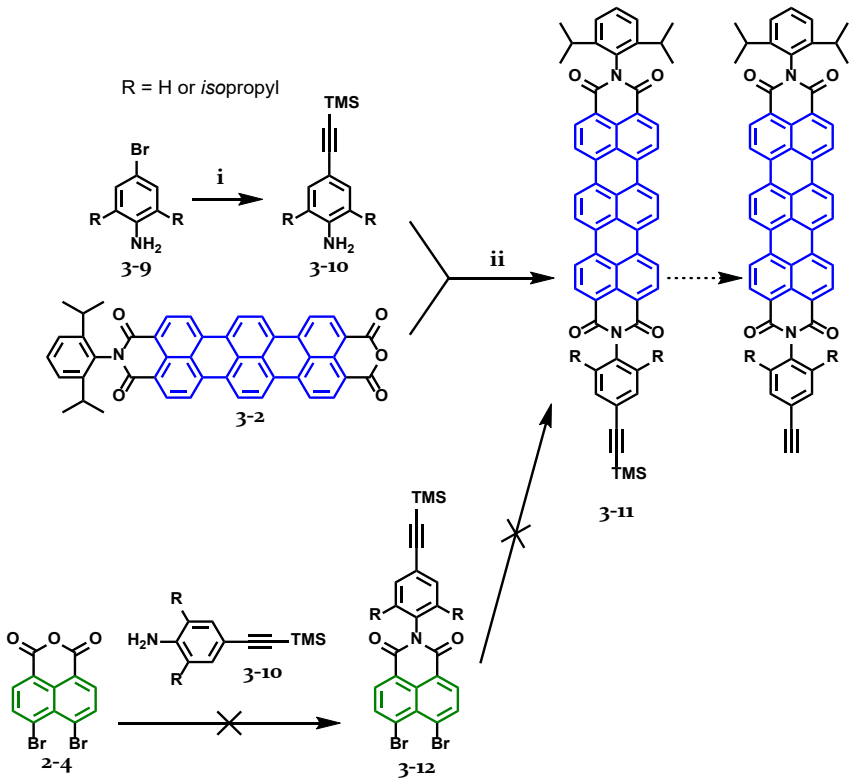

Scheme 3-5. Synthesis of ethynyl-TDI. Conditions: i) trimethylsilylacetylene, CuI, $Pd(PPh_3)_2Cl_2$, ET_3N, THF, 75 °C, 16 h; ii) quinoline, 190 °C, 16 h.

Unfortunately, **3-11** (R = H) could only be observed on one occasion in quinoline at 190 °C without the addition of any catalyst, as shown in the MALDI-TOF spectrum in Figure 3-4. This reaction has so far not been reproducible on a larger scale for further characterization, and ^{1}H NMR analysis was inconclusive due to the limited amount of substance available. Any attempt to repeat the imidization reaction produced the same results as discussed above, namely degradation products of the terrylene compound.

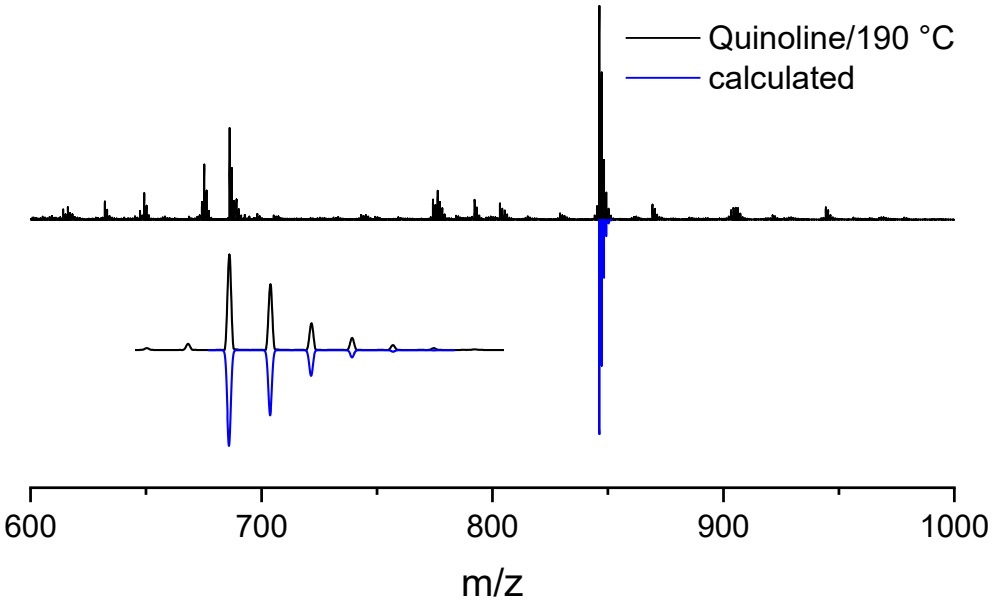

Figure 3-4. MALDI-TOF spectrum of the crude TMS-protected ethynyl-TDI **3-11** with R = H.

Synthesizing the **3-10**-substituted dibromo-NMI **3-12** to obtain TDI **3-11** via the cascade approach was also unsuccessful. Even though imidization of the NMI with less reactive amines gave reliable results in the past, in this case, the acidic conditions appear to suppress any reaction.

While the choice of solvents for the imidization with dibromo-NMA **2-4** requires the addition of an acid to prevent substitution at the bromine groups and is thus limited, the impact of catalysts (see Table 3-1) on this reaction still remains to be explored. Further research in this area could provide better insight into the – at first

glance – simple imidization reaction, and consequently give access to imide motifs that cannot be attained otherwise.

3.3 Synthesis of an Asymmetric TDI

To proof that TMIDE **3-1** can be reproducibly used as a building block for asymmetric TDIs, 1-heptyloctylamine was used to synthesize asymmetric TDI **3-13** (Scheme 3-6). The reaction succeeded at common imidization conditions in imidazole in good yields at a 100 mg scale. TDI **3-13** was characterized by MALDI-TOF MS (Figure 3-5) and NMR spectroscopy (Figure 3-6).

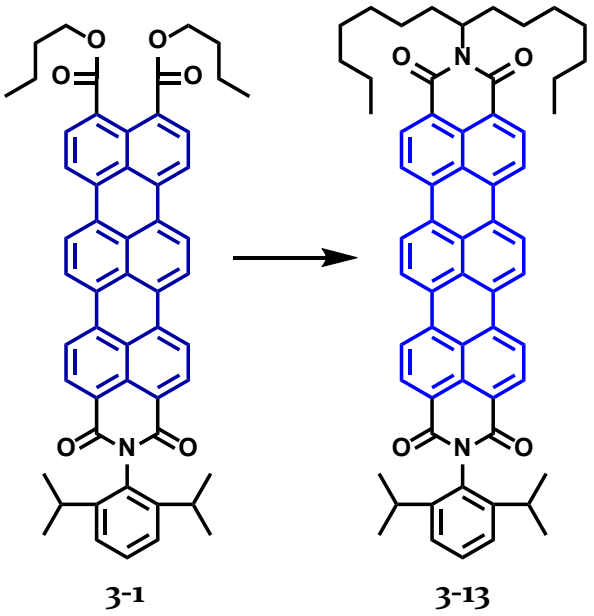

3-1 **3-13**

Scheme 3-6. Synthesis of asymmetric TDI **3-13**. Conditions: imidazole, 170 °C, 16 h.

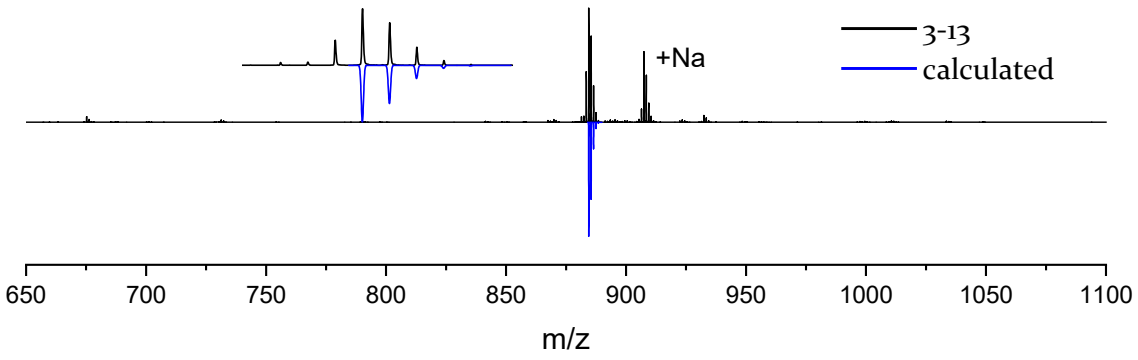

Figure 3-5. MALDI-TOF spectrum of **3-13**.

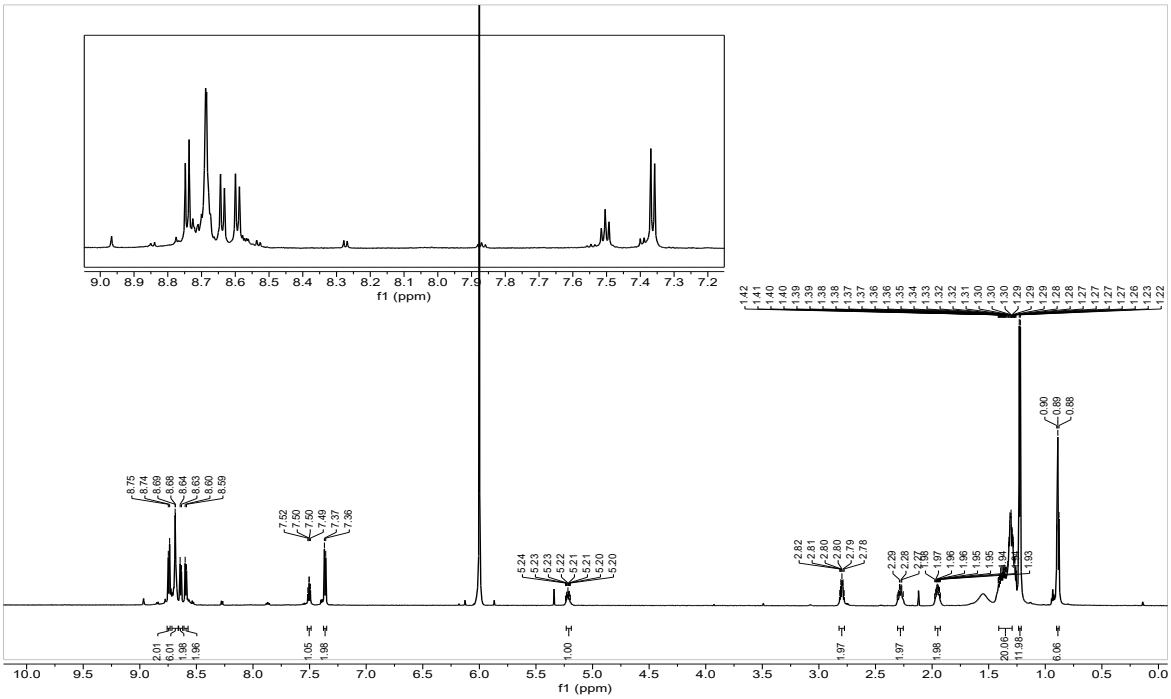

Figure 3-6. ^{1}H NMR spectrum of **3-13**, $C_2D_2Cl_4$, 343 K.

This further corroborates the assumption that the success of imidization reactions in rylene chemistry is primarily guided by the solubility of both reactants; influences that impact the reactivity (solubility, steric demand and electron deficiency of the nucleophile) then require harsher reaction conditions and/or addition of a catalyst, and fully understanding the imidization behavior of terrylene-based compounds will be subject of further research.

3.4 SUMMARY

This chapter has shown the synthesis of an asymmetric terrylene building block that is accessible on a large scale without the need for column chromatography. This building block was successfully used in a subsequent imidization reaction to receive asymmetric TDI **3-13** in excellent yields.

Unsuccessful however were reproducible imidization reactions with less reactive amines that bear functional groups for further cross-coupling to PAHs at a later stage. It has been shown by MALDI-TOF analysis that TDI **3-11** could be synthesized starting from TMIMA **3-2** on a milligram scale, but efforts to repeat this process on a larger scale were without results. During the process of obtaining the target compound, several approaches were pursued and undesired side-reactions were identified, giving insights into future possibilities of optimizing reaction conditions. This leads to the conclusion that the asymmetric building block can generally be a precursor for asymmetrical TDIs even with less reactive nucleophiles, but more research is necessary to develop a reliable protocol that tolerates a broad variety of amines and anilines to be used in imidization reaction with TDI-precursor building blocks.

Largely unexplored remain the possibilities of successfully synthesizing dibromo-NMIs with these problematic amines/anilines. From experience, imidization of naphthalene compounds succeed under milder reaction temperatures than are necessary for terrylene imides, and could in turn avoid the degradation of starting material that was observed in the described terrylene cases under the necessarily harsh conditions. Further investigations into the impact of catalysts could give access to dibromonaphthalene imides with less reactive amines, and consequently to the desired TDIs.

Chapter 4

SYNTHESIS OF A TDI LIGAND FOR IRON(II) SPIN CROSSOVER COMPLEXES

4.1 INTRODUCTION

The difficulties and importance of desymmetrization of rylene diimides have been discussed in chapter 1 based on literature and in chapter 3 based on the experimental results received in this work. In chapter 3, the two asymmetric building blocks TMIDE **3-1** and TMIMA **3-2,** synthesized by the cascade cross-coupling approach developed in chapter 2, were introduced. As an example for their roles as precursors for custom-tailored nanocolorants in highly specialized applications, they will be converted to TDIs attached to coordinating ligands. Eventually, these TDI will serve as the chromophore-ligands in coordination complexes for photophysical studies of the spin states of these coordination complexes.

4.1.1 LIGAND FIELD THEORY AND LIESST-EFFECT

Coordination compounds exist in either high spin or low spin state, which are both determined by factors like the charges of metal and ligands or the type of ligand. According to ligand field theory, ligands with strong field strength Δ_O lead to a high energy difference (crystal field splitting energy) between orbitals. A selection of ligands in order of decreasing field strength and their influence on the spin state in an octahedral d^6 complex is shown in Figure 4-1. If this energy exceeds the pairing energy, a coordination compound is considered to be a low spin (LS) compound, and high spin (HS) if the ligand field strength is weaker than the pairing energy.[130] Thermal spin crossover (SCO) can occur if the energy difference between LS and HS is on the order of thermal energy k_BT (Figure 4-2).[131]

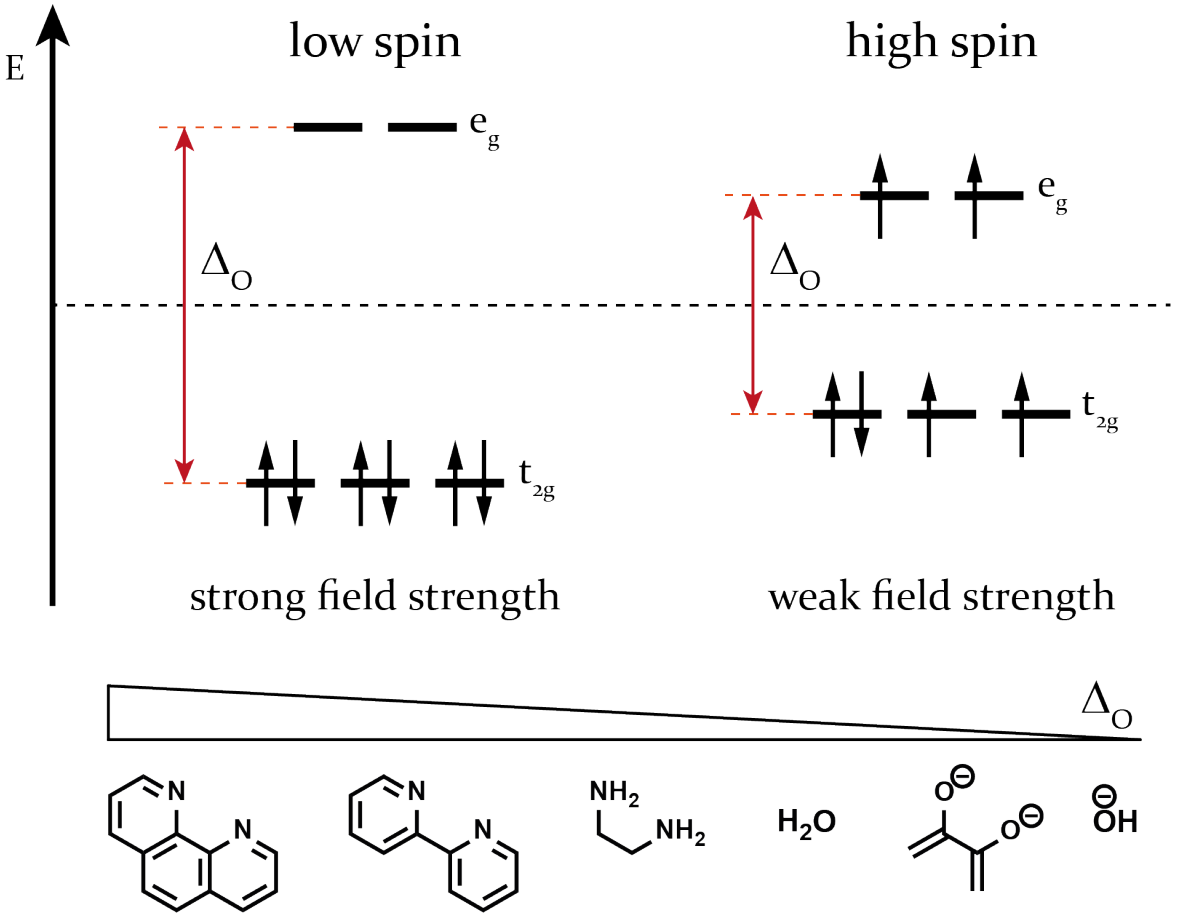

Figure 4-1. Schematic representation of the influence of ligand field strength on the spin state in an octahedral d^6 complex.

Some transition metal complexes are known to undergo SCO under certain conditions. This change of the spin state can be induced via change of temperature, change of pressure, in a magnetic field or with irradiation of light.[132] The *Light-Induced Excited Spin State Trapping*, or LIESST-effect, is of special interest and was discovered by *Spiering at al.* in Mainz in 1984.[133] The LIESST-effect describes the behavior of a sample, typically of Fe(II)-complexes, below a temperature at which thermal SCO does not occur. Irradiation of the sample at 514 nm (wavelength of Argon laser) excites the LS state and is followed by two intersystem crossing processes (via the intermediate state IS) to the HS state. Because the decay of the ^{5}T high spin state to the ^{1}A low spin state is spin- and parity-forbidden, the HS state is metastable at low temperatures.

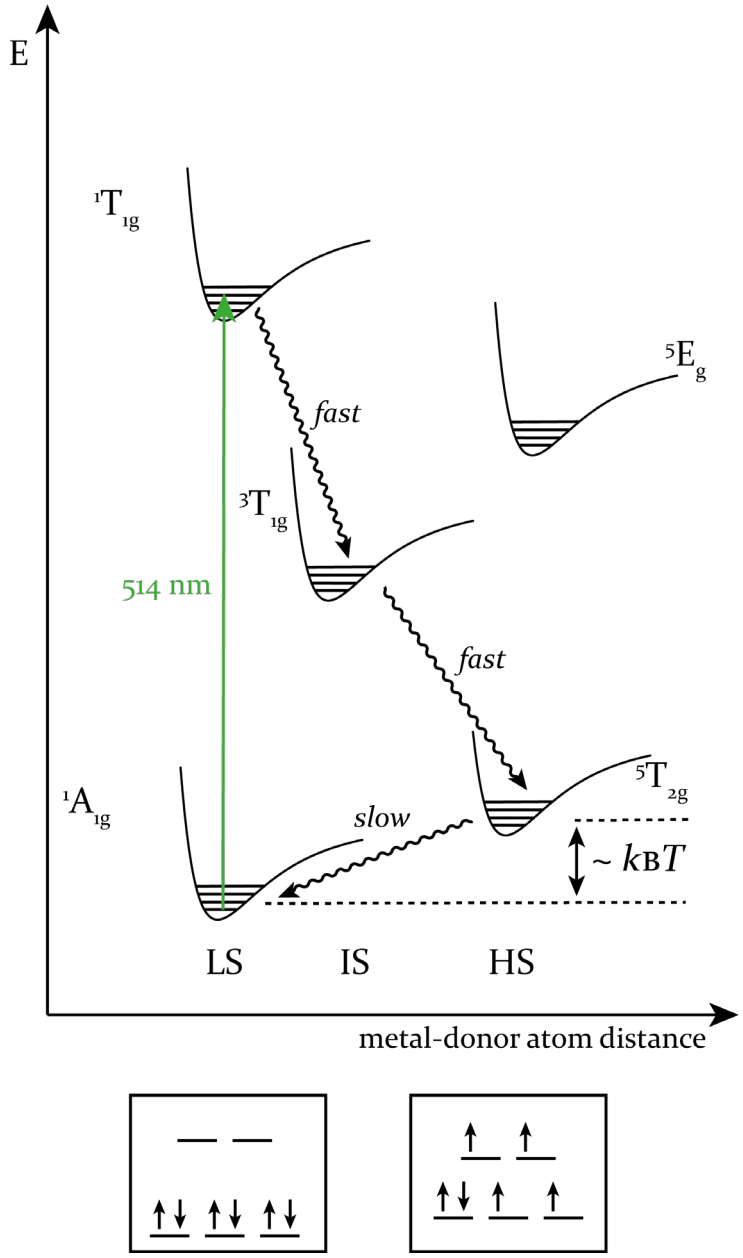

Figure 4-2. Simplified Jablonski diagram for the photophysical processes of the LIESST effect in Fe(II) complexes. Simplified illustration showing only the $^1A_1 \rightarrow {}^5T_2$ transition, derived from the literature.[132]

Spin crossover results in magnetic, optical, vibrational and structural changes of the complex. These changes allow detection of the LS-HS conversion via various methods, including Mössbauer and IR spectroscopy, or DSC analysis.[134] But until now, no emission spectroscopy has been used to detect this kind of spin crossover.

4.1.2 Concept for the Synthesis

Using the concept of fluorescence probing discussed in chapter 3, a yet unexplored possibility for the detection of HS-LS switching based on TDI as the chromophore will be investigated. If a chromophore probe is placed near the coordination compound, changes that result from the different distributions of 3d electrons in the LS and HS state should affect the electron distribution and bond lengths of the chromophore. Single molecule fluorescence spectroscopy could then give insight into the influence of the spin states on the photophysical properties such as emission maxima and fluorescence or triplet-state lifetimes of the coordination complex.

The goal of this chapter is to determine if the cascade cross-coupling approach can be used to synthesize a TDI that is linked to a chelating ligand capable of complexing Fe(II). The envisioned coordination compound **4-1** can be seen in Figure 4-3. Irradiation is conducted at 514 nm to enforce the *LIESST*-effect, therefore no absorption of the chromophore should take place at this wavelength. As evidenced in the absorption spectrum in Figure 2-9, TDI is the ideal chromophore for this task with the first absorption maximum found above 550 nm. Typically, the reversed *LIESST* effect can be observed when radiating the sample at 820 nm, which is above the absorption range of TDI.[132] Should the TDI-ligand prove to be a viable ligand for iron(II) SCO complexes, it should be possible to spectroscopically detect switching between the high and low spin complex on a single molecule level.

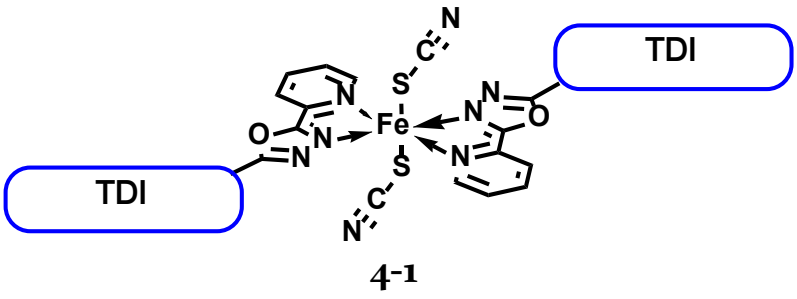

4-1

Figure 4-3. Concept of the Fe(II)-TDI coordination complex.

4.2 Synthesis of the TDI-Pyridine-Oxadiazole Ligand

The molecule design that was employed in this work is based on $[Fe^{II}(L)_2(SCN)_2]$ complexes, with 2,5-di(2-pyridyl)-1,3,4-oxadiazole (**4-2)** as the Ligand L, that have been used in *LIESST* effect studies before.[135] Incorporation into a TDI scaffold via the imide position requires the presence of a primary amine functionality. For this purpose, 5-(pyridin-2-yl)-1,3,4-oxadiazol-2-amine (**4-3)** was synthesized by the *Rentschler* group, that will act as a bidentate chelating ligand with the required amine attached (Figure 4-4).

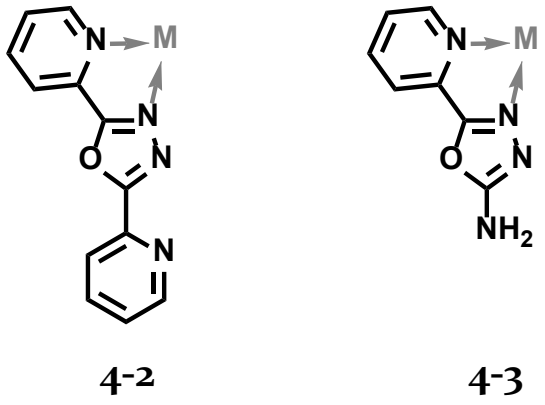

4-2 **4-3**

Figure 4-4. Bidentate chelating ligands 2,5-di(2-pyridyl)-1,3,4-oxadiazole **4-2** (left) and 5-(pyridin-2-yl)-1,3,4-oxadiazol-2-amine **4-3** (right).

With 5-(pyridin-2-yl)-1,3,4-oxadiazol-2-amine in hand, first attempts of imidization with TMIDE **3-1** were unsuccessful (Scheme 4-1). Even though on a first glance, steric hindrance and low nucleophilicity didn't suggest posing a problem in the imidization with amine **4-3**, no TDI could be observed via TLC nor MALDI-TOF analysis. The tested reaction conditions were similar to those listed in Table 3-1, and equally, hydrolysis and decarboxylation occurred at the majority of reaction conditions.

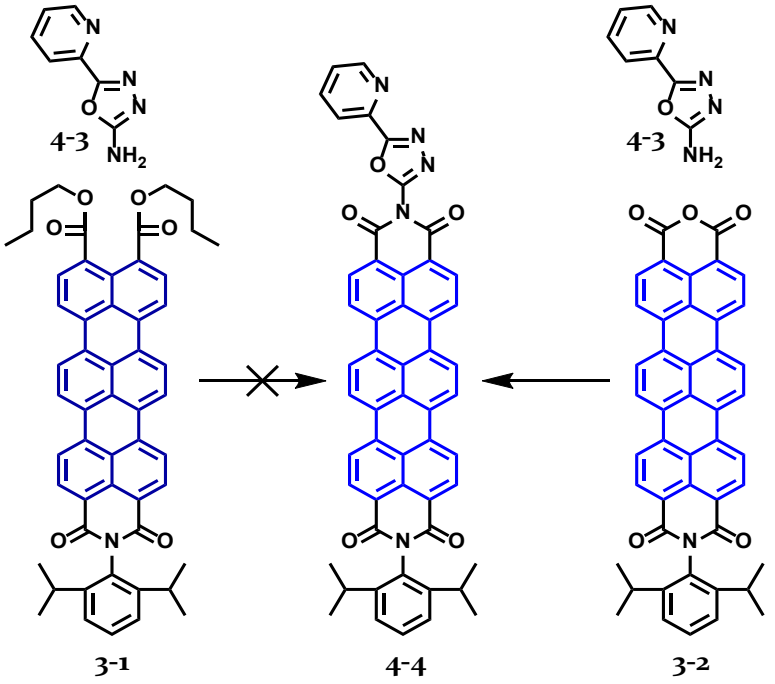

Scheme 4-1. Synthesis of TDI-pyridin-oxadiazole ligand **4-4**. Conditions: quinoline, 190 °C, 48 h.

Imidization of **4-3** and TMIMA **3-2** in quinolone at 190 °C was partially successful, as can be seen in the MALDI-TOF spectrum in Figure 4-5. However, after 48 h, only a small amount of TMIMA was converted to the target TDI **4-4**, suggesting a low reactivity of the nucleophile **4-3**.

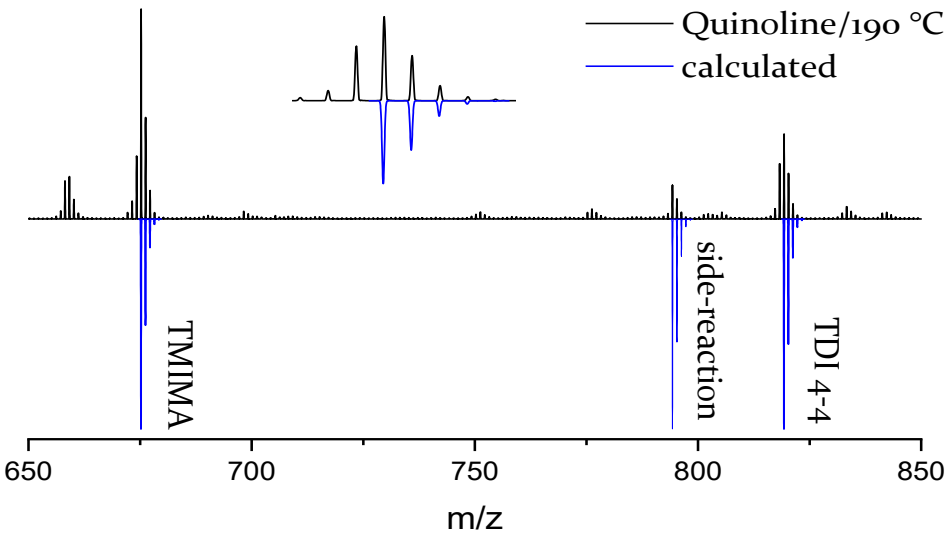

Figure 4-5. MALDI-TOF spectrum of the crude TDI-pyridin-oxadiazole ligand **4-4**.

Unfortunately, the low reaction rate resulted in the unwanted side reactions illustrated in Scheme 4-2; usually, the initial nucleophilic substitution of the amine is followed by hydrolysis and the imide is formed. In this case however, the low reaction rate in addition to the harsh reaction conditions (high temperatures, slightly basic solvent that can act as a nucleophilic catalyst) seems to result in a competing decarboxylation reaction. While unusual, this mono-decarboxylation process has been reported in the past on several occasions.[136–138]

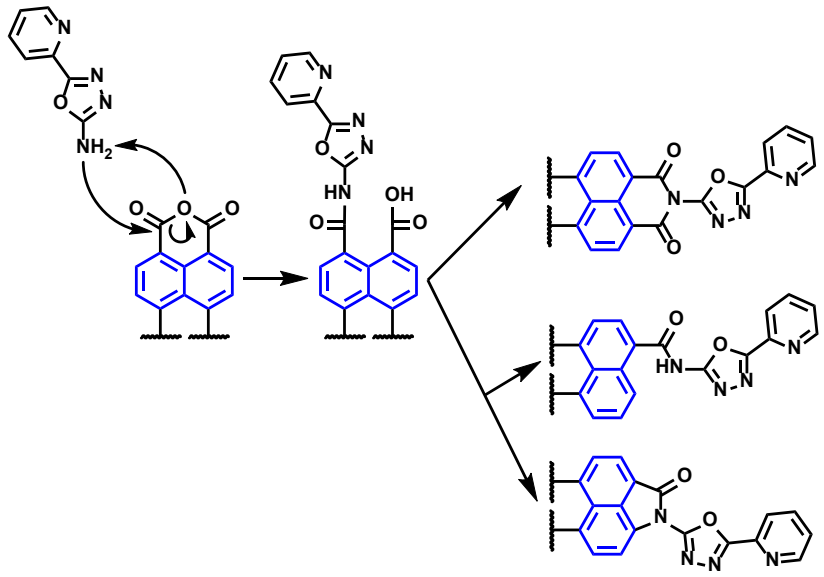

Scheme 4-2. Competing imidization and decarboxylation processes.

The solubility of TDI **4-2** however was too low for TDI **4-2** to be isolated from the starting material and the decarboxylated side product via column chromatography. This not only complicated characterization, but posed potential problems in successive complexation reactions. Typically, concentrated solutions of metal salt and ligand are prepared, and the complex forms by slow diffusion. It is important to use both components in a known ratio to have control over the coordination geometries, and a suspension of inseparable starting material and TDI-ligand with poor solubility is detrimental to this requirement.[135,139] Nonetheless, due to the increased solubility of TDI **4-4** compared to TMIMA **3-2** in chloroform, samples of **4-4** were collected for subsequent complexation reactions by filtration of the reaction mixture and collection of the filtrate with a higher **4-4** to **3-2** ratio.

In order to purify and fully characterize the TDI-ligand, a more soluble derivative was synthesized as outlined in Scheme 4-3:

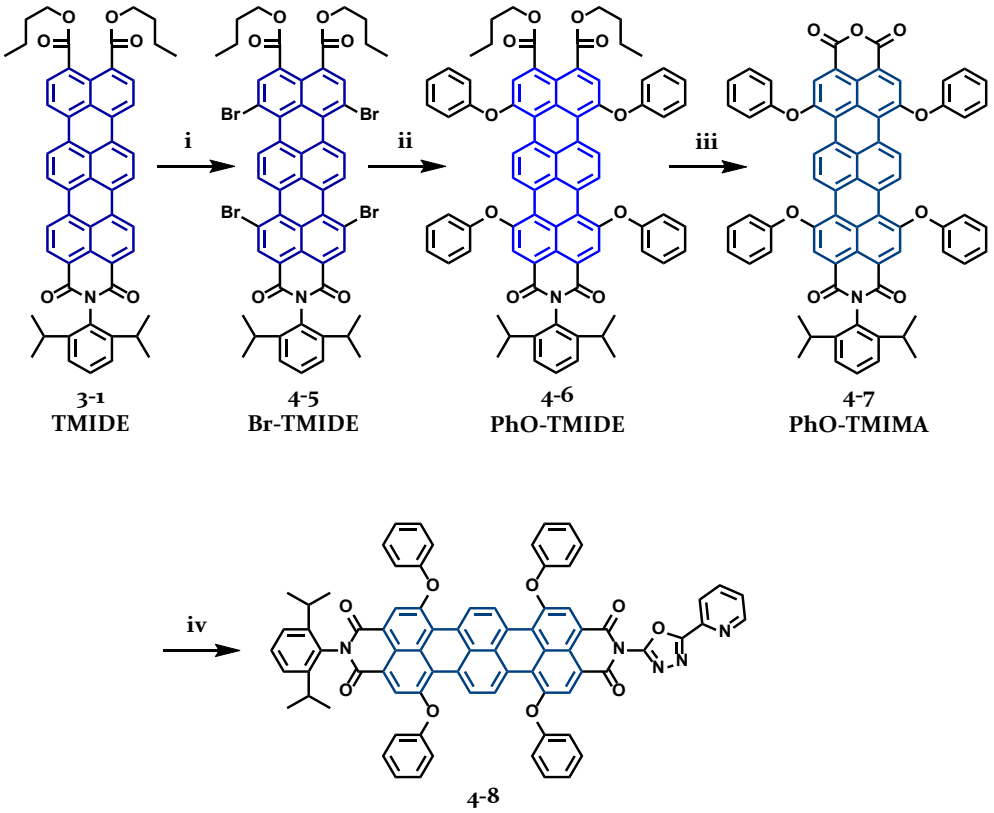

Scheme 4-3. Synthesis of bay-substituted TDI-ligand. Conditions: i) Br_2, $CHCl_3$, 60 °C, 3 h, 95 %; ii), phenol, K_2CO_3, NMP, 120 °C, 16 h, 85 %; iii) *p*-TsOH, toluene, 110 °C, 16 h, 97 %; iv) **4-3**, quinoline, 183 °C, 24 h, 10 %.

Bromination of TMIDE **3-1** in chloroform gave 3,6,11,14-tetrabromo-TMIDE without any over- or underbrominated TMIDE as side-products. This is important, as separation of different bromination products via column chromatography is time consuming, especially on a large scale. Figure 4-6 displays the MALDI-TOF spectrum after bromination and precipitation. In addition to the signal with the highest intensity that is ascribed to the TMIDE **4-5**, a signal with $\Delta m/z = 33.8$ can be seen. This signal neither matches the m/z of tri-brominated TMIDE nor its respective potassium salt, and was therefore assumed to be a fragment of **4-5** caused by the ionization process.

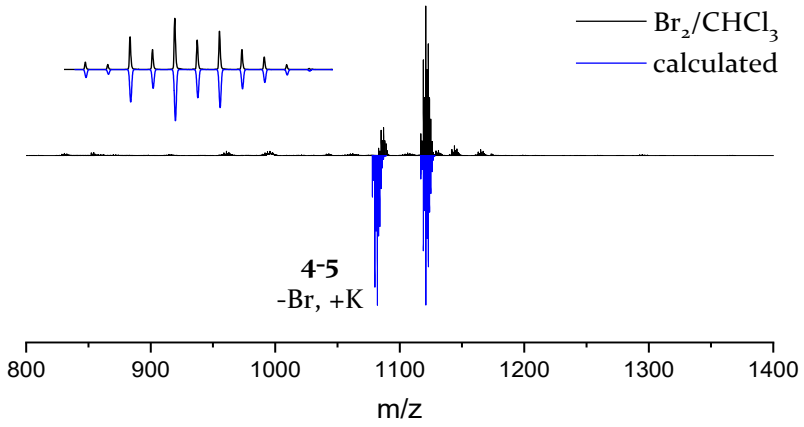

Figure 4-6. MALDI-TOF spectrum of tetrabrominated TMIDE **4-5**.

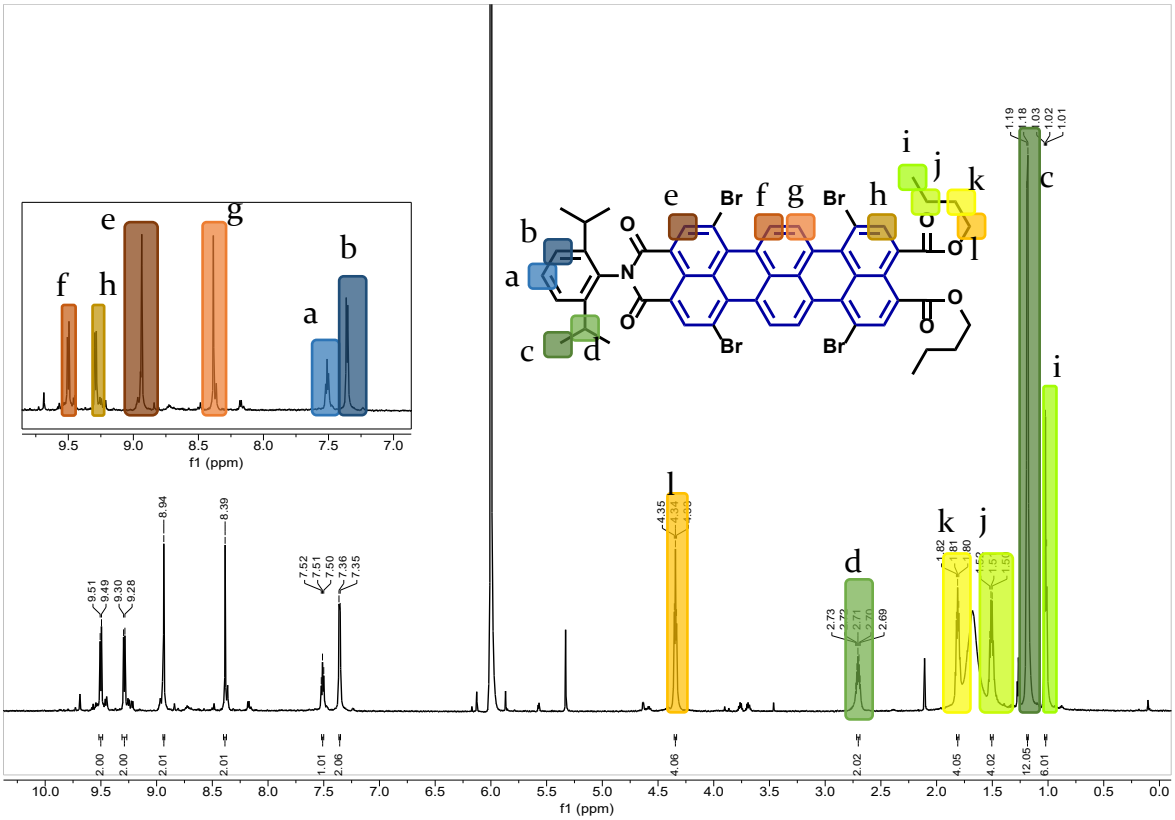

Figure 4-7. ^{1}H NMR spectrum of Br-TMIDE **4-5**, $C_2D_2Cl_4$, 298 K.

This conclusion was further corroborated by the lack of presence of additional compounds both in TLC analysis and in the ^{1}H NMR spectrum in Figure 4-7. Because extensive chromatographic purification was expected for the final target compound, **4-5** was used without further purification to investigate the origin of the additional mass signal with $\Delta m/z = 33.8$. By stirring with phenol and potassium carbonate in

NMP at 120 °C following the well-reported nucleophilic *bay*-substitution procedure,[52] tetra-phenoxylated TMIDE **4-6** could be obtained after filtering over silica in 85 % yield.

Figure 4-8 shows the absorption and emission spectra of TMIDEs **3-1**, **4-5** and **4-6** in toluene and Table 4-1 summarizes the optical data. Phenoxylation of TMIDE results in a bathochromic shift of 9 nm from $\lambda_{abs,max}$ = 633 nm (for TMIDE **3-1**) to 642 nm, and should therefore not interfere with the *LIESST* irradiation wavelengths of 514 nm and 820 nm after the subsequent imidization reaction (and thus a further bathochromic shift, see Table 2-2). It is expected that the absorption profiles of both unsubstituted and *bay*-phenoxylated TDIs will be suitable to investigate the *LIESST*-effect.

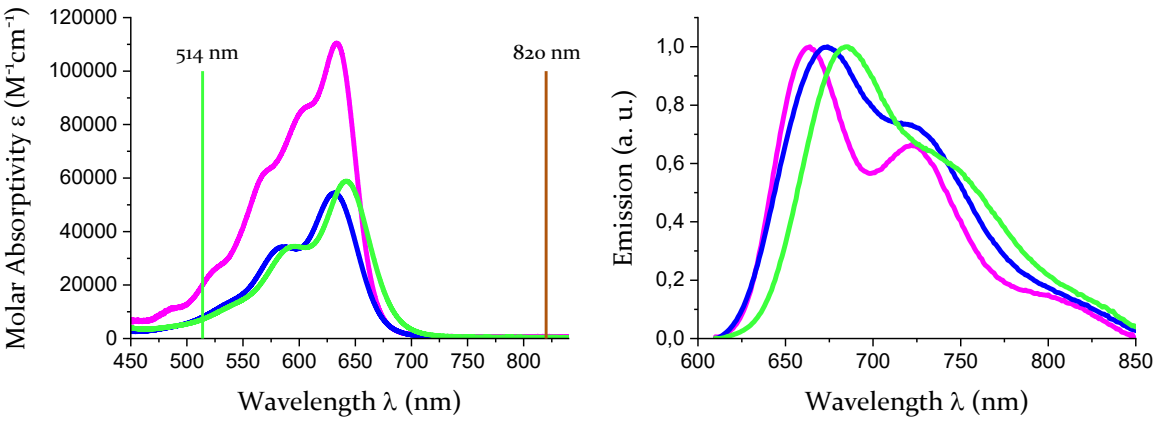

Figure 4-8. UV-VIS absorption (left) and emission (right) spectra of compound TMIDE **3-1** (magenta), Br-TMIDE **4-5** (blue), and PhO-TMIDE **4-6** (green) in toluene, conc. ~10^{-6} M

Table 4-1. Optical data of TMIDE **3-1**, Br-TMIDE **4-5**, and PhO-TMIDE **4-6.**

	$\lambda_{abs,max}$ (nm)	ε_0 ($M^{-1}cm^{-1}$)	$\lambda_{em,max}$ (nm)
3-1	633	110478	664
4-5	631	54410	674
4-6	642	58861	684

Acidic hydrolysis in toluene with *p*-toluenesulfonic acid as the catalyst provided the moderately soluble tetra-phenoxylated PhO-TMIMA **4-7** as the precursor for the

phenoxylated TDI-ligand **4-8** in close to quantitative yield (Scheme 4-4).[46] Due to the presence of *bay*-phenoxy substituents, *p*-toluenesulfonic acid instead of sulfuric acid (see Scheme 3-2) had to be used as the acidic catalyst, as the latter would lead to sulfonation of the substituents.[140]

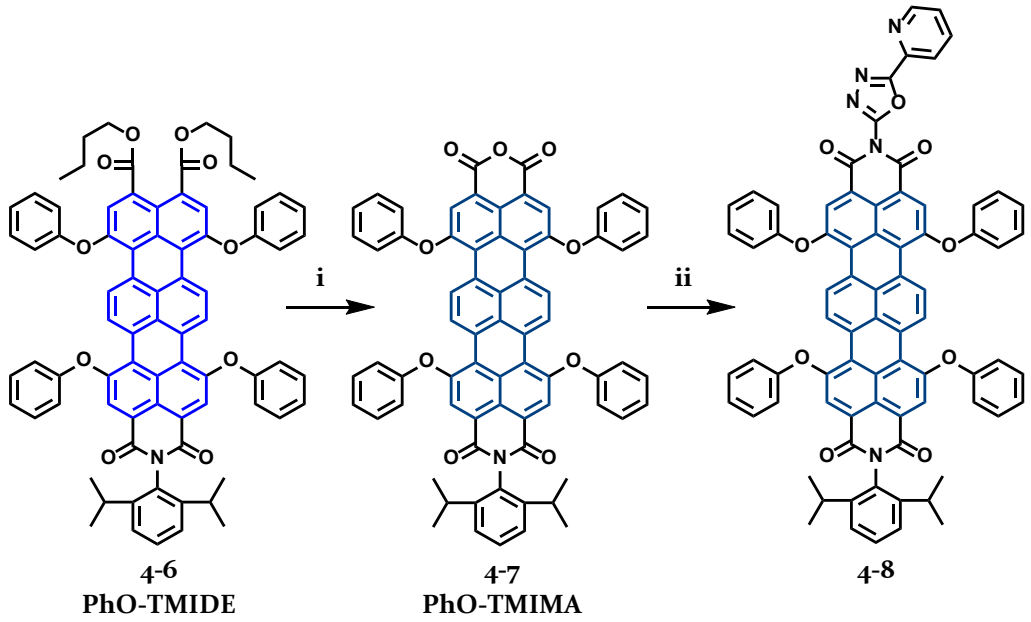

Scheme 4-4. Hydrolysis and imidization reactions to receive TDI-ligand **4-8**. Conditions: i) *p*-TsOH, toluene, 110 °C, 16 h, 97 %; ii) **4-3**, quinoline, 183 °C, 24 h, 10 %.

The following imidization reaction suffered from the same side reactions that were discussed previously. In addition to decarboxylation, the high temperatures necessary for the imidization reaction between PhO-TMIMA **4-7** and the amine **4-3** resulted in the loss of phenoxy groups in the target compound. Precise control of the reaction temperature (too low and no imidization can be observed, too high and side reactions dominate the product mixture) and control of the progress via TLC was necessary to terminate the reaction at the right time.

Nonetheless, the increased solubility compared to unsubstituted TDI-ligand **4-4** made column chromatography ($CHCl_3$/MeOH 50:1) possible. After purification, 9 mg of the target compound **4-8** could be obtained in 10 % yield. Considering the complex mixture of side products with similar R_f values as well as the improved, but still low, solubility, this yield was acceptable for the intended purpose.

In the MALDI-TOF spectrum in Figure 4-9, a signal (<5 % in m/z intensity) of TDI **4-8** with only three phenoxy-substituents is visible. It is unclear whether the cause for the apparent loss of phenoxy-substituents is due to the harsh reaction conditions (basic solvent, high temperature) or fragmentation caused by the ionization process during MALDI-TOF measurements. The characterization of the precursor material did not reveal the presence of underbrominated species and can be excluded as the reason for the apparent impurity. TDI **4-8** was purified two times by consecutive column chromatography ($CHCl_3$/MeOH 10:1 and 95:5) and subsequently by size exclusion chromatography. After this purification process, TLC analysis did not reveal the presence of a second, triphenoxylated TDI, supporting the assumption that the additional signal in Figure 4-9 is caused by the ionization process.

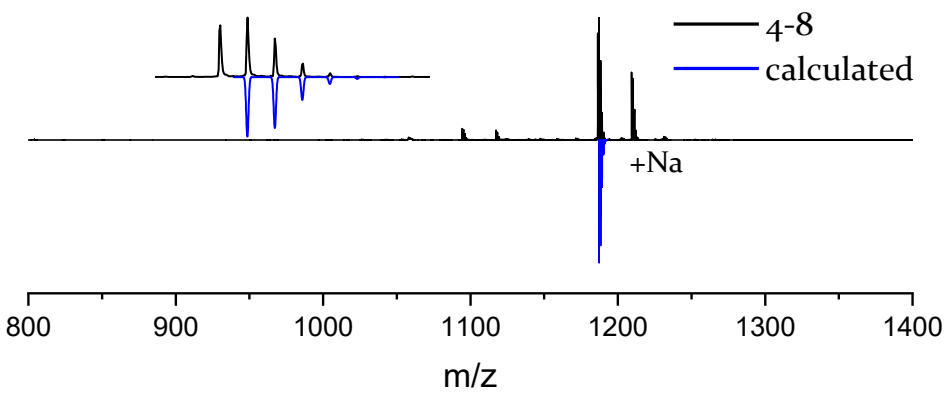

Figure 4-9. MALDI-TOF spectrum of TDI **4-8**.

The identity of **4-8** was further confirmed by 1D and 2D NMR analysis in Figure 4-10 and Figure 4-11. High temperature measurements were necessary to resolve most signals, but due to the large number of aromatic protons, chemical shifts and coupling patterns in the area between 7.20 ppm and 7.60 ppm cannot be fully resolved. 2D NMR experiments however allowed the assignment of the respective protons b, g, h, I, j and k to one of the two unresolved multiplets.

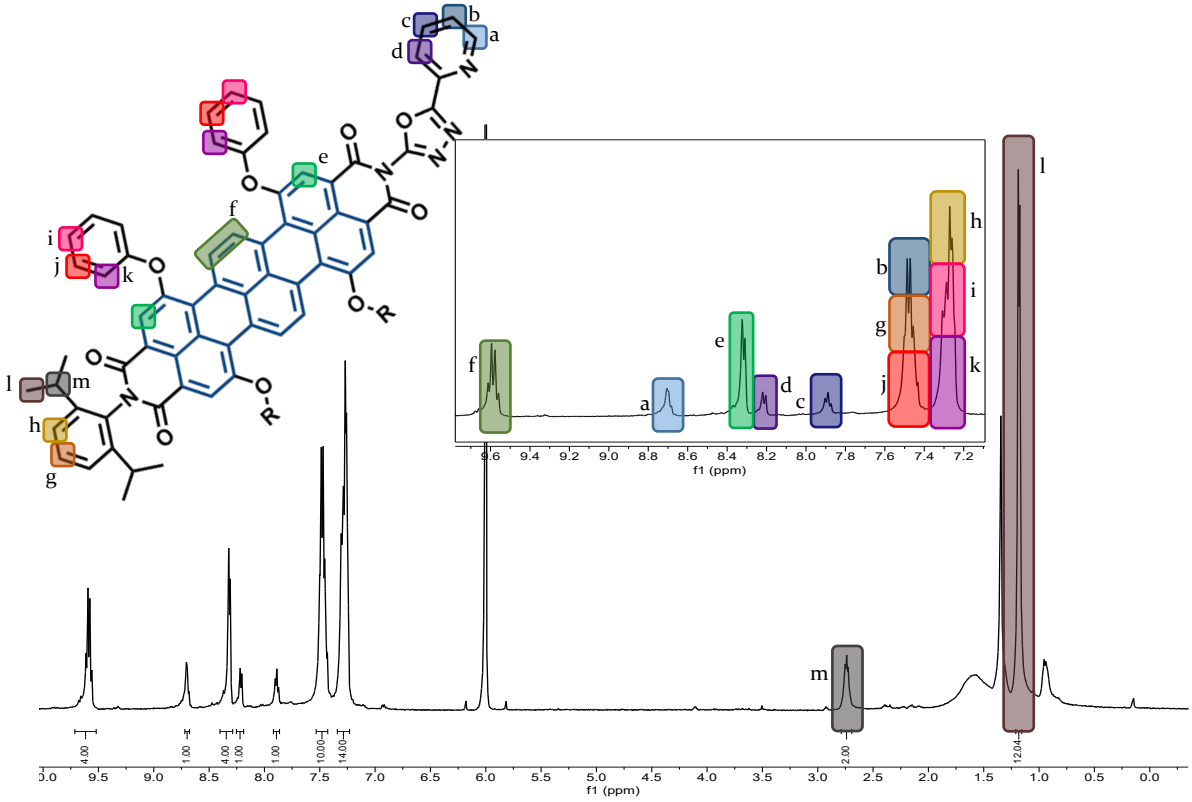

Figure 4-10. ^{1}H NMR of TDI-Ligand **4-8**, $C_2H_2Cl_4$, 373 K.

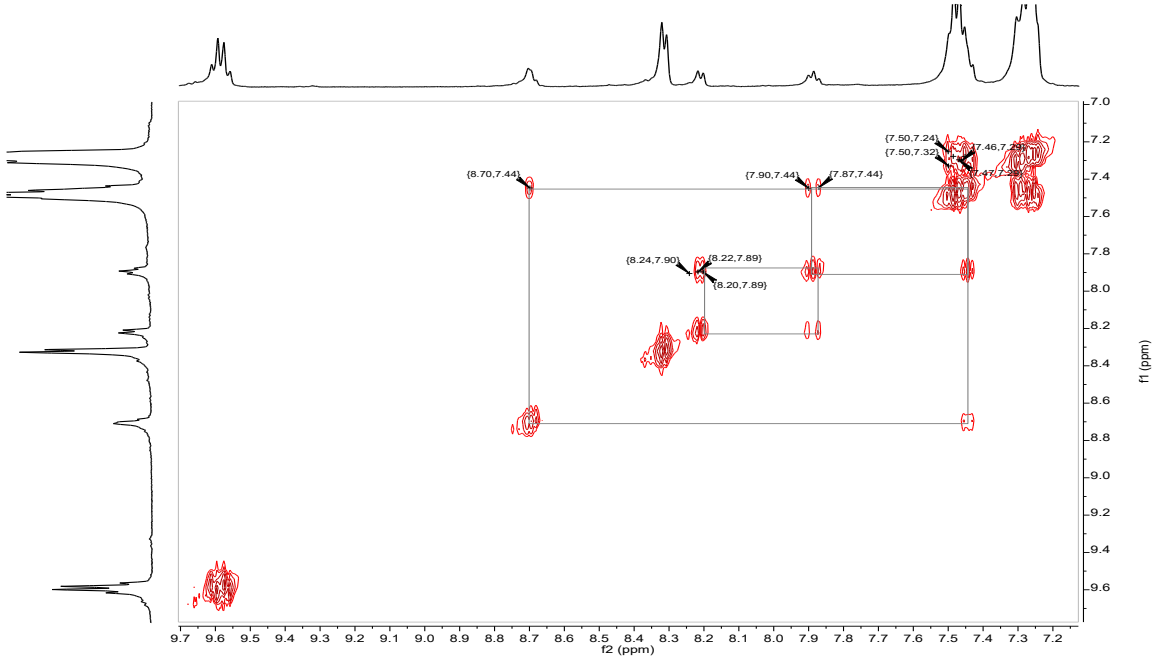

Figure 4-11. ^{1}H-^{1}H COSY NMR of TDI-Ligand **4-8**, $C_2H_2Cl_4$, 373 K.

The absorption spectrum of TDI ligand **4-8** in Figure 4-12 clearly shows that both wavelengths for *LIESST* and reversed-*LIESST* effects at 514 nm and 820 nm lie outside the absorption range of the chromophore. Therefore, irradiation of the complex to induce spin crossover does not excite the chromophore, and emission detection is detached from switching between high- and low-spin states. Consequently, the TDI ligand fulfills the basic requirements for emission-based detection of light-induced spin crossover on a single molecule level in the envisioned Fe(II) coordination complex.

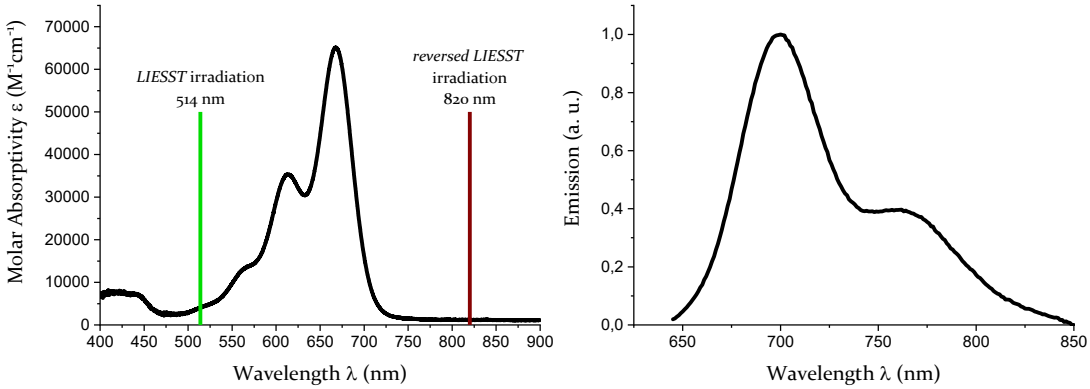

Figure 4-12. UV-VIS absorption (left) and emission (right) spectrum of TDI ligand **4-8** in toluene, conc. ~10^{-6} M.

PHOTOPHYSICAL PROPERTIES OF THE COORDINATION COMPLEX

The complexation reactions are part of ongoing research in the *Rentschler* group. Figure 4-13 illustrates the expected $[Fe(II)L_2(SCN)_2]$ coordination complex.

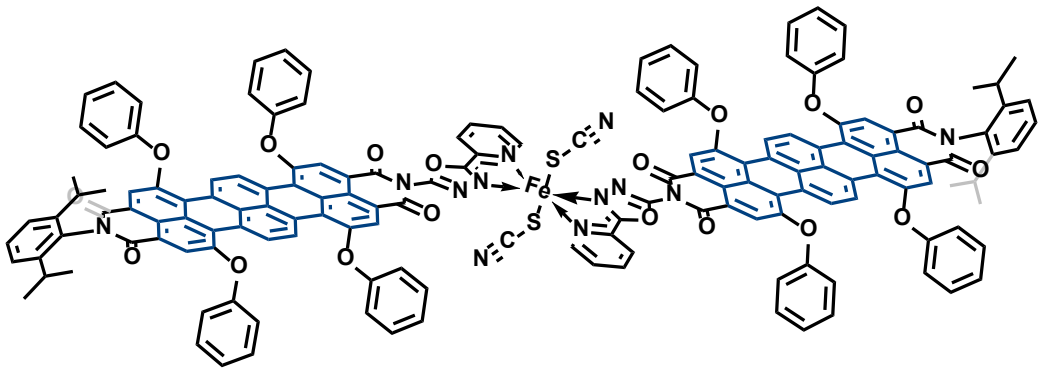

Figure 4-13. Schematic representation of the $[Fe(II)L_2(SCN)_2]$ complex.

With the ambient-stable TDI-Ligands provided by our group in hand, initial complexation reactions were carried out by *Julian Eppelsheimer* and *Fabian Fürmeyer*. To prepare the $Fe(SCN)_2$ solution, $FeSO_4$ and KSCN were dissolved in MeOH separately, combined, and the precipitated K_2SO_4 was filtered from the $Fe(SCN)_2$ solution. The two TDI-ligands were each dissolved in chloroform and layered with the $Fe(SCN)_2$ solution in inert atmosphere in a glovebox in separate vials. After several days, a change in color of the solution with TDI **4-4** could be observed, suggesting that a complexation reaction was successful. After exposition to ambient conditions, the color reverted back, as demonstrated in Figure 4-14.

Figure 4-14. Assumed complex solution inside (left) and outside (right) of the glovebox.

Upon comparison of the absorption spectrum (measured in sealed cuvettes in inert atmosphere) of the assumed coordination complex with the spectra of TDI and $Fe(SCN)_2$ (Figure 4-15), a broad, intense band with an absorption maximum at $\lambda_{abs,max}$ = 514 nm became visible that was not present in either reactant solution. The high intensity and bathochromic shift relative to the $Fe(SCN)_2$ absorption band suggests a charge-transfer transition.

In order to further investigate the photophysical properties of the coordination complex in inert atmosphere, polymer solutions (ZEONEX® 330R) with aliquots of the complex solution were prepared inside the glovebox. After polymerization on

glass slides in the inert atmosphere, the samples were sealed with a second slide to ensure oxygen-free handling of the samples outside the glovebox.

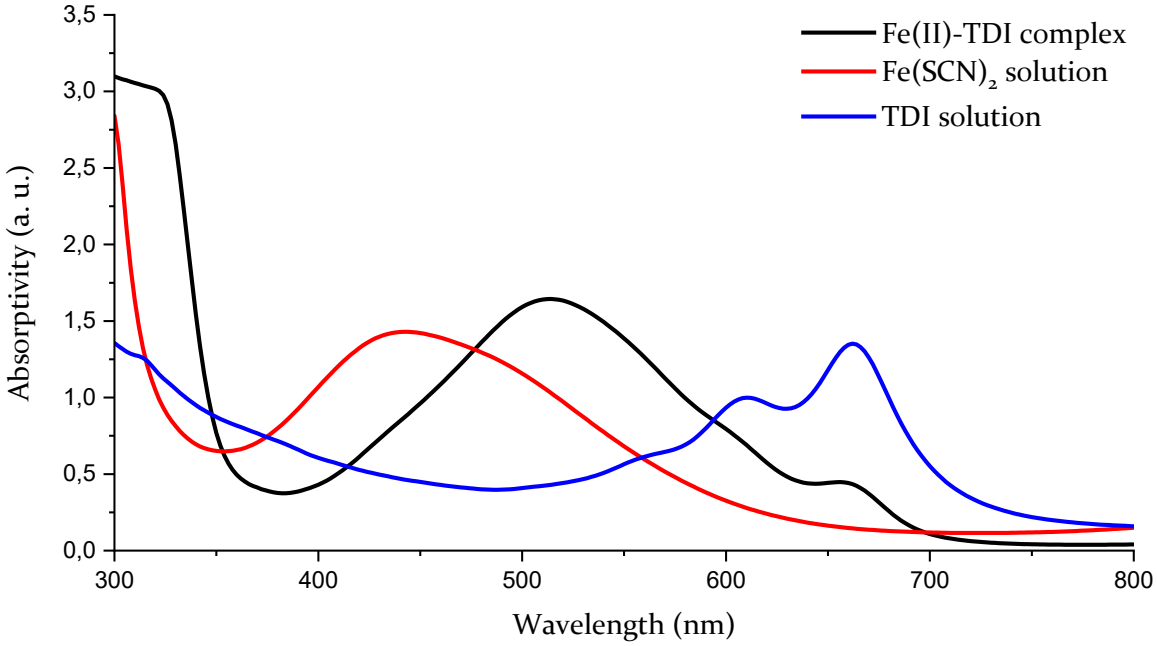

Figure 4-15. Absorption spectra of the *bay*-unsubstituted TDI Ligand **4-4** (blue, in $CHCl_3$), $Fe(SCN)_2$ solution (red, in MeOH) and the suspected Fe(II)-TDI complex (black, in $CHCl_3$/MeOH). Data provided by *Julian Eppelsheimer*.

Investigations into the photophysical properties of the ensemble as well as on the single molecule level at low temperatures are part of the ongoing research by *Marius Bauer* of the *Basché* group.

4.3 Summary

In this chapter, the tetra-phenoxy substituted TDI ligand **4-8** was successfully synthesized based on the TMIDE precursor developed in chapter 3. Imidization reactions suffered from the same side-reactions discussed elaborately in earlier chapters, but the reaction rate caused by the low reactivity of the pyridine-oxadiazole amine allowed insights into the decarboxylation processes that cause these side-products. The introduction of phenoxy-substituents into the *bay*-positions increased the solubility of the monoanhydride precursor **4-7** sufficiently for imidization reactions to

take place, although still under harsh conditions; the increased solubility nonetheless made isolation of TDI ligand **4-8** possible.

In accordance with the requirements stated in the introduction, the absorption range of **4-8** lies between both irradiation wavelengths that are used for the light-induced spin crossover. Consequently, the TDI ligand should be the ideal chromophore for emission-based single-molecule detection of the *LIESST*-effect

The knowledge about side-reactions gained in this chapter might also help to improve conditions for imidization reactions in the future. The hypothesis that a lack of solubility of the terrylene precursor is the main reason for unsuccessful imidization reactions was further corroborated. Whilst only a small amount of *bay*-unsubstituted TMIMA **3-2** was converted to the target compound **4-4** even after 48 h, the introduction of phenoxy substituents improving the solubility allowed the successful synthesis, purification and characterization of the envisioned TDI ligand **4-8**. Conclusively, when designing new functional terrylene-based materials, the solubility of the reactants needs to play a central role in the decision-making process.

Chapter 5
WATER-SOLUBLE TDI CATIONS AS FLUORESCENT PROBES

5.1 INTRODUCTION

Chapter 3 and 4 focused on the synthesis of monofunctional TDIs and their application as fluorescent probes via direct attachment to a second molecule. The adaptability of rylene imides to be modified according to the requirements of each task was utilized to custom-tailor an auxiliary TDI probe to gain information on the spin states in a coordination complex.

In contrast, a symmetric TDI based on the cascade cross-coupling approach will be synthesized in this chapter to be used as the probing chromophore in a host-guest chemosensor. Instead of gaining information about a molecule via the photophysical properties of the directly attached TDI probe, the host-guest chemosensor is going to be used to monitor changes in concentration of an analyte without direct attachment to the TDI probe via a fluorescence turn-on/turn-off mechanism.

Reaction monitoring via chemosensors, especially of enzymatic redox and hydrolysis reactions, is a topic of high interest that ranges from utilizing electrochemical sensing to graphene- and carbon nanotube-based chemosensors.[141–147] By tracking the change in concentration of analytes, knowledge about the enzymatic activity can be gained. Detection of these changes in concentration is often emission based as it is highly sensitive and allows for real-time response. However, intrinsic fluorescence is uncommon in substrate-product pairs, and often indistinguishable from each other.[148] A way to circumvent this restriction is fluorescent labeling of the substrate. This, however, increases the cost and effort that goes into studies of enzymatic activity, as it requires additional synthetic steps. Furthermore, altering the substrate on a molecular level can lead to non-representative results, because the introduced fluorophore can severely change substrate binding, catalytic turnover or solubility.[149]

One way of reaction monitoring enzymatic activity that avoids fluorescence labeling is the utilization of a self-assembling host-guest system based on a macrocyclic host and a chromophore as the fluorescent guest molecule, demonstrated by *Biedermann et al.* (Figure 5-1).[150] As the host, cucurbit[8]uril (CB[8]) was chosen because its cavity space had the appropriate dimensions to fit PDI as the chromophore together with a wide range of aromatic analytes inside (based on DFT calculations)[150].

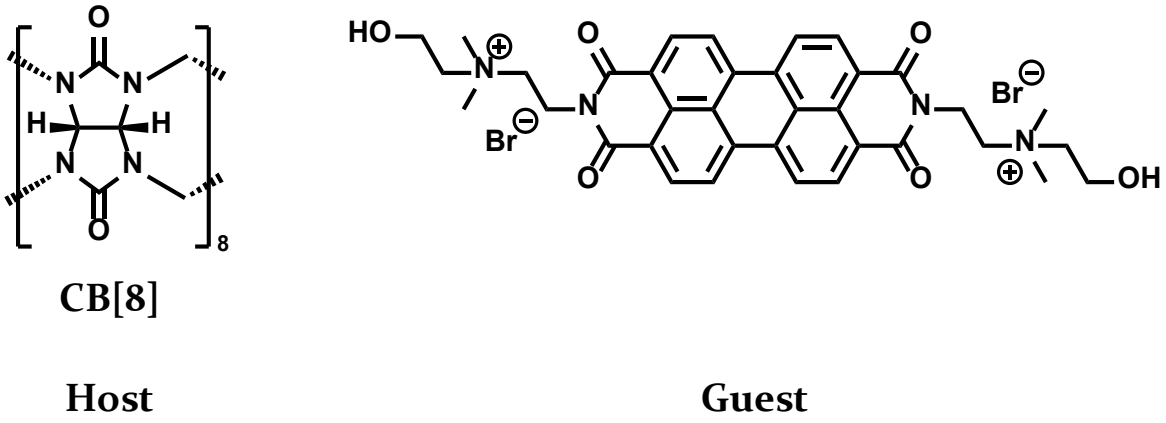

Figure 5-1. CB[8] and dicationic PDI used in previous work.[150]

Tracking of enzymatic activity with the described CB[8]-PDI chemosensor is based on the Associative Binding Assay (ABA, Figure 5-2) mechanism. The self-assembly of CB[8]-host and the guest molecule as the first step in forming the chemosensor is driven by the enthalpic gain caused by the replacement of 'cavity-water' during the complexation,[151] as well as attractive ion-dipole interactions with the carbonyl portals of CB[8].[152] During the tracking of enzymatic activity, aromatic substrates and products bind to the PDI of the CB[8]-PDI chemosensor complex via attractive π-interactions with different binding rates. This leads to quenched emission of the PDI, which can be quantified and directly related to the concentration ratio of the substrate-product mixture. Owing to the high sensitivity and immediate response of fluorescence detection, real-time reaction monitoring at low concentrations becomes possible.[153]

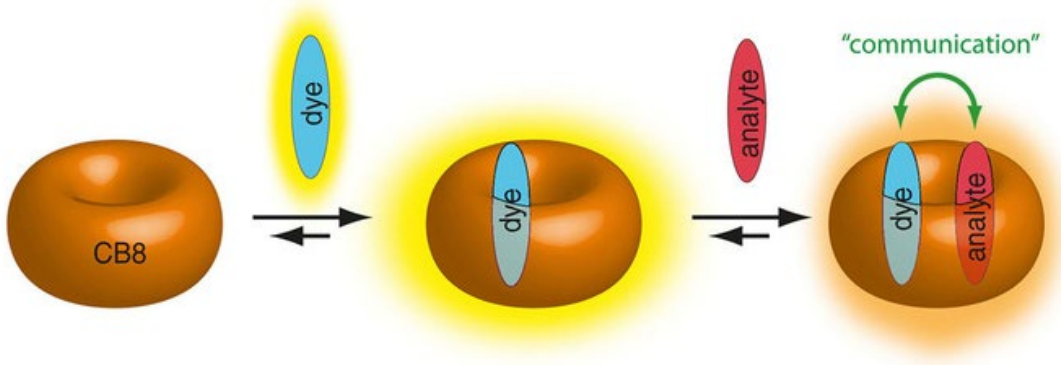

Figure 5-2. Schematic representation of the chemosensing mechanism of the associative binding essay.[148]

Incorporation of a TDI as the chromophore would allow for wider spectroscopic range of detection, and the increased aromatic surface area of the rylene core could potentially extend the number of detectable analytes. This chapter will explore whether a dicationic TDI analogue similar to the PDI in Figure 5-1 can be synthesized and self-assembled into a CB[8]-TDI complex with similar fluorescence turn-on-turn-of behavior in aqueous solution.

5.2 Synthesis of the Dicationic TDIs

Typically, rylene imides can achieve water solubility by introducing water-solubility enhancing functionalities such as quaternary ammonium cations or sulfonic acids either in the imide- or *bay*-positions as described in chapter 1. The limited cavity space of CB[8] does not allow *bay*-substitution on the rylene core however, water solubility must therefore be introduced via the imide substituents.

Starting point for the synthesis of a dicationic TDI was the symmetrical TTE building block **2-9** (Scheme 5-1). Imidization with 3-aminopropyldimethylamin in imidazole was carried out in a pressure vessel at 160 °C for 24 h. The reaction mixture was precipitated in a 10:1 mixture of THF/H_2O and washed several times, which removed all residual starting material. After drying the deep blue compound, TDI **5-1** was received in 65 % yield. Figure 5-3 shows the MALDI-TOF spectrum of

N,*N*'-Bis(dimethylaminopropyl)-terrylene-3,4,11,12-tetracarboximide **5-1**. The solubility was not sufficient for ^{1}H NMR measurements.

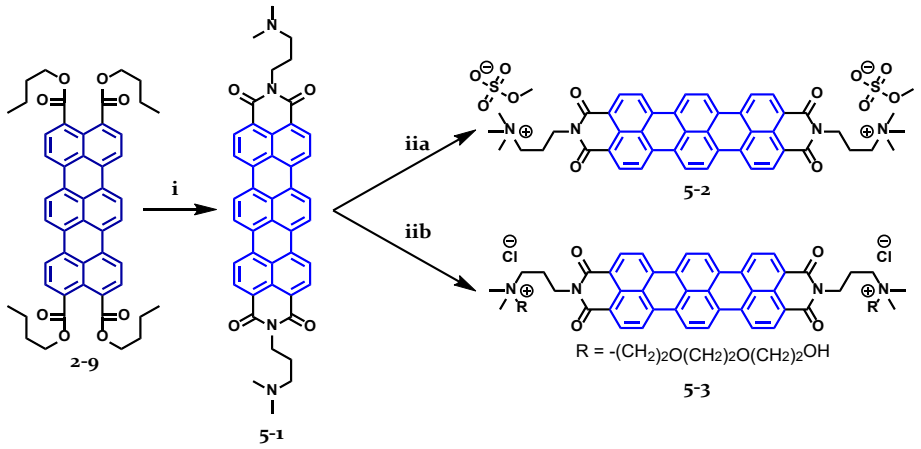

Scheme 5-1. Synthesis of dicationic TDIs **5-2** and **5-3**. Conditions: i) dimethylaminopropylamine, imidazole, 160 °C, 24 h, 65 %; iia) dimethylsulfate, 110 °C, 24 h, 95 %; iib) triethylene glycol monochlorohydrin, DMF, 110 °C, 24 h, 95 %.

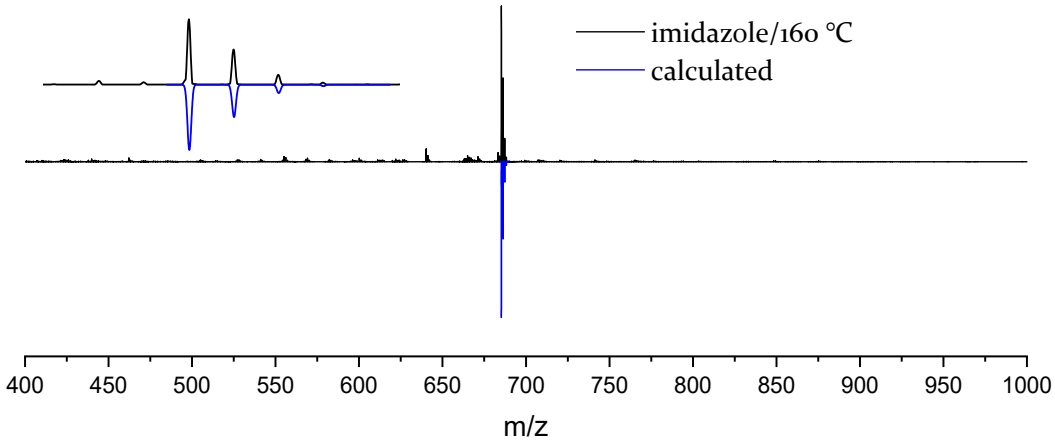

Figure 5-3. MALDI-TOF spectrum of TDI **5-1**.

TDI **5-1** was quaternized with dimethyl sulfate and triethylene glycol monochlorohydrin. For this purpose, two samples were prepared with **5-1** suspended in dimethyl sulfate (Scheme 5-1, top) or DMF/triethylene glycol monochlorohydrin (Scheme 5-1, bottom) respectively. Each sample was stirred at 110 °C for 24 h. Both TDIs were

isolated from the quaternizing reagents by precipitation of the reaction solution in THF, followed by repeated washing. TDIs **5-2** and **5-3** were obtained in 95 % yield.

In Figure 5-4, the ESI-MS of both the methylated TDI **5-2** and the Me-TDI-CB[8] complex in water/MeOH are displayed, with their respective calculated masses at the bottom row. The charge of the TDI and the TDI-CB[8] complex is '2+', therefore both appear as double-charged ions at half their nominal mass.

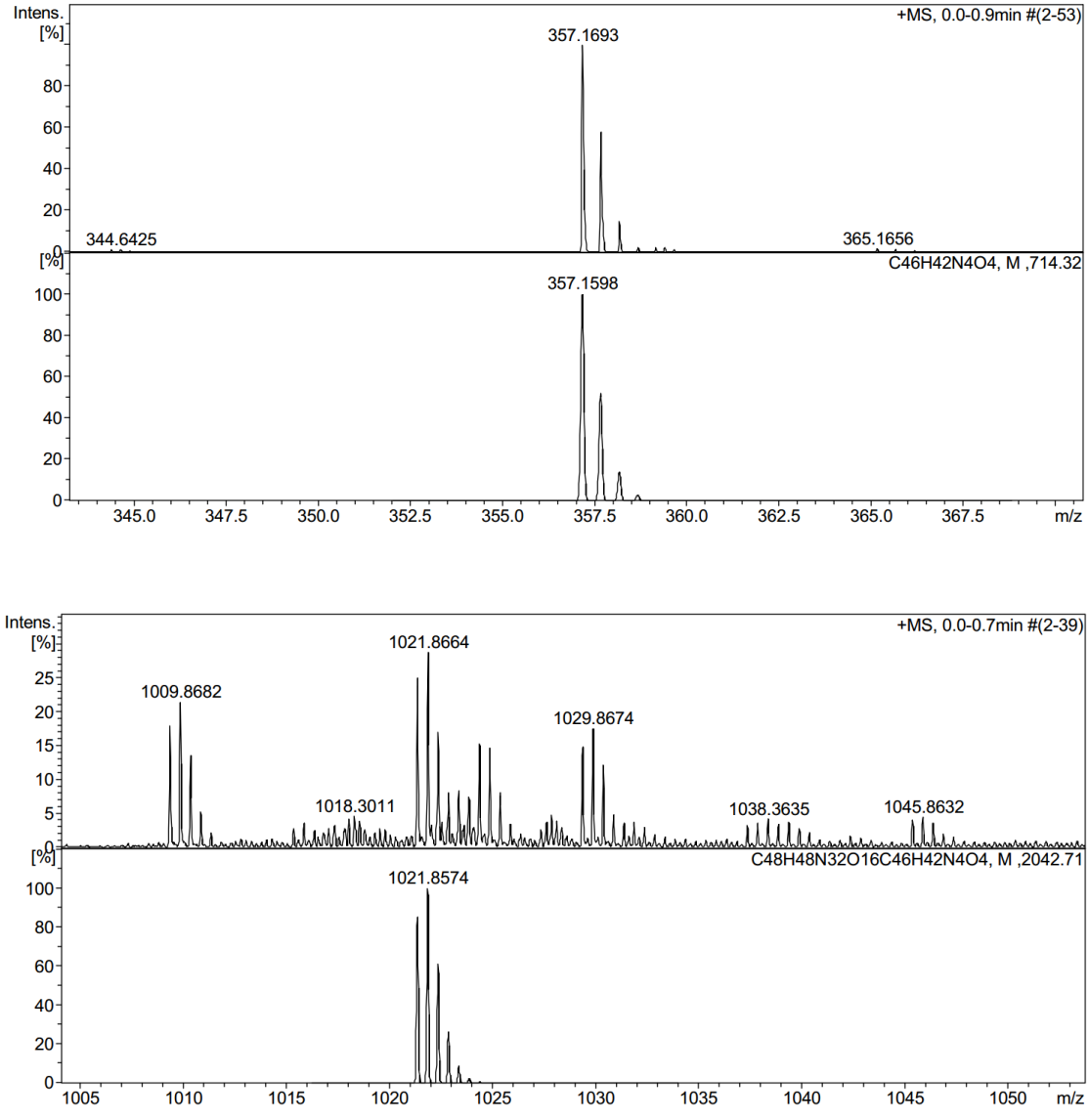

Figure 5-4. ESI-MS spectra of Me-TDI^{2+} **5-2** (top) and Me-TDI^{2+}-CB[8] complex (bottom) in water. Measured by *Amrutha Prabodh* at KIT, Institute of Nanotechnology, Karlsruhe.

While the TDI-CB[8] complex can be detected in ESI-MS (m/z = 1021.8664), the nature of the additional signals is unclear. However, the two minor impurities in the TDI spectrum in Figure 5-4 (m/z = 344.6425 and 365.1656) have the same Δm/z as the two closest impurities in the TDI-CB[8] complex (m/z = 1009.8682 and 1029.8674), but a higher signal intensity relative to the target compounds. It appears that either the impurity-CB[8] complexes possess a higher signal intensity in ESI-MS, or the unknown impurities have a higher affinity to bind to the CB[8]. Possible however is that these 'impurities' are only ESI-MS artifacts that are amplified in the CB[8] complex. For example, the detected mass m/z = 1029.8674 matches the calculated mass of the 'methylated' [TDI-CB[8]+Me^{2+}] (m/z = 1029.8756), and m/z = 1038.3635 matches the 'methanolated' [TDI-CB[8]+$MeOH^{2+}$] (m/z = 1038.3770).[154]

The ESI-MS spectrum in Figure 5-5 depicts TEG-TDI **5-3** as the double-charged ion with a detected mass of m/z = 475.3252 as the main signal.

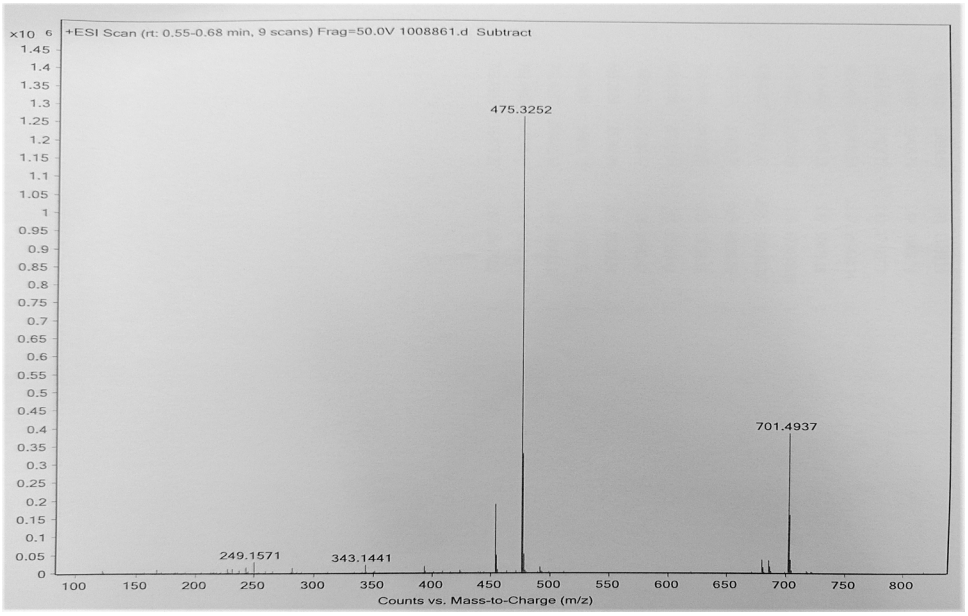

Figure 5-5. ESI-MS spectrum of TEG-TDI^{2+} **5-3**.

The nature of the second, lower-intensity signal of m/z = 701.4937 is unclear. As the sample was prepared by dissolving **5-3** in water and filtering the solution with a 0.2 µm syringe filter, remnants of the water-insoluble TDI **5-1** (m/z = 684.2737) can

be ruled out. It is also unlikely that the quaternization was incomplete and the hypothetical TDI-monocation of **5-3** (m/z = 816.3601) is responsible for the unassignable signal.

Unfortunately, both TDIs were not sufficiently soluble for NMR spectroscopy in water or DMSO. One equivalent of CB[8] was added to **5-3** to induce the self-assembly into the CB[8]-TDI complex and mitigate aggregation. Signals in the aromatic region became visible (Figure 5-6, top), but the signal-to-noise ratio did not allow integration or assignment of these signals. This behavior was expected, as in the CB[8]-PDI complex discussed in the literature, only broad signals of the cationic PDI could be observed as well (Figure 5-7).[150] The larger, planar surface area of TDI compared to PDI leads to decreased solubility, explaining the worse signal-to-noise ratio in the TDI case.

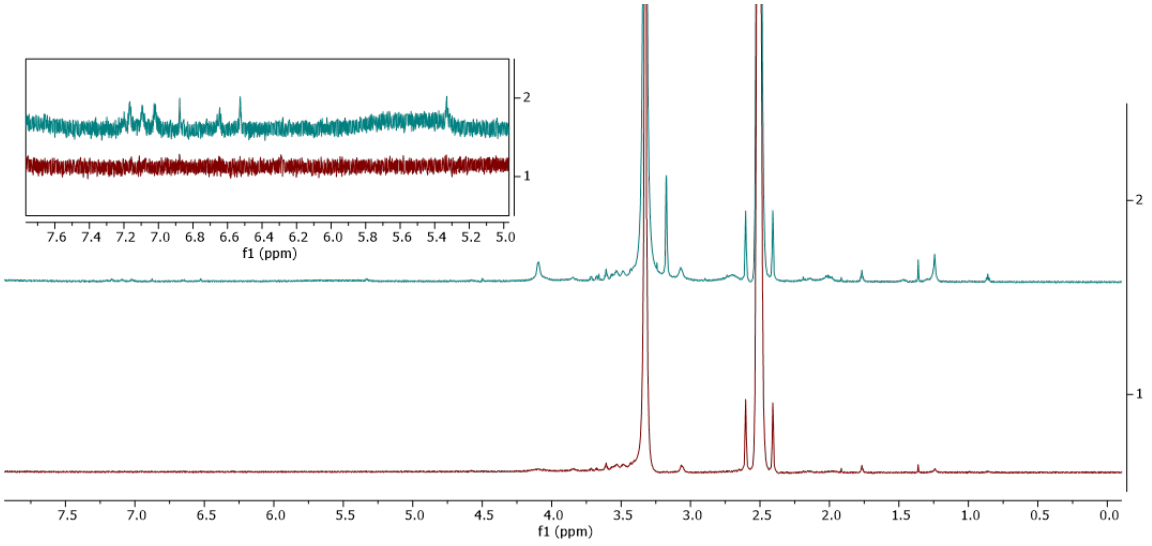

Figure 5-6. ^{1}H NMR spectra of **5-3** (bottom) and **5-3** + **CB[8]** (top), $(CD_3)_2SO$, 298 K.

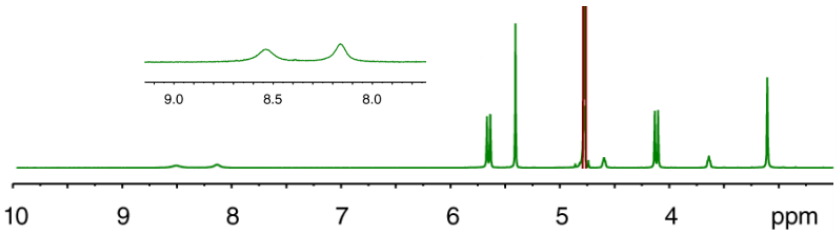

Figure 5-7. ^{1}H NMR spectrum of the CB[8]-PDI complex in D_2O.[150]

Due to the high tendency of aggregation, HPLC analysis was only successful with the TEG-TDI **5-3**. Figure 5-8 shows the analytical HPLC elugram of TEG-TDI **5-3** on a C1-modified reversed phase HPLC column with a solvent-gradient of H_2O/0.1 % TFA (90:10) → THF/0.1 % TFA (10:90). In the elugram, only TDI-based compounds are visible, as evidenced by their absorption wavelengths between 500 nm and 700 nm and the characteristic electronic transition band structure. Inconclusive is the presence of three different signals around the 4-minute mark. As only analytical HPLC was possible, these three compounds could not be further analyzed to verify whether quaternization was not complete (TDI/TDI^{+}/TDI^{2+}), or the dissociation happened during the chromatography. To fully verify whether this hypothesis is true, separation on a C1-HPLC column on a preparative scale would be necessary, which was not available.

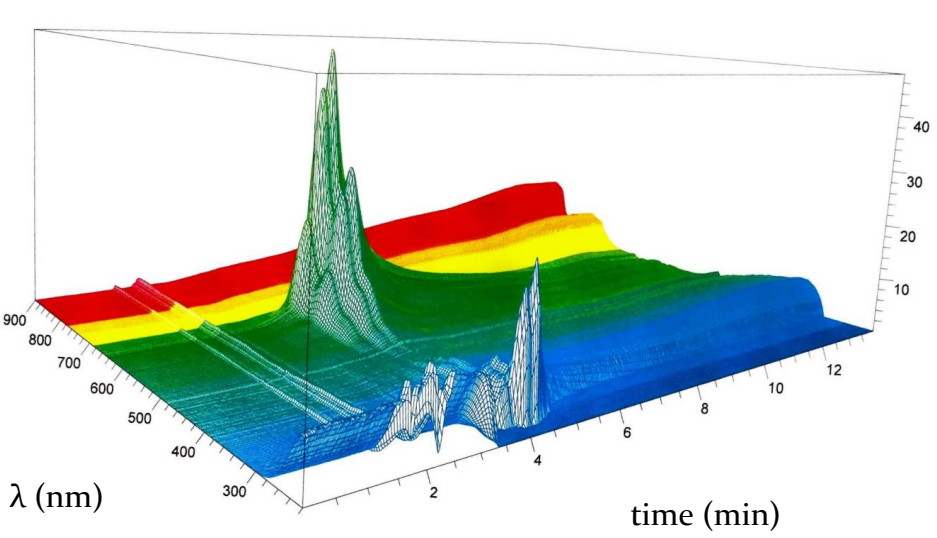

Figure 5-8. HPLC elugram of TEG-TDI **5-3** on a C1-modified reversed phase column in THF/H_2O/TFA.

5.3 Optical Properties and Fluorescent Switching of the Dicationic TDIs

Absorption and emission spectra of the two dicationic TDIs were recorded in H_2O (Figure 5-9). Without CB[8], both TDIs suffered from aggregating effects reminiscent of perylene H-aggregates at high concentrations (Figure 5-10).[155] In the reference spectrum in Figure 5-10 showing H-aggregating behavior of PDI, the absorption maxima of the monomer (red) and the aggregated species (green) are highlighted.

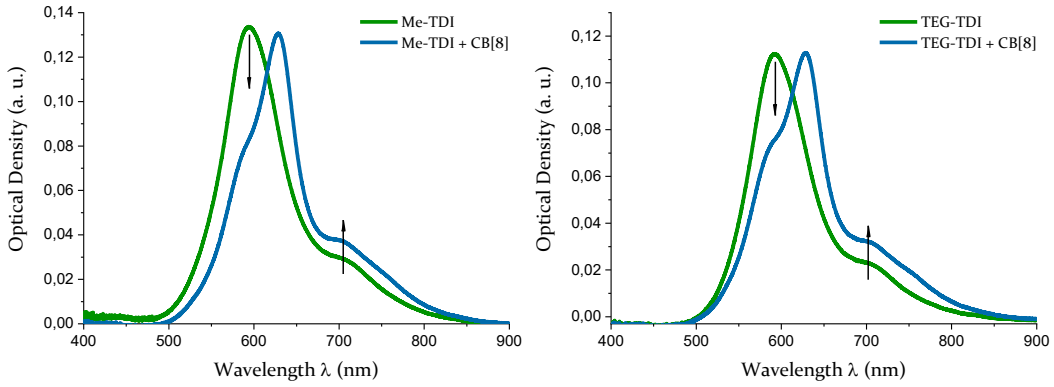

Figure 5-9. Absorption spectra of Me-TDI **5-2** (left) and TEG-TDI **5-3** (right) before (green) and after (blue) the addition of CB[8] in H_2O, conc. ~ 20 µM.

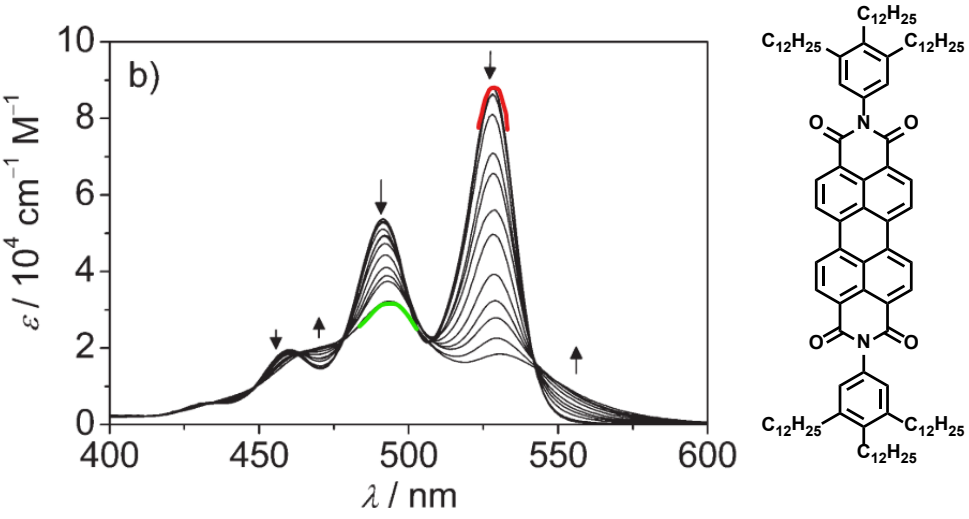

Figure 5-10. Absorption spectrum of the H-aggregate of PDI in toluene with increasing concentration.[155]

With the addition of CB[8] and formation of the host-guest complex, a shift of intensities of the electronic transition bands starts to emerge, while still maintaining the general shape of aggregated rylene imides. This is indicated by the presence of a broad absorption band instead of the three, characteristic absorption bands of fully dissolved rylene diimides.[156]

When comparing the transition between the aggregated and monomeric state of the PDI-CB[8] case (Figure 5-11) with the absorption spectra of TDI **5-2** and **5-3** in H_2O (Figure 5-9),[150] it is suggested that both TDIs **5-2** and **5-3** exist as aggregates. At a 1:1 ratio of PDI/CB[8], the clear separation between the 0-0 (as the absorption maximum), 0-1 and 0-2 transitions (yellow graph in the absorption spectrum in Figure 5-11) indicates the complete deaggregation of the chromophore. In contrast, the complexation of TDI even with an excess amount of CB[8] did not prevent aggregation as effectively as in the PDI case. In the absorption spectrum in Figure 5-9, the addition of CB[8] lead to a bathochromic shift of the absorption maximum, but no clear separation between transition bands was visible, proving that complexation of TDI with CB[8] is either not complete or CB[8] is not the ideal host-molecule to completely suppress TDI aggregation.

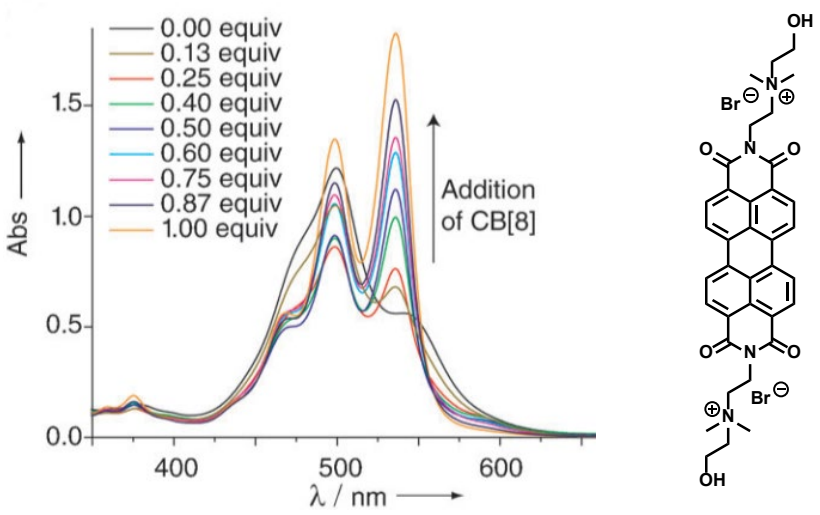

Figure 5-11. Complexation of cationic PDI with increasing amounts of CB[8] in H_2O, conc. ~20 µM.[150]

More important for chemical sensing than the absorption spectrum, however, is the emission behavior of the host-guest complex. Initial UV/Vis titrations investigating the viability of using a TDI cation as the chromophore in the described chemosensor host-guest complex were carried out by *Amrutha Prabodh* of the *Biedermann* group at the Karlsruhe Institute of Technology. CB[8] was added to a 20 µM solution of Me-TDI in H_2O and absorption and emission spectra were recorded (Figure 5-12). It is apparent that whilst no TDI emission is detectable due to the previously discussed aggregating effects, the addition of CB[8] lead to a significant increase in emission intensity. This experiment verified the expected behavior of increasing emission intensity upon addition of a macrocycle to form host-guest complexes. Although aggregation was not completely inhibited, as discussed in the last section, the decrease in aggregation was effective enough to allow TDI emission. Going forward, it is reasonable to screen the complexation with additional, larger macrocyclic hosts with a similar diameter to elucidate the possibilities of completely preventing aggregation in the same way as the PDI case.

The UV/Vis titration, however, did not prove whether the TDI is placed in the center of the CB[8] (as illustrated in Figure 5-2). Determining the structure of the macrocyclic complex is central to the cause of using TDI-CB[8] as a chemosensor via

the mechanism described in the introductory section. Therefore, further research will focus on shedding light on the complex structure via DOSY experiments, obtaining potential crystal structures or estimating the binding strength via isothermal titration calorimetry.

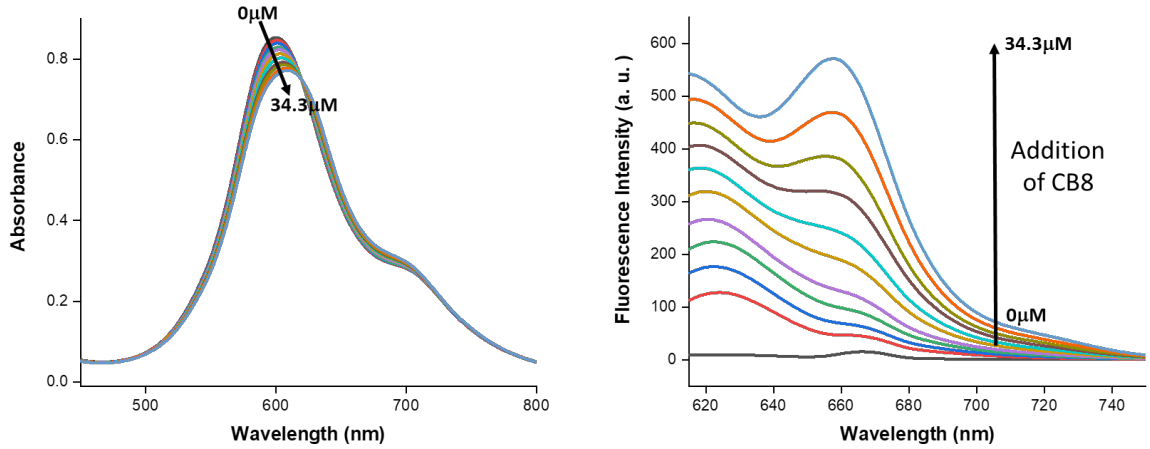

Figure 5-12. UV-Vis absorption (left) and emission (right) titration of Me-TDI **5-2** with increasing concentration of CB[8] in H_2O. Measured by *Amrutha Prabodh* at KIT, Institute of Nanotechnology, Karlsruhe.

5.4 SUMMARY

In this chapter, the TTE building block **2-9** was converted to dicationic-TDI precursor **5-1** in good yield. Dimethylaminopropylamine was chosen as the imide substituent, allowing the introduction of water-solubilizing functionalities via quaternization. Two dicationic, quaternized TDIs **5-2** and **5-3** were synthesized with methyl and triethyleneglycol as alkyl side-chains, respectively. Their aggregating behavior in H_2O and DMSO did not allow ^1H NMR spectroscopy, instead relying only on ESI-MS, UV/Vis and HPLC as characterization methods.

As was evidenced by the UV-Vis spectra in water, both the methyl- and the triethyleneglycol-quaternized TDIs were aggregated without the addition of CB[8], as π-π stacking of the rylene core could not be efficiently prevented by linear imide substituents. Upon addition of CB[8] in a titration experiment the emission increased, suggesting that a host-guest complex forms which partially breaks aggregation of the chromophore. This lays the groundwork for all further chemosensing-related research, as the switching of fluorescence via an aggregation-deaggregation equilibrium is the basis for the envisioned associative chemosensing method employed by the group of *Biedermann*.

Further research will focus on the chemosensing of aromatic analytes in enzymatic redox and hydrolysis reactions with the TDI-CB[8] complex, as well as further corroborating the complex structure. Both go hand-in-hand, as it's essential that the analyte can bind to the TDI inside the cavity space of CB[8] to meet the requirements of the underlying ABA-mechanism.

Chapter 6
ELECTRON-DEFICIENT (HETERO-)PAHS

6.1 INTRODUCTION

In the previous chapters, the scope of the cascade cross-coupling protocol has already been expanded beyond the coupling of naphthalenes as the 'terminal' and 'core' units. By altering the combination of coupling partners, different variations of perylene and terrylene carboxylic imides and esters have been synthesized. This chapter will build on this idea in an effort to obtain PAHs and heterocyclic PAHs based on the rylene motif in one or two-step syntheses.

PAHs and their heterocyclic counterparts exhibit unique optical and electronic properties and have thus found widespread application as organic electronics and photovoltaics.[157–159] While organic p-type semiconductors (hole conducting) are more common, a smaller number of n-type semiconductors (electron conducting) has been reported and access is often limited by complex synthesis.[160]

In order to be classified as good n-type semiconducting material, it should be solution processable, the semiconductor should be stable in air, have low injection barriers and high charge carrier mobilities.[161] Ambient stable electron injection and transport is a necessity to avoid of trapping of H_2O and O_2, which are most common under ambient conditions. A low-lying LUMO energy has been theoretically proven and empirically demonstrated to be a criterion to fulfill these requirements.[162]

Hetero-doping of PAHs or replacement of phenylene units with heteroaromates can alter both HOMO and LUMO drastically,[163,164] whereas substitution of the rylene series with electron-deficient groups like imides generally lowers the LUMO-level, as described in chapter 1. An example that demonstrates how the HOMO and LUMO energies can be tuned by the combination of hetero-doped, extended naphthalene cores with electron withdrawing imide groups is shown in the acene diimide series in Figure 6-1.[165]

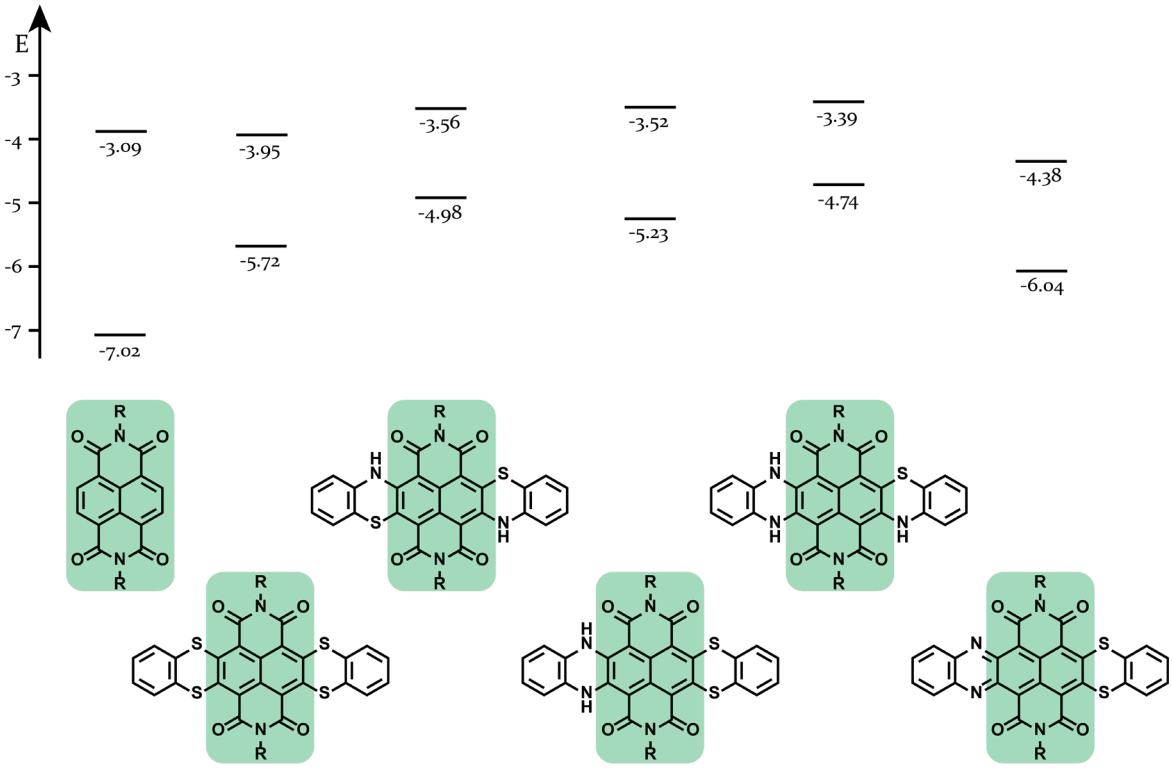

Figure 6-1. HOMO and LUMO energies (in eV) of an acene diimide series.

Functionalization of PAHs with imide substituents would be favorable to the applications described, due to their high electron-deficiency and potentially increased solubility compared to non-substituted PAHs. However, not many procedures for imide-substituted (heterocyclic) PAHs are reported, typically requiring the synthesis of the carboxylic acid anhydride-bearing PAH scaffold or post-functionalization of rylene imides.[165–168] The difficulties of these steps have been described extensively in this work, and an alternative approach based on the cascade cross-coupling reaction starting from readily available compounds could give access to a variety of PAHs and heterocyclic PAHs based on the rylene imide scaffold that would otherwise not be obtainable. This chapter will therefore focus on the variation of the 'core'-building block (Scheme 6-1) in order to investigate the influence of different substitution patterns and heteroatom doping on their optical and electronic properties.

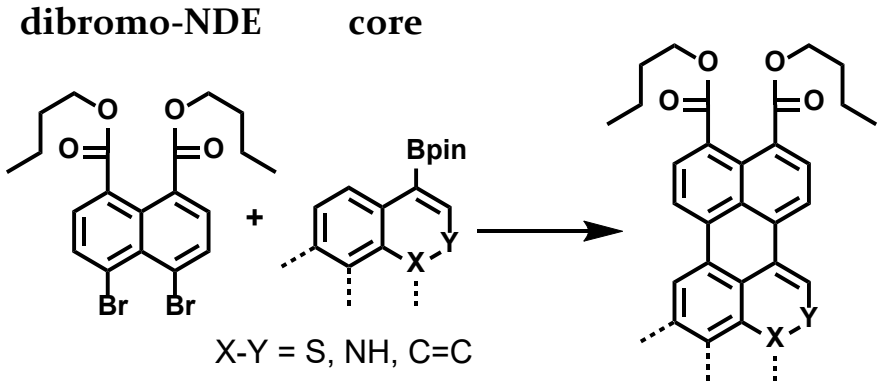

Scheme 6-1. Schematic representation of synthesis of (heterocyclic) carboxylic ester substituted PAHs.

In particular, this chapter will expand the scope of the cascade cross-coupling reaction of dibromo-NDE **2-10** with the 'core' building blocks shown in Figure 6-2. Coupling with both boronic esters of pyrene is expected to result in two examples of electron-deficient PAHs, a concept that has been investigated by *Seifert et al.* in the synthesis of PAH-imides.[169] Coupling of **2-10** with benzothiophene- and indole-based boronic esters on the other hand will lead to two examples of carboxylic ester substituted PAHs with heteroatoms incorporated directly into the scaffold.

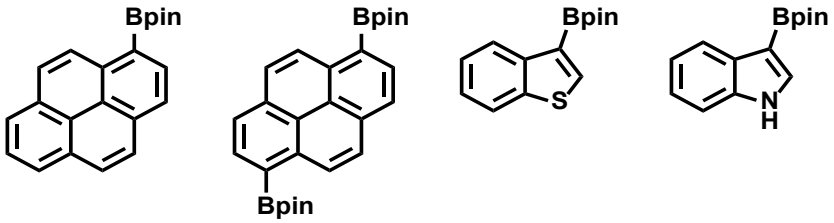

Figure 6-2. 'Core' building blocks used in this chapter.

6.2 Synthesis of Pseudo-Rylene Esters

Scheme 6-2 outlines the cascade cross-coupling reactions of dibromo-NDE **2-10** with the boronic esters of pyrene, benzothiophene and indole. All cross-coupling reactions were successful with the conditions established in chapter 2. In contrast to the syntheses of rylene esters in the previous chapters, purification via precipitation was not sufficient in this case. After column chromatography, the three compounds

6-1 – **6-3** were received in yields of 61 % to 86 %. The MALDI-TOF MS of compounds **6-1**, **6-2** and **6-3** in Figure 6-3 and NMR spectra in Figure 6-4 confirmed their identities.

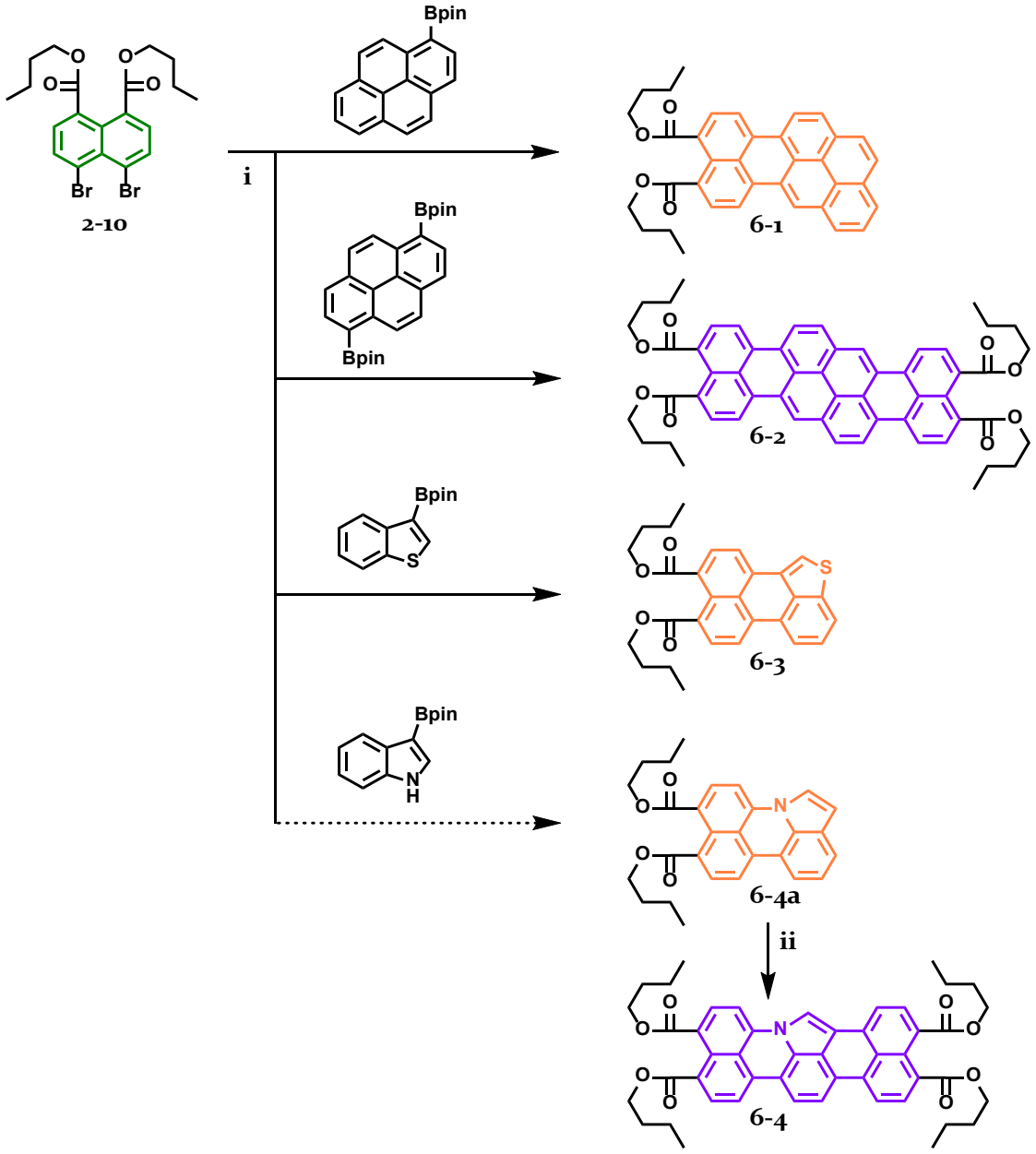

Scheme 6-2. Synthesis of carboxylic esters **6-1** - **6-4**. Conditions: i) Pd_2dba_3/PCy_3, K_2CO_3, *o*-dichlorobenzene, 165 °C, 16 h, 73 % for **6-1**, 61 % for **6-2**, 85 % for **6-3**; ii) Pd_2dba_3/PCy_3/SPhos, K_2CO_3, *o*-dichlorobenzene, 165 °C, 16 h, 35 %.

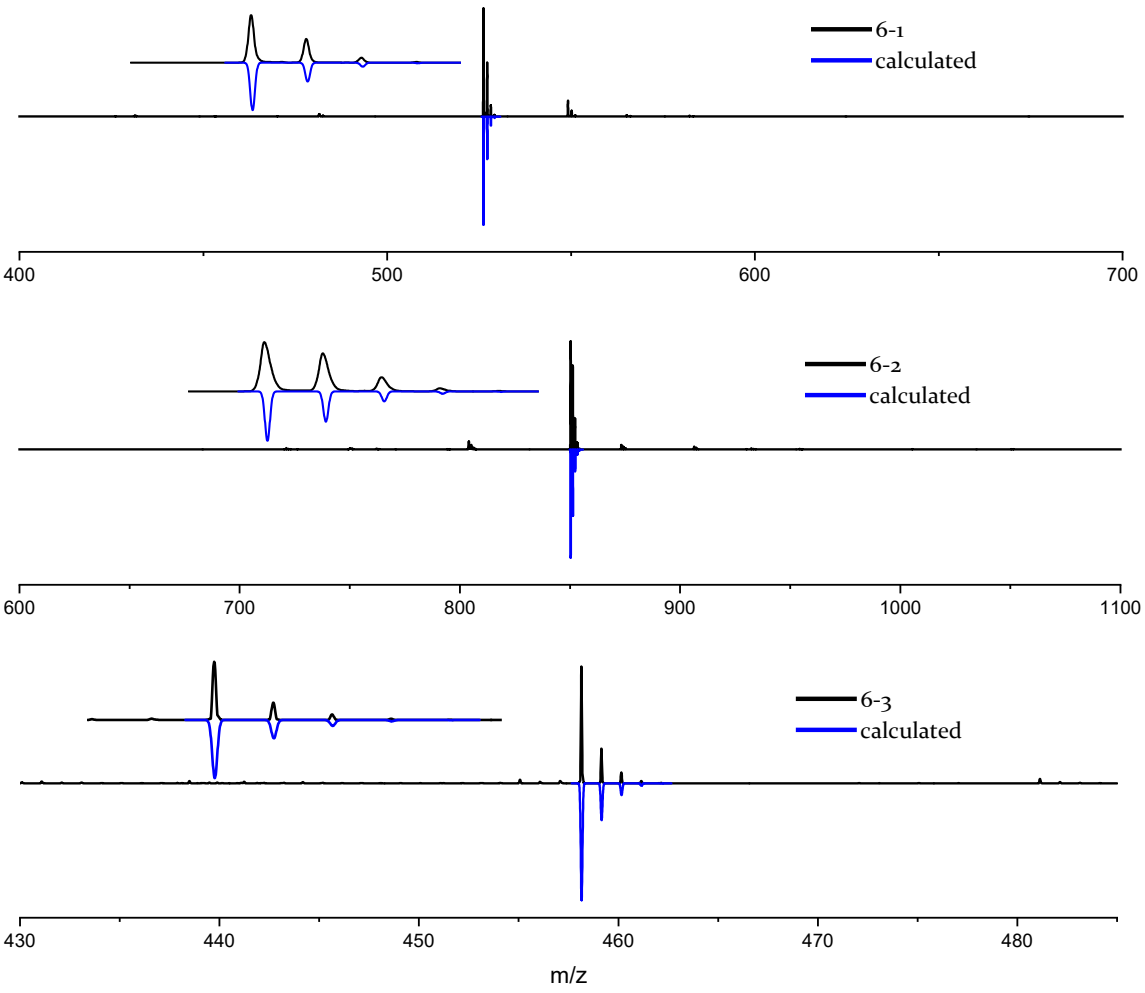

Figure 6-3. MALDI-TOF MS of compounds **6-1**, **6-2** and **6-3**.

Due to the high tendency for π-stacking of both pyrene-based carboxylic esters **6-1** and **6-2**, high-temperature measurements (393 K) were necessary to fully resolve all proton signals in the ^{1}H NMR spectra in Figure 6-4. In contrast, the spectrum of benzothiophene derivative **6-3** was fully resolved at ambient temperatures, due to the size-difference between the p-orbitals of sulphur and the neighboring p-orbitals of carbon, which appears to have effectively prevented π-stacking. When comparing the spectra of the two pyrene-esters **6-1** and **6-2** based on the same structural motif, the symmetric nature of the tetraester **6-2** becomes immediately evident by the less-crowded aromatic region, which can be assigned to five distinguishable groups of protons.

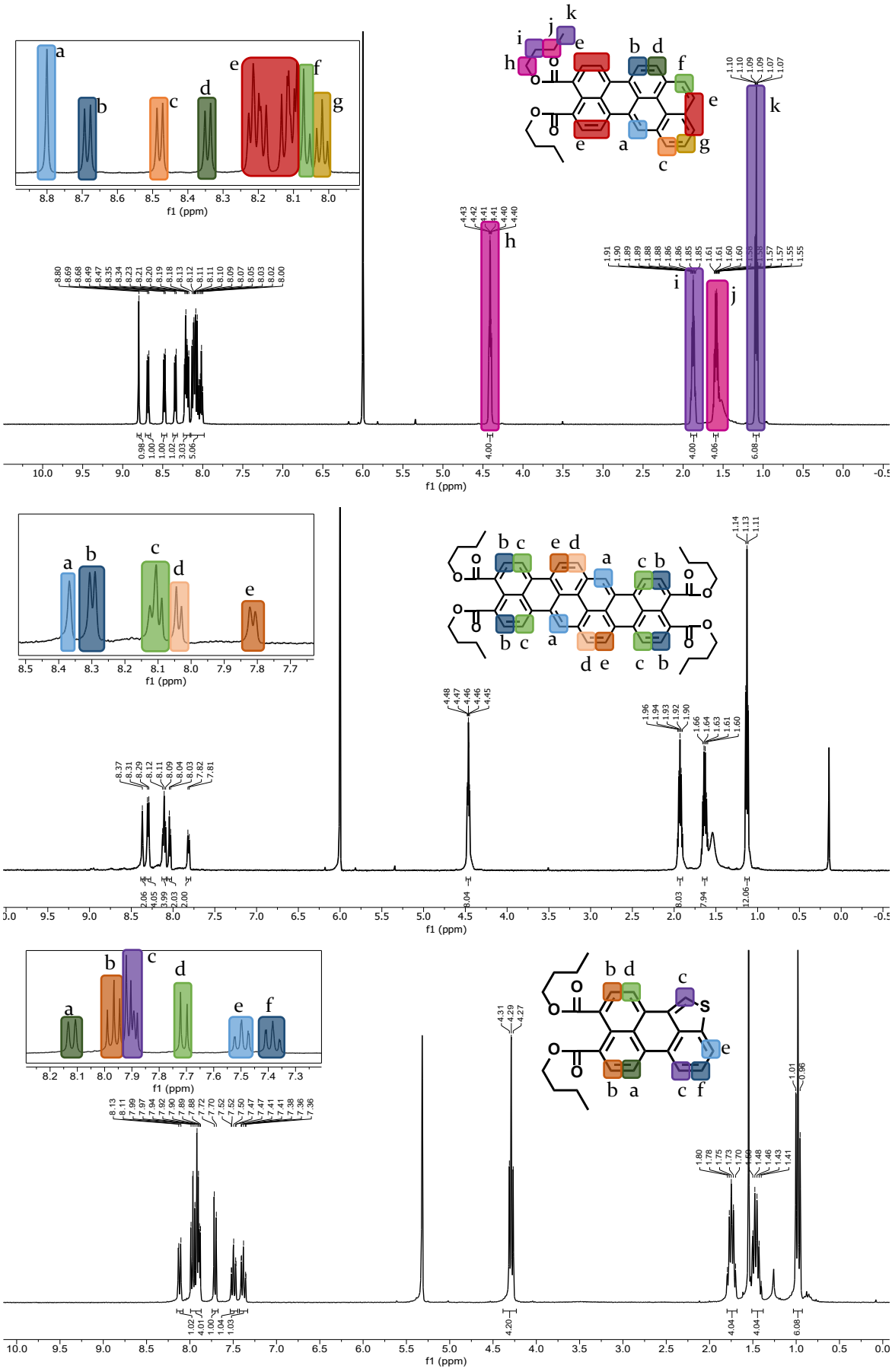

Figure 6-4. ^{1}H NMR spectra of **6-1** (top), **6-2** (center) in $C_2D_2Cl_4$, 393 K and **6-3** (bottom) in CD_2Cl_2, 274 K.

This series of carboxylic esters highlights the scope of the cascade cross-coupling protocol, enabling the variation of carboxylic rylene scaffolds in a bottom-up synthesis, instead of being limited to post-synthetic modifications. Furthermore, the possibilities of altering the carboxylic ester or imide substituents allows possible access to a wide range of yet unexplored (hetero-)PAH motifs, particularly for investigations into their self-assembling properties.

6.3 Triple-Cascade Cross-Coupling

Noteworthy is the reaction between dibromo-NDE and the 3-boronic ester of indole in Scheme 6-3:

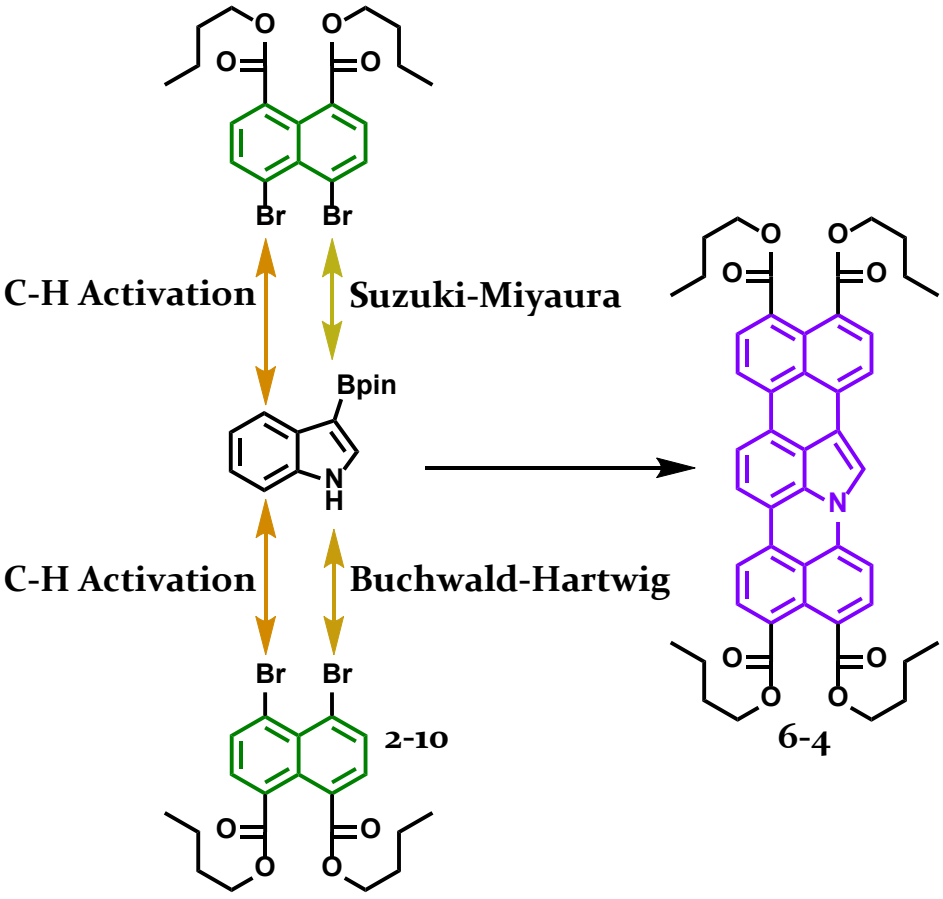

Scheme 6-3. Possible explanation for the occurrence of the violet side-product during the cascade reaction with indole and dibromo-NDE **2-10**. Conditions: Pd_2dba_3/PCy_3/SPhos, K_2CO_3, *o*-dichlorobenzene, 165 °C, 16 h, 35 %.

During the initial reaction condition screening via TLC analysis, a violet compound was visible next to an orange compound, which matched the expected color of the indole-based diester **6-4a**. This reaction intermediate could be identified by TLC analysis and mass spectrometry, but isolation of the compounds via column chromatography was unsuccessful due to similar polarities and tailing of the different compounds. Due to the excess of dibromo-NDE **2-10**, conversion to the tetraester **6-4** was the most probable explanation for the appearance of a violet chromophore, which was corroborated by mass spectrometry upon further investigation. This unintended reaction suggests that an additional coupling reaction other than *Suzuki-Miyaura* followed by C-H activation cyclization has occurred. This third aryl-aryl cross-coupling reaction in the coupling cascade forms a carbon-nitrogen bond as outlined in Scheme 6-3. Because a palladium catalyst was already present, *Buchwald-Hartwig* amination seemed to be the most likely explanation for this unintended follow-up reaction.

In order to verify this assumption, efforts went into selectively synthesizing indole-based tetraester **6-4**. The addition of a second, *Buchwald-Hartwig* active ligand to the catalytic system was the logical step.[170] After screening several available ligand combinations, the catalytic system of $Pd_2(dba)_3$ with PCy_3 and SPhos as ligands resulted in the violet compound as the major product, as confirmed by TLC analysis.

The identity of **6-4** was confirmed after full workup and column chromatography via MALDI-TOF MS (Figure 6-5) and ^1H NMR spectroscopy (Figure 6-6). Surprising was the low solubility compared to the structurally related terrylene and pyrene-based carboxylic tetraesters **2-9** and **6-2**. Even at 120 °C, the signal-to-noise ratio was low and the signals couldn't be fully resolved. Due to the angle in the scaffold caused by the sp2 hybridized nitrogen atom (Figure 6-6, ~ 160°, calculated from the geometry-optimized structure), the loss of symmetry lead to a large number of aromatic proton signals, further impeding their assignment. The angle along the long axis is also a possible explanation for the decreased solubility, as it could make columnar stacking, and therefore aggregation, easier.

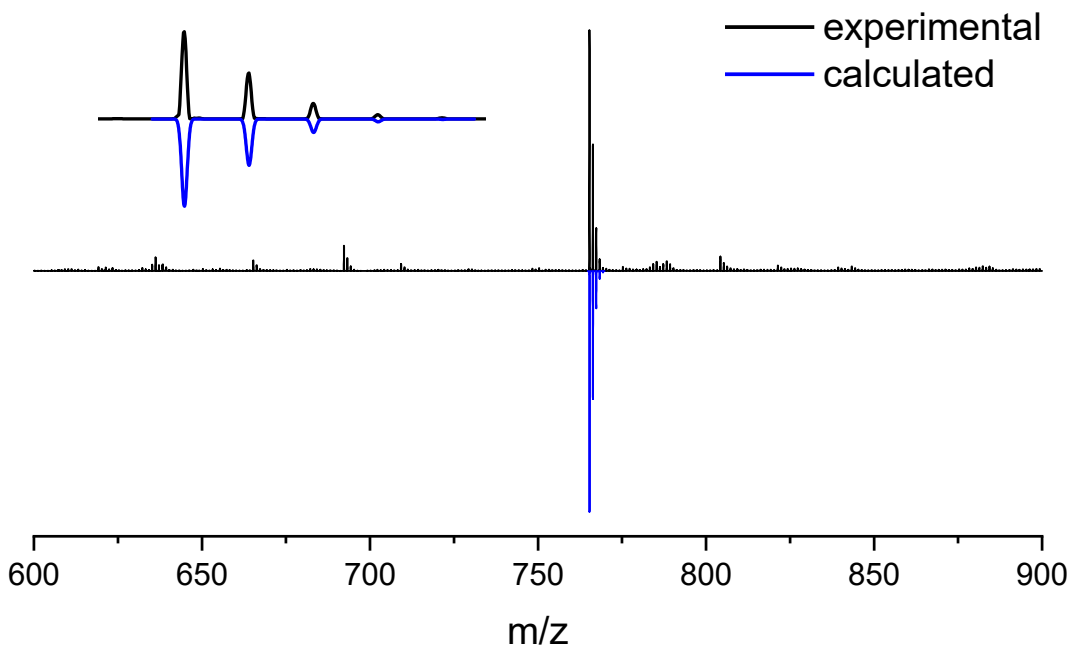

Figure 6-5. MALDI-TOF spectrum of indole-based tetraester **7-4**.

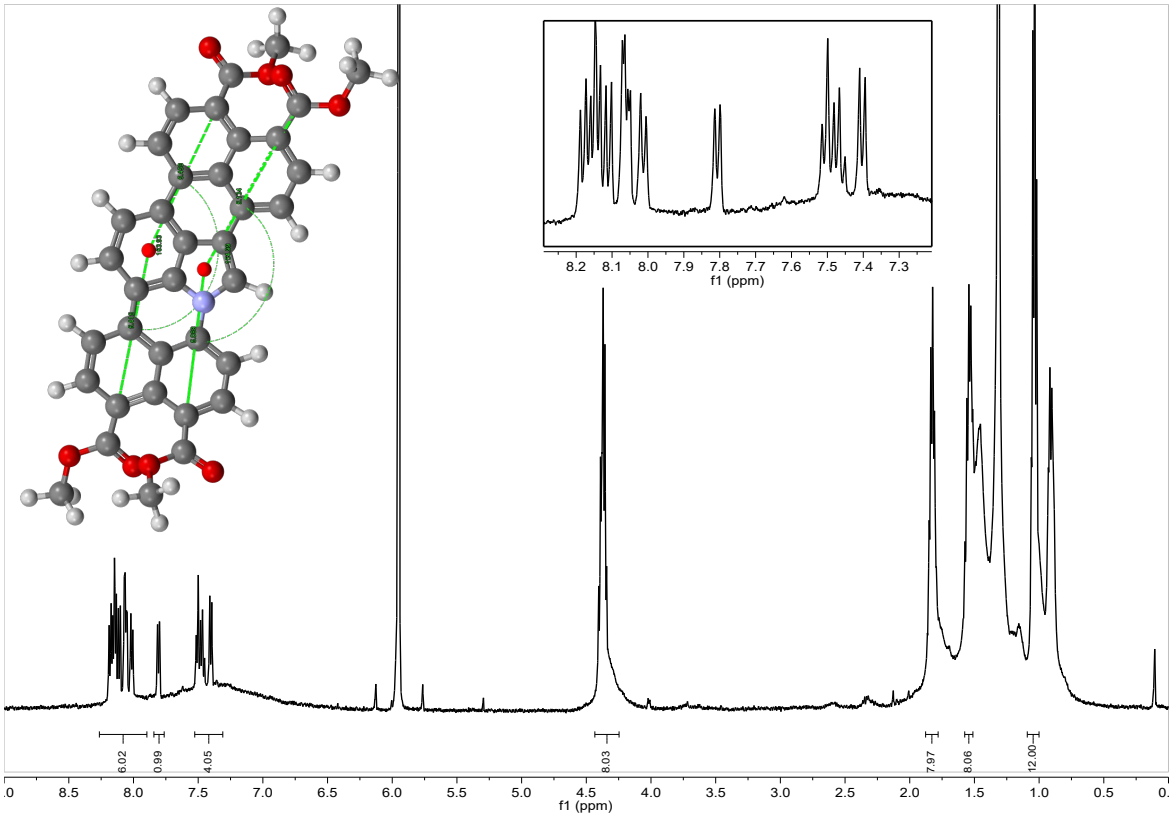

Figure 6-6. ^{1}H NMR of indole-based tetraester **7-4**, $C_2H_2Cl_4$, 393 K.

This reaction is especially remarkable, because triple-cascade cross-coupling reactions are rare and most often utilized as tools in total synthesis.[171–173] The one-pot formation of heterocyclic PAHs that involves three different types of cross-coupling reactions however remains largely unexplored and could pave the way towards molecular design choices that are otherwise not synthetically achievable.

6.4 Synthesis of a PAH-Diimide

To prove that the aforementioned pseudorylene esters are viable building blocks for (heterocyclic) PAH imides, the pyrene-based tetraester **6-2** was converted to the diimide **6-5** via imidization with 1-heptyloctylamine in imidazole (Scheme 6-4). After column chromatography, the diimide was received in 57 % yield as a dark blue solid. The compound was characterized by MALDI-TOF MS (Figure 6-7) and NMR spectroscopy (Figure 6-8). As in the tetraester case **6-2**, the high symmetry is reflected in the NMR by the clearly separated signals in the protonic region.

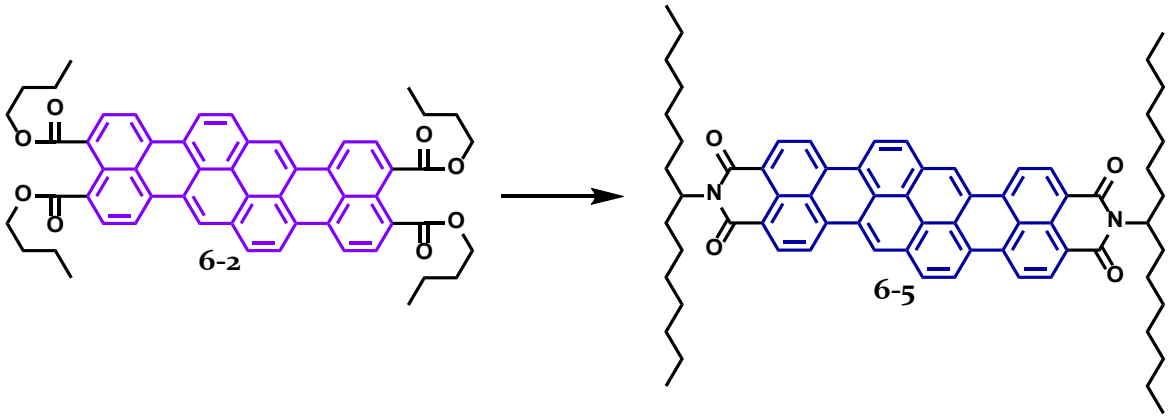

Scheme 6-4. Synthesis of the pyrene-based diimide **6-5**. Conditions: 1-heptyloctylamine, imidazole, 160 °C, 16 h, 57 %.

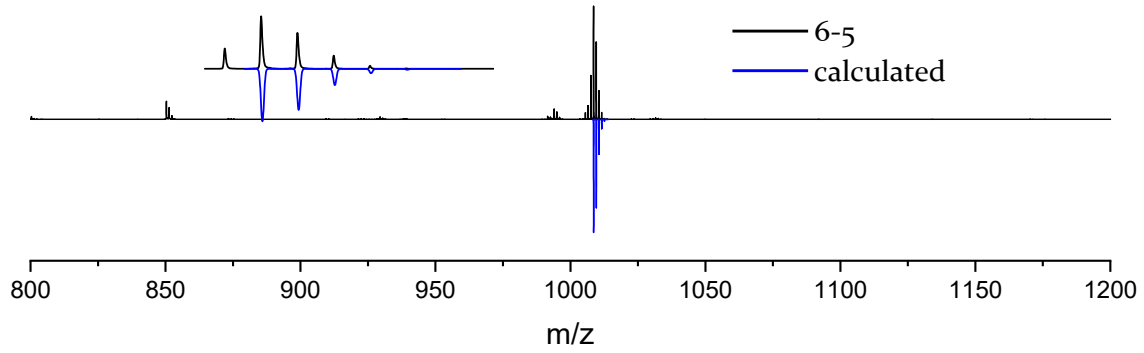

Figure 6-7. MALDI-TOF MS of **6-5**.

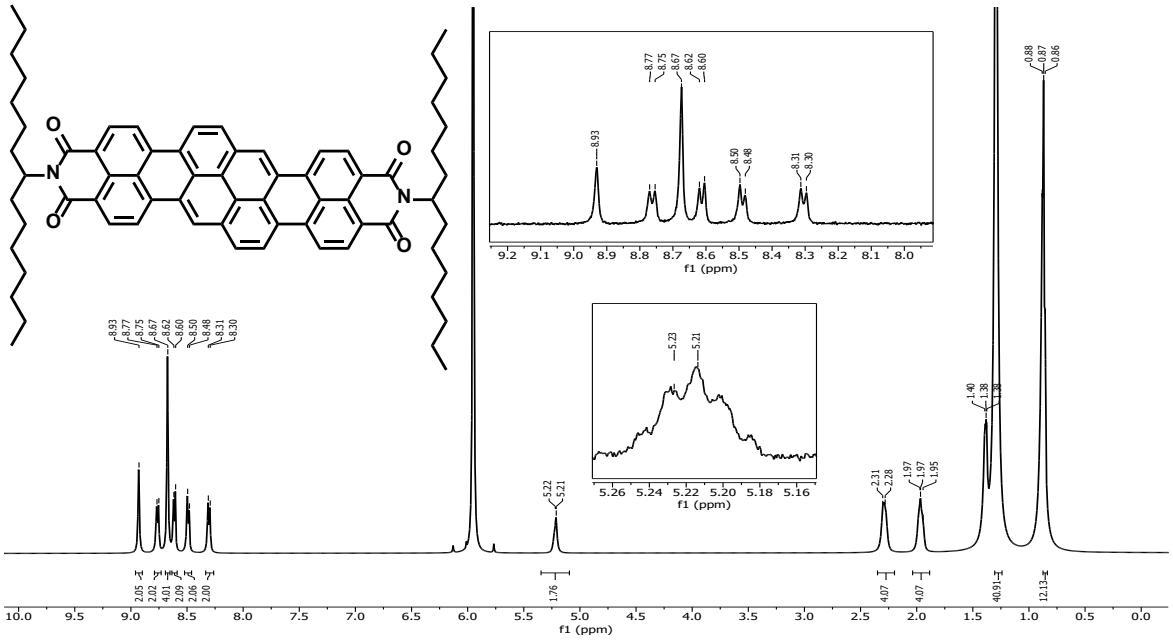

Figure 6-8. ^{1}H NMR spectrum of **6-5**, $C_2D_2Cl_4$, 298 K.

The ability to modify the imide substituent without repeating the whole reaction sequence, and instead relying on an imide-precursor, could help using such building blocks in future applications like organic semiconductors, where variation of the imide substituent can be used to tune the material properties.[174,175]

6.5 Optical and Electronic Properties

To gain insight into the optical and electronic properties of the pseudorylene esters and imide **6-1** – **6-5**, the compounds were characterized by UV-Vis absorption and emission spectra (Figure 6-9) as well as cyclic voltammetry. The results are summarized in Table 6-1. Entries **6-1b** and **6-3b** are the 2,6-di*iso*propylphenyl substituted imides of their respective esters and were synthesized and published by *Shoyama et al.* recently.[92] Their work, which is based on our new facile synthesis of the dibromo-NMI building block **2-21**,[97] focused on expanding the scope of coupling partners for **2-4** to include a variety of PAHs ranging from anthracene, pyrene and coronene to bowl-shaped corannulene.[92,176] Furthermore, efforts by the *Würthner* group went into improving the reaction yields by variation of the solvent and base, culminating in 1-chloronaphthalene as the ideal solvent for the cascade cross-coupling protocol.[177]

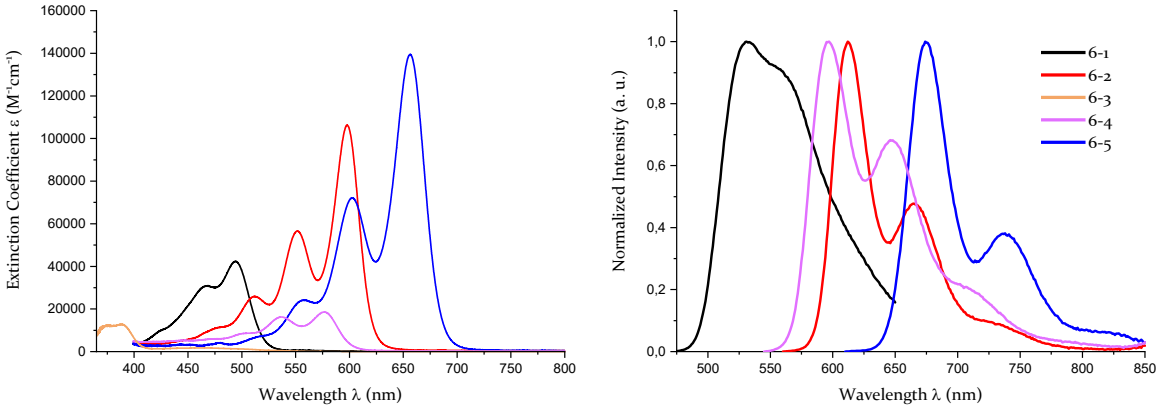

Figure 6-9. UV-Vis absorption (left) and emission (right) spectra of **6-1** (black), **6-2** (red),**6-3** (orange), **6-4** (violet) and **6-5** (blue) in dichloromethane, conc. ~ 10^{-7} M.

When comparing the absorption and emission profiles of TDI **2-16** (Figure 2-9) with those of the pyrene-based diimide **6-5**, similar characteristics become apparent. In both cases, absorption/emission maxima and extinction coefficient are of similar magnitude, which is without surprise considering the structural relationship between the naphthalene- and pyrene-core. The same comparison can be drawn in the pyrene- and terrylene-based carboxylic tetraesters **6-2** and **2-9.** With a slightly larger

molar absorptivity in the pyrene-example (due to the increased size of the conjugated backbone), the approximately same bathochromic shifts in both absorption and emission maxima can be seen when going from carboxylic ester to carboxylic diimide.

Table 6-1. Optical end electronic properties of compounds **6-1** – **6-5**.

	$\lambda_{abs,max}$ (nm)	ε_0 ($M^{-1}cm^{-1}$)	$\lambda_{em,max}$ (nm)	*LUMO* (eV)	*HOMO* (eV)
TTE 2-9	595	83400	610	-3.4	-5.3
TDI 2-16	652	105000	666	-3.7	-5.5
PMI 2-23	507	34670	545	-3.3	-5.6
6-1	494	42529	530	-3.2	-5.4
6-1b	547	43000	598	-3.5	-5.6
6-2	598	105899	612	-3.3	-5.3
6-3	390	12712		-3.3	-5.9
6-3b	497	30000	536	-3.3	-5.7
6-4	576	18633	595	-3.3	-5.3
6-5	656	139219	675	-3.7	-5.4

In the case of the hetero-doped indole-based tetraester **6-4,** a hypsochromically shifted absorption and emission maximum compared to the structurally related TTE **2-9** can be explained by the slightly smaller aromatic backbone due to the five-membered ring in the scaffold. Interestingly, both heterocyclic rylenes **6-3** and **6-4** show low extinction coefficients compared to the other compounds of this series. Additionally, almost no emission could be detected in the case of benzothiophene-based diester **6-3**. Possible explanations for this behavior are the lesser degree of aromaticity (due to poorer overlap of the 3p orbitals of the sulphur atoms with the 2p orbitals of the neighboring carbon atoms) and a push-pull like character caused by the increased electron-density in the rylene scaffold.

Figure 6-10 summarizes the HOMO and LUMO energies of the PAHs synthesized in this chapter for a comparison with the related terrylene-based compounds from chapter 2,[97] and the recent work by *Seifert et al.*[169] and *Shoyama et al.*[92]

As a general trend, the LUMO energies of the carboxylic imides are lower compared to their respective carboxylic ester analogues, which is in accordance to the expected behavior due to the increased electron deficiency caused by the imide substituents. When comparing each respective ester/imide pair, this trend of becomes obvious in their color in solution as well, as a general blue-shift, caused by the decreased bandgap, can be observed.

All terrylene-based compounds display similar HOMO-LUMO gaps, deriving from their structural similarity. Conclusively, π-extension by substitution of the central naphthalene- with a pyrene-unit has a lesser effect on the energy levels than the extension by additional naphthalene-units as shown in the rylene diimide series in Figure 1-2.

In the PMI-related PAH series, all compounds exhibit similar LUMO-values with a larger HOMO-LUMO gap compared to the terrylene-based compounds of this series. This is in accordance with the expected behavior due to the smaller π-conjugated scaffold. As in the terrylene-based PAHs, the influence of core-variation has a lesser influence on the color in solution than lateral extension or the electron density determined by the number of carboxylic ester or imide substituents.

The largest HOMO-LUMO gap of the series can be found in the benzothiophene-based carboxylic ester **6-3**, reflecting the large hypsochromic shift of the absorption band. In contrast, the gap of the indole-based carboxylic ester **6-4** is only slightly larger than that of TTE **2-9**.

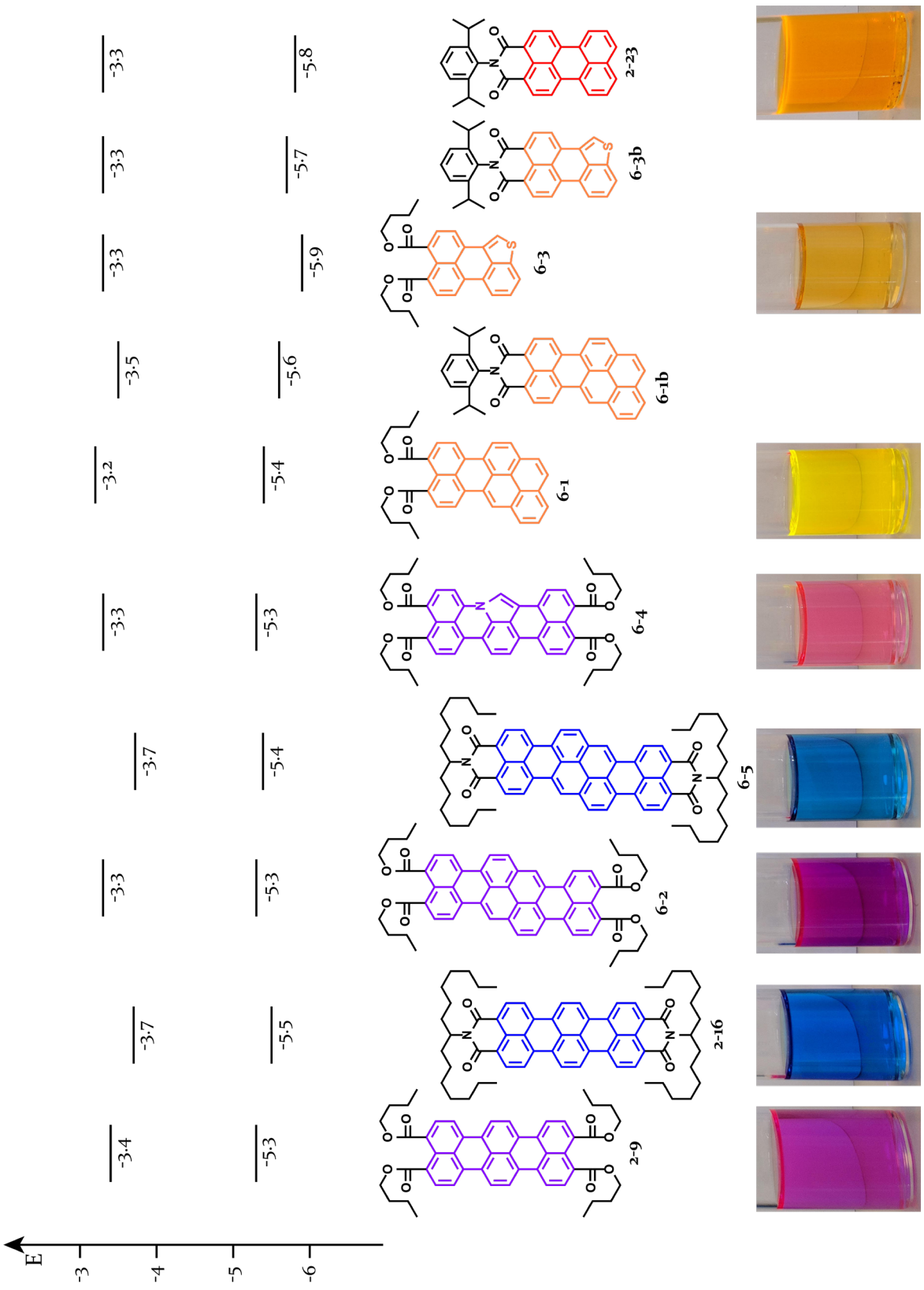

Figure 6-10. HOMO-LUMO energies (in eV) of the electron-deficient PAH series, calculated from the redox potentials in CH_2Cl_2 solutions (0.1 M TBAHFP) with ferrocene as internal standard.

6.6 SUMMARY

This chapter has shown the successful syntheses of different electron-deficient PAHs and heterocyclic PAHs based on the cascade coupling approach starting from small, readily available building blocks. With the synthesis of the pseudoterrylene indole tetraester, a one-pot, triple cascade reaction consisting of *Suzuki-Miyaura* and *Buchwald-Hartwig* cross-coupling followed by C-H activation cyclization was discovered. Until very recently, the introduction of heteroatoms into the rylene imide scaffold was mostly limited to the extension or substitution of the rylene core (see chapter 1) or modification of the *peri* and imide positions, for example the vinylogization of rylene anhydrides with acetylanilines.[178] The ability to design and synthesize large PAHs based on a variety of small, readily available building blocks with moderate to good solubility could facilitate the access towards a multitude of PAHs not available before. With the inclusion of a *Buchwald-Hartwig* amination into the cascade reaction, even heterocyclic PAHs with more than only one type of heteroatom are conceivable.

Investigation into the optical and electronic properties of the PAH series discussed in this chapter offered insights into the influences different 'core' (pyrene, heterocycles) and 'terminal' (carboxylic esters and imides) building blocks have on absorption and emission maxima as well as their band gaps. In particular, the introduction of sulphur into the scaffold increased the HOMO-LUMO gap by a larger amount than in the case of nitrogen. However, only one nitrogen-doped (**6-4**) and one sulphur-doped (**6-3**) example has been synthesized, and a larger number of hetero-PAHs is necessary to understand the relationship between material properties and the nature, amount and placement of the heteroatom(s) in the electron-deficient PAH scaffold. Further work on the triple-cascade cross-coupling protocol could therefore provide an essential synthetic tool to supply functional materials with precisely designed molecular structures that could help to better understand these relationships

Chapter 7
SYNTHESIS OF A TRIANGULAR TRICHROMOPHORE

7.1 INTRODUCTION

One of the central functions of light-harvesting complexes in nature is excitation energy transfer (EET). Until now, the steps involved are still not completely understood. To comprehend these processes at the single-molecule level, many multichromophoric systems have been synthesized and investigated in the past, including linear,[84,179–183] dendrimeric,[184–186] and zigzag rylene imides.[187] However, all these systems share a great disadvantage. The chromophores are linked via flexible spacer groups, which results in a large number of geometric states as well as a variable distance between the chromophores. Because the goal is the investigation of energy transfer pathways at the single-molecule level, minimizing these variables by employing clever molecular design choices to achieve defined, rigid geometries is preferred.

A molecular design that would circumvent the drawbacks is a cyclic arrangement of two or more chromophores, as this would fix the rylene chromophores in place relative to each other and ensure better defined electronic and excitonic coupling patterns. This strategy was first pursued in 2010, using a polymerization approach with *bay*-substituted PDIs.[188] Elaborate efforts went into the photophysical characterization of these macrocyclic multichromophores, but detailed insights into the electronic coupling patterns were still limited by the flexibility of the macrocyclic backbone as well as the presence of *bay*-substituents.[189–191]

Therefore, a triangular tri-PDI, based on the cyclization method for cycloparaphenylenes developed by *Jasti*,[192] was designed. This triangular arrangement (Figure 7-1) used cis-1,4-dimethoxy cyclohexadiene linkers to ensure a high rigidity of the chromophores and did not rely on the presence of *bay*-substituents for increased solubility during the synthesis. While this required greater synthetic effort, the energy

transfer pathways from donor-PDIs D1 and D2 to the acceptor-PDI A could be identified via polarization-resolved single-molecule spectroscopy at 1.2 K. [a]

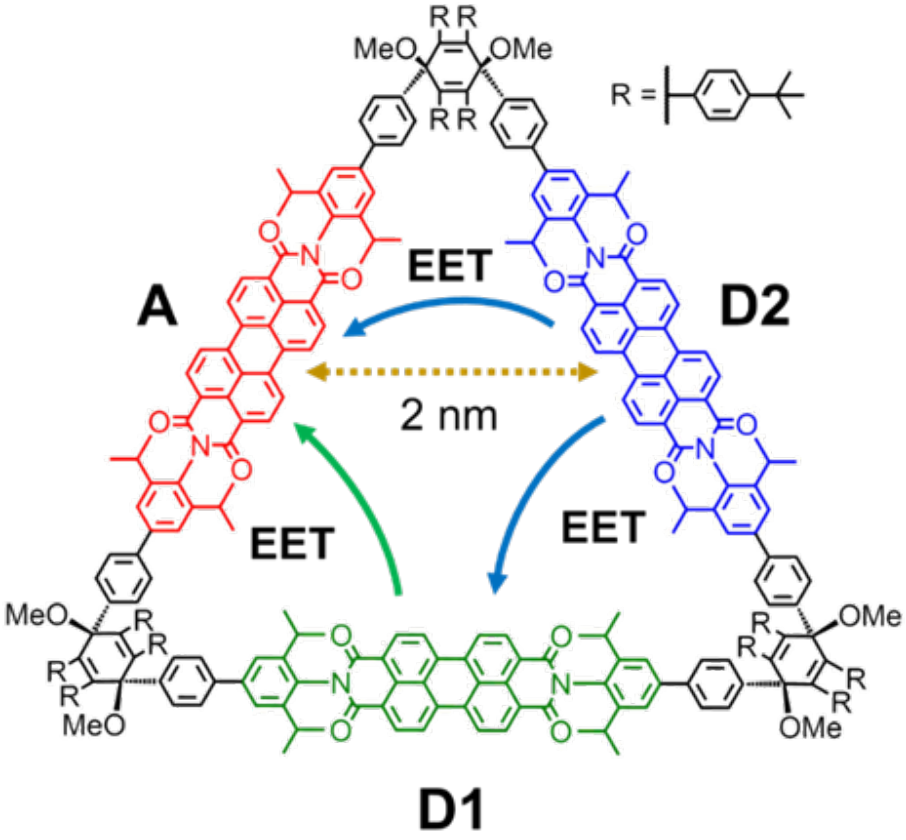

Figure 7-1. Schematic representation of the energy transfer pathway in a triangular PDI.

This chapter's goal will be the synthesis of a similar macrocycle, with a dedicated acceptor chromophore in place of PDI **A**. The EET from donor to acceptor moieties in the macrocycle in Figure 7-1 relies in slight orientational differences between the three chromophores to direct which chromophore acts as the donor and acceptor. Replacing one of the chromophores would lead to a clear energy difference and could allow even more detailed insights into the energy or even electron transfer pathways in a rigid, triangular trichromophore.

[a] Manuscript in preparation by Simon J. Hauschildt, Daniel Uersfeld, Patrick Dewald, Paul Schmid, Bernd Engels, Klaus Müllen, and Thomas Basché.

Two options are possible to replace PDI **A** with a dedicated acceptor. Reminiscent of the linear Acceptor-Donor-Acceptor multichromophore published by our group,[84] TDI can serve as the dedicated acceptor molecule for PDI donors. Alternatively, *bay*-substituted PDIs with bathochromically shifted absorption bands are viable acceptors for unsubstituted PDIs. The choice of one over the other choice will be discussed in the respective section.

7.2 Synthesis of a Symmetric Triangular Macrocycle

In a first step, a triangular trichromophore based on our past work (Figure 7-1) with R = methyl instead of the bulky *tert*-butylphenyl was synthesized as the reference compound for future research into the energy transfer processes in a dedicated donor-acceptor macrocycle.

The triangular macrocycle is built from two different building-blocks; a bifunctional chromophore and a bifunctional cis-1,4-dimethoxy cyclohexadiene based linker-molecule 'kink' (**7-3**, Scheme 7-1).

The synthesis of the 'kink' building-block follows a procedure employed in the bottom-up synthesis for carbon nanotubes,[193] and started with a lithium-halogen exchange reaction between 1,4-dibromobenzene and tetramethyl-*p*-benzoquinone. With the methyl substituted benzoquinone, cis-isomer **7-1** was received in 95 % yield. After methylation and borylation, the diboronic acid pinacol ester of the kink building block **7-3** was acquired in an overall yield of 67 %.

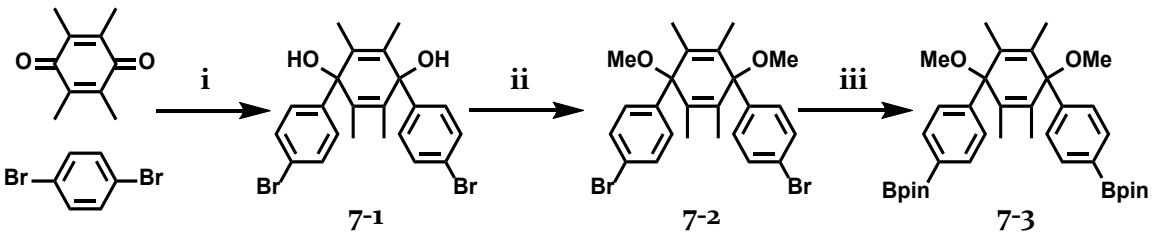

Scheme 7-1. Synthesis of the 'kink' building block **7-3**. Conditions: i) *n*-BuLi, THF, -78 °C, 95 %; ii) NaH, MeI, THF, -78 °C, 90 %; iii) B_2pin_2, $Pd(dppf)Cl_2xCH_2Cl_2$, KOAc, 1,4-dioxane, 80 °C, 65 %.

Followed by *Suzuki-Miyaura* coupling of **7-3** with the para-dibromo substituted PDI **7-4**, the two macrocycle precursors **7-5** and **7-6** could be obtained (Scheme 7-2). Only a highly reactive catalyst system of $Pd(OAc)_2$ and SPhos was able to facilitate a coupling reaction between the two building blocks. This was surprising, because neither solubility nor steric hinderance were expected concerns with compounds **7-3** and **7-4**.

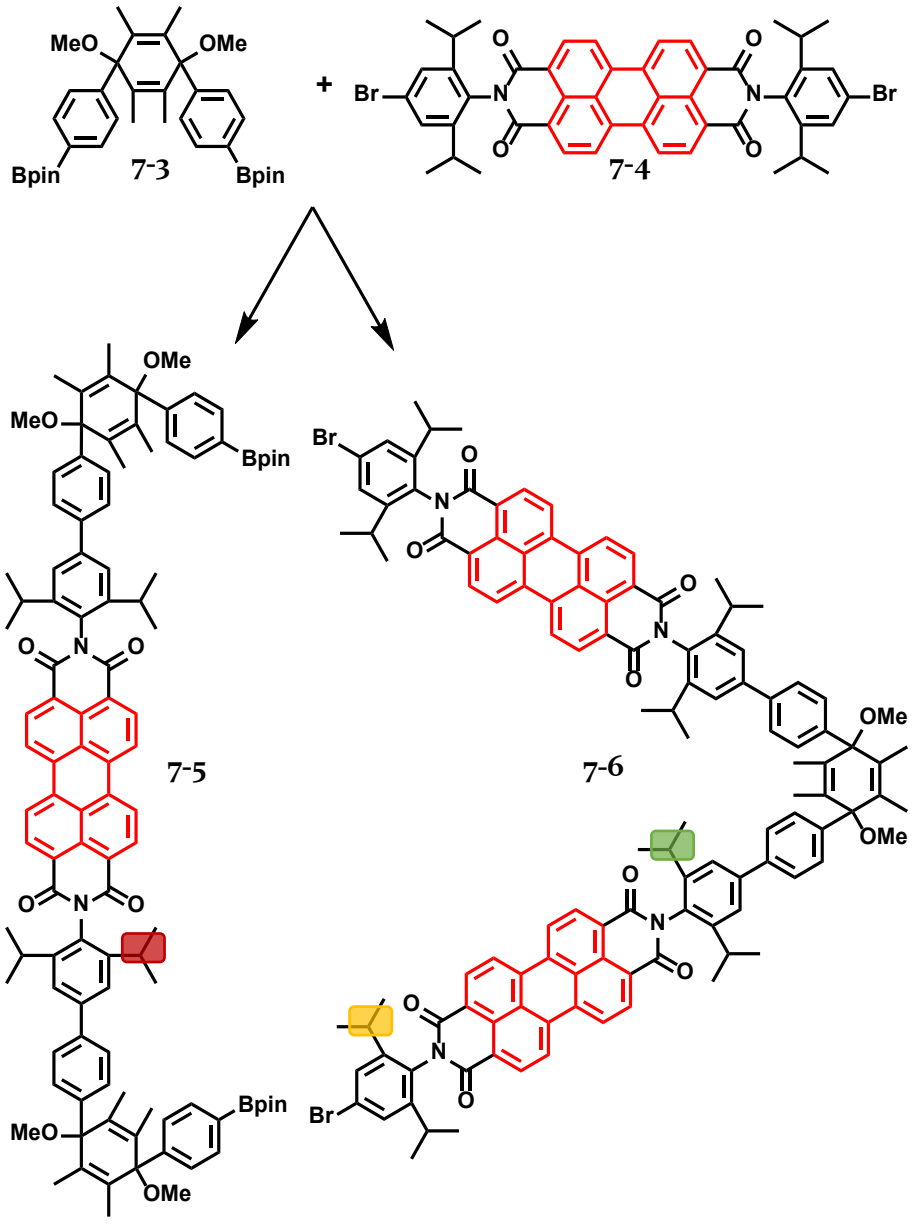

Scheme 7-2. Synthesis of the two kink-PDI building blocks **7-5** and **7-6**. Conditions: $Pd(OAc)_2$, SPhos, K_2CO_3, toluene, H_2O, 85 °C, 10 % for **7-5**, 15 % for **7-6**.

The downside of highly reactive catalyst systems however is the risk of defunctionalization during the reaction. In the presented case, whether precursors **7-5** or **7-6** are received as the products was only be controlled by the ratio of the 'kink'-linker **7-3** to PDI **7-4**. The symmetric nature of all reactants involved leaves either the bromo or boronic ester functionalities (depending on the ratio) exposed to defunctionalization during the reaction. This is a prerequisite for the subsequent cyclization step and these side-reactions cannot be completely avoided.

Another unwanted side-reaction that severely reduced product yield was oligomerization during the coupling reaction towards **7-5** and **7-6**. Based on the *Ruggli-Ziegler* principle, a high concentration favors *inter*molecular instead of *intra*molecular reactions. This principle is based on the higher collision rate between molecules at higher concentrations with a probability for intramolecular reactions that is independent of concentration. Additionally, large excess of one reactant in AA/BB systems can minimize oligomerization by increasing the probability for reaction between monomeric reaction partners. The relatively low solubility of PDI compared to the linker, however, lead to precipitation of the PDI in higher concentration, impeding the control over the reactant-ratios. Therefore, a trade-off was necessary between high concentration to promote reaction between monomeric coupling partners on one hand, and a sufficient dilution to prevent precipitation of reactants and intermediates with low solubility.

Nonetheless, both precursors **7-5** and **7-6** were obtained after silica column and size exclusion chromatography in 10 – 15 % yield. The size-difference between the reactants **7-3**/**7-4**, building blocks **7-5**/**7-6** and higher oligomeric products made separation based on their hydrodynamic radius an effective tool in the isolation of the building blocks.

The ^{1}H NMR spectra of **7-5** (top) and **7-6** (bottom) are shown in Figure 7-2. The most significant difference to distinguish both building blocks are the signals belonging to the *iso*propyl substituents of the PDI units color-marked in Scheme 7-2 and enlarged in Figure 7-2. In the case of **7-5**, the PDI unit is the symmetric center of the

compound, resulting in only one signal. In contrast, **7-6** has to different sets of *iso*-propyl substituents, which is reflected in the two sets of signals marked in Figure 7-2.

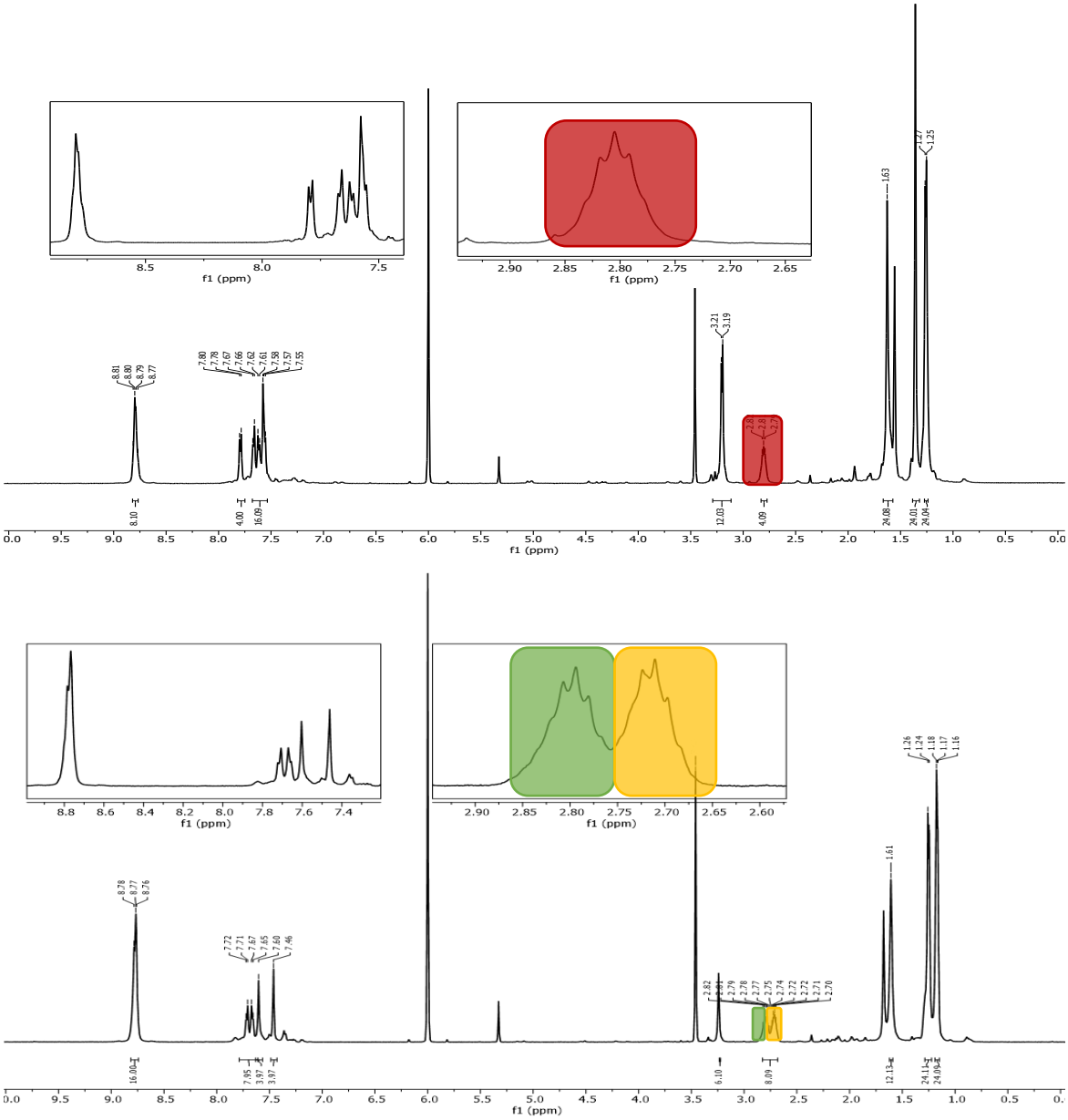

Figure 7-2. ^{1}H NMR spectra of **7-5** (top) and **7-6** (bottom), CD_2Cl_2, 298 K.

In the MALDI-TOF spectra of **7-5** and **7-6** in Figure 7-3, their masses appeared reduced by one methoxy-unit, caused by the fragmentation during MALDI-TOF measurements. This behavior is typical for 1,4-dimethoxy-cyclohexadiene based macrocycles and is documented in the literature.[194]

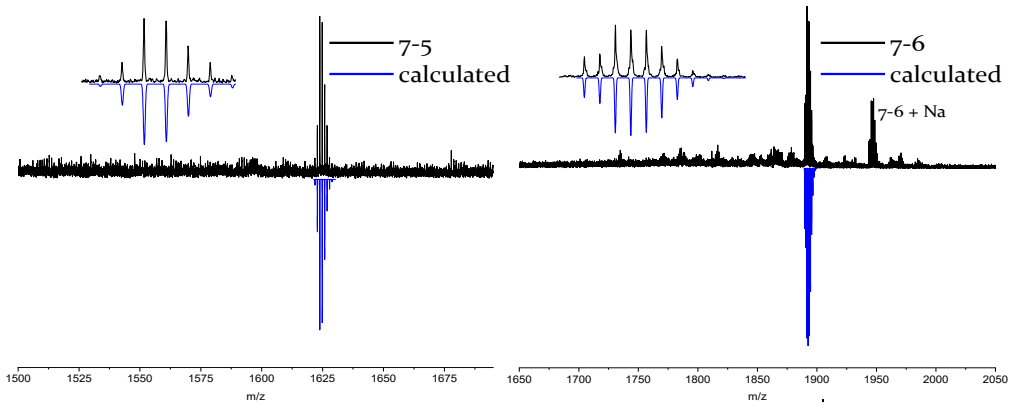

Figure 7-3. MALDI-TOF MS of compounds **7-5** and **7-6**.

In initial test reactions, one of the building blocks was slowly added to the reaction solution to ensure immediate cyclization after coupling between **7-5** and **7-6** without the need for high dilution. However, due to the apparent low rate, no cyclization could be observed. Therefore, with similar reaction conditions as before but in high dilution (5 mM) to prevent intermolecular oligomerization, precursors **7-5** and **7-6** successfully cyclized to the triangular macrocycle **7-7** (Scheme 7-3). After removal of defunctionalized starting material and oligomerized side-products via silica column and size-exclusion chromatography, the macrocycle was received in 8 % yield.

The MALDI-TOF spectrum in Figure 7-4 (reduced by the mass of one methoxy-unit) and ^{1}H NMR spectrum in Figure 7-5 proved the identity of the macrocycle.

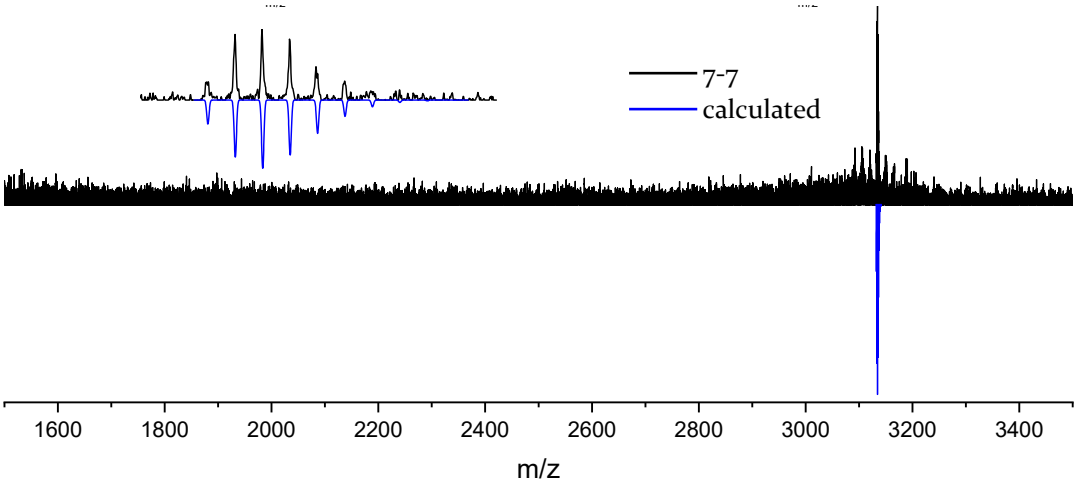

Figure 7-4. MALDI-TOF MS of macrocycle **7-7**.

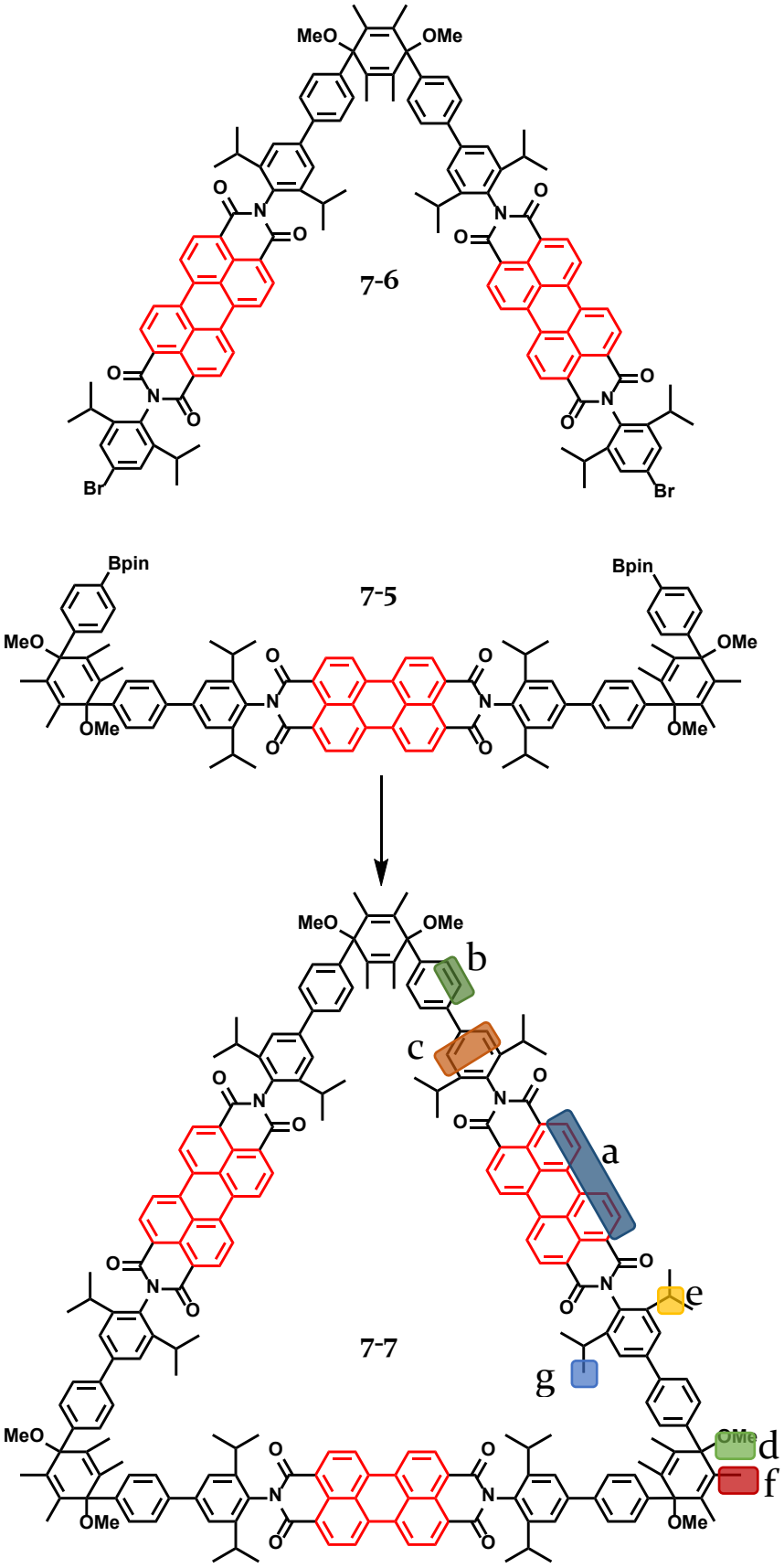

Scheme 7-3. Synthesis of the tri-PDI cycle **7-7**, protons marked for ^{1}H NMR signal assignment. Conditions: $Pd(OAc)_2$, SPhos, K_3PO_4, toluene, H_2O, 85 °C, 8 %.

Due to the symmetric nature of **7-7**, ^{1}H NMR spectroscopy was an effective tool to distinguish the macrocycle from a possible non-cyclized trimer. Two characteristics unmistakably proved the existence of a macrocycle; the three separated groups of aromatic protons (PDI core, 2,6-di*iso*propylphenyl, 1,4-diphenyl) as well as the septet belonging to the *iso*propyl groups. Due to its asymmetry, a non-cyclized trimer would show a larger number of proton signals and could therefore be successfully distinguished from the macrocycle.

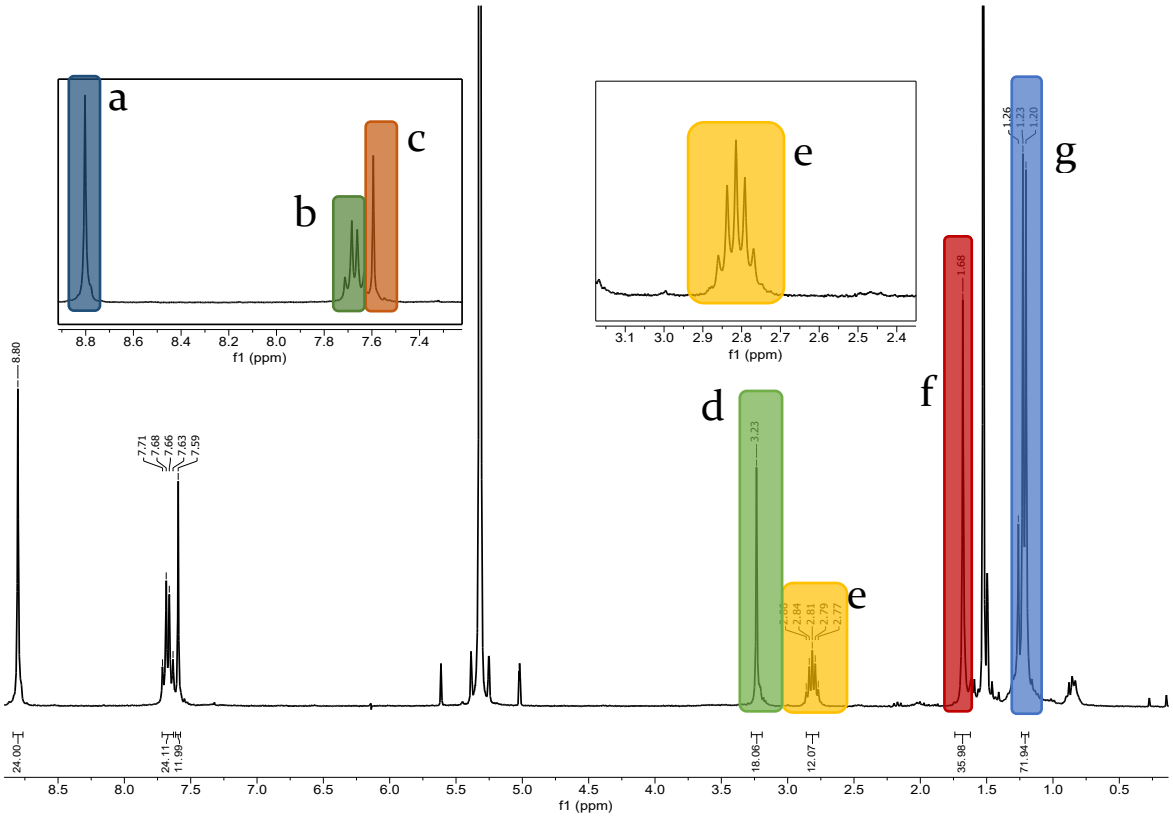

Figure 7-5. ^{1}H NMR spectrum of macrocycle **7-7** in CH_2Cl_2, 298 K.

In the UV/Vis absorption and emission spectra of **7-5**, **7-6** and **7-7** in toluene, the typical PDI absorption and emission bands belonging to the 0-0, 0-1 and 0-2 transitions can be seen. As was expected for the ensemble spectra at room temperature, both building blocks and the macrocycle had the same absorption and emission maxima $\lambda_{abs,max}$ = 528 nm and $\lambda_{abs,max}$ = 538 nm. Due to the number of chromophores per molecule (one PDI in **7-5**, two PDIs in **7-6**, three PDIs in macrocycle **7-7**), the extinction coefficient of macrocycle **7-7** was around three times higher than in the case of mono-PDI building block **7-5**. The extinction coefficient of **7-5** (ε = 70769 $M^{-1}cm^{-1}$) matched the value of DIPP-PDI (ε = 70980 $M^{-1}cm^{-1}$),[195] proving that the linker molecules had no influence on the absorption cross section determining the extinction coefficient.

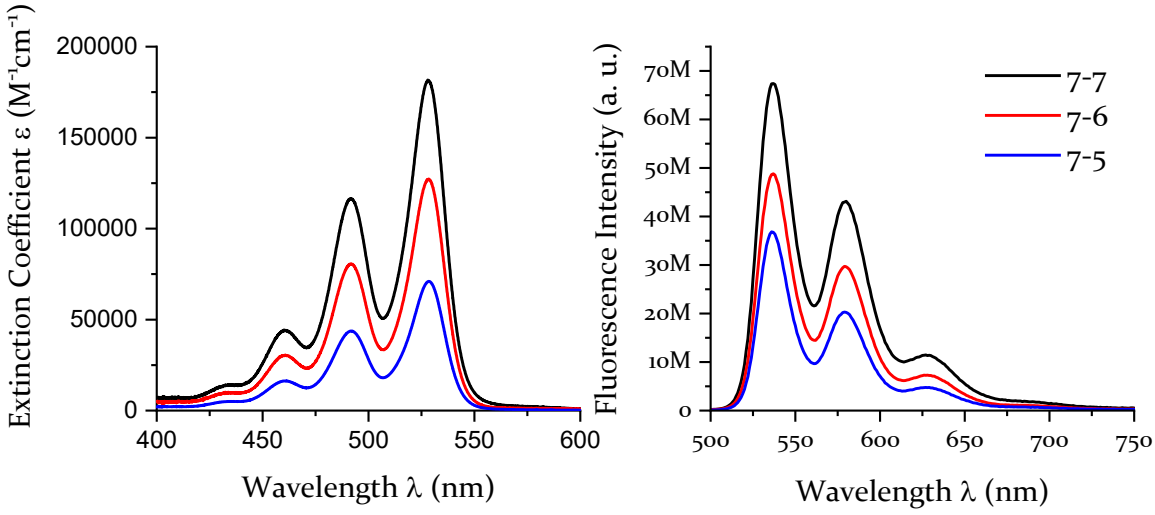

Figure 7-6. UV/Vis absorption (left) and emission (right) spectra of compounds **7-5**, **7-6** and **7-7**, toluene, conc. = 9.9^{-6} M (absorption), 9.9^{-7} M (emission).

Fluorescence lifetimes of **7-5** – **7-7** (± 0.02 ns) were calculated from the fluorescence decay curves measured by *Marius Bauer* in Figure 7-7 and are of the same magnitude as the lifetime of DIPP-PDI (τ = 3.68 ns). Energy transfer would translate into reduced fluorescence lifetimes at the emission wavelength of the donor. However, as the energy difference of the PDIs stems from orientational variation and is only

observable at low temperatures on the single molecule level, the experimental results in the ensemble at room temperature are consistent with the expected behavior.

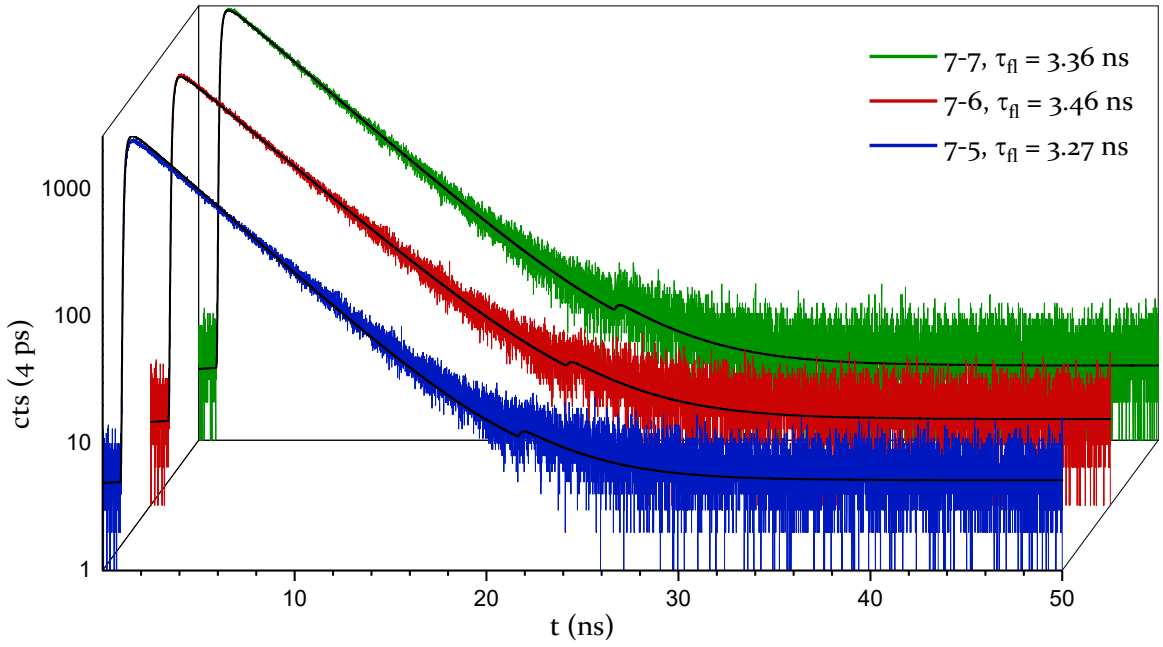

Figure 7-7. Fluorescence decay curves of **7-7** (green), **7-6** (red) and **7-5** (blue) in toluene, conc. = 9.9^{-7} M, λ_{exc} = 488 nm, λ_{em} = 538 nm. Measurements by *Marius Bauer*.

7.3 Synthesis of a Donor-Acceptor Macrocycle

After the successful synthesis of the symmetric triangular trichromophore **7-7**, as a next step, one of the PDIs should be exchanged for a dedicated acceptor chromophore. A logical approach would be the insertion of one or two TDIs instead of PDI to act as the acceptor moiety, a design that would mimic the linear Acceptor-Donor-Acceptor multichromophore that has been investigated in the past.[84,196]

Two arguments speak against a design like this, however. First, much like in chapter 3, neither syntheses of *para*-bromo substituted TDI **7-8** succeeded (Scheme 7-4). In the case of imidization, no reaction could be observed at all, whereas the cascade coupling approach resulted in a complicated mixture of different coupling products, without any evidence for the difunctionalized TDI. Alternatively, one of the earlier approaches towards TDIs could be used to synthesize TDI **7-8**, which would require a lengthy synthesis without a guarantee of a successful cyclization afterwards.

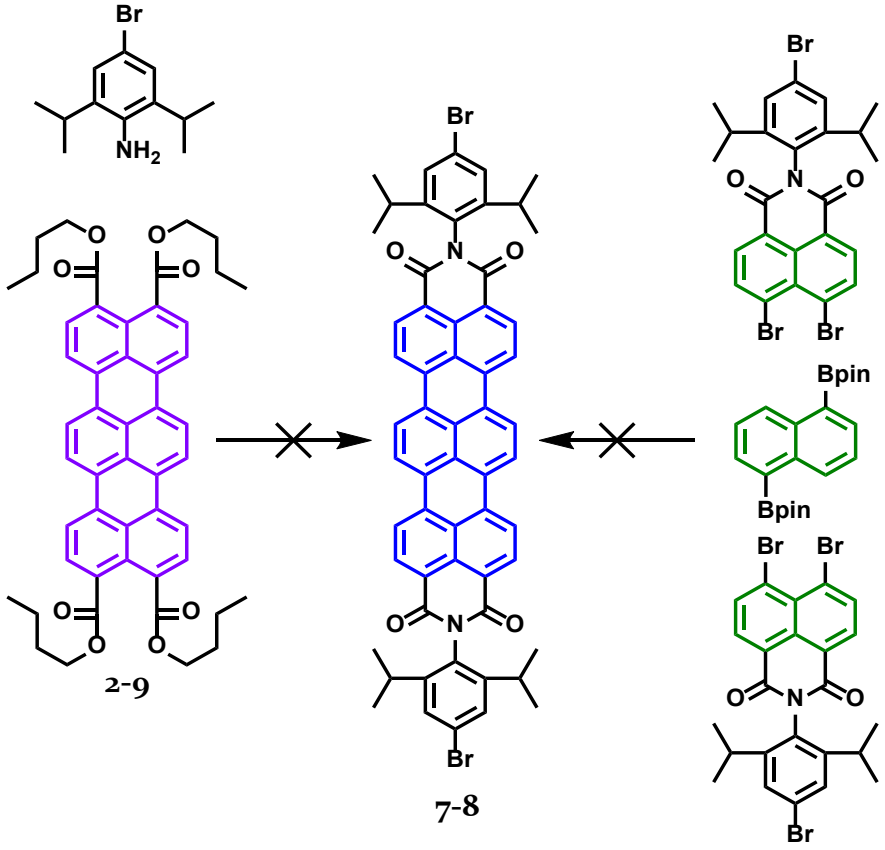

Scheme 7-4. Unsuccessful syntheses of *para*-dibromo TDI **7-8**.

The second argument against using TDI is of geometrical nature. A great part of calculations that are the basis for understanding the experimental results of the macrocycle in Figure 7-1 are based on the hypothesis of an equiangular triangular shape of the macrocycle. When basing future research on energy or electron transfer in a dedicated donor-acceptor macrocycle on **7-7** as the reference material, the increased length of TDI in a mixed TDI-PDI derivative of **7-7** would lead to a distorted triangular shape. Interpreting experimental results between the reference macrocycle **7-7** and a hypothetical TDI_n-PDI_m-macrocycle would be dramatically more difficult. Furthermore, even though the 'kink'-linker molecules are flexible to a degree,[194] it is unclear if the narrow kinking angle necessary for a cyclization reaction between TDI- and PDI-precursors would be possible. Given the already low yields of the symmetric macrocycle **7-7**, the prospects of a successful cyclization were too low to follow the TDI-PDI-macrocycle approach.

Alternatively, an amino-substituted PDI as the acceptor unit was envisioned. Following a literature-reported direct amination procedure,[197] *bay*-pyrrolidine substituted PDI **7-9** was synthesized in 69 % yield (Scheme 7-5). According to the provided spectroscopic data, this pyrrolidine-substituted PDI absorbs in the range of 550 – 750 nm, which is the region of TDI absorptivity and should therefore be suited for energy transfer experiments between PDI and pyrrolidine-PDI.

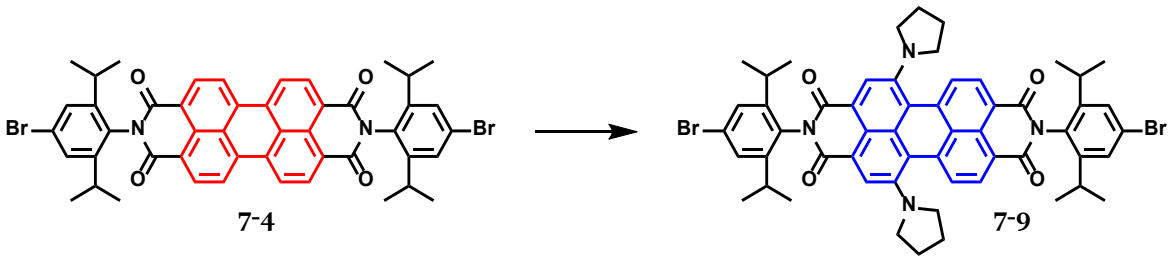

Scheme 7-5. Synthesis of the pyrrolidine-substituted PDI **7-9**. Conditions: pyrrolidine, $KMnO_4$, $AgNO_3$, r.t., 16 h, 65 %.

With pyrrolidine-PDI **7-9**, macrocycle precursor **7-10** was synthesized (Scheme 7-6) in 33 % yield after column chromatography. Surprisingly, $Pd(PPh_3)_4$ was sufficient as a catalyst with moderate reactivity. This suggests that the problems of the *Suzuki-Miyaura* couplings in the previous section might be caused by low solubility of the unsubstituted PDI, or be of electronic nature. Due to the pyrrolidine substituents at the *bay*-positions, the resulting pyrrolidine-PDI is more soluble and more electron rich, and both effects could contribute to cross-coupling reactivity.

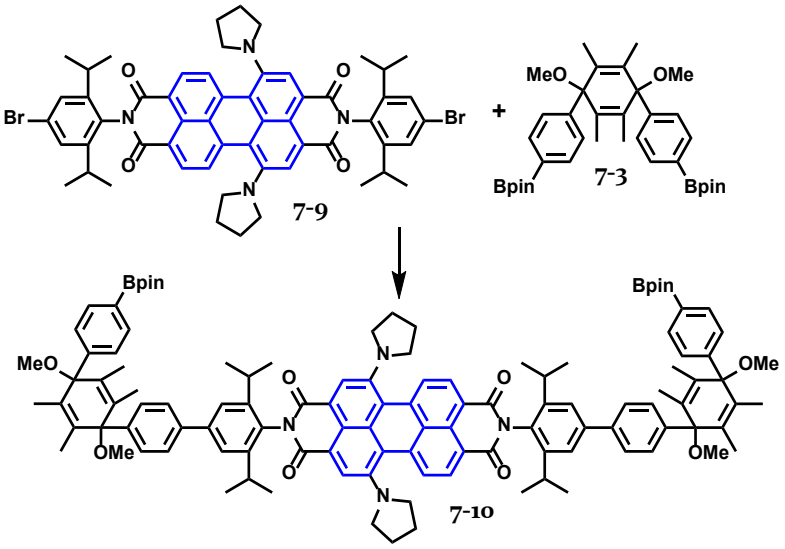

Scheme 7-6. Synthesis of the pyrrolidine-PDI building block **7-10**. Conditions: $Pd(PPh_3)_4$, K_2CO_3, toluene, EtOH, H_2O, 80 °C, 16 h, 33 %.

Figure 7-8 shows the MALDI-TOF spectrum of the pyrrolidine-PDI precursor **7-10**, and the calculated isotopic pattern matches the experimental results. The additional signals stem from fragmentation during MALDI-TOF MS measurements. These fragments are attributed to the loss of the four methoxy-groups (m/z = 30) of the 'kink'-linker and is documented in the literature.[194]

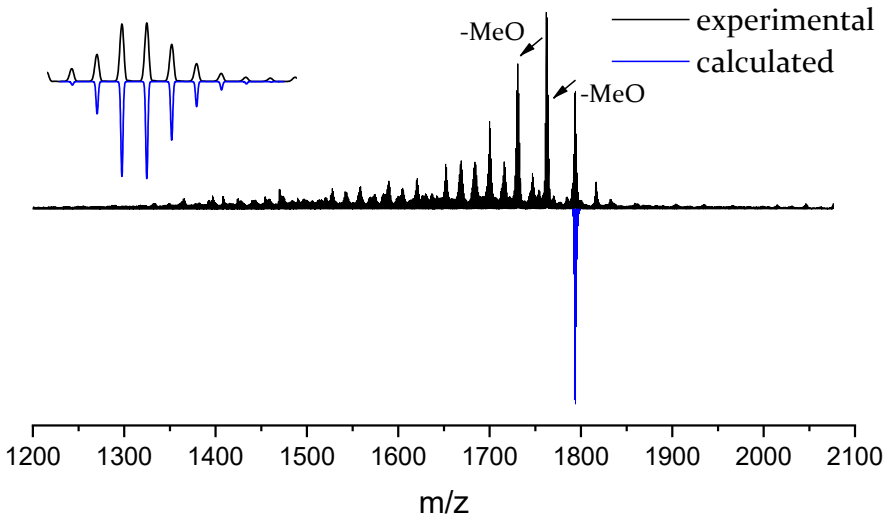

Figure 7-8. MALDI-TOF spectrum of pyrrolidin-PDI precursor **7-10**.

Both precursors **7-6** and **7-10** were then subjected to cyclization reactions in an attempt to synthesize donor-acceptor macrocycle **7-11** (Scheme 7-7). Under the conditions listed in Table 7-1, no reaction could be observed by TLC and MALDI-TOF MS analysis.

Table 7-1. Reaction conditions for the cyclization between **7-6** and **7-10.**

	Catalyst	Base	Solvent	Temperature
1	$Pd(PPh_3)_4$	K_2CO_3	Toluene/H_2O	80 °C
2	$Pd(PPh_3)_4$	K_2CO_3	1,4-Dioxane/H_2O	80 °C
3	$Pd(dppf)Cl_2$	K_2CO_3	Toluene/H_2O	80 °C
4	$Pd(dppf)Cl_2$	K_2CO_3	1,4-Dioxane/H_2O	80 °C
5	$Pd(OAc)_2$/SPhos	K_2CO_3	Toluene/H_2O	80 °C
6	$Pd(OAc)_2$/SPhos	K_2CO_3	1,4-Dioxane/H_2O	80 °C

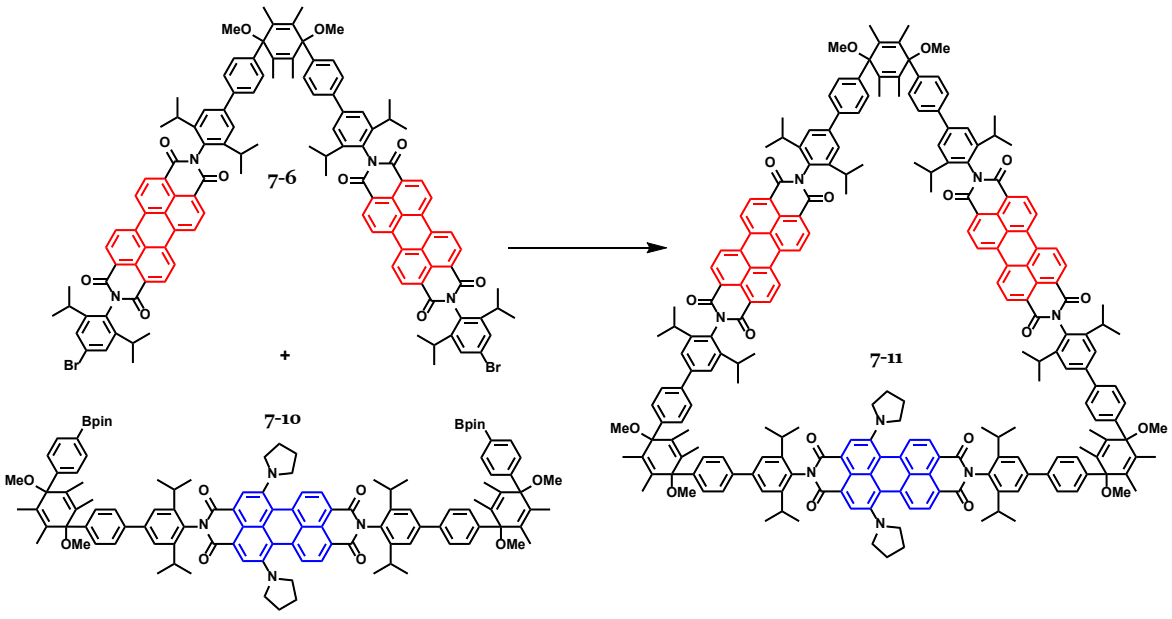

Scheme 7-7. Envisioned synthesis of the donor-acceptor macrocycle **7-11**.

Upon inspection of the sample vial with the precursor **7-10**, the otherwise dark blue solid was covered with a brown coating. MALDI-TOF MS analysis (Figure 7-9) of the substance revealed the complete loss of the boronic ester groups. This was surprising, as the boronic esters of rylene imides are generally stable under ambient

conditions and this behavior has not been observed with boronic esters of rylene dyes before. At the time of this writing, the reason for the instability of **7-10** is unclear.

To further pursue the goal of obtaining a pyrrolidine-substituted PDI macrocycle, newly prepared precursor **7-10** should be strictly kept under argon while a reference sample should be exposed to ambient conditions in order to clarify whether the increased electron density caused by the amine substituents results in degradation of **7-10**.

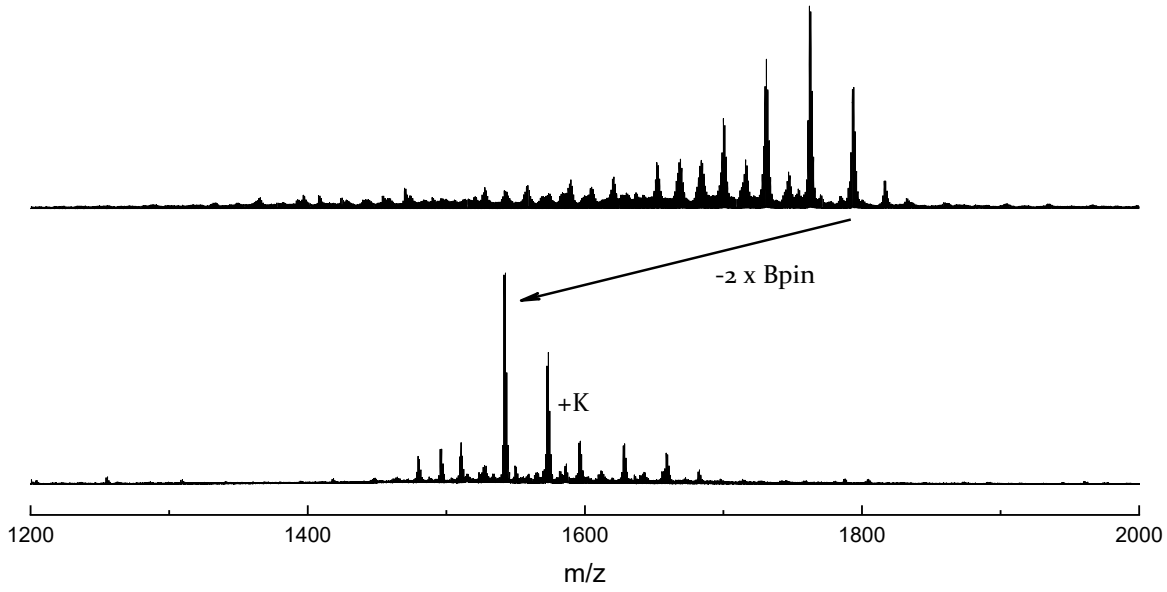

Figure 7-9. MALDI-TOF showing the degradation of the pyrrolidine-PDI precursor **7-10** under the exposure to ambient conditions.

7.4 Summary

This chapter demonstrated the successful synthesis of the triangular macrocycle **7-7** with three unsubstituted PDIs serving as chromophores for energy transfer studies. This macrocycle is envisioned as the reference material for an otherwise identical macrocycle in which one or two of the PDIs will be exchanged for an acceptor molecule with identical length. With this restriction, TDI as the acceptor chromophore was disregarded, although energy transfer on multichromophores consisting of a mix of PDI and TDI has been studied in the past.

The special geometrical restrictions of this rigid triangular macrocycle demanded for a chromophore of the same length as the reference material but an absorption profile similar to TDI. For this reason, pyrrolidine-substituted PDI **7-9** was chosen and a macrocycle precursor **7-10** based on pyrrolidine-PDI was synthesized. However, all attempts of cyclization were futile. Inspection of the precursor sample revealed the degradation of the substance under the loss of the boronic ester substituents. Future attempts at cyclization with amine-substituted macrocycle precursors should therefore take special care to keep the compounds from being exposed to ambient conditions.

SUMMARY AND CONCLUDING REMARKS

In summary, a novel approach based on a cascade cross-coupling protocol has been established that enabled the synthesis of symmetric and asymmetric rylene imides and esters. Using this protocol, TDI building blocks were prepared on a gram scale and with minimal efforts required for purification, starting from readily available material. The scope of materials derived from these building blocks ranges from terrylene-based symmetric and asymmetric dyes and pigments to functional materials for photophysical studies into the spin states of coordination complexes and as potential guest-chromophores in host-guest chemosensors for enzymatic redox and hydrolysis reactions. The cascade cross-coupling protocol was also expanded towards PAH-based carboxylic esters and imides including heteroaromatic scaffolds, and a triple cascade reaction consisting of three distinct cross-coupling reactions was discovered.

During this work, several synthetic obstacles encountered were overcome by either improved reaction conditions or alternate molecular designs, but others still remain. This includes the central, unanswered question whether reliable conditions can be established that allow a comprehensive number of amines and anilines to serve as nucleophiles in the imidization reaction with terrylene and naphthalene building blocks. Currently, the unpredictable success rate of the imidization reaction hampers the universal applicability of the cascade approach. Whereas sterically unhindered amines were generally sufficiently reactive, sterically hindered anilines and aromatic amines with poor solubility resulted in low yields or no reaction at all. However, hydrolysis and decarboxylation were identified as the main side-reactions, caused by the necessity for harsh reaction conditions in these problematic cases. Going forward, the largest room for improvement lies in the exploration of nucleophilic catalysts that would allow imidization reactions under milder conditions for low-reactivity amines and anilines.

In conclusion, a new approach towards synthesizing terrylene and PAH imides has been discovered that significantly facilitates the access to rylene- and PAH-based nanocolorants by streamlining the synthesis and purification methods required. These advantages, that minimize the obstacle of lengthy, low-yielding syntheses, could raise the interest of the scientific community in these rylene-based materials to the same level only PDIs have reached so far.

EXPERIMENTAL SECTION

MATERIALS AND METHODS

All compounds were purchased from Sigma-Aldrich, Fisher Scientific, VWR, TCI Europe, Acros, or were provided by BASF, and were used without purification. Reactions in inert atmosphere were performed using standard *Schlenk*-techniques using argon as inert gas. Work-up and purification were performed under air with reagent-grade solvents. Column chromatography was performed using silica gel (particle size of 0.04 – 0.063 mm or 0.063 – 0.200 mm from Macherey-Nagel), and silica coated aluminum sheets with fluorescence indicator from Macherey-Nagel were used for TLC analysis. All ^{1}H and ^{13}C NMR spectra were recorded on a Bruker AVANCE 300, Bruker AVANCE III 500, Bruker AVANCE III 700 or Bruker AVANCE III 850 spectrometer in the listed deuterated solvent supplied by Sigma-Aldrich. Field desorption (FD) mass spectrometry was performed on a VG Instruments ZAB 2-SE-FPD. High-resolution MALDI-TOF mass spectrometry was performed on a Waters Corp. SYNAPT G2 Si high resolution time-of-flight mass spectrometer. All samples were recorded as solid-state samples with tetracyanoquinodimethane as matrix. Electrospray ionization mass spectrometry was performed on an Agilent 6545 QTOF-MS spectrometer. Solution UV/Vis absorption and emission spectra were recorded at room temperature in the listed solvents (HPLC grade) in a 10 mm standard quartz cell. Melting points were recorded using Büchi B-545 melting point at a heating rate of 5 °C/min. Cyclic voltammetry was performed on an EG&G Princeton Applied Research potentiostat model 273. A palladium-carbon electrode (1.5 mm diameter) was used as the working electrode with platinum and silver wires as a counter and reference electrodes, respectively. Measurements were carried out in 0.1 Bu_4NPF_6 solutions in anhydrous, degassed CH_2Cl_2 or THF using ferrocene/ferrocenium as internal standard. Infrared spectra were recorded on a Nicolet FT-IR 730. Elemental analysis of solid samples was performed on an Elementar vario EL Cube.

4,5-Dibromo-1,8-naphthalenedicarboxylic anhydride (2-4)

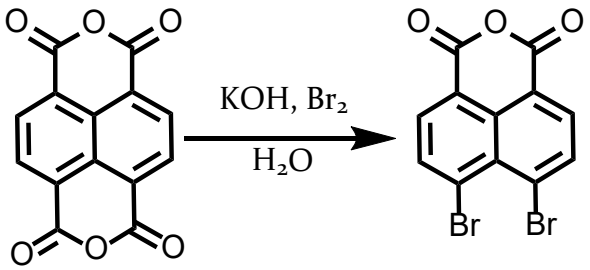

To a stirred suspension of 1,4,5,8-naphthalenetetracarboxylic dianhydride (10.03 g, 37.3 mmol) in 350 mL H_2O was added KOH (10.51 g, 186.4 mmol) and the suspension was heated to 85 °C. To the hot solution was added Br_2 (4.7 mL, 93.2 mmol) dropwise and the solution was stirred for 1 h. After the reaction was allowed to cool to room temperature, 20 mL HCl was added. The precipitate was filtered, washed with water and MeOH to afford 4,5-dibromo-1,8-naphthalenedicarboxylic anhydride (12.61 g, 95 %) as a light brown, poorly soluble solid. The compound was used without further purification.

Terrylene-3,4,11,12-tetra(*n*-butylcarboxylate) (2-9)

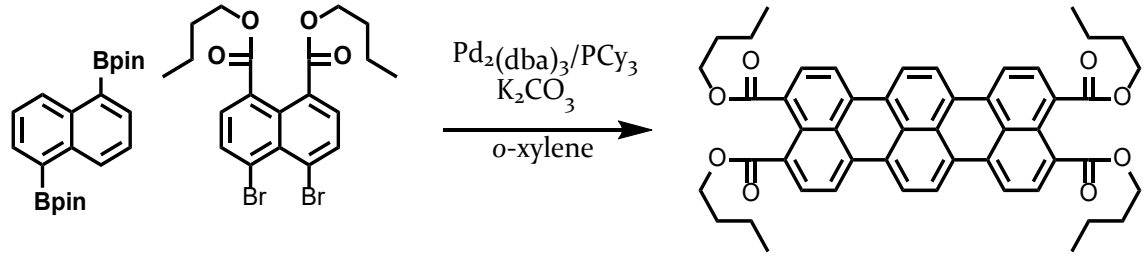

A mixture of 1,5-naphthalenediboronic acid pinacol ester **2-11** (1.39 g, 3.6 mmol), **2-10** (3.90 g, 8.0 mmol), K_2CO_3 (5.97 g, 43.2 mmol), $Pd_2(dba)_3$ (665.6 mg, 729 µmol), tricyclohexylphosphine (818.0 mg, 2.9 mmol) and 115 mL *o*-xylene was stirred at 145 °C under argon atmosphere. After stirring for 24 h, the reaction was cooled to room temperature and poured into MeOH. The precipitate was filtered, dissolved in dichloromethane, washed with water and brine and dried over $MgSO_4$. After removal of the solvent, the title compound was redissolved in dichloromethane and

precipitated from MeOH, filtered, washed with ethanol and methanol to afford compound **2-9** (2.10 g, 75 %) as violet solid.

^{1}H NMR (700 MHz, $C_2D_2Cl_4$) δ = 8.22 (s, 4H), 8.18 (d, *J* = 7.9 Hz, 4H), 8.00 (d, *J* = 7.8 Hz, 4H), 4.31 (t, *J* = 6.8 Hz, 8H), 1.82 – 1.73 (m, 8H), 1.53 – 1.45 (m, 8H), 0.99 (t, *J* = 7.4 Hz, 12H).

^{13}C NMR (176 MHz, CD_2Cl_2) δ = 169.1, 133.8, 130.6, 130.0, 129.7, 129.7, 129.1, 127.6, 122.8, 120.2, 65.7, 31.3, 19.9, 14.3.

HR-MS (MALDI-TOF): m/z = 776.3338, calcd. for $C_{50}H_{48}O_8$: m/z = 776.3349.

UV/Vis: $\lambda_{abs,max}$ = 595 nm, ε_0 = 83400 $M^{-1}cm^{-1}$, $\lambda_{em,max}$ = 610 nm.

FT-IR: $\tilde{\nu}$ [cm^{-1}] = 2959, 2928, 2872, 2846, 1710, 1581, 1525, 1508, 1460, 1446, 1402, 1379, 1324, 1261, 1199, 1169, 1150, 1103, 1060, 1033, 944.

Mp = 214 – 216 °C.

4,5-Dibromonaphthalene-1,8-di(*n*-butylcarboxylate) (2-10)

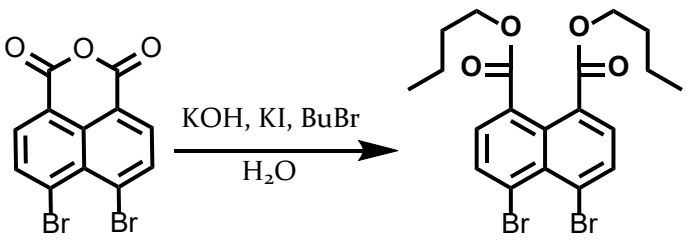

To a suspension of **2-4** (4.01 g, 11.2 mmol) in 150 mL H_2O was added KOH (3.2 g, 56.2 mmol) and the suspension was heated to 85 °C. The solution was precipitated in acetone/isopropanol and filtered. The resulting potassium salt, KI (186.5 mg, 1.1 mmol), butylbromide (7.2 mL, 67.4 mmol) and Aliquat 336 (1 mL) were added and the reaction was stirred overnight. After cooling to RT, the organic layer was dissolved in dichloromethane, washed with water and brine and dried with $MgSO_4$. The raw mixture was filtered on a pad of silica (dichloromethane/petroleum ether 1:10) to separate the title compound from Aliquat 336 and alkylbromide. After removal of

the solvent, compound **2-10** was mixed with hexane, cooled in liquid nitrogen and upon crystallization, was filtered and washed while still cold, to afford the title compound as a pale-yellow solid (3.55 g, 65 %).

^{1}H NMR (300 MHz, CD_2Cl_2) δ 8.04 (d, J = 7.8 Hz, 2H), 7.78 (d, J = 7.8 Hz, 2H), 4.25 (t, J = 6.8 Hz, 4H), 1.73 (m, J = 8.5, 6.6 Hz, 4H), 1.51 – 1.38 (m, 4H), 0.97 (t, J = 7.4 Hz, 6H).

^{13}C NMR (75 MHz, CD_2Cl_2) δ 168.2, 135.3, 132.2, 131.6, 130.8, 130.3, 124.7, 66.1, 31.1, 19.8, 14.1.

FD-MS: m/z = 486.3, calcd. for $C_{20}H_{22}Br_2O_4$: m/z = 486.2.

FT-IR: $\tilde{\nu}$ [cm^{-1}] = 2958, 2872, 1715, 1585, 1552, 1503, 1462, 1284, 1260, 1156, 1187, 1103, 1063, 1037, 938, 842, 801, 770, 744, 1397, 1381, 1351, 1434, 985, 901.

Mp = 45 – 46 °C.

N,N'-Bis(1-heptyloctyl)-terrylene-3,4,11,12-tetracarboximide (2-16)

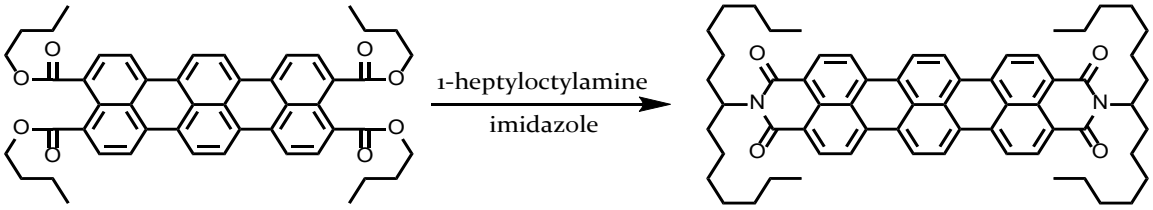

A mixture of **2-9** (301.2 mg, 386 µmol), 1-heptyloctylamine[198] (702.6 mg, 3.1 mmol) and imidazole (4 g) was stirred at 170 °C for 16 h. After cooling to 100 °C, the reaction mixture was poured into 300 mL diluted aqueous HCl and stirred for 1 h. The precipitate was filtered, washed with diluted HCl, water and MeOH. The solid was dissolved in dichloromethane and filtered through a pad of silica. The solution was concentrated in vacuo and precipitated in MeOH, filtered and washed with MeOH to afford compound **2-16** (216.7 mg, 60 %) as blue solid.

^{1}H NMR (700 MHz, $C_2D_2Cl_4$) δ = 8.59 (d, *J* = 8.1 Hz, 4H), 8.53 (s, 4H), 8.46 (d, *J* = 8.0 Hz, 4H), 5.15 (m, 2H), 2.26 – 2.18 (m, 4H), 1.93 – 1.85 (m, 4H), 1.39 – 1.20 (m, 40H), 0.82 (t, *J* = 7.0 Hz, 12H).

^{13}C NMR (176 MHz, CD_2Cl_2) δ = 165.0, 164.0, 135.3, 130.8, 129.9, 128.3, 125.9, 124.1, 121.5, 55.0, 33.0, 32.5, 30.2, 29.9, 27.8, 23.3, 14.5.

HR-MS (MALDI-TOF): m/*z* = 934.5648, calcd. for $C_{64}H_{74}N_2O_4$: m/*z* = 934.5649.

UV/Vis: $\lambda_{abs,max}$ = 652 nm, ε_0 = 105000 $M^{-1}cm^{-1}$, $\lambda_{em,max}$ = 666 nm.

FT-IR: $\tilde{\nu}$ [cm^{-1}] = 2953, 2921, 2853, 1923, 1693, 1647, 1583, 1507, 1460, 1417, 1395, 1378, 1351, 1321, 1302, 1249, 1206, 1175, 1145, 1107, 1024, 959.

Mp = 280 °C.

N,N'-Bis(*n*-octyl)-terrylene-3,4,11,12-tetracarboximide (2-17)

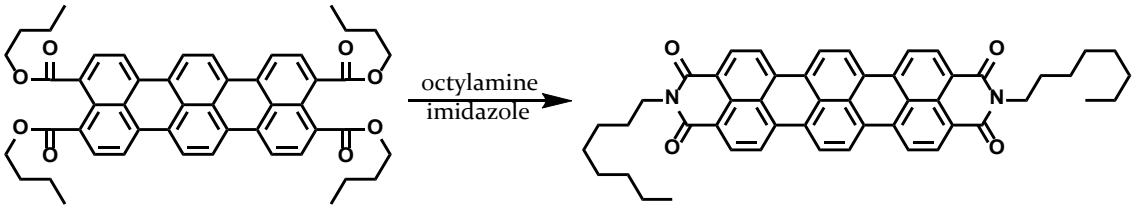

A mixture of **2-9** (203.4 mg, 262 µmol), *n*-octylamine (0.35 mL, 2.1 mmol) and imidazole (5 g) was stirred at 170 °C for 16 h in a sealed pressure vessel. After cooling to 100 °C, the reaction mixture was poured into 100 mL diluted aqueous HCl (2N) and stirred for 1 h. The precipitate was filtered, washed with aqueous HCl, water and MeOH. The precipitate was dissolved in hot H_2SO_4 and water was added dropwise until the green solution turned into a blue suspension. After the suspension cooled to room temperature, the precipitate was filtered, washed with water, ethanol and methanol to afford compound **2-17** (139.3 mg, 72 %) as blue solid.

HR-MS (MALDI-TOF): m/*z* = 738.3460, calcd. for $C_{50}H_{46}N_2O_4$: m/*z* = 738.3458

FT-IR: $\tilde{\nu}$ [cm^{-1}] = 2952, 2925, 2850, 2361, 2336, 2114, 1992, 1690, 1651, 1583, 1507, 1462, 1431, 1382, 1352, 1330, 1307, 1258, 1210, 1167, 1087, 1046, 1013, 960.

Mp > 370 °C.

N,N'-Bis(phenyl)-terrylene-3,4,11,12-tetracarboximide (2-18)

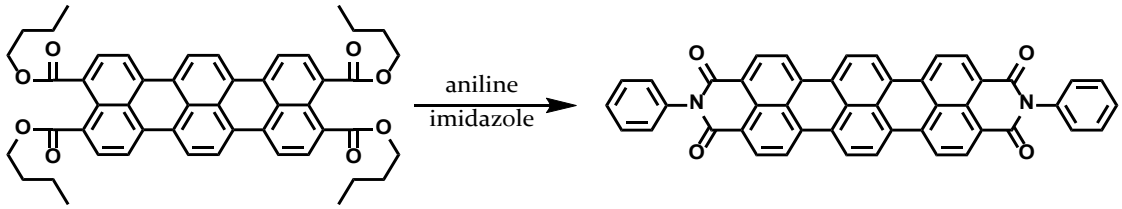

A mixture of **2-9** (202.7 mg, 261 µmol), aniline (0.20 mL, 2.2 mmol) and imidazole (5 g) was stirred at 170 °C in a sealed pressure vessel for 16 h. After cooling to 100 °C, the reaction mixture was poured into 100 mL diluted aqueous HCl (2N) and stirred for 1 h. The precipitate was filtered, washed with aqueous HCl, water and MeOH. The precipitate was dissolved in hot H_2SO_4 and water was added dropwise until the green solution turned into a blue suspension. After the suspension cooled to RT, the precipitate was filtered, washed with water, ethanol and methanol to afford compound **2-18** (131.3 mg, 75 %) as blue solid.

HR-MS (MALDI-TOF): m/z = 666.1566, calcd. for $C_{46}H_{22}N_2O_4$: m/z = 666.1580.

FT-IR: $\tilde{\nu}$ [cm^{-1}] = 2361, 2339, 1700, 1655, 1584, 1560, 1542, 1523, 1505, 1455, 1420, 1379, 1364, 1333, 1304, 1255, 1203, 1179, 1139, 1014, 1044, 964.

Mp = > 370 °C.

N,N'-Bis(2,6-di*iso*propylphenyl)-terrylene-3,4,11,12-tetracarboximide (2-19)

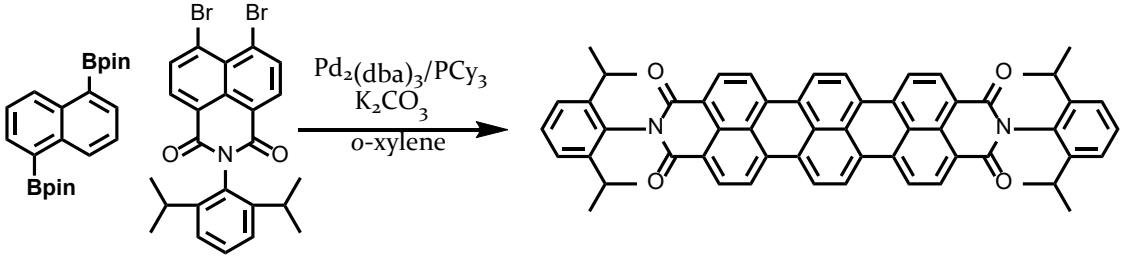

A mixture **2-11** (350.1 mg, 920 µmol), **2-21** (1.10 g, 2.1 mmol), K_2CO_3 (1.53 g, 11.4 mmol), $Pd_2(dba)_3$ (167.9 mg, 184 µmol), tricyclohexylphosphine (206.4 mg,

736 µmol) and 70 mL *o*-xylene was stirred at 145 °C under argon atmosphere. After stirring for 24 h, the mixture was cooled to room temperature and poured into MeOH. The precipitate was filtered, dissolved in dichloromethane, washed with water and brine and dried over $MgSO_4$. The organic layer was concentrated in vacuo and filtered through a pad of silica. After removal of the solvent, the compound was redissolved in dichloromethane and precipitated in MeOH, filtered and washed with ethanol and methanol to afford compound **2-19** (461.3 mg, 60 %) as blue solid.

^{1}H NMR (500 MHz, $C_2D_2Cl_4$) δ = 8.70 (d, *J* = 8.0 Hz, 4H), 8.65 (s, 4H), 8.58 (d, *J* = 7.8 Hz, 4H), 7.42 (t, *J* = 7.8 Hz, 2H), 7.29 (d, *J* = 7.8 Hz, 4H), 2.83 – 2.74 (m, 4H), 1.19 (d, *J* = 6.8 Hz, 24H).

^{13}C NMR (126 MHz, $C_2D_2Cl_4$) δ = 163.68, 146.35, 136.29, 131.84, 131.61, 130.68, 129.34, 124.65, 124.04, 122.79, 121.82, 121.15, 100.01, 74.46, 29.53, 23.98.

HR-MS (MALDI-TOF): m/*z* = 835.3531, calcd. for $C_{58}H_{47}N_2O_4^+$ $[M+H]^+$: m/*z* = 835.3530.

FT-IR: $\tilde{\nu}$ [cm^{-1}] = 2962, 2926, 2870, 2361, 2337, 1702, 1662, 1584, 1503, 1465, 1447, 1419, 1377, 1356, 1331, 1303, 1289, 1253, 1201, 1184, 1138, 1100, 1057, 1034, 1013, 961, 939.

Mp > 370 °C.

N,N'-Bis(2,2,3,3,4,4,4-heptafluorobutyl)-terrylene-3,4,11,12-tetracarboximide (2-20)

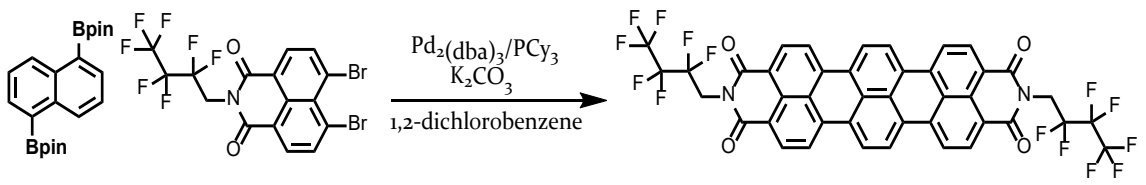

A mixture of compound **2-11** (170.3 mg, 448 µmol), **2-22** (528.1 mg, 984 µmol), K_2CO_3 (741.8 mg, 5.3 mmol), $Pd_2(dba)_3$ (81.8 mg, 90 µmol), tricyclohexylphosphine (100.5 mg, 358 µmol) and 15 mL 1,2-dichlorobenzene was stirred at 180 °C under

argon atmosphere. After stirring for 24 h, the mixture was cooled to room temperature and poured into MeOH. After filtration, the precipitate was dissolved in hot H_2SO_4 and water was added dropwise until the green solution turned into a blue suspension. After the suspension cooled to room temperature, the precipitate was filtered, washed with water, ethanol and methanol to afford compound **2-20** (131.2 mg, 33 %) as blue solid.

HR-MS (MALDI-TOF): m/*z* = 878.0842, calcd. for $C_{42}H_{16}F_{14}N_2O_4$: m/*z* = 878.0887

FT-IR: $\tilde{\nu}$ [cm^{-1}] = 2665, 2362, 2334, 2117, 2090, 1996, 1862, 1705, 1664, 1579, 1505, 1419, 1377, 1344, 1328, 1303, 1209, 1174, 1114, 1079, 1053, 967, 990, 905.

Mp > 370 °C.

N-(2,6-Di*iso*propylphenyl)-4,5-dibromo-1,8-naphthalimide (2-21)

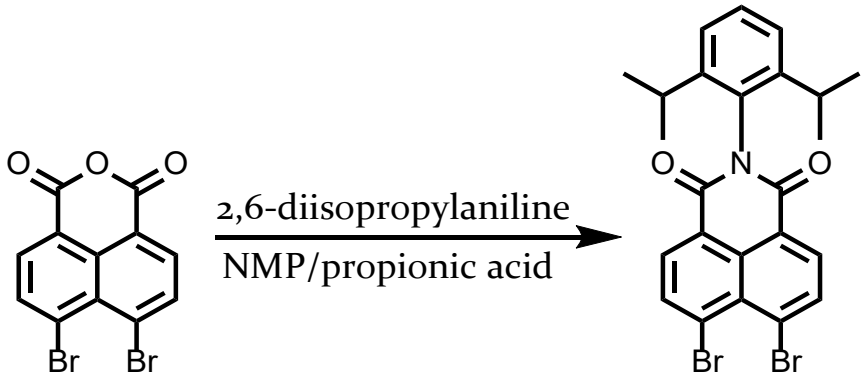

To a solution of **2-4** (5.02 g, 14.1 mmol) in 30 mL *N*-methyl-2-pyrrolidone and 30 mL propionic acid was added 2,6-di*iso*propylaniline (10.04 g, 56.2 mmol) and the reaction was stirred at 160 °C overnight. After cooling to room temperature, the reaction mixture was poured into water, filtered, washed with water and methanol to afford compound **2-21** (4.01 g, 55 %) as pale yellow solid.

^{1}H NMR (700 MHz, $C_2D_2Cl_4$) δ = 8.36 (d, *J* = 7.8 Hz, 2H), 8.21 (d, *J* = 7.7 Hz, 2H), 7.39 (t, *J* = 7.8 Hz, 1H), 7.24 (d, *J* = 7.8 Hz, 2H), 2.57 (sept, *J* =7.0 Hz, 2H), 1.07 (d, *J* = 6.7 Hz, 12H).

^{13}C NMR (176 MHz, CD_2Cl_2) δ = 163.9, 147.7, 146.5, 136.9, 132.5, 130.2, 129.0, 125.2, 124.7, 124.5, 123.8, 29.7, 24.2.

HR-MS (MALDI-TOF): m/z = 513.9958, calcd. for $C_{24}H_{21}Br_2NO_2$: m/z = 514.0012.

FT-IR: $\tilde{\nu}$ [cm^{-1}] = 2962, 2929, 2867, 1770, 1754, 1726, 1711, 1669, 1591, 1550, 1506, 1468, 1458, 1418, 1369, 1336, 1305, 1242, 1216, 1196, 1180, 1158, 1144, 1313, 1098, 1055, 977, 937, 913.

Mp = 298 - 300 °C.

N-(2,2,3,3,4,4,4-HEPTAFLUOROBUTYL)-4,5-DIBROMO-1,8-NAPHTHALIMIDE (2-22)

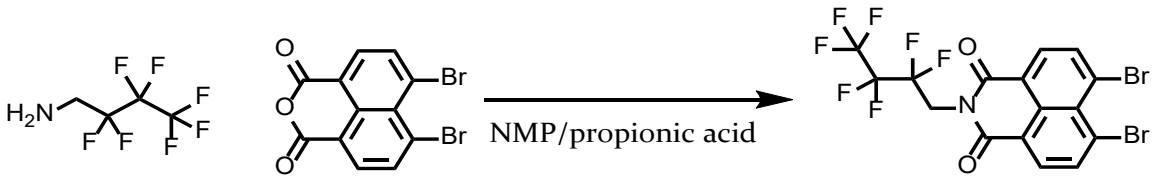

To a solution of **2-4** (6.52 g, 18.3 mmol) in 40 mL *N*-methyl-2-pyrrolidone and 40 mL propionic acid was added heptafluoro-*n*-butylamine (5 mL, 36.7 mmol) and the reaction was stirred at 160 °C in a sealed pressure vessel overnight. After cooling to RT, the reaction mixture was poured into MeOH, filtered, washed with water and methanol to afford compound **2-22** (5.39 g, 55 %) as pale yellow solid.

^{13}C NMR (126 MHz, $C_2D_2Cl_4$) δ = 162.7, 136.4, 132.1, 129.2, 122.3, 38.6, 3.6, 1.5.

HR-MS (MALDI-TOF): m/z = 534.8701, calcd. for $C_{16}H_6Br_2F_7NO_2$: m/z = 534.6854.

FT-IR: $\tilde{\nu}$ [cm^{-1}] = 2927, 2852, 2363, 2336, 1772, 1732, 1712, 1660, 1593, 1550, 1506, 1379, 1357, 1338, 1296, 1226, 1179, 1160, 1122, 1096, 1048, 973, 947, 901.

Mp = 223 – 225 °C.

N-(2,6-DI*ISO*PROPYLPHENYL)-PERYLENE-3,4-DICARBOXIMIDE (2-23)

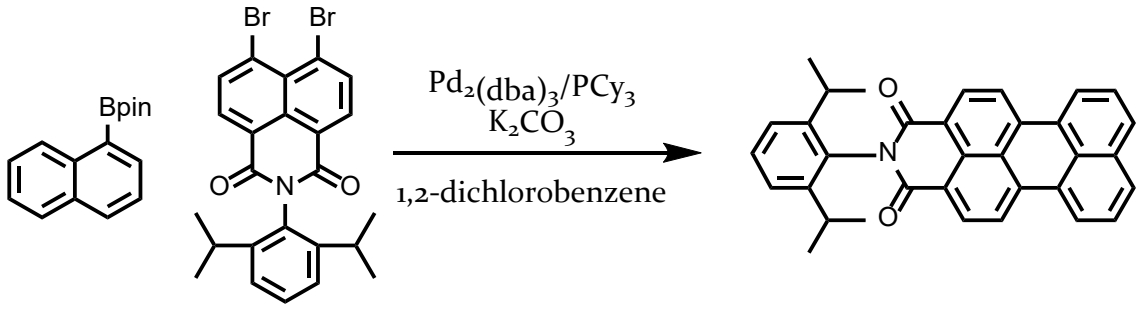

A mixture of 1-naphthalene boronic acid pinacol ester (50.1 mg, 197 µmol), **2-21** (111.5 mg, 216 µmol), K_2CO_3 (163.1 mg, 1.2 mmol), $Pd_2(dba)_3$ (17.9 mg, 20 µmol), tricyclohexylphosphine (22.1 mg, 79 µmol) and 8 mL 1,2-dichlorobenzene was stirred at 180 °C under argon atmosphere. After stirring for 24 h, the reaction was cooled to room temperature and poured into MeOH. The precipitate was filtered, dissolved in dichloromethane, washed with water and brine and dried over $MgSO_4$. The organic layer was concentrated in vacuo and filtered through a pad of silica. After removal of the solvent, the compound was redissolved in dichloromethane and precipitated in MeOH, filtered and washed with ethanol and methanol to afford compound **2-23** (61.6 mg, 65 %) as red solid.

^{1}H NMR (700 MHz, $C_2D_2Cl_4$) δ = 8.58 (d, *J* = 7.9 Hz, 2H), 8.41 (d, *J* = 4.6 Hz, 4H), 7.88 (d, *J* = 7.8 Hz, 2H), 7.61 (t, *J* = 7.6 Hz, 2H), 7.40 (t, *J* = 7.5 Hz, 1H), 7.26 (d, *J* = 7.9 Hz, 2H), 2.76 – 2.70 (m, 2H), 1.15 (d, *J* = 6.2 Hz, 12H).

^{13}C NMR (176 MHz, CD_2Cl_2) δ = 164.6, 146.7, 138.2, 134.9, 132.4, 132.2, 131.6, 131.2, 131.2, 129.8, 129.7, 128.5, 127.7, 124.6, 124.6, 121.5, 120.9, 29.6, 24.3.

HR-MS (MALDI-TOF): m/*z* = 481.2062, calcd. for $C_{34}H_{27}NO_2$: m/*z* = 481.2042.

N-(1-HEPTYLOCTYL)-TERRYLENE-3,4-DICARBOXIMIDE (2-26)

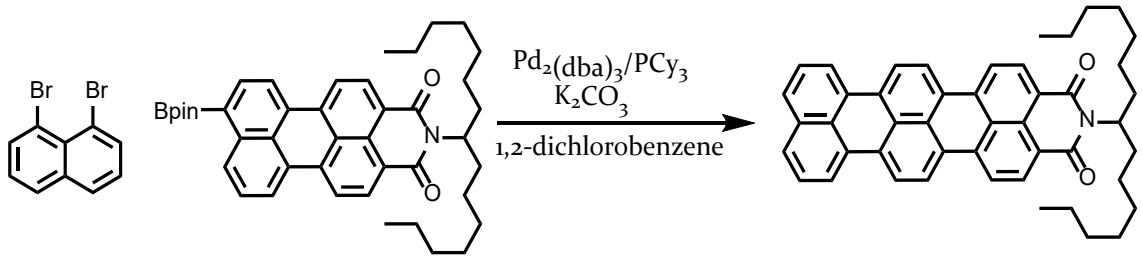

A mixture of 1,8-dibromonaphthalene (71.7 mg, 251 µmol), **11**[27] (150.1 mg, 228 µmol), K_2CO_3 (189.1 mg, 1.4 mmol), $Pd_2(dba)_3$ (20.8 mg, 23 µmol), tricyclohexylphosphine (25.6 mg, 91 µmol) and 8 mL 1,2-dichlorobenzene was stirred at 180 °C under argon atmosphere. After stirring for 24 h, the reaction was cooled to room temperature and poured into MeOH. The precipitate was filtered, dissolved in dichloromethane, washed with water and brine and dried over $MgSO_4$. The organic layer was concentrated in vacuo and filtered through a pad of silica. After removal of the solvent, the compound was redissolved in dichloromethane and precipitated in MeOH, filtered and washed with ethanol and methanol to afford compound **2-26** (44.9 mg, 30 %) as blue solid.

^{1}H NMR (500 MHz, $C_2D_2Cl_4$) δ = 8.53 (d, J = 7.6 Hz, 2H), 8.42 (d, J = 7.8 Hz, 2H), 8.38 – 8.24 (m, 6H), 7.77 (d, J = 7.8 Hz, 2H), 7.54 (t, J = 7.7 Hz, 2H), 5.23 – 5.02 (m, 1H), 2.31 – 2.18 (m, 2H), 1.98 – 1.81 (m, 2H), 1.47 – 1.15 (m, 20H), 0.84 (s, 6H).

^{13}C NMR (126 MHz, $C_2D_2Cl_4$) δ = 164.6, 136.7, 134.9, 133.7, 131.4, 130.7, 130.4, 129.4, 129.0, 127.2, 124.5, 122.2, 121.7, 120.1, 54.9, 32.9, 31.9, 29.7, 29.3, 27.3, 22.6, 13.9.

HR-MS (MALDI-TOF): m/*z* = 656.3500, calcd. for $C_{47}H_{46}NO_2^+$ $[M+H]^+$: m/*z* = 656.3523.

UV/Vis: $\lambda_{abs,max}$ = 603 nm, ε_0 = 46200 $M^{-1}cm^{-1}$, $\lambda_{em,max}$ = 680 nm.

FT-IR: $\tilde{\nu}$ [cm^{-1}] = 3054, 2956, 2923, 2849, 2363, 2338, 1693, 1651, 1592, 1577, 1559, 1500, 1460, 1423, 1393, 1371, 1352, 1339, 1289, 1267, 1246, 1208, 1175, 1165, 1138, 1109, 1069, 1032, 971, 939, 914.

Mp > 370 °C.

N-(2,6-DI*ISO*PROPYLPHENYL)-TERRYLENE-3,4-DICARBOXIMIDE (2-28)

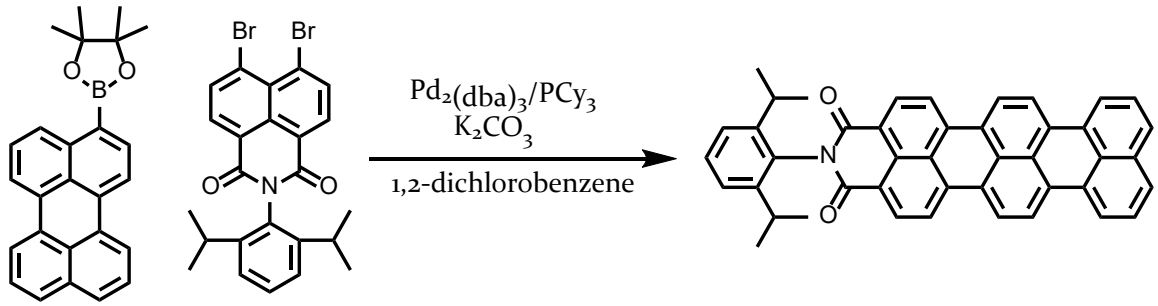

A mixture of 3-perylene boronic acid pinacol ester[199] (301.2 mg, 796 µmol), **2-21** (449.5 mg, 872 µmol), K_2CO_3 (657.6 mg, 4.8 mmol), $Pd_2(dba)_3$ (72.8 mg, 79 µmol), tricyclohexylphosphine (88.9 mg, 317 µmol) and 25 mL 1,2-dichlorobenzene was stirred at 180 °C under argon atmosphere. After stirring for 24 h, the reaction was cooled to room temperature and poured into MeOH. The precipitate was filtered, dissolved in dichloromethane, washed with water and brine and dried over $MgSO_4$. The organic layer was concentrated in vacuo and filtered through a pad of silica. After removal of the solvent, the compound was redissolved in dichloromethane and precipitated in MeOH, filtered and washed with ethanol and methanol to afford compound **2-28** (191.7 mg, 40 %) as blue solid.

^{1}H NMR (500 MHz, $C_2D_2Cl_4$) δ = 8.60 (d, *J* = 7.9 Hz, 2H), 8.48 (d, *J* = 8.4 Hz, 2H), 8.36 (m, 6H), 8.24 (d, *J* = 8.1 Hz, 2H), 7.79 (d, *J* = 8.1 Hz, 2H), 7.57 (t, *J* = 7.9 Hz, 2H), 7.41 (t, *J* = 7.9 Hz, 1H), 7.28 (d, *J* = 7.9 Hz, 2H), 2.86 – 2.70 (m, 2H), 1.18 (d, *J* = 6.8 Hz, 12H).

The compound was not sufficiently soluble for ^{13}C NMR measurements.

HR-MS (MALDI-TOF): m/*z* = 606.2424, calcd. for $C_{44}H_{32}NO_2^+$ $[M+H]^+$: m/*z*= 606.2428.

FT-IR: $\tilde{\nu}$ [cm^{-1}] = 2964, 2903, 2864, 1769, 1732, 1692, 1651, 1593, 1575, 1558, 1503, 1469, 1447, 1376, 1356, 1342, 1314, 1290, 1259, 1223, 1213, 1199, 1181, 1157, 1088, 1016, 931.

Mp > 370 °C.

N-(2,6-DI*ISO*PROPYLPHENYL)-TERRYLENE-3,4,11,12-TETRACARBOXY MONOIMIDE DIBUTYLESTER (3-1)

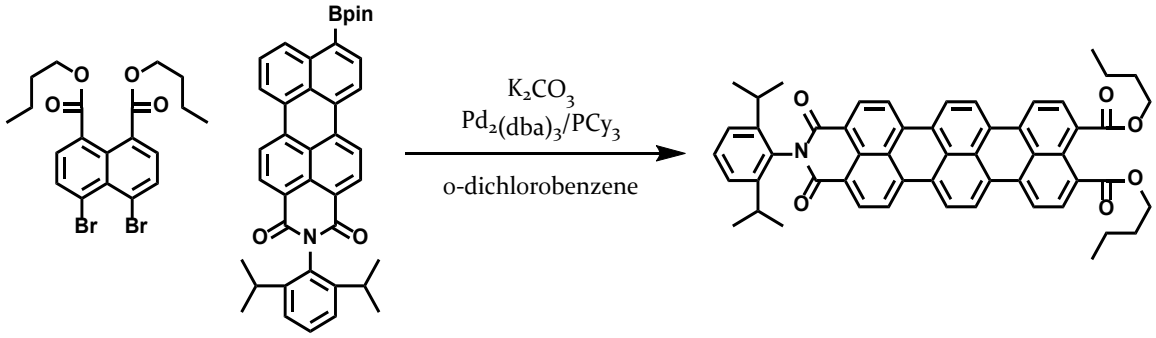

A mixture of 2-10 (750 mg, 1.54 mmol), 3-2[200] (749.8 mg, 1.23 mmol), K_2CO_3 (1.71 g, 12.3 mmol), $Pd_2(dba)_3$ (140.79 mg, 154.3 µmol), tricyclohexylphosphine (86.5 mg, 308.5 µmol) and 30 mL 1,2dichlorobenzene was stirred at 180 °C under argon atmosphere. After stirring for 24 h, the reaction was cooled to room temperature and poured into MeOH. The precipitate was filtered, dissolved in dichloromethane, washed with water and brine and dried over $MgSO_4$. The organic layer was concentrated in vacuo and filtered through a pad of silica with DCM, followed by ethyl acetate as the eluents, to receive **3-1** (808 mg, 65 %) as blue solid.

^{1}H NMR (500 MHz, $C_2D_2Cl_4$) δ = 8.64 (d, *J* = 8.0 Hz, 2H), 8.43 (t, 4H), 8.31 (d, *J* = 8.5 Hz, 2H), 8.28 (d, *J* = 8.1 Hz, 2H), 8.05 (d, *J* = 7.9 Hz, 2H), 7.50 (t, *J* = 7.9 Hz, 1H), 7.36 (d, *J* = 7.9 Hz, 2H), 4.35 (t, *J* = 6.8 Hz, 4H), 2.76 (h, *J* = 6.8 Hz, 2H), 1.88 – 1.77 (m, 4H), 1.59 – 1.45 (m, 4H), 1.20 (d, *J* = 6.8 Hz, 12H), 1.03 (t, *J* = 7.4 Hz, 6H).

^{13}C NMR (126 MHz, $C_2D_2Cl_4$) δ = 168.35, 163.60, 145.41, 136.39, 132.94, 131.74, 131.65, 131.03, 130.32, 130.25, 130.14, 129.31, 129.18, 128.49, 128.05, 127.87, 126.18, 124.40, 123.90, 120.89, 120.84, 120.67, 65.34, 30.51, 29.01, 23.98, 19.21, 13.84.

HR-MS (MALDI-TOF): m/*z* = 805.3266, calcd. for $C_{54}H_{47}NO_6$: m/*z* = 805.3403.

UV/Vis: $\lambda_{abs,max}$ = 633 nm, ε_0 = 110478 $M^{-1}cm^{-1}$, $\lambda_{em,max}$ = 664 nm.

Mp = 250 - 254 °C.

N-(2,6-Di*iso*propylphenyl)-terrylene-3,4,11,12-tetracarboxy monoimide monoanhydride (3-2)

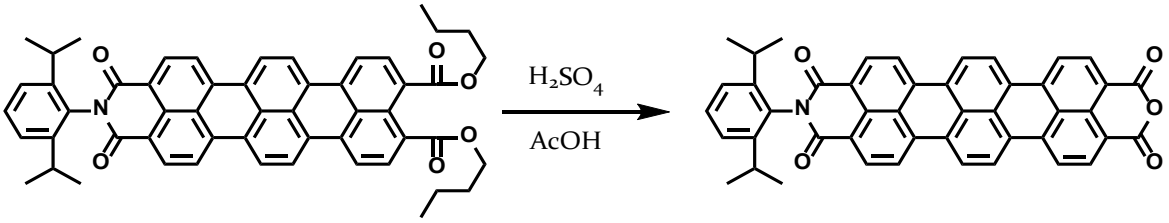

Compound **3-1** (100 mg, 124 µmol) was dissolved in 5 mL acetic acid and 10 mL sulfuric acid was added. After stirring for 16 h at 110 °C, the solution was precipitated in water, filtered and washed with water and methanol. After drying, 79 mg (100 %) of the blue solid **3-2** was received.

The compound was not sufficiently soluble for NMR measurements.

HR-MS (MALDI-TOF): m/*z* = 675.1980, calcd. for $C_{46}H_{29}NO_5$: m/*z* = 675.2046.

Mp > 370 °C.

N-(2,6-Di*iso*propylphenyl)-N-(4-trimethylsilylethynyl)-terrylene-3,4,11,12-tetracarboxy diimide (3-11)

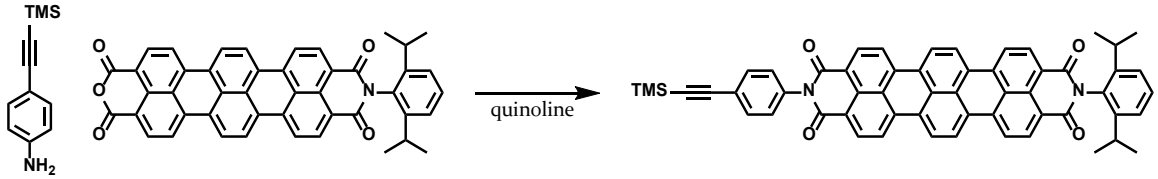

3-3 (10 mg, 15 µmol) and **3-8** were dissolved in 2 mL freshly distilled quinoline and stirred for 16 h under argon at 190 °C. After cooling to room temperature, the reaction mixture was precipitated in diluted hydrochloric acid, filtered and washed with water and methanol. After filtering over a pad of silica, 0.9 mg (7 %) of the blue solid **3-11** was received.

HR-MS (MALDI-TOF): m/*z* = 846.2988, calcd. for $C_{57}H_{42}N_2O_4Si$: m/*z* = 846.2914.

N-(2,6-Di*iso*propylphenyl)-N-(1-heptyloctyl)-terrylene-3,4,11,12-tetracarboxy diimide (3-13)

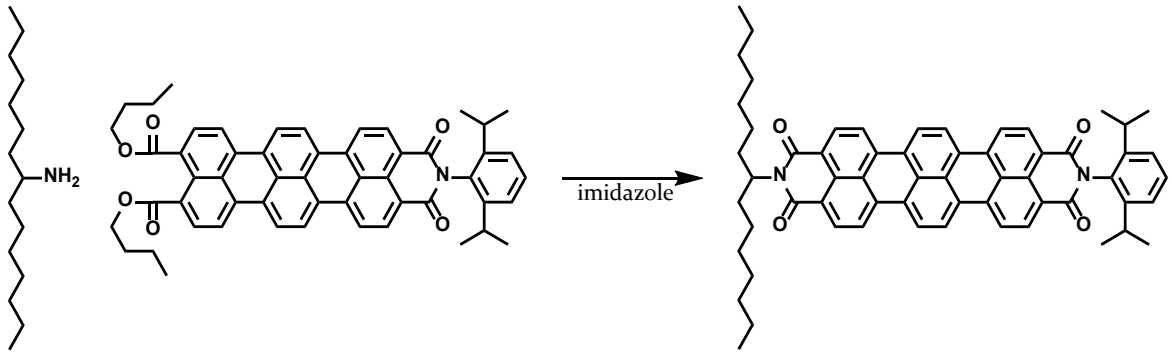

3-1 (100 mg, 124 µmol) and 1-heptyloctylamine (140 mg, 615 µmol) were mixed with 3 g imidazole and stirred for 16 h under argon at 170 °C. After cooling to 100 °C, the reaction mixture was precipitated in diluted hydrochloric acid, filtered and washed with water and methanol. After filtering over a pad of silica, 83 mg (75 %) of the blue solid **3-13** was received.

^{1}H NMR (700 MHz, $C_2D_2Cl_2$) δ = 8.74 (d, *J* = 7.9 Hz, 2H), 8.69 (d, *J* = 2.1 Hz, 6H), 8.64 (d, *J* = 8.1 Hz, 2H), 8.59 (d, *J* = 8.1 Hz, 2H), 7.50 (t, *J* = 7.9 Hz, 1H), 7.36 (d, *J* = 7.9 Hz, 2H), 5.27 – 5.16 (m, 1H), 2.85 – 2.75 (m, 2H), 2.33 – 2.21 (m, 2H), 2.00 – 1.91 (m, 2H), 1.43 – 1.24 (m, 20H), 1.22 (d, *J* = 6.8 Hz, 12H), 0.89 (t, *J* = 7.0 Hz, 6H).

^{13}C NMR (from 2D-^{1}H,^{13}C HSQC spectrum, 176 MHz, $C_2D_2Cl_4$) δ = 131.4, 130.9, 128.8, 124.0 123.5, 121.2, 121.1, 54.3, 32.1, 31.3, 29.0, 28.8, 28.7, 26.6, 23.6, 22.1, 13.6.

HR-MS (MALDI-TOF): m/*z* = 884.4599, calcd. for $C_{61}H_{60}N_2O_4$: m/*z* = 884.4553.

Mp = 252 - 253 °C.

1,6,9,14-TETRABROMO-N-(2,6-DI*ISO*PROPYLPHENYL)-TERRYLENE-3,4,11,12-TETRACARBOXY MONOIMIDE DIBUTYLESTER (4-5)

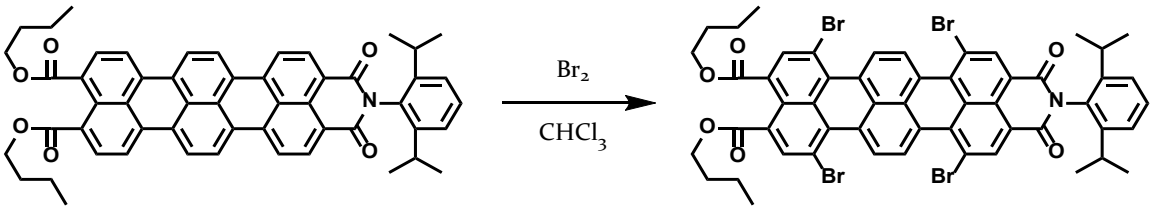

3-1 (1 g, 1.24 mmol) was dissolved in 50 mL chloroform and 0.4 mL bromine (7.5 mmol) was added. Under the exclusion of light, the reaction was stirred at 60 °C for 3 h. After cooling to room temperature, the reaction mixture was washed with aqueous sodium thiosulfate, the organic phase was dried with magnesium sulfate and concentrated in vacuum. The concentrated chloroform solution was precipitated in hexane, filtered and dried to receive **4-5** as a blued solid (1.32 g, 95 %).

^{1}H NMR (700 MHz, $C_2D_2Cl_4$) δ = 9.50 (d, *J* = 8.4 Hz, 2H), 9.29 (d, *J* = 8.4 Hz, 2H), 8.94 (s, 2H), 8.39 (s, 2H), 7.51 (t, *J* = 7.8 Hz, 1H), 7.36 (d, *J* = 7.6 Hz, 2H), 4.34 (t, *J* = 6.9 Hz, 4H), 2.71 (hept, *J* = 13.9, 7.0 Hz, 2H), 1.86 – 1.78 (m, 4H), 1.56 – 1.49 (m, 4H), 1.19 (d, *J* = 6.7 Hz, 12H), 1.02 (t, *J* = 7.5 Hz, 6H).

^{13}C NMR (from 2D-^{1}H,^{13}C HSQC spectrum, 176 MHz, $C_2D_2Cl_4$) δ = 137.9, 136.6, 129.2, 127.7, 126.8, 123.8, 65.6, 30.2, 28.8, 23.7, 18.9, 13.5.

HR-MS (MALDI-TOF): m/*z* = 1116.9530, calcd. for $C_{54}H_{43}Br_4NO_6$: m/*z* = 1116.9824.

UV/Vis: $\lambda_{abs,max}$ = 631 nm, ε_0 = 54410 $M^{-1}cm^{-1}$, $\lambda_{em,max}$ = 674 nm.

Mp = 310 - 313 °C.

1,6,9,14-TETRAPHENOXY-N-(2,6-DI*ISO*PROPYLPHENYL)-TERRYLENE-3,4,11,12-TETRACARBOXY MONOIMIDE DIBUTYLESTER (4-6)

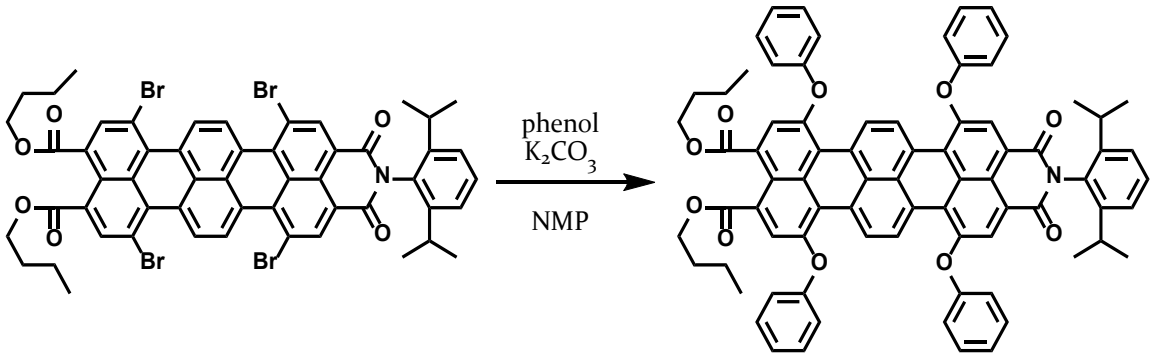

4-5 (200 mg, 178 µmol), phenol (134 mg, 1.43 mmol) and K_2CO_3 (197 mg, 1.43 mmol) were dissolved in 10 mL NMP and were stirred for 16 h under argon at 110 °C. After cooling to room temperature, the reaction mixture was precipitated in diluted hydrochloric acid, filtered, washed with water and methanol. After filtering over a pad of silica, **4-6** was received as a blue solid (178 mg, 85 %).

^{1}H NMR (700 MHz, $C_2D_2Cl_4$) δ = 9.45 (d, *J* = 8.9 Hz, 2H), 9.24 (d, *J* = 8.9 Hz, 2H), 8.22 (s, 2H), 7.66 (s, 2H), 7.51 – 7.37 (m, 7H), 7.28 – 7.26 (m, 4H), 7.25 – 7.21 (m, 8H), 7.20 – 7.18 (m, 4H), 4.21 (t, *J* = 6.8 Hz, 4H), 2.65 (hept, *J* = 6.8 Hz, 2H), 1.69 – 1.64 (m, 4H), 1.36 – 1.31 (m, 4H), 1.11 (d, *J* = 6.9 Hz, 12H), 0.90 (t, *J* = 7.3 Hz, 6H).

^{13}C NMR (from 2D-^{1}H,^{13}C HSQC spectrum, 176 MHz, $C_2D_2Cl_4$) δ = 129.9, 129.8, 128.4, 127.3, 125.5, 124.1, 123.5, 122.8, 122.4, 119.0, 119.1 65.1, 30.0, 28.6, 23.7, 18.8, 13.5.

HR-MS (MALDI-TOF): m/*z* = 1173.4301, calcd. for $C_{78}H_{63}NO_{10}$: m/*z* = 1173.4452.

UV/Vis: $\lambda_{abs,max}$ = 642 nm, ε_0 = 58861 $M^{-1}cm^{-1}$, $\lambda_{em,max}$ = 684 nm.

Mp = 155 - 157 °C.

1,6,9,14-Tetraphenoxy-N-(2,6-di*iso*propylphenyl)-terrylene-3,4,11,12-tetracarboxy monoanhydride monoimide (4-7)

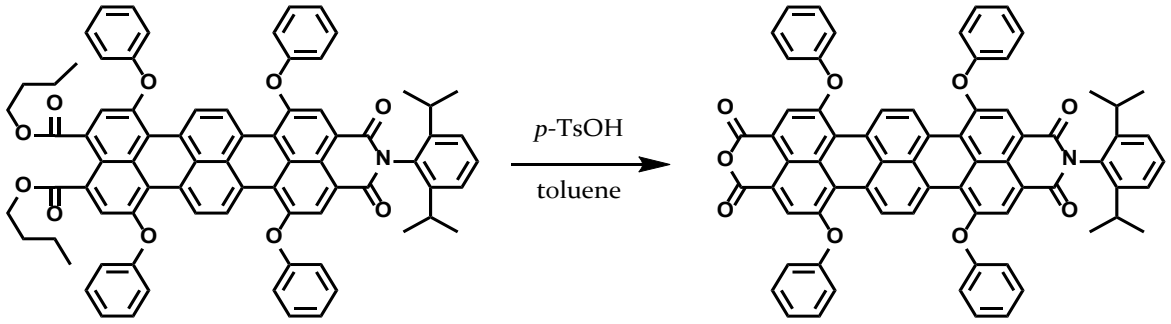

4-6 (150 mg, 128 µmol) and *para*-toluene sulfonic acid (110 mg, 640 µmol) were dissolved in 10 mL toluene and stirred for 16 h at 100 °C. After cooling to room temperature, the solution was precipitated in methanol, filtered, washed with methanol and dried to receive **4-7** as a dark green solid (130 mg, 97 %).

The compound was not sufficiently soluble for NMR measurements.

HR-MS (MALDI-TOF): m/*z* = 1043.2710, calcd. for $C_{70}H_{45}NO_9$: m/*z* = 1043.3094.

Mp > 370 °C.

1,6,9,14-Tetraphenoxy-N-(2,6-di*iso*propylphenyl)-N-(5-(pyridin-2-yl)-1,3,4-oxadiazol)-terrylene-3,4,11,12-tetracarboxy diimide (4-8)

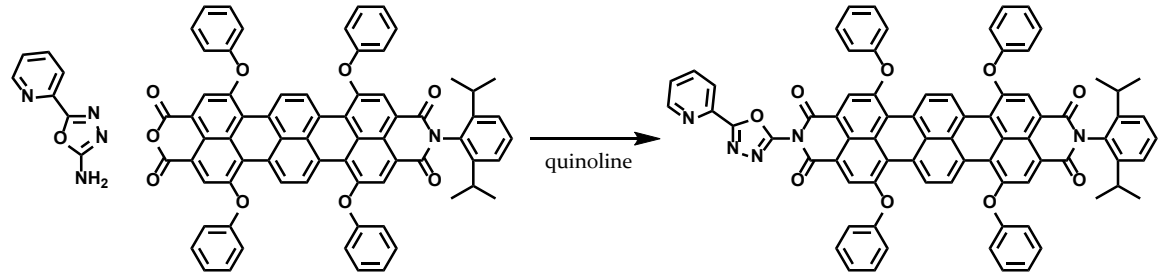

4-7 (70 mg, 67 µmol) and **4-3** (32 mg, 200 µmol) were dissolved in 5 mL freshly distilled quinoline, degassed and purged with argon and stirred for 24 h at 183 °C. After cooling to room temperature, the reaction mixture was precipitated in diluted hydrochloric acid, filtered and washed with water and methanol. The solid was

purified by column chromatography ($CHCl_3$/MeOH 10:1) followed by size exclusion chromatography (THF). **4-8** was received as a dark green solid (8 mg, 10 %).

^{1}H NMR (500 MHz, $C_2D_2Cl_4$) δ = 9.83 – 9.50 (m, 4H), 8.87 – 8.63 (m, 1H), 8.49 – 8.28 (m, 4H), 8.21 (d, *J* = 7.9 Hz, 1H), 7.89 (t, *J* = 7.7 Hz, 1H), 7.64 – 7.40 (m, 10H), 7.39 – 7.13 (m, 14H), 2.74 (hept, 2H), 1.18 (d, *J* = 6.8 Hz, 12H).

^{13}C NMR (from 2D-^{1}H,^{13}C HSQC spectrum, 176 MHz, $C_2D_2Cl_4$) δ = 149.1, 137.0, 130.0, 130.1, 128.6, 128.7, 124.6, 124.4, 124.0, 122.8, 122.9, 121.2, 119.2, 29.1, 28.7, 23.4.

HR-MS (MALDI-TOF): m/z = 1187.3667, calcd. for $C_{77}H_{49}N_5O_9$ m/z = 1187.3530.

UV/Vis: $\lambda_{abs,max}$ = 667 nm, ε_0 = 64615 $M^{-1}cm^{-1}$, $\lambda_{em,max}$ = 700 nm.

N,N-Bis(dimethylaminopropyl)-terrylene-3,4,11,12-tetracarboximide (5-1)

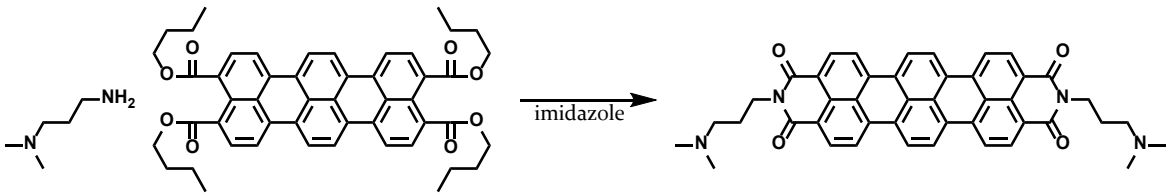

2-9 (250 mg, 322 µmol) and dimethylaminopropylamine (263 mg, 2.57 mmol) were mixed with 5 g imidazole and stirred for 24 h at 160 °C. After cooling to 100 °C, the reaction mixture was precipitated in water, filtered and washed with water and methanol. **5-1** was received as a blue solid (143 mg, 65 %).

The compound was not sufficiently soluble for NMR measurements.

HR-MS (MALDI-TOF): m/*z* = 685.2576, calcd. for $C_{44}H_{36}N_4O_4^+$ $[M+H]^+$: m/*z* = 685.2809.

Mp > 370 °C.

N,N'-Bis(dimethylaminopropyl)-terrylene-3,4,11,12-tetracarboximide dimethylammonium diiiodide (5-2)

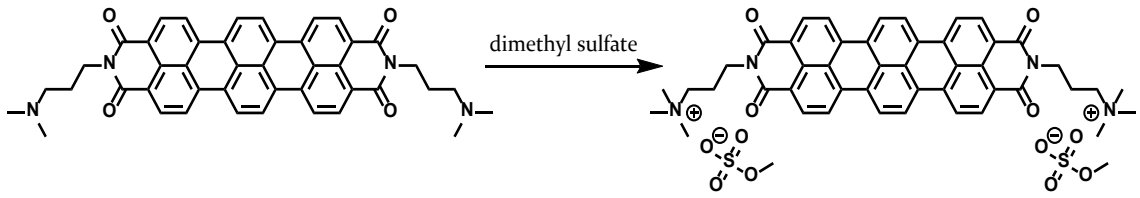

5-1 (25 mg, 36 µmol) was dissolved in 4 mL dimethylsulfate and the reaction was stirred at 110 °C for 24 h in a sealed vial. The reaction mixture was precipitated in THF and washed three times with THF, filtered and dried. **5-2** was received as a blue solid (35 mg, 95 %).

The compound was not sufficiently soluble for NMR measurements.

HR-MS (ESI): m/z = 357.1693, calcd. for $C_{46}H_{42}N_4O_4^{2+}$: m/z = 357.1598.

Mp > 370 °C.

N,N'-Bis(dimethylaminopropyl)-terrylene-3,4,11,12-tetracarboximide ditriethyleneglycol dichloride (5-3)

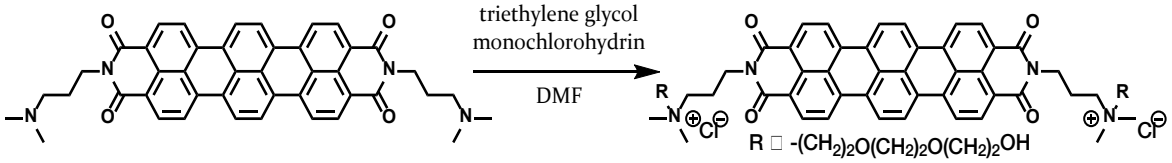

5-1 (25 mg, 36 µmol) was dissolved in 5 mL DMF, 2 mL triethylene glycol monochlorohydrin was added and the reaction was stirred at 110 °C for 24 h in a sealed vial. The reaction mixture was precipitated in THF and washed three times with THF, filtered and dried. **5-3** was received as a blue solid (38 mg, 95 %).

The compound was not sufficiently soluble for NMR measurements.

HR-MS (ESI): m/z = 475.3252, calcd. for $C_{56}H_{60}N_4O_{10}^{2+}$: m/z = 475.2227.

Mp > 370 °C.

NAPHTHO[8,1,2-BCD]PERYLENE-9,10-DICARBOXY DIBUTYLESTER (6-1)

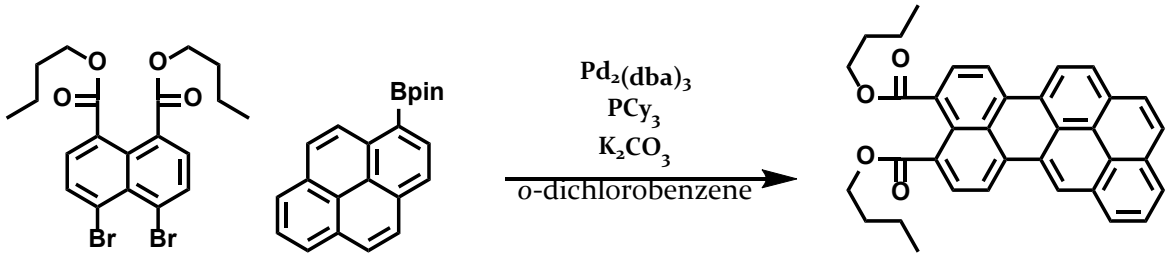

2-10 (50 mg, 103 µmol), 1-pyrenylboronic acid pinacol ester (27 mg, 82 µmol), K_2CO_3 (56.8 mg, 411 µmol), $Pd_2(dba)_3$ (18.8 mg, 21 µmol) and PCy_3 (11.5 mg, 41 µmol) were dissolved in 3.5 mL *o*-dichlorobenzene, degassed and purged with argon. The reaction mixture was stirred at 165 °C under argon for 16 h. After cooling to room temperature, the reaction mixture was mixed with hexane and filtered over silica to remove the *o*-dichlorobenzene. After the solvent was removed in vacuum, the compound was purified by column chromatography with ethyl acetate/hexane (1:3) to receive **6-1** as an orange solid (39 mg, 73 %).

^{1}H NMR (500 MHz, $C_2D_2Cl_4$) δ = 8.80 (s, 1H), 8.69 (d, *J* = 8.4 Hz, 1H), 8.48 (d, *J* = 8.0 Hz, 1H), 8.34 (d, *J* = 7.9 Hz, 1H), 8.25 – 8.17 (m, 3H), 8.15 – 7.99 (m, 5H), 4.41 (td, *J* = 6.8, 2.6 Hz, 4H), 1.88 (pd, *J* = 6.9, 1.9 Hz, 4H), 1.64 – 1.54 (m, 4H), 1.09 (td, *J* = 7.4, 1.6 Hz, 6H).

^{13}C NMR (126 MHz, $C_2D_2Cl_4$) δ = 168.28, 168.25, 134.66, 134.29, 131.57, 131.37, 131.27, 130.41, 129.99, 129.74, 129.71, 129.65, 129.26, 129.00, 127.75, 127.16, 126.96, 126.68, 126.31, 126.24, 126.09, 125.40, 124.81, 124.68, 123.31, 121.38, 119.84, 119.57, 64.83, 30.64, 19.10, 13.45.

HR-MS (MALDI-TOF): m/z = 526.1893, calcd. for $C_{36}H_{30}O_4$: m/z = 526.2144.

UV/Vis: $\lambda_{abs,max}$ = 494 nm, ε_0 = 42529 $M^{-1}cm^{-1}$, $\lambda_{em,max}$ = 530 nm.

Mp = 252 - 254 °C.

DIBENZO[LM,YZ]PYRANTHRENE-3,4,12,13-TETRACARBOXY TETRABUTYLESTER (6-2)

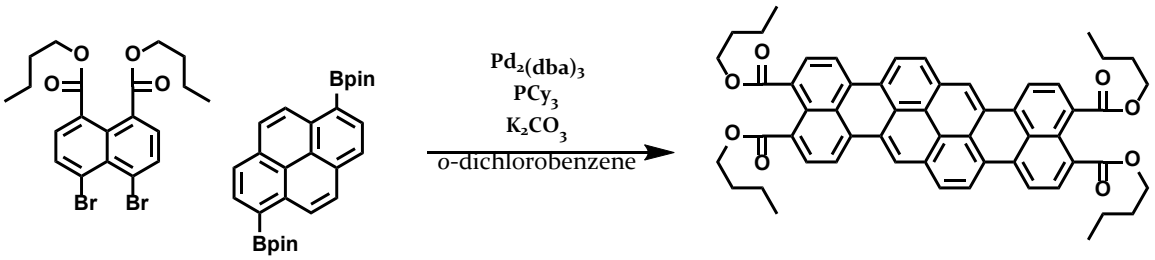

2-10 (141 mg, 291 µmol), 1,6-pyrenyldiboronic acid pinacol ester (60 mg, 132 µmol), K_2CO_3 (146 mg, 1.1 mmol), $Pd_2(dba)_3$ (48.2 mg, 53 µmol) and PCy_3 (29.6 mg, 106 µmol) were dissolved in 4.5 mL *o*-dichlorobenzene, degassed and purged with argon. The reaction mixture was stirred at 165 °C under argon for 16 h. After cooling to room temperature, the reaction mixture was mixed with hexane and filtered over silica to remove the *o*-dichlorobenzene. After the solvent was removed in vacuum, the compound was purified by column chromatography with ethyl acetate/hexane (1:3) to receive **6-2** as a violet solid (68 mg, 61 %).

^{1}H NMR (500 MHz, $C_2D_2Cl_4$) δ = 8.37 (s, 2H), 8.30 (d, *J* = 8.1 Hz, 4H), 8.11 (t, *J* = 8.9 Hz, 4H), 8.04 (d, *J* = 7.8 Hz, 2H), 7.81 (d, *J* = 8.3 Hz, 2H), 4.46 (t, 8H), 1.93 (p, *J* = 7.0 Hz, 8H), 1.63 (h, *J* = 7.4 Hz, 8H), 1.13 (t, *J* = 7.4 Hz, 12H).

^{13}C NMR (126 MHz, $C_2D_2Cl_4$) δ = 168.28, 168.23, 133.98, 133.60, 131.17, 130.32, 129.97, 129.90, 129.62, 129.48, 129.23, 128.88, 127.68, 126.97, 124.97, 124.18, 122.50, 121.87, 119.98, 119.88, 64.94, 30.69, 19.14, 13.50.

HR-MS (MALDI-TOF): m/z = 850.3092, calcd. for $C_{56}H_{50}O_8$: m/z = 850.3506.

UV/Vis: $\lambda_{abs,max}$ = 598 nm, ε_0 = 105899 $M^{-1}cm^{-1}$, $\lambda_{em,max}$ = 612 nm.

Mp = 322 - 324 °C.

PHENALENO[1,2,3-CD][1]-BENZOTHIOPHENE-8,9-DICARBOXY DIBUTYLESTER (6-3)

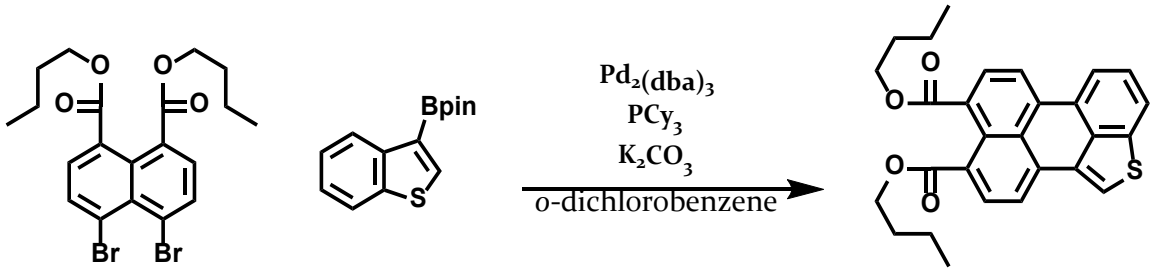

2-10 (50 mg, 103 µmol), 3-benzothiophene boronic acid pinacol ester (21.4 mg, 82 µmol), K_2CO_3 (56.8 mg, 411 µmol), $Pd_2(dba)_3$ (18.8 mg, 21 µmol) and PCy_3 (11.5 mg, 41 µmol) were dissolved in 3.5 mL *o*-dichlorobenzene, degassed and purged with argon. The reaction mixture was stirred at 165 °C under argon for 16 h. After cooling to room temperature, the reaction mixture was mixed with hexane and filtered over silica to remove the *o*-dichlorobenzene. After the solvent was removed in vacuum, the compound was purified by column chromatography with ethyl acetate/hexane (1:3) to receive **6-3** as an orange solid (40 mg, 85 %).

^{1}H NMR (300 MHz, CD_2Cl_2) δ = 8.12 (d, J = 7.9, 1.0 Hz, 1H), 8.04 – 7.83 (m, 4H), 7.71 (d, J = 7.2 Hz, 1H), 7.50 (dt, J = 8.0, 7.1, 1.1 Hz, 1H), 7.38 (dt, J = 8.3, 7.2, 1.3 Hz, 1H), 4.29 (t, 4H), 1.75 (p, J = 8.2, 6.6, 1.4 Hz, 4H), 1.53 – 1.40 (m, 4H), 0.98 (t, J = 7.4, 1.0 Hz, 6H).

HR-MS (MALDI-TOF): m/z = 458.1455, calcd. for $C_{28}H_{26}O_4S$: m/z = 458.1552.

UV/Vis: $\lambda_{abs,max}$ = 390 nm, ε_0 = 12712 $M^{-1}cm^{-1}$.

Mp = 86 °C.

BENZO[KL]NAPHTHO[1',8':4,5,6]ISOINDOLO[7,1,2-CDE]ACRIDINE-1,8,9,16-TETRACARBOXY TETRABUTYLESTER (6-4)

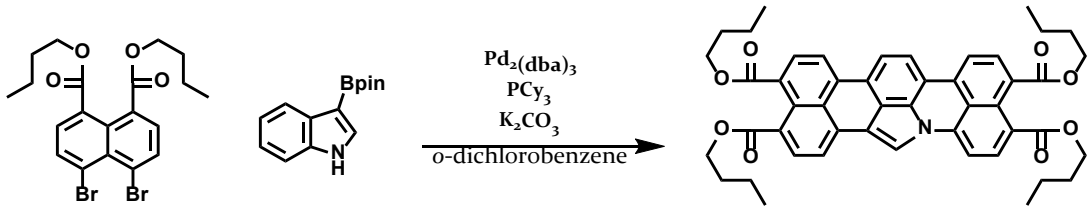

2-10 (88 mg, 181 µmol), 3-indole boronic acid pinacol ester (20 mg, 82 µmol), K_2CO_3 (91 mg, 658 µmol), $Pd_2(dba)_3$ (30.1 mg, 32 µmol) and PCy_3 (18.5 mg, 68 µmol) were dissolved in 4.5 mL *o*-dichlorobenzene, degassed and purged with argon. The reaction mixture was stirred at 165 °C under argon for 16 h. After cooling to room temperature, the reaction mixture was mixed with hexane and filtered over silica to remove the *o*-dichlorobenzene. After the solvent was removed in vacuum, the compound was purified by column chromatography with chloroform to receive **6-4** as a violet solid (22 mg, 35 %).

^{1}H NMR (500 MHz, $C_2D_2Cl_4$) δ = 8.29 – 7.94 (m, 6H), 7.81 (d, *J* = 7.4 Hz, 1H), 7.62 – 7.34 (m, 4H), 4.37 (t, *J* = 11.5, 6.7 Hz, 8H), 1.91 – 1.77 (m, 8H), 1.60 – 1.51 (m, 8H), 1.03 (t, *J* = 7.4 Hz, 12H).

^{13}C NMR (126 MHz, $C_2D_2Cl_4$) δ = 168.79, 168.70, 138.06, 136.39, 131.54, 130.68, 129.32, 128.58, 127.97, 123.95, 65.59, 65.41, 65.30, 65.30, 30.72, 30.67, 29.78, 19.39, 14.04, 14.02 (due to the low solubility, not all ^{13}C signals could be resolved).

HR-MS (MALDI-TOF): m/z = 765.2944, calcd. for $C_{48}H_{47}NO_8$: m/z = 765.3302.

UV/Vis: $\lambda_{abs,max}$ = 576 nm, ε_0 = 18633 $M^{-1}cm^{-1}$, $\lambda_{em,max}$ = 595 nm.

Mp = 118 - 123 °C.

N,N'-(1-HEPTYLOCTYL)-DIBENZO[LM,YZ]PYRANTHRENE-3,4,12,13-TETRACARBOXYDIIMIDE (6-5)

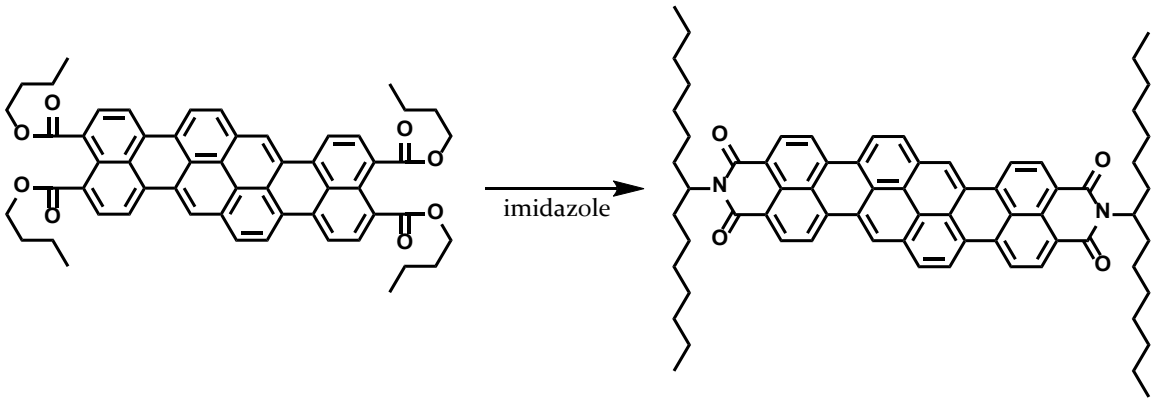

6-2 (100 mg, 118 µmol) and 1-heptyloctylamine (160 mg, 705 µmol) were mixed with 5 g imidazole and stirred at 160 °C for 16 h. After cooling to 100 °C, the reaction mixture was precipitated in diluted hydrochloric acid, filtered, washed with water and methanol. The compound was purified by column chromatography with ethyl acetate/hexane (1:3) to receive **6-5** as a blue solid (68 mg, 57 %).

^{1}H NMR (500 MHz, $C_2D_2Cl_4$) δ = 8.93 (s, 2H), 8.76 (d, *J* = 8.3 Hz, 2H), 8.67 (s, 4H), 8.61 (d, *J* = 7.8 Hz, 2H), 8.49 (d, *J* = 8.1 Hz, 2H), 8.31 (d, *J* = 8.4 Hz, 2H), 5.27 – 5.17 (m, 2H), 2.35 – 2.24 (m, 4H), 1.96 (d, *J* = 13.9 Hz, 4H), 1.33 – 1.27 (m, 40H), 0.94 – 0.84 (m, 12H).

^{13}C NMR (126 MHz, $C_2D_2Cl_4$) δ = 166.29, 165.17, 149.08, 135.65, 132.03, 129.87, 128.45, 128.27, 124.69, 124.46, 123.00, 121.10, 54.60, 32.45, 31.58, 29.45, 29.40, 29.32, 28.94, 26.92, 22.31, 13.69 (due to the low solubility, not all ^{13}C signals could be resolved).

HR-MS (MALDI-TOF): m/z = 1008.5764, calcd. for $C_{71}H_{77}NO_4$ $[M+H]^+$: m/z = 1008.5926.

UV/Vis: $\lambda_{abs,max}$ = 656 nm, ε_0 = 139219 $M^{-1}cm^{-1}$, $\lambda_{em,max}$ = 675 nm.

Mp = 298 - 302 °C.

1,4-Bis(4'-bromophenyl)-1,4-dihydroxy-2,3,5,6-tetramethyl-cyclohexa-2,5-diene (7-1)

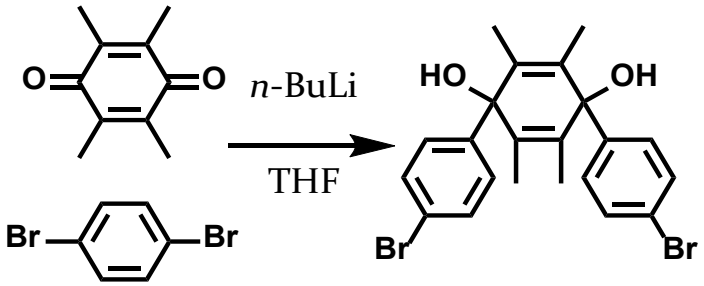

In a flame-dried, argon-purged Schlenk flask, 1,4-dibromobenzene (17.24 g, 73 mmol) was dissolved in 150 mL anhydrous THF and cooled to -78 °C. Slowly, *n*-butyllithium (45.7 mL, 73 mmol) was added and the solution was stirred for 1 h. In a separate sealed flask, tetramethyl-*p*-benzoquinone (3 g, 18.3 mmol) was dissolved in anhydrous THF and transferred to the flask containing the 1,4-dibromobenzene solution. The solution was stirred for 16 h while slowly reaching room temperature. After the addition of water, the organic phase was extracted with ethyl acetate, washed with water and brine and dried with magnesium sulfate. After removing the solvent under reduced pressure, the title compound was precipitated by the addition of cold methanol and ultrasound treatment to receive 8.3 g (95 %) of **7-1** as a white solid.

^{1}H NMR (500 MHz, CD_2Cl_2) δ = 7.49 (d, 4H), 7.36 (d, 4H), 1.50 (s, 12H).

^{13}C NMR (126 MHz, CD_2Cl_2) δ = 143.69, 133.14, 132.43, 132.40, 132.15, 131.87, 131.66, 131.57, 129.34, 128.96, 121.11, 75.61, 23.46, 20.26, 18.40, 14.64, 11.88.

MS (FD): m/z = 478.2, calcd. for $C_{22}H_{22}Br_2O_2$: m/z = 478.00.

Mp: disintegration.

1,4-Bis(4'-bromophenyl)-1,4-dimethoxy-2,3,5,6-tetramethyl-cyclohexa-2,5-diene (7-2)

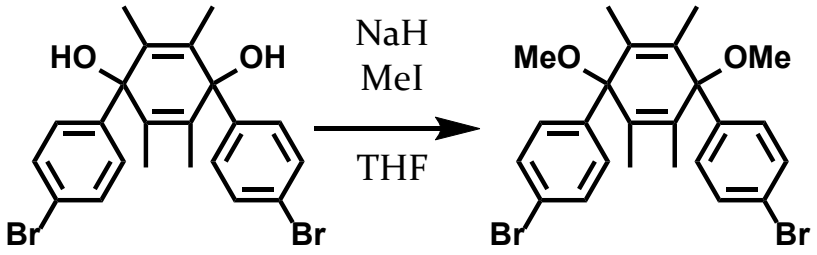

In a flame-dried, argon-purged Schlenk flask, **7-1** (4.05 g, 8.5 mmol) was dissolved in 150 mL anhydrous THF and cooled to -78 °C. Sodium hydride (270 mg, 11.3 mmol) was added, followed by methyl iodide (4.2 mL, 67.8 mmol) after 1 h and the solution was stirred for 16 h while slowly reaching room temperature. After the addition of water, the organic phased was extracted with ethyl acetate, washed with water and brine and dried with magnesium sulfate. After removing the solvent under reduced pressure, the title compound was precipitated by the addition of methanol to receive 3.86 g (90 %) of **7-2** as a white solid.

^{1}H NMR (500 MHz, CD_2Cl_2) δ = 7.43 (d, *J* = 8.2 Hz, 4H), 7.33 (d, *J* = 8.2 Hz, 4H), 3.12 (s, 6H), 1.50 (s, 12H).

^{13}C NMR (126 MHz, CD_2Cl_2) δ = 143.52, 134.04, 131.28, 129.62, 121.18, 80.88, 51.21, 30.26, 13.86.

MS (FD): m/z = 506.3, calcd. for $C_{24}H_{26}Br_2O_2$: m/z = 506.03.

Mp = 188 - 192 °C.

1,4-Bis(phenylboronic acid pinacol ester)-1,4-dimethoxy-2,3,5,6-tetramethyl-cyclohexa-2,5-diene (7-3)

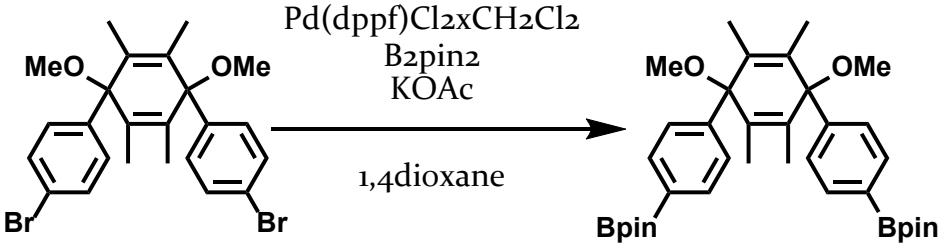

In a flame-dried, argon-purged Schlenk flask, **7-2** (1 g, 1.98 mmol), KOAc (3.1 g, 31.6 mmol) and bis(pinacolato)diboron (1.5 g, 5.9 mmol) were suspended in 50 mL anhydrous 1,4-dioxane and degassed for 30 m. $Pd(dppf)Cl_2xCH_2Cl_2$ (129 mg, 158 µmol) was added and the reaction was stirred for 16 h at 80 °C. After the addition of water, the solvent was concentrated under reduced pressure, the reaction mixture mixed with ethyl acetate, washed with water and brine and the organic phase was dried with magnesium sulfate. After the solvent was removed under reduced pressure, the mixture was mixed with dichloromethane, filtered over a pad of silica and the solvent was removed. After precipitation in methanol, 770 mg (65 %) of **7-3** was received as a white solid.

^{1}H NMR (500 MHz, CD_2Cl_2) δ 7.69 (d, *J* = 7.7 Hz, 4H), 7.48 (d, *J* = 7.7 Hz, 4H), 3.14 (s, 6H), 1.50 (s, 12H), 1.33 (s, 24H).

^{13}C NMR (126 MHz, CD_2Cl_2) δ 147.46, 134.56, 133.99, 127.19, 84.28, 81.42, 51.16, 25.24, 13.93.

MS (FD): m/z = 600.4, calcd. for $C_{36}H_{50}B_2O_6$: m/z = 600.38.

Mp: 231 – 234 °C.

BIS((4‘‘‘-PHENYLBORONIC ACID PINACOL ESTER)-1’’,-4’’-DI-METHOXY-1’’,4’’-BIPHENYL-2’’,3’’,5’’,6’’-TETRAMETHYL)-CYCLO-HEXADIENYL-[N,N’-BIS(2’,6’-DI*ISO*PROPYLPHENYL)-PERYLENE-3,4,9,10-TETRACARBOXYDIIMIDE] (7-5)

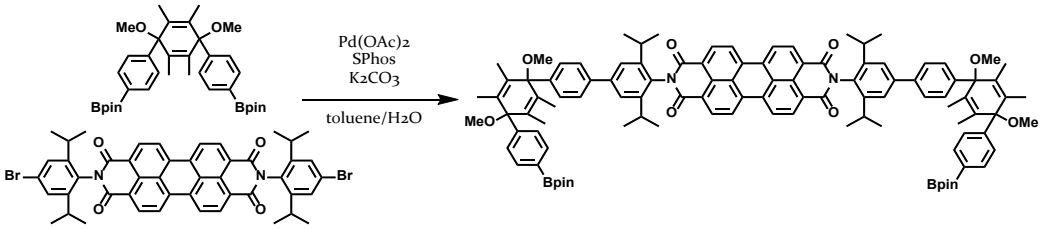

In a flame-dried, argon-purged Schlenk flask, **7-9** (415 mg, 691 µmol), **7-4** (200 mg, 230 µmol) and K_2CO_3 (630 mg, 4.6 mol) were suspended in 5 mL toluene and the reaction mixture was degassed for 30 m. In an argon atmosphere, 0.5 mL H_2O, $Pd(OAc)_2$ (5.17 mg, 23 µmol) and SPhos (23.57 mg, 58 µmol) were added, the flask was sealed and stirred at 85 °C for 16 h. Water was added, the reaction mixture was extracted with ethyl acetate, washed with water and brine and the organic phase was dried with magnesium sulfate. After removal of the solvent, the reaction mixture was filtered over a pad of silica, followed by size exclusion chromatography to receive 38 mg (10 %) of **7-5** as a red solid.

^{1}H NMR (500 MHz, $C_2D_2Cl_4$) δ = 8.85 – 8.74 (m, 8H), 7.79 (d, *J* = 7.7 Hz, 4H), 7.67 (d, *J* = 7.7 Hz, 4H), 7.62 (d, *J* = 8.0 Hz, 4H), 7.59 – 7.54 (m, 8H), 3.20 (d, *J* = 6.8 Hz, 12H), 2.81 (hept, *J* = 7.0 Hz, 4H), 1.63 (s, 24H), 1.36 (s, 24H), 1.26 (d, *J* = 6.7 Hz, 24H).

^{13}C NMR (126 MHz, $C_2D_2Cl_4$) δ = 163.32, 146.98, 145.79, 142.89, 141.59, 139.19, 134.95, 134.09, 133.39, 133.18, 132.02, 129.93, 129.84, 127.50, 126.62, 126.38, 123.37, 123.16, 122.74, 83.65, 80.66, 80.50, 50.77, 50.75, 50.67, 29.21, 24.85, 24.04, 13.77, 13.67.

HR-MS (MALDI-TOF): m/z = 1623.8445, calcd. for $C_{107}H_{114}B_2N_2O_{11}$ $[M\text{-}1H]^-$: m/z = 1623.8536.

UV/Vis: $\lambda_{abs,max}$ = 528 nm, ε_0 = 70769 $M^{-1}cm^{-1}$, $\lambda_{em,max}$ = 538 nm.

Mp: disintegration > 345 °C.

4‘-Bis[(N-(4‘‘‘-bromo-2‘‘‘,6‘‘‘-di*iso*propylphenyl))-(N‘-(2‘‘‘,6‘‘‘-diisopropylphenyl)-perylene-3‘‘,4‘‘,9‘‘,10‘‘-tetracarboxydiimide)]-1,4-dimethoxy-2,3,5,6-tetramethyl-1,4-phenylcyclohexadiene (7-6)

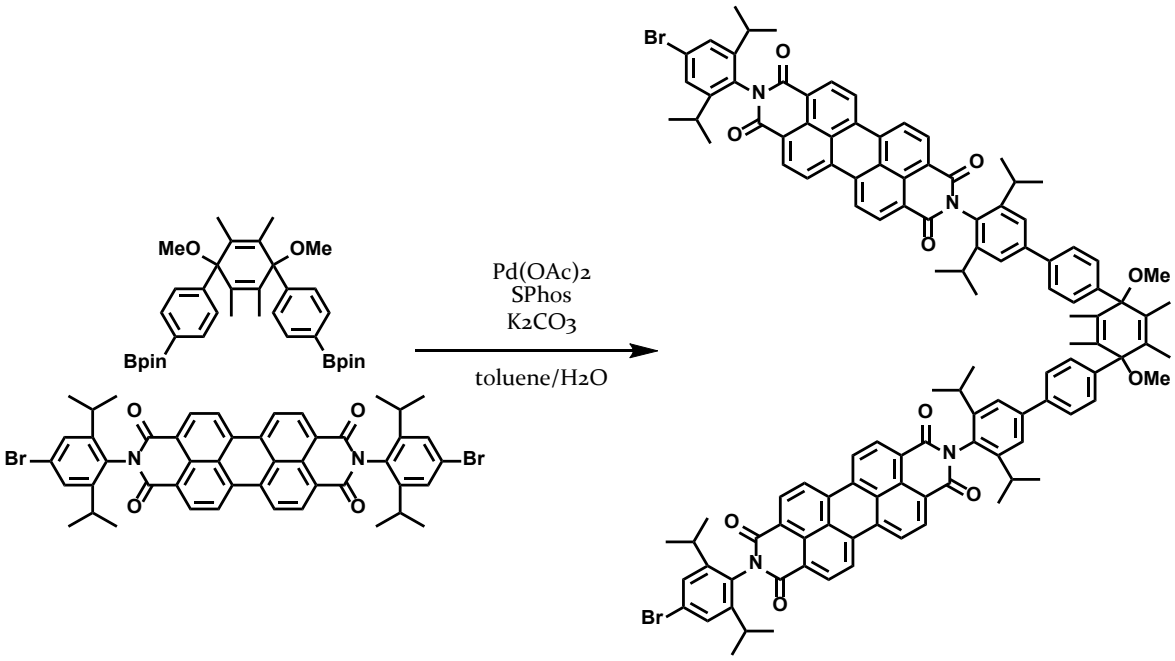

In a flame-dried, argon-purged Schlenk flask, **7-3** (100 mg, 167 µmol), **7-4** (434 mg, 500 µmol) and K_2CO_3 (460 mg, 3.3 mmol) were suspended in 5 mL toluene and the reaction mixture was degassed for 30 m. In an argon atmosphere, 0.5 mL H_2O, $Pd(OAc)_2$ (3.7 mg, 17 µmol) and SPhos (16.91 mg, 42 µmol) were added, the flask was sealed and stirred at 85 °C for 16 h. Water was added, the reaction mixture was extracted with ethyl acetate, washed with water and brine and the organic phase was dried with magnesium sulfate. After removal of the solvent, the reaction mixture was filtered over a pad of silica, followed by size exclusion chromatography to receive 48 mg (15 %) of **7-6** as a red solid.

^{1}H NMR (500 MHz, $C_2D_2Cl_4$) δ = 8.81 – 8.74 (m, 16H), 7.71 (d, *J* = 7.9 Hz, 4H), 7.66 (d, *J* = 8.0 Hz, 4H), 7.60 (s, 4H), 7.46 (s, 4H), 3.46 (s, 6H), 2.87 – 2.68 (m, 8H), 1.61 (s, 12H), 1.25 (d, *J* = 6.8 Hz, 24H), 1.17 (d, 24H).

^{13}C NMR (126 MHz, $C_2D_2Cl_4$) δ = 163.29, 163.10, 148.06, 145.84, 142.98, 141.54, 139.06, 135.12, 134.83, 133.37, 132.12, 132.01, 129.92, 129.81, 127.60, 127.42, 126.61, 126.36,

123.55, 123.45, 123.33, 123.22, 123.13, 122.84, 122.68, 80.60, 50.78, 50.71, 29.21, 29.16, 24.03, 23.99, 23.78, 13.76.

HR-MS (MALDI-TOF): m/z = 1889.6105, calcd. for $C_{119}H_{104}Br_2N_4O_9$ $[M-1H]^-$: m/z = 1889.6097.

UV/Vis: $\lambda_{abs,max}$ = 528 nm, ε_0 = 125770 $M^{-1}cm^{-1}$, $\lambda_{em,max}$ = 538 nm.

Mp > 370 °C.

TRIS[1,4-DIMETHOXY-2,3,5,6-TETRAMETHYL-1,4-PHENYLCYCLOHEXADIENE]-TRIS[N,N'-BIS(2''',6'''-DI*ISO*PROPYLPHENYL)-PERYLENE-3'',4'',9'',10''-TETRACARBOXYDIIMIDE] (7-7)

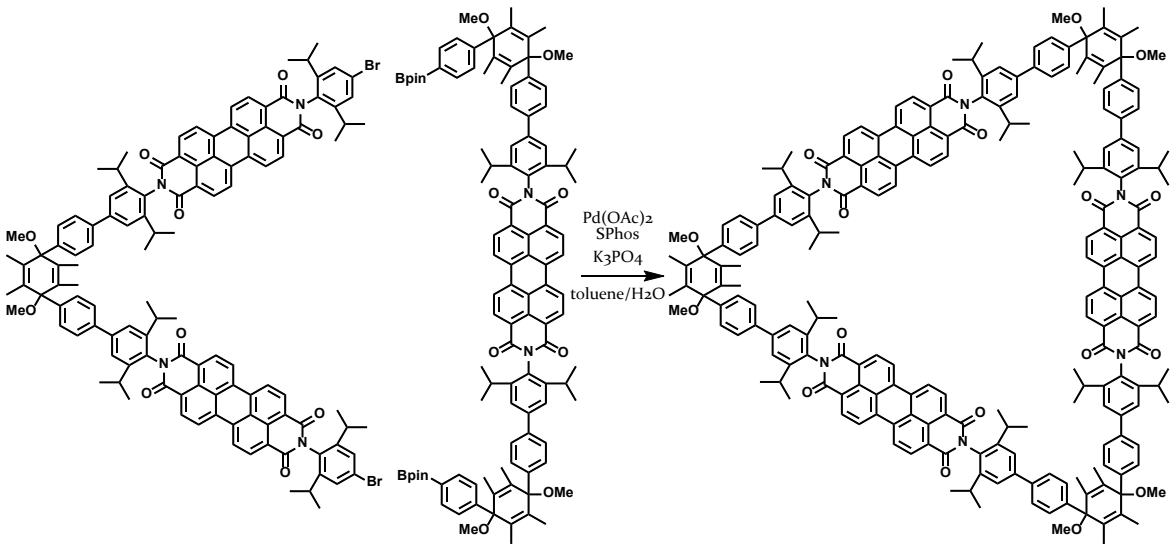

In a flame-dried, argon-purged Schlenk flask, **7-5** (52.9 mg, 28 µmol), **7-6** (50.0 mg, 30 µmol) and K_3PO_4 (116.5 mg, 550 µmol) were suspended in 6 mL toluene and the reaction mixture was degassed for 30 m. In an argon atmosphere, 0.5 mL H_2O, $Pd(OAc)_2$ (616 µg, 2.8 µmol) and SPhos (2.8 mg, 6.9 µmol) were added, the flask was sealed and stirred at 85 °C for 48 h. Water was added, the reaction mixture was extracted with ethyl acetate, washed with water and brine and the organic phase was dried with magnesium sulfate. After removal of the solvent, the reaction mixture

was filtered over celite, followed by size exclusion chromatography to receive 6.9 mg (8 %) of **7-7** as a red solid.

^{1}H NMR (300 MHz, CD_2Cl_2) δ = 8.83 – 8.76 (m, 24H), 7.72 – 7.63 (m, 24H), 7.59 (s, 12H), 3.23 (s, 18H), 2.81 (hept, *J* = 6.8 Hz, 12H), 1.68 (s, 36H), 1.22 (d, *J* = 6.8 Hz, 72H).

Not enough material was available for ^{13}C NMR measurements.

HR-MS (MALDI-TOF): m/z = 3132.4589, calcd. for $C_{215}H_{196}N_6O_{17}$ $[M-1H]^-$: m/z = 3132.4584.

UV/Vis: $\lambda_{abs,max}$ = 528 nm, ε_0 = 181698 $M^{-1}cm^{-1}$, $\lambda_{em,max}$ = 538 nm.

BIS((4‘‘‘-PHENYLBORONIC ACID PINACOL ESTER)-1’’,-4’’-DIMETHOXY-1’’,4’’-BIPHENYL-2’’,3’’,5’’,6’’-TETRAMETHYL)-CYCLOHEXADIENYL-[N,N’-BIS(2’,6’-DI*ISO*PROPYLPHENYL)-PERYLENE-(1,6-DIPYRROLIDIN)-3,4,9,10-TETRACARBOXYDIIMIDE] (7-10)

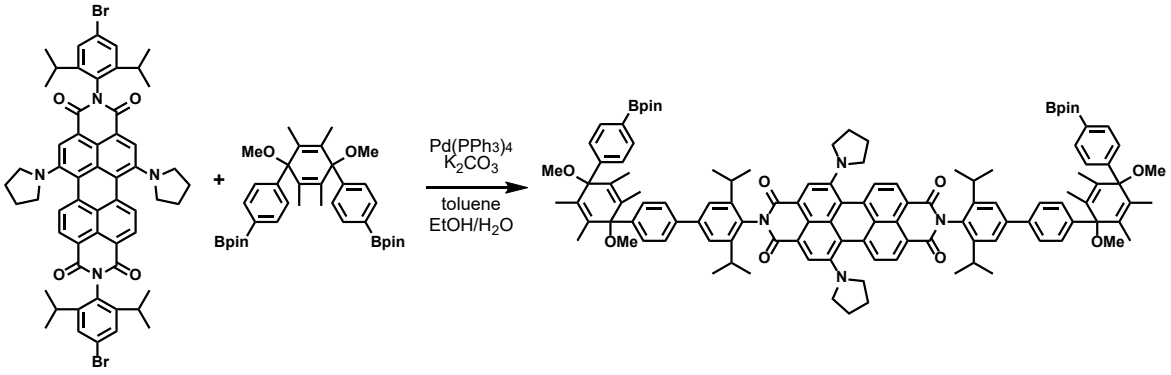

In a flame-dried, argon-purged Schlenk flask, N,N’-bis(2’,6’-di*iso*propylphenyl)-perylene-(1,6-dipyrrolidin)-3,4,9,10-tetracarboxydiimide[197] (112 mg, 111 µmol), **7-3** (200 mg, 334 µmol) and K_2CO_3 (184 mg, 1.3 mmol) were suspended in 3 mL toluene and the reaction mixture was degassed for 30 m. In an argon atmosphere, 0.5 mL degassed H_2O, 0.5 mL degassed EtOH and $Pd(PPh_3)_4$ (12.8 mg, 11 µmol) were added, the flask was sealed and stirred at 80 °C for 16 h. Water was added, the reaction mixture was extracted with ethyl acetate, washed with water and brine and the organic

phase was dried with magnesium sulfate. After removal of the solvent, the reaction mixture was purified by column chromatography (ethyl acetate/hexane 1:1) to receive 65.8 mg (33 %) of **7-10** as a blue solid.

HR-MS (MALDI-TOF): m/z = 1792.9876, calcd. for $C_{116}H_{130}B_2N_4O_{12}$: m/z = 1792.9871.

Due to the instability under ambient conditions, no further characterization could be performed.

LIST OF PUBLICATIONS

(1) D. Uersfeld, S. Stappert, C. Li, K. Müllen, *Adv. Synth. Catal.* **2017**, *359*, 4184.

(2) Manuscript in preparation by S. J. Hauschildt, D. Uersfeld, P. Dewald, P. Schmid, B. Engels, K. Müllen, and T. Basché.

REFERENCES

[1] K. Hübner, *Chemie unserer Zeit* **2006**, *40*, 274–275.

[2] C. Graebe, C. Liebermann, *Berichte der Dtsch. Chem. Gesellschaft* **1869**, *2*, 14–14.

[3] H. Schiff, *Ann. der Chemie und Pharm.* **1863**, *127*, 342–347.

[4] S. H. Kim, in *Funct. Dye.*, Elsevier, **2006**, pp. 5–6.

[5] N. Kobayashi, T. Fukuda, H. Tian, F. Meng, J. D. Hepworth, B. M. Heron, *Functional Dyes*, Elsevier, **2006**.

[6] C. Wang, H. Dong, W. Hu, Y. Liu, D. Zhu, *Chem. Rev.* **2012**, *112*, 2208–2267.

[7] H. Dong, H. Zhu, Q. Meng, X. Gong, W. Hu, *Chem. Soc. Rev.* **2012**, *41*, 1754–1808.

[8] J. Shinar, Ed. , *Organic Light-Emitting Devices*, Springer New York, New York, NY, **2004**.

[9] I. D. W. Samuel, G. A. Turnbull, *Chem. Rev.* **2007**, *107*, 1272–1295.

[10] T. Terai, T. Nagano, *Curr. Opin. Chem. Biol.* **2008**, *12*, 515–521.

[11] E. Clar, *Chem. Ber.* **1948**, *81*, 52–63.

[12] R. Scholl, C. Seer, R. Weitzenböck, *Berichte der Dtsch. Chem. Gesellschaft* **1910**, *43*, 2202–2209.

[13] M. Kardos, *Verfahren Zur Darstellung Eines Küpenfarbstoffes Der Naphthalinreihe*, **1913**, DE276357.

[14] A. Herrmann, K. Müllen, *Chem. Lett.* **2006**, *35*, 978–985.

[15] F. Würthner, *Chem. Commun.* **2004**, 1564–1579.

[16] M. Greene, in *High Perform. Pigment.*, Wiley-VCH Verlag GmbH & Co. KGaA, Weinheim, FRG, **n.d.**, pp. 249–261.

[17] C. Li, H. Wonneberger, *Adv. Mater.* **2012**, *24*, 613–636.

[18] X. Zhan, A. Facchetti, S. Barlow, T. J. Marks, M. A. Ratner, M. R. Wasielewski, S. R. Marder, *Adv. Mater.* **2011**, *23*, 268–284.

[19] A. Mansour, M. El-Shaarawy, S. El-Bashir, M. El-Mansy, M. Hammam, *Polym. Int.* **2002**, *51*, 393–397.

[20] M. Davies, C. Jung, P. Wallis, T. Schnitzler, C. Li, K. Müllen, C. Bräuchle, *ChemPhysChem* **2011**, *12*, 1588–1595.

[21] Y. Nagao, *Prog. Org. Coatings* **1997**, *31*, 43–49.

[22] R. R. Reghu, H. K. Bisoyi, J. V Grazulevicius, P. Anjukandi, V. Gaidelis, V. Jankauskas, *J. Mater. Chem.* **2011**, *21*, 7811.

[23] S. K. Lee, Y. Zu, A. Herrmann, Y. Geerts, K. Müllen, A. J. Bard, *J. Am. Chem. Soc.* **1999**, *121*, 3513–3520.

[24] W. Göhde, U. C. Fischer, H. Fuchs, J. Tittel, T. Basché, C. Bräuchle, A. Herrmann, K. Müllen, *J. Phys. Chem. A* **1998**, *102*, 9109–9116.

[25] X. Zhao, Y. Xiong, J. Ma, Z. Yuan, *J. Phys. Chem. A* **2016**, *120*, 7554–7560.

[26] S. Berngruber, Synthesis and Characterization of Dendritic, Water Soluble Terrylene and Quaterrylene Derivatives, Friedrich-Alexander-Universität Erlangen-Nürnberg, **2014**.

[27] N. G. Pschirer, C. Kohl, F. Nolde, J. Qu, K. Müllen, *Angew. Chemie Int. Ed.* **2006**, *45*, 1401–1404.

[28] Y. Avlasevich, C. Li, K. Müllen, *J. Mater. Chem.* **2010**, *20*, 3814.

[29] Y. Geerts, H. Quante, H. Platz, R. Mahrt, M. Hopmeier, A. Böhm, K. Müllen, *J. Mater. Chem.* **1998**, *8*, 2357–2369.

[30] A. Rademacher, S. Märkle, H. Langhals, *Chem. Ber.* **1982**, *115*, 2927–2934.

[31] F. Graser, E. Hädicke, *Liebigs Ann. der Chemie* **1980**, *1980*, 1994–2011.

[32] Z. Chen, A. Lohr, C. R. Saha-Möller, F. Würthner, *Chem. Soc. Rev.* **2009**, *38*, 564–584.

[33] E. Hädicke, F. Graser, *Acta Crystallogr. Sect. C Cryst. Struct. Commun.* **1986**, *42*, 195–198.

[34] G. Geissler, H. Remy, *Verfahren Zur Herstellung von Fluoreszenzfarbstoffen*, **1962**, DE1130099 (B).

[35] F. Würthner, T. E. Kaiser, C. R. Saha-Möller, *Angew. Chemie Int. Ed.* **2011**, *50*, 3376–3410.

[36] P. M. Kazmaier, R. Hoffmann, *J. Am. Chem. Soc.* **1994**, *116*, 9684–9691.

[37] G. Seybold, *Dye. Pigment.* **1989**, *11*, 303–317.

[38] H. Langhals, *Heterocycles* **1995**, *40*, 477–500.

[39] N. E. Aksakal, Y. Chumakov, F. Yuksel, *J. Chem. Crystallogr.* **2018**, *0*, 3.

[40] S.-G. Liu, G. Sui, R. A. Cormier, R. M. Leblanc, B. A. Gregg, *J. Phys. Chem. B* **2002**, *106*, 1307–1315.

[41] J. Shang, H. Tang, H. Ji, W. Ma, C. Chen, J. Zhao, *Chinese J. Catal.* **2017**, *38*, 2094–2101.

[42] S. Leroy-Lhez, J. Baffreau, L. Perrin, E. Levillain, M. Allain, M.-J. Blesa, P. Hudhomme, *J. Org. Chem.* **2005**, *70*, 6313–6320.

[43] D. Franke, M. Vos, M. Antonietti, N. A. J. M. Sommerdijk, C. F. J. Faul, *Chem. Mater.* **2006**, *18*, 1839–1847.

[44] Y. Nagao, Y. Tanabe, T. Misono, *Nippon Kagaku Kaishi* **1979**, 528–534.

[45] E. Spietschka, H. Troester, *Perylene-3,4,9,10-Tetracarboxylic-Acid-Monoanhydride-Monoalkali Salts, Process for Their Preparation and Their Use*, **1981**, DE3008420.

[46] C. Xue, R. Sun, R. Annab, D. Abadi, S. Jin, *Tetrahedron Lett.* **2009**, *50*, 853–856.

[47] S. B. Stappert, Synthesis and Photophysical Characterization of Nanocolorants for Energy-Transfer Studies, Johannes Gutenberg-Universität Mainz, **2016**.

[48] C. Kirmaier, H. Song, E. Yang, J. K. Schwartz, E. Hindin, J. R. Diers, R. S. Loewe, K. Tomizaki, F. Chevalier, L. Ramos, et al., *J. Phys. Chem. B* **2010**, *114*, 14249–14264.

[49] H. Eilingsfeld, M. Patsch, *Chlorierungsverfahren*, **1976**, DE2519790 (A1).

[50] Z. Chen, M. G. Debije, T. Debaerdemaeker, P. Osswald, F. Würthner, *ChemPhysChem* **2004**, *5*, 137–140.

[51] Y. Zagranyarski, L. Chen, D. Jänsch, T. Gessner, C. Li, K. Müllen, *Org. Lett.* **2014**, *16*, 2814–2817.

[52] G. Seybold, A. Stange, *Fluorescent Aroxysubstituted 3,4,9,10-Perylenetetracarboxylic Acid-Diimides and Their Use for the Concentration of Lights in Small Area*, **1986**, DE3545004 (A1).

[53] F. Würthner, *Pure Appl. Chem.* **2006**, *78*, 2341–2349.

[54] C. Kohl, T. Weil, J. Qu, K. Müllen, *Chem. - A Eur. J.* **2004**, *10*, 5297–5310.

[55] K. Peneva, G. Mihov, F. Nolde, S. Rocha, J. Hotta, K. Braeckmans, J. Hofkens, H. Uji-i, A. Herrmann, K. Müllen, *Angew. Chemie Int. Ed.* **2008**, *47*, 3372–3375.

[56] B. A. Jones, A. Facchetti, M. R. Wasielewski, T. J. Marks, *J. Am. Chem. Soc.* **2007**, *129*, 15259–15278.

[57] C. Li, J. Schöneboom, Z. Liu, N. G. Pschirer, P. Erk, A. Herrmann, K. Müllen, *Chem. - A Eur. J.* **2009**, *15*, 878–884.

[58] A. Hagfeldt, G. Boschloo, L. Sun, L. Kloo, H. Pettersson, *Chem. Rev.* **2010**, *110*, 6595–6663.

[59] H. Qian, W. Yue, Y. Zhen, S. Di Motta, E. Di Donato, F. Negri, J. Qu, W. Xu, D. Zhu, Z. Wang, *J. Org. Chem.* **2009**, *74*, 6275–6282.

[60] S. Nakazono, Y. Imazaki, H. Yoo, J. Yang, T. Sasamori, N. Tokitoh, T. Cédric, H. Kageyama, D. Kim, H. Shinokubo, et al., *Chem. - A Eur. J.* **2009**, *15*, 7530–7533.

[61] F. O. Holtrup, G. R. J. Müller, H. Quante, S. De Feyter, F. C. De Schryver, K. Müllen, *Chem. - A Eur. J.* **1997**, *3*, 219–225.

[62] K. Müllen, H. Quante, A. Böhm, *Substituierte Quaterrylentetracarbonsäurediimide*, **1996**, WO9622332.

[63] K. Müllen, H. Quante, *Quaterrylentetracarbonsäureimide*, **1992**, DE4236885.

[64] H. Langhals, A. Walter, E. Rosenbaum, L. B.-Å. Johansson, *Phys. Chem. Chem. Phys.* **2011**, *13*, 11055–11059.

[65] C. Jung, B. K. Müller, D. C. Lamb, F. Nolde, K. Müllen, C. Bräuchle, *J. Am. Chem. Soc.* **2006**, *128*, 5283–5291.

[66] M. Haase, C. G. Hübner, F. Nolde, K. Müllen, T. Basché, *Phys. Chem. Chem. Phys.* **2011**, *13*, 1776–1785.

[67] K. Peneva, G. Mihov, F. Nolde, S. Rocha, J. Hotta, K. Braeckmans, J. Hofkens, H. Uji-i, A. Herrmann, K. Müllen, *Angew. Chemie Int. Ed.* **2008**, *47*, 3372–3375.

[68] J. Mapel, M. Currie, T. D. Heidel, M. Baldo, S. Goffri, *Solar Concentrator and Devices and Methods Using Them*, **2009**, WO/2009/091773.

[69] G. Hu, R. Liu, E. J. Alexy, A. K. Mandal, D. F. Bocian, D. Holten, J. S. Lindsey, *New J. Chem.* **2016**, *40*, 8032–8052.

[70] H. Langhals, U. Ritter, *New Naphthalene, Perylene, Benzoperylene, Terrylene, Quaterrylene Bisimide and Trisimide Anions, as Salts, e.g. Tetrabutylammonium- or Potassium-Salts, Useful e.g. to Prepare Dyes, Preferably Vats Dye, to Color Cotton, Paper and Nylon*, **2008**, DE102008036495.

[71] F. Nolde, J. Qu, C. Kohl, N. G. Pschirer, E. Reuther, K. Müllen, *Chem. - A Eur. J.* **2005**, *11*, 3959–3967.

[72] H. Langhals, S. Christian, A. Hofer, *J. Org. Chem.* **2013**, *78*, 9883–9891.

[73] M. A. Omary, H. H. Patterson, in *Encycl. Spectrosc. Spectrom.*, Elsevier, **1999**, pp. 1372–1391.

[74] T. Förster, *Ann. Phys.* **1948**, *437*, 55–75.

[75] H. N. Kim, L. Puhl, F. Nolde, C. Li, L. Chen, T. Basché, K. Müllen, *Chemistry* **2013**, *19*, 9160–9166.

[76] M. Cotlet, R. Gronheid, S. Habuchi, A. Stefan, A. Barbafina, K. Müllen, J. Hofkens, F. C. De Schryver, *J. Am. Chem. Soc.* **2003**, *125*, 13609–13617.

[77] S. A. Latt, H. T. Cheung, E. R. Blout, *J. Am. Chem. Soc.* **1965**, *87*, 995–1003.

[78] L. Stryer, *Annu. Rev. Biochem.* **1978**, *47*, 819–846.

[79] A. Bohnen, K. Koch, W. Lüttke, K. Müllen, *Angew. Chemie Int. Ed. English* **1990**, *29*, 525–527.

[80] K.-H. Koch, K. Müllen, *Chem. Ber.* **1991**, *124*, 2091–2100.

[81] Y. Zagranyarski, L. Chen, Y. Zhao, H. Wonneberger, C. Li, K. Müllen, *Org. Lett.* **2012**, *14*, 5444–5447.

[82] J. Kelber, H. Bock, O. Thiebaut, E. Grelet, H. Langhals, *European J. Org. Chem.* **2011**, *2011*, 707–712.

[83] P. D. Frischmann, F. Würthner, *Org. Lett.* **2013**, *15*, 4674–4677.

[84] S. Stappert, C. Li, K. Müllen, T. Basché, *Chem. Mater.* **2016**, *28*, 906–914.

[85] D. Jänsch, I. Ivanov, Y. Zagranyarski, I. Duznovic, M. Baumgarten, D. Turchinovich, C. Li, M. Bonn, K. Müllen, *Chem. - A Eur. J.* **2017**, *23*, 4870–4875.

[86] R. Giovannini, P. Knochel, *J. Am. Chem. Soc.* **1998**, *120*, 11186–11187.

[87] D. G. Hall, in *Boronic Acids*, Wiley-VCH Verlag GmbH & Co. KGaA, Weinheim, Germany, **2011**, pp. 1–133.

[88] H. a Wegner, L. T. Scott, A. de Meijere, *J. Org. Chem.* **2003**, *68*, 883–887.

[89] J. M. Quimby, L. T. Scott, *Adv. Synth. Catal.* **2009**, *351*, 1009–1013.

[90] S. Saïdi-Besbes, É. Grelet, H. Bock, *Angew. Chemie Int. Ed.* **2006**, *45*, 1783–1786.

[91] X. Mo, M.-M. Shi, J.-C. Huang, M. Wang, H.-Z. Chen, *Dye. Pigment.* **2008**, *76*, 236–242.

[92] K. Shoyama, M. Mahl, S. Seifert, F. Würthner, *J. Org. Chem.* **2018**, *83*, 5339–5346.

[93] S. Benning, H.-S. Kitzerow, H. Bock, M.-F. Achard, *Liq. Cryst.* **2000**, *27*, 901–906.

[94] T. Hassheider, S. A. Benning, H.-S. Kitzerow, M.-F. Achard, H. Bock, *Angew. Chemie Int. Ed.* **2001**, *40*, 2060–2063.

[95] I. Seguy, P. Jolinat, P. Destruel, J. Farenc, R. Mamy, H. Bock, J. Ip, T. P. Nguyen, *J. Appl. Phys.* **2001**, *89*, 5442–5448.

[96] M. Oukachmih, P. Destruel, I. Seguy, G. Ablart, P. Jolinat, S. Archambeau, M. Mabiala, S. Fouet, H. Bock, *Sol. Energy Mater. Sol. Cells* **2005**, *85*, 535–543.

[97] D. Uersfeld, S. Stappert, C. Li, K. Müllen, *Adv. Synth. Catal.* **2017**, *359*, 4184–4189.

[98] P. Y. Bruice, in *Org. Chem.* (Ed.: J. Zalesky), Pearson Education, Santa Barbara, **2017**, pp. 696–738.

[99] S. M. Dyar, E. A. Margulies, N. E. Horwitz, K. E. Brown, M. D. Krzyaniak, M. R. Wasielewski, *J. Phys. Chem. B* **2015**, *119*, 13560–13569.

[100] J. M. Mativetsky, M. Kastler, R. C. Savage, D. Gentilini, M. Palma, W. Pisula, K. Müllen, P. Samorì, *Adv. Funct. Mater.* **2009**, *19*, 2486–2494.

[101] U. Lewandowska, W. Zajaczkowski, L. Chen, F. Bouillière, D. Wang, K. Koynov, W. Pisula, K. Müllen, H. Wennemers, *Angew. Chemie Int. Ed.* **2014**, *53*, 12537–12541.

[102] S. Das, S. Lee, M. Son, X. Zhu, W. Zhang, B. Zheng, P. Hu, Z. Zeng, Z. Sun, W. Zeng, et al., *Chem. - A Eur. J.* **2014**, *20*, 11410–11420.

[103] A. S. Weingarten, R. V. Kazantsev, L. C. Palmer, M. McClendon, A. R. Koltonow, A. P. S. Samuel, D. J. Kiebala, M. R. Wasielewski, S. I. Stupp, *Nat. Chem.* **2014**, *6*, 964–970.

[104] A. S. Weingarten, R. V Kazantsev, L. C. Palmer, D. J. Fairfield, A. R. Koltonow, S. I. Stupp, *J. Am. Chem. Soc.* **2015**, *137*, 15241–15246.

[105] Y. Zhang, Y. Xiao, Y. Xie, L. Zhu, D. Shi, C. Cheng, *Org. Electron.* **2015**, *21*, 184–191.

[106] H. Wonneberger, Light Harvesting and Orbital Tuning, Johannes Gutenberg-Universität Mainz, **2012**.

[107] G.-F. Zhang, H. Wang, M. P. Aldred, T. Chen, Z.-Q. Chen, X. Meng, M.-Q. Zhu, *Chem. Mater.* **2014**, *26*, 4433–4446.

[108] F. Nolde, W. Pisula, S. Müller, C. Kohl, K. Müllen, *Chem. Mater.* **2006**, *18*, 3715–3725.

[109] D. Bauman, R. Hertmanowski, E. Chrzumnicka, T. Martynski, in (Eds.: T.R. Wolinski, M. Warenghem, S.-T. Wu), **2005**, pp. 594713–594719.

[110] L. X. Chen, S. Xiao, L. Yu, *J. Phys. Chem. B* **2006**, *110*, 11730–11738.

[111] T. Edvinsson, C. Li, N. Pschirer, J. Schöneboom, F. Eickemeyer, R. Sens, G. Boschloo, A. Herrmann, K. Müllen, A. Hagfeldt, *J. Phys. Chem. C* **2007**, *111*, 15137–15140.

[112] U. Lewandowska, S. Corra, W. Zajaczkowski, N. A. K. Ochs, M. S. Shoshan, J. Tanabe, S. Stappert, C. Li, E. Yashima, W. Pisula, et al., *Chem. - A Eur. J.* **2018**, *24*, 12623–12629.

[113] U. Lewandowska, W. Zajaczkowski, S. Corra, J. Tanabe, R. Borrmann, E. M. Benetti, S. Stappert, K. Watanabe, N. A. K. Ochs, R. Schaeublin, et al., *Nat. Chem.* **2017**, *9*, 1068–1072.

[114] T. van der Boom, R. T. Hayes, Y. Zhao, P. J. Bushard, E. A. Weiss, M. R. Wasielewski, *J. Am. Chem. Soc.* **2002**, *124*, 9582–9590.

[115] X. Li, L. E. Sinks, B. Rybtchinski, M. R. Wasielewski, *J. Am. Chem. Soc.* **2004**, *126*, 10810–10811.

[116] M. J. Ahrens, L. E. Sinks, B. Rybtchinski, W. Liu, B. A. Jones, J. M. Giaimo, A. V Gusev, A. J. Goshe, D. M. Tiede, M. R. Wasielewski, *J. Am. Chem. Soc.* **2004**, *126*, 8284–8294.

[117] B. Rybtchinski, L. E. Sinks, M. R. Wasielewski, *J. Am. Chem. Soc.* **2004**, *126*, 12268–12269.

[118] C. Curutchet, B. Mennucci, G. D. Scholes, D. Beljonne, *J. Phys. Chem. B* **2008**, *112*, 3759–3766.

[119] E. Schwartz, V. Palermo, C. E. Finlayson, Y.-S. Huang, M. B. J. Otten, A. Liscio, S. Trapani, I. González-Valls, P. Brocorens, J. J. L. M. Cornelissen, et al., *Chem. - A Eur. J.* **2009**, *15*, 2536–2547.

[120] T. M. Wilson, M. J. Tauber, M. R. Wasielewski, *J. Am. Chem. Soc.* **2009**, *131*, 8952–8957.

[121] F. J. Céspedes-Guirao, A. B. Ropero, E. Font-Sanchis, Á. Nadal, F. Fernández-Lázaro, Á. Sastre-Santos, *Chem. Commun.* **2011**, *47*, 8307–8309.

[122] F. J. Céspedes-Guirao, L. Martín-Gomis, K. Ohkubo, S. Fukuzumi, F. Fernández-Lázaro, Á. Sastre-Santos, *Chem. - A Eur. J.* **2011**, *17*, 9153–9163.

[123] J. B. Birks, *Photophysics of Aromatic Molecules*, Wiley-Interscience, London, **1970**.

[124] B. Fückel, G. Hinze, J. Wu, K. Müllen, T. Basché, *ChemPhysChem* **2012**, *13*, 938–945.

[125] S. Jin, M. Supur, M. Addicoat, K. Furukawa, L. Chen, T. Nakamura, S. Fukuzumi, S. Irle, D. Jiang, *J. Am. Chem. Soc.* **2015**, *137*, 7817–7827.

[126] G.-J. Huang, M. A. Harris, M. D. Krzyaniak, E. A. Margulies, S. M. Dyar, R. J. Lindquist, Y. Wu, V. V. Roznyatovskiy, Y.-L. Wu, R. M. Young, et al., *J. Phys. Chem. B* **2016**, *120*, 756–765.

[127] H. Langhals, *Chem. Ber.* **1985**, *118*, 4641–4645.

[128] L. Feiler, H. Langhals, K. Polborn, *Liebigs Ann.* **1995**, *1995*, 1229–1244.

[129] E. Valeur, M. Bradley, *Chem. Soc. Rev.* **2009**, *38*, 606–631.

[130] G. A. Lawrance, in *Introd. to Coord. Chem.*, John Wiley & Sons, Ltd, Chichester, UK, **n.d.**, pp. 41–82.

[131] A. Hauser, Springer, Berlin, Heidelberg, **n.d.**, pp. 49–58.

[132] J. A. Real, A. B. Gaspar, M. C. Muñoz, *Dalt. Trans.* **2005**, *0*, 2062–2079.

[133] S. Decurtins, P. Gütlich, C. P. Köhler, H. Spiering, A. Hauser, *Chem. Phys. Lett.* **1984**, *105*, 1–4.

[134] P. Gütlich, G. Yann, T. Woike, *Coord. Chem. Rev.* **2001**, *219–221*, 839–879.

[135] J. Klingele, D. Kaase, M. Schmucker, Y. Lan, G. Chastanet, J.-F. Létard, *Inorg. Chem.* **2013**, *52*, 6000–6010.

[136] G. F. L. Ehlers, K. R. Fisch, W. R. Powell, *J. Polym. Sci. Part A-1 Polym. Chem.* **1970**, *8*, 3511–3527.

[137] H. Langhals, P. von Unold, M. Speckbacher, *Liebigs Ann.* **1997**, *1997*, 467–468.

[138] H. Langhals, *Helv. Chim. Acta* **2005**, *88*, 1309–1343.

[139] M. Klingele, *Coord. Chem. Rev.* **2003**, *241*, 119–132.

[140] J. Qu, C. Kohl, M. Pottek, K. Müllen, *Angew. Chemie Int. Ed.* **2004**, *43*, 1528–1531.

[141] K. Schügerl, *J. Biotechnol.* **2001**, *85*, 149–173.

[142] D. Wahler, J.-L. Reymond, *Curr. Opin. Chem. Biol.* **2001**, *5*, 152–158.

[143] D. Wahler, J.-L. Reymond, *Curr. Opin. Biotechnol.* **2001**, *12*, 535–544.

[144] D. R. Thévenot, K. Toth, R. A. Durst, G. S. Wilson, *Anal. Lett.* **2001**, *34*, 635–659.

[145] J. Wang, *Electroanalysis* **2005**, *17*, 7–14.

[146] A. Qureshi, W. P. Kang, J. L. Davidson, Y. Gurbuz, *Diam. Relat. Mater.* **2009**, *18*, 1401–1420.

[147] Y. Shao, J. Wang, H. Wu, J. Liu, I. A. Aksay, Y. Lin, *Electroanalysis* **2010**, *22*, 1027–1036.

[148] S. Sinn, F. Biedermann, *Isr. J. Chem.* **2018**, *58*, 357–412.

[149] J.-L. Reymond, V. S. Fluxà, N. Maillard, *Chem. Commun.* **2008**, 34–46.

[150] F. Biedermann, E. Elmalem, I. Ghosh, W. M. Nau, O. A. Scherman, *Angew. Chemie Int. Ed.* **2012**, *51*, 7739–7743.

[151] F. Biedermann, W. M. Nau, H.-J. Schneider, *Angew. Chemie* **2014**, *126*, 11338–11352.

[152] J. Lagona, P. Mukhopadhyay, S. Chakrabarti, L. Isaacs, *Angew. Chemie Int. Ed.* **2005**, *44*, 4844–4870.

[153] V. Westphal, M. A. Lauterbach, A. Di Nicola, S. W. Hell, *New J. Phys.* **2007**, *9*, 435–435.

[154] B. O. Keller, J. Sui, A. B. Young, R. M. Whittal, *Anal. Chim. Acta* **2008**, *627*, 71–81.

[155] Z. Chen, B. Fimmel, F. Würthner, *Org. Biomol. Chem.* **2012**, *10*, 5845–5855.

[156] F. Würthner, Z. Chen, V. Dehm, V. Stepanenko, *Chem. Commun.* **2006**, 1188–1190.

[157] M. Stępień, E. Gońka, M. Żyła, N. Sprutta, *Chem. Rev.* **2017**, *117*, 3479–3716.

[158] T. Jin, J. Zhao, N. Asao, Y. Yamamoto, *Chem. - A Eur. J.* **2014**, *20*, 3554–3576.

[159] A. Narita, X.-Y. Wang, X. Feng, K. Müllen, *Chem. Soc. Rev.* **2015**, *44*, 6616–6643.

[160] H. Zhylitskaya, M. Stępień, *Org. Chem. Front.* **2018**, *5*, 2395–2414.

[161] X. Gao, Y. Hu, *J. Mater. Chem. C* **2014**, *2*, 3099–3117.

[162] H. Usta, C. Risko, Z. Wang, H. Huang, M. K. Deliomeroglu, A. Zhukhovitskiy, A. Facchetti, T. J. Marks, *J. Am. Chem. Soc.* **2009**, *131*, 5586–5608.

[163] U. H. F. Bunz, J. U. Engelhart, B. D. Lindner, M. Schaffroth, *Angew. Chemie Int. Ed.* **2013**, *52*, 3810–3821.

[164] F. Bureš, *RSC Adv.* **2014**, *4*, 58826–58851.

[165] C. Li, C. Xiao, Y. Li, Z. Wang, *Org. Lett.* **2013**, *15*, 682–685.

[166] C. Huang, S. Barlow, S. R. Marder, *J. Org. Chem.* **2011**, *76*, 2386–2407.

[167] Y. Avlasevich, S. Müller, P. Erk, K. Müllen, *Chem. - A Eur. J.* **2007**, *13*, 6555–6561.

[168] S. Alibert-Fouet, I. Seguy, J.-F. Bobo, P. Destruel, H. Bock, *Chem. - A Eur. J.* **2007**, *13*, 1746–1753.

[169] S. Seifert, D. Schmidt, F. Würthner, *Org. Chem. Front.* **2016**, *3*, 1435–1442.

[170] D. Peixoto, A. Locati, C. S. Marques, A. Goth, J. P. P. Ramalho, A. J. Burke, *RSC Adv.* **2015**, *5*, 99990–99999.

[171] K. C. Nicolaou, D. J. Edmonds, P. G. Bulger, *Angew. Chemie Int. Ed.* **2006**, *45*, 7134–7186.

[172] C. Grondal, M. Jeanty, D. Enders, *Nat. Chem.* **2010**, *2*, 167–178.

[173] C. M. R. Volla, I. Atodiresei, M. Rueping, *Chem. Rev.* **2014**, *114*, 2390–2431.

[174] S. Ghosh, X.-Q. Li, V. Stepanenko, F. Würthner, *Chem. - A Eur. J.* **2008**, *14*, 11343–11357.

[175] R. Schmidt, J. H. Oh, Y.-S. Sun, M. Deppisch, A.-M. Krause, K. Radacki, H. Braunschweig, M. Könemann, P. Erk, Z. Bao, et al., *J. Am. Chem. Soc.* **2009**, *131*, 6215–6228.

[176] S. Seifert, D. Schmidt, K. Shoyama, F. Würthner, *Angew. Chemie Int. Ed.* **2017**, *56*, 7595–7600.

[177] M. Mahl, K. Shoyama, J. Rühe, V. Grande, F. Würthner, *Chem. - A Eur. J.* **2018**, *24*, 9409–9416.

[178] D. Jänsch, C. Li, L. Chen, M. Wagner, K. Müllen, *Angew. Chemie Int. Ed.* **2015**, *54*, 2285–2289.

[179] G. Hinze, R. Métivier, F. Nolde, K. Müllen, T. Basché, *J. Chem. Phys.* **2008**, *128*, 124516-1-124516–12.

[180] B. Fückel, G. Hinze, F. Nolde, K. Müllen, T. Basché, *Phys. Rev. Lett.* **2009**, *103*, 1030031–1030034.

[181] R. Métivier, F. Nolde, K. Müllen, T. Basché, *Phys. Rev. Lett.* **2007**, *98*, 047802-1-047802-4.

[182] R. Liu, M. W. Holman, L. Zang, D. M. Adams, *J. Phys. Chem. A* **2003**, *107*, 6522–6526.

[183] F. P. Diehl, C. Roos, A. Duymaz, B. Lunkenheimer, A. Köhn, T. Basché, *J. Phys. Chem. Lett.* **2014**, *5*, 262–269.

[184] C. Flors, I. Oesterling, T. Schnitzler, E. Fron, G. Schweitzer, M. Sliwa, A. Herrmann, M. van der Auweraer, F. C. de Schryver, K. Müllen, et al., *J. Phys. Chem. C* **2007**, *111*, 4861–4870.

[185] S. Stöttinger, G. Hinze, G. Diezemann, I. Oesterling, K. Müllen, T. Basché, *Nat. Nanotechnol.* **2014**, *9*, 182–186.

[186] R. Métivier, F. Kulzer, T. Weil, K. Müllen, T. Basché, *J. Am. Chem. Soc.* **2004**, *126*, 14364–14365.

[187] A. Issac, R. Hildner, C. Hippius, F. Würthner, J. Köhler, *ACS Nano* **2014**, *8*, 1708–1717.

[188] F. Schlosser, V. Stepanenko, F. Würthner, *Chem. Commun. (Camb).* **2010**, *46*, 8350–8352.

[189] J. Lee, V. Stepanenko, J. Yang, H. Yoo, F. Schlosser, D. Bellinger, B. Engels, I. G. Scheblykin, F. Würthner, D. Kim, *ACS Nano* **2013**, *7*, 5064–5076.

[190] S. Ham, J. Yang, F. Schlosser, F. Würthner, D. Kim, *J. Phys. Chem. Lett.* **2014**, *5*, 2830–2835.

[191] F. Schlosser, J. Sung, P. Kim, D. Kim, F. Würthner, *Chem. Sci.* **2012**, *3*, 2778–2785.

[192] R. Jasti, J. Bhattacharjee, J. B. Neaton, C. R. Bertozzi, *J. Am. Chem. Soc.* **2008**, *130*, 17646–17647.

[193] T. Nishiuchi, X. Feng, V. Enkelmann, M. Wagner, K. Müllen, *Chemistry* **2012**, *18*, 16621–5.

[194] F. E. Golling, M. Quernheim, M. Wagner, T. Nishiuchi, K. Müllen, *Angew. Chem. Int. Ed. Engl.* **2014**, *53*, 1525–1528.

[195] M. Haase, Einzelmolekülspektroskopie an Einer Homologen Reihe von Rylendiimiden Und an Einem Bichromophoren Modellsystem Für Elektronischen Energietransfer, Johannes Gutenberg-Universität Mainz, **2010**.

[196] B. Fückel, G. Hinze, F. Nolde, K. Müllen, T. Basché, *J. Phys. Chem. A* **2010**, *114*, 7671–7676.

[197] L. George, Z. Ahmed, H. Lemmetyinen, A. Efimov, *European J. Org. Chem.* **2015**, *2015*, 584–590.

[198] N. J. L. K. Davis, R. W. MacQueen, D. A. Roberts, A. Danos, S. Dehn, S. Perrier, T. W. Schmidt, *J. Mater. Chem. C* **2016**, *4*, 8270–8275.

[199] K. E. Brown, B. S. Veldkamp, D. T. Co, M. R. Wasielewski, *J. Phys. Chem. Lett.* **2012**, *3*, 2362–2366.

[200] T. Weil, M. A. Abdalla, C. Jatzke, J. Hengstler, K. Müllen, *Biomacromolecules* **2005**, *6*, 68–79.